Phosphorylation of the transcription factor Cyclops from *L. japonicus* modulates its activity and its interaction with CCaMK

Dissertation zur Erlangung des Doktorgrades der Naturwissenschaften an der Fakultät für Biologie der Ludwig-Maximilians-Universität München

vorgelegt von

Philipp Robert Bellon

München, Juni 2021

Erstgutachter:	Prof. Dr. Martin Parniske
Zweitgutachter:	Dr. Macarena Marín
Dissertation eingereicht am:	07. Juni 2021
Tag der mündlichen Prüfung:	21. Juli 2021

Eidesstattliche Erklärung

Ich versichere hiermit an Eides statt, dass die vorgelegte Dissertation von mir selbständig und ohne unerlaubte Hilfe angefertigt ist.

München, den 07. Juni 2021

Philipp Bellon

Erklärung

Hiermit erkläre ich, dass die Dissertation nicht ganz oder in wesentlichen Teilen einer anderen Prüfungskommission vorgelegt worden ist. Ich habe mich nicht anderweitig einer Doktorprüfung ohne Erfolg unterzogen.

München, den 07. Juni 2021

Philipp Bellon

Table of Contents

I Abbreviation Index

°C	Degree Celsius
Δ	Delta
A	Alanine
aa	Amino Acid
ABA	Abscisic Acid
ABC	ATP-Binding Cassette
AD	Activation Domain
AM	Arbuscular Mycorrhiza
AMF	Arbuscular Mycorrhiza Fungi
AMT	Ammonium Transporter
AON	Autoregulation of Nodulation
APL	Altered Phloem Development
ASL18/LBD16a	Asymmetric Leaves 2-like 18/Lateral organ Boundaries Domain 16a
ATP	Adenosine triphosphate
BCP1	Blue Copper-binding Protein 1
BD	DNA-Binding Domain
BiFC	Bimolecular Fluorescence Complementation
bp	Base pairs
BR	Brassinosteroid
Ca^{2+}	Calcium
CaM	Calmodulin
CBD	Calmodulin-Binding Domain
CBP	CREB-Binding Protein
CC	Coiled-coil
CCaMK	Calcium- and Calmodulin-Dependent Kinase
CDPK	Calcium-Dependent Protein Kinase
CDPKII	Calcium Dependent Protein Kinase II
CE	*Cytokinin response-element*

CEBiP	Chitin Elicitor Binding Protein
CEP	C-terminally encoded Peptide
CERK1	Chitin Elicitor Receptor Kinase 1
ChIP	Chromatin Immunoprecipitation
CIP73	CCaMK Interacting Protein of approximately 73 kD
CLE	Clavata3/embryo surrounding region-related
CNGC	Cyclic Nucleotide-Gated Channel
CO	Chitooligosaccharide
Co-IP	Co-Immunoprecipitation
CO_2	Carbon dioxide
CRA2	Compact Root Architecture 2
Cyc-Re	*Cyclops Response-Element*
$Cyclops^{min}$	C-terminal fragment of Cyclops (aa 255-518)
$Cyclops^{1-255}$	N-terminal fragment of Cyclops (aa 1-255)
D	Aspartic acid
D27	Dwarf27
DIP	DELLA-Interacting Protein
DMI	Does not Make Infection
DNA	Deoxyribonucleic Acid
dpi	Days post inoculation
*Ds*Red	*Discosoma species* red fluorescent protein
EF1α	Elongation Factor 1α
eGFP	Enhanced Green Fluorescent Protein
eIT	Epidermal IT
EMSA	Electrophoretic Mobility Shift Assay
ENOD	Early nodulin
EPR3	Exopolysaccharide Receptor 3
ER	Endoplasmatic Reticulum
EV	Empty Vector
FLIM	Fluorescence Lifetime Imaging
FLT	Fluorescence Lifetime
FRET	Förster Resonance Energy Transfer

GA	Gibberellic Acid
GlcNAc	N-acetylglucosamine
GOF	Gain-of-function
GPAT	Glycerol-3 phosphate-O-acyltransferase
h	hour
HA	Hemaglutinin
HAR1	Hypernodulation Aberrant Root formation 1
HIP	HSC/HSP70 Interacting Protein
HMGR1	3-Gydroxy-3-Methylglutaryl CoA Reductase 1
HSF1	Heat Shock Factor 1
IPD3	Interacting Protein of DMI3
IPN2	Interacting Protein of NSP2
IT	Infection Thread
kb	Kilobases
kD	Kilodalton
KPI	Kunitz Protease Inhibitor
LCA	Last Common Ancestor
LCO	Lipochitooligosaccharide
LIN	Lumpy Infections
Lj	*Lotus japonicus*
Ll	*Lilium longiflorum*
LNP	Lectin Nucleotide Phosphohydrolase
LOF	Loss-of-function
LRR	Leucine-rich Repeat
LYK	LysM motif eceptor-like Kinase
LysM	Lysine motif
MAG	Monoacylglycerol
MAPK	Mitogen-activated Protein Kinase
MBP	Myelin Basic Protein
mCherry	Monomeric mCherry
MF	Mycorrhization Factor
MIG	Mycorrhiza-induced GRAS

Mp	*Marchantia paleacea*
MSP	Major Sperm Protein
MST	Monosaccharide Transporter
Mt	*Medicago truncatula*
MVA	Mevalonate
MYA	Million-years-ago
N_2	Atmospheric dinitrogen
NAP1	Nck-associated Protein 1
NCR peptides	Nodule-specific Cysteine-rich peptides
NF	Nodulation Factor
NF-Y	Nuclear Factor Y
NFP	Nod Factor Perception
NFR	Nod Factor Receptor
NiCK4	NFR5-interacting Cytoplasmic Kinase 4
NIN	Nodule Inception
NIN^N	N-terminal fragment of NIN (aa 1-296)
NLP	NIN-like Protein
NLS	Nuclear Localization Signal
nM	Nanomolar
NMR	Nuclear Magnetic Resonance
NO	Nitric Oxide
NOPE1	No Perception 1
NPC	Nuclear Pore Complex
NPL	Nodule Pectate Lyase
ns	Nanosecond
NSP	Nodulation Signalling Pathway
NUE	Nitrogen Use Efficiency
NUP	Nuclear Porin
Os	*Oryza sativa*
P(i)	(Inorganic) Phosphorus
PAM	Periarbuscular Membrane
PAS	Periarbuscular Space

PGN	Peptidoglucan
Ph	*Phaseolus hybrida*
Ph	*Petunia hybrida*
PIR1	121F-specific p53 inducible RNA
PIT	Pre-Infection Thread
PM	Plasmamembrane
pmol	Picomol
PPA	Pre-Penetration Apparatus
pro	*Promoter*
PT	Phosphate Transporter
RAD1	Required for Arbuscule Development 1
RAM1	Reduced Arbuscular Mycorrhiza 1
RAM2	Reduced Arbuscular Mycorrhiza 2
RGS	Regulator of G-Signalling
RH	Root Hair
RHC	Root Hair Curling
RPG	Rhizobium-directed Polar Growth
RINRK1	Rhizobial Infection Receptor-like Kinase 1
RLK	Receptor-like Kinase
RLU	Relative Light Units
RNA	Ribonucleic Acid
RNAi	RNA interference
RNS	Root Nodule Symbiosis
ROP6	Rho-like small GTPase 6
S	Serine
SbtM	Subtilisin-like serine protease
SCP	Serine Carboxypeptidase
SD medium	Synthetic dropout medium
SERCA	Sarco/endoplasmic reticulum calcium ATPase
SIE3	SymRK-Interacting E3 ubiquitin ligase 3
SINA4	Seven In Absentia 4
SIP	SymRK-interacting Protein

Sl	*Solanum lycopersicum*
SL	Strigolactone
SLR	Slender rice
SN	Spontaneous Nodule
snf	*spontaneous nodule formation*
STR	Stunted Arbuscule
STY	Stylish
SUT	Sucrose Transporter
SymRK	Symbiosis Receptor-like Kinase
T	Threonine
TAF	TBP-associated Factor
TBP	TATA-binding Protein
TSS	Transcriptional Start Site
U	Uracil
UAS	Upstream Activating Sequence
Ubi	Ubiquitin
VAMP	Vesicle-associated Membrane Protein
VPY	Vapyrin
W	Tryptophane
wpi	Weeks post inoculation
WT	Wildtype
Y	Tyrosine
Y2H	Yeast two-hybrid
YFP	Yellow Fluorescent Protein
Zm	*Zea mays*
μg	Microgram
μl	Microliter
μm	Micrometer

II List of Publications

Philipp Bellon, the author of this thesis, contributed to the following manuscript as follows:

Manuscript 1: Distinct phosphosites of Cyclops promote transcription factor activity and disturb interaction with CCaMK

Reference: **Philipp Bellon**, Katja Zic, Clara Pappenberger, Giulia Gobbato, and Martin Parniske (in preparation)

Manuscript 2: Redox sensitive cysteine residues in the Calcium and calmodulin dependent protein kinase are required for infection thread development

Reference: Víctor Giménez-Oya, Marion Cerri, **Philipp Bellon**, Meritxell Antolín-Llovera, Martin Parniske (in preparation)

Philipp Bellon contributed to the preparation and presentation of the following posters:

Poster presentation at the European Nitrogen Fixation Conference (ENFC) 2016, in Budapest:

"Do you want to join the complex? Towards the identification of new CCaMK/Cyclops components." Reference: Aline Sandré, Chloé Cathebras, Jayne Lambert, **Philipp Bellon**, Rosa Elena Andrade, Xiaoyun Gong and Martin Parniske

Poster presentation at the SFB924 conference 2017, in Freising:

"Multiple phosphorylation sites of Cyclops influence the transcriptional regulation of the *NIN* promoter." Reference: **Philipp Bellon**, Katja Katzer, Martin Parniske

Poster presentation at the European Nitrogen Fixation Conference (ENFC 2018, in Stockholm:

"Transcriptional regulation of Cyclops is dependent on its phosphorylation status." Reference: **Philipp Bellon**, Martin Parniske

III Summary

Legumes form root endosymbioses with nutrient-delivering fungi and nitrogen-fixing rhizobia, called arbuscular mycorrhiza (AM) and root nodule symbiosis (RNS), respectively (Lanfranco et al., 2018; Roy et al., 2019). The establishment of both symbioses is controlled by a regulatory protein complex comprising a calcium- and calmodulin-dependent kinase (CCaMK) and its phosphorylation target Cyclops, a DNA-binding transcriptional regulator (Tirichine et al., 2006; Singh et al., 2014).

In vivo and *in vitro* studies of Cyclops identified 32 phosphorylated amino acid residues (Grimsrud et al., 2010; Singh et al., 2014; Marx et al., 2016; Jin et al., 2018; Diploma Katja Katzer, 2011). The goal of this study was to reveal the functional relevance of Cyclops phosphorylation sites beyond eight that were previously characterized (Singh et al., 2014; Jin et al., 2018). To this end, combinations of phosphomimetic (S/T/Y to D) and phosphoablative (S/T/Y to A) amino acids replacement within the Cyclops protein were generated and their functional impact on transcriptional activation and symbiotic performance was tested.

Transactivation assays in *Nicotiana benthamiana* leaves and yeast suggest that 14 phosphorylation sites in the Cyclops$^{1\text{-}255}$ region synergistically contribute to the expression of the Cyclops target genes *Reduced Arbuscular Mycorrhiza 1* (*RAM1*) and *Nodule Inception* (*NIN*). In the *L. japonicus ccamk-13* mutant, four Cyclops versions with 5, 6, 9 or 10 phosphomimetic replacements mediated an increase in nodule numbers and supported rhizobial presence in nodules, but not fungal entry into the root and arbuscule formation. Complementation of the *cyclops-3* mutant, with respective Cyclops versions resulted in a lower number of infected nodules, indicating that the phosphorylation status of Cyclops may be regulated in a tissue- and time-specific manner during symbioses establishment. Protein-protein interaction studies in yeast suggest that the phosphorylation of Cyclops^{S236} blocks its interaction with CCaMK.

These data led to a model in which CCaMK phosphorylates Cyclops under calcium- and calmodulin-stimulated conditions at multiple sites within in the Cyclops$^{1\text{-}255}$ region. This phosphorylation strongly increases its transcriptional activation strength and initiates the expression of target genes like *NIN* and *RAM1*. The subsequent phosphorylation of S236 weakens Cyclops' interaction with CCaMK, indicating an intrinsic autoregulatory mechanism.

IV Zusammenfassung

Leguminosen formen Wurzelendosymbiosen mit nährstofffliefernden Pilzen (Arbuskuläre Mykorrhiza) und stickstofffixierenden Rhizobien (Wurzelknöllchensymbiose) (Lanfranco et al., 2018; Roy et al., 2019). Beide Symbiosen werden von einem Proteinkomplex reguliert, der aus der Kalzium- und Calmodulin-abhängigen Kinase CCaMK und deren Phosphorylierungssubstrat Cyclops besteht, einem DNA-bindenden Transkriptionsfaktor (Tirichine et al., 2006; Singh et al., 2014). *In vivo* und *in vitro* Studien haben bis jetzt 32 Phosphorylierungsstellen an Cyclops entdeckt (Grimsrud et al., 2010; Singh et al., 2014; Marx et al., 2016; Jin et al., 2018; Diploma Katja Katzer, 2011). Bis jetzt wurden acht Phophorylierungsstellen funktionell charakterisiert und das Ziel dieser Arbeit war diese Zahl erweitern. Dafür wurden Cyclopsversionen mit phosphoablativen (S/T/Y zu D) und phosphomimetischen (S/T/Y zu A) Aminosäureaustäuschen generiert und deren Relevanz für transkriptionelle Aktivierung und symbiotischen Erfolg wurde getestet. Transaktivierungsexperimente in *Nicotiana benthamiana* und Hefe weisen darauf hin, dass 14 Phosphorylierungsstellen in der Cyclops$^{1\text{-}255}$ Region gemeinsam zur Expressionsstärke der Cyclops Zielgene *Reduced Arbuscular Mycorrhiza 1* (*RAM1*) und *Nodule Inception* (*NIN*) beitragen. In der *L. japonicus ccamk-13* Mutante vermittelten Cyclopsversionen mit 5, 6, 9 und 10 mimetischen Aminosäuremutationen vermehrte Knöllchenbildung und das Vorhandensein von Rhizobien in diesen Knöllchen, aber nicht die die Infektion mit Mykorrhizapilz oder Arbuskulentwicklung. Die Komplementation der *cyclops-3* Mutante mit entsprechenden den gleichen Cyclopsversionen resultierte in einer reduzierten Anzahl von infizierten Knöllchen im Vergleich zu Wildtyp Cyclops, was darauf hinweisen könnte, dass der Phosphorylierungsstatus von Cyclops einer zeitlichen und räumlichen Regulierung unterliegt. Durch Interaktionsstudien in Hefe wurden Hinweise erarbeitet, dass die Phosphorylierung von Cyclops^{S236} die Interaction mit CCaMK blockiert. Die Ergebnisse dieser Arbeit auf einen Mechanismus hin, bei dem Cyclops$^{1\text{-}255}$ von CCaMK im Vorhandensein vom Kalzium und Calmodulin an mehreren Stellen phosphoryliert wird. Dadurch wird die Expression von *NIN* und *RAM1* stark erhöht. Die Phosporylierung von Cyclops^{S236D} vermindert daraufhin die Interaktion von Cyclops und CCaMK, was auf einen intrinsischen regulatorischen Mechanismus hinweisen könnte.

V Introduction

1 Root endosymbioses

1.1 The significance of symbiosis

Symbiosis is a widespread phenomenon within the tree of life. Although the term has been under century-long debate, it denotes long term interactions of two organisms, the symbionts, of generally mutualistic nature. The reciprocal and distinct benefits generated in these interactions are diverse but can be distinguished in four general categories: access to new metabolic capabilities, protection from antagonists, improved mobility, and inter-species cultivation. This gain of novel capabilities mediates an advantage for both partners, which is subjected to a positive selection pressure and therefore evolutionary stable (Douglas, 2011).

To overcome nutrient limitations in the soil, plants engage with *Glomeromycota* fungi to form a symbiosis called arbuscular mycorrhiza (AM), or with phylogenetically diverse α- and β- protobacteria, collectively called rhizobia, to form the root nodule symbiosis (RNS) (MacLean et al., 2017; Roy et al., 2019). In exchange for photosynthetically fixed carbons, arbuscular mycorrhiza fungi (AMF) mainly deliver phosphorus (P) to the plant, which is incorporated into DNA, RNA as well as phospholipids, and plays a critical role in ATP-based energy homeostasis (George et al., 1995; Mitsuhashi et al., 2005; Maathuis, 2009; Gaude et al., 2012). Plants use dedicated transport systems to take up P in the form of soluble inorganic P (Pi) molecules, like $H_2PO_4^-$ (Chen et al., 2008; Nussaume et al., 2011; Shen et al., 2011). However, up to 90% of the soil's P content is fixed in the form of organic matter and minerals and is therefore inaccessible to plants (Maathuis, 2009). Due to slow conversion rates into plant-accessible P and substantial runoff into ground and sea waters, P availability is notoriously limited (Maathuis, 2009; Menge et al., 2012). To compensate for the limitation of this macro element in agriculture, it is supplied in the form of P fertilizers, which are produced from finite, non-renewable sources like phosphate-rock (Walan et al., 2014). Various studies predict a maximum in global phosphate-rock production (peak phosphate) to be reach between 2033 – 2136 (Fixen, 2009; Vaccari, 2009; Cordell et al., 2011; Sverdrup and Ragnarsdottir, 2011; Mohr and Evans, 2013). A sustainable solution for food production that could overcome these problems would be the development and agricultural use of optimal AMF inoculums to increase the portion of plant-accessible P in the soil (Dalpé and Monreal, 2004).

Similar to P, nitrogen (N) is essential for plant development (George et al., 1995). It can be taken up directly in the form of nitrate (NO_3^-) and ammonium (NH_4^+) via members of the nitrate transporter (NRT) and ammonium transporter (AMT) families, respectively, and it is mainly incorporated into amino acids (aa), the bases of DNA and photosynthetic pigments (Tischner, 2000; Orsel et al., 2002; Miller and Cramer, 2005). To boost agricultural performance, N is mainly delivered to plants via N-based fertilizers which are almost exclusively produced via the Haber-Bosch process, annually consuming 1 – 2% of the world's energy supply (Smil, 2004; Smith et al., 2007). Due to leaching to ground and surface waters and emission to air, the nitrogen use efficiency (NUE) is calculated to be as low as 18% (Westhoek et al., 2014). Those N losses lead to damages on ecological, health-related and monitory levels (Sutton et al., 2011). Additional problems arise from a heavily beef and dairy based diet in Europe, which generates a strong demand for legumes like soybean (*Glycine max*) from countries like Brazil. The associated supply chain leads to a new manmade N cycle that is spanning the entire globe and is associated with increased emissions of CO_2 due to production and transport via road, river and ocean (da Silva et al., 2010). Based on atmospheric dinitrogen (N_2) fixation via the bacterial enzyme nitrogenase, RNS-forming plants benefit from an improved N supply (Poole et al., 2018). Therefore, a detailed understanding of the underlying genetic and molecular mechanisms could allow to bioengineer RNS in a wide variety of crop plants, promising a more sustainable and ecological food production (Charpentier and Oldroyd, 2010; Huisman and Geurts, 2020). To this end, the model legumes *Lotus japonicus* (*Lj*) and *Medicago truncatula* (*Mt*) were extensively studied in laboratories over the last decades.

1.2 Arbuscular mycorrhiza

The association with AMF substantially increases the root surface through a highly expanded and fine hyphal network that unlocks P resources otherwise inaccessible to the plant (Walder et al., 2012). Some fungal hyphae penetrate the plant root intracellularly to form highly branched structures in cortical cells, called arbuscules, which represent the main surface of nutrient exchange between the symbionts (Gutjahr and Parniske, 2013). Apart from small amounts of ammonia, AMF mainly deliver phosphate and water to the plant (Javot et al., 2007; Guether et al., 2009). In return, the plant delivers hexoses and β-monoacylglycerols (β-MAGs) to the fungus, accounting for up to 20% of its photosynthetically fixed carbons (Shachar-Hill et al., 1995; Pfeffer et al., 1999; Bago et al., 2002; Bravo et al., 2017; Jiang et al., 2017; Keymer et al., 2017; Luginbuehl et al., 2017). In addition to

improved nutrient supply, plants engaged in AM benefit from increased biotic and abiotic stress tolerance, increased resistance to pathogens and an improved soil structure (Gianinazzi et al., 2010). Approximately 80% of all land plants engage with AMF and fossil records of AM are dated to an age of approximately 400 million years, which raised the hypothesis that the establishment of this symbiosis was crucial for the colonisation of land by plants (Remy et al., 1994; Taylor et al., 1995; Fitter, 2006).

The association between fungus and plant is a multistep process. After mutual exchange of signalling molecules, contact between hyphae and roots as well as the physicochemical composition of the root surface itself leads to the formation of a fungal invasion structure, called the hyphopodium (Bastmeyer et al., 2002; Wang et al., 2012). To prepare for fungal accommodation, the plant forms a tubular cytoplasmic bridge called pre-penetration apparatus (PPA), which is comprised of microtubules, actin filament and the endoplasmatic reticulum (ER) (Genre et al., 2005; Siciliano et al., 2007; Genre et al., 2008). The major sperm protein (MSP) and ankyrin-repeat domain containing protein Vapyrin (*Mt*VPY) has been implicated in cellular reorganization during fungal infection, but its exact function remains unknown (Pumplin et al., 2010; Murray et al., 2011). The fungal path through the root is pre-defined by the nucleus, which moves ahead of the hyphae containing PPA (Genre et al., 2008). Once the fungal hyphae reach the cortex, they elongate along the longitudinal root axis, penetrate cortical cells and form arbuscules (Gutjahr and Parniske, 2013). Arbuscule development correlates with vacuolar deformation, proliferation of mitochondria and plastids, as well as the formation of a plastidial network around the arbuscule (Fester et al., 2001; Lohse et al., 2005; Pumplin and Harrison, 2009). Direct contact between arbuscules and the plant cytosol is prevented by the formation of a plant-derived periarbuscular membrane (PAM) (Harrison, 2005). Thereby, the fungal plasmamembrane (PM) and the PAM generate a common apoplast called periarbuscular space (PAS) (Gutjahr and Parniske, 2013). Due to the presence of multiple transport systems, both membranes and the PAS represent the main site of nutrient exchange between the symbionts (Parniske, 2008; Lanfranco et al., 2018).

For PAM development, two exocytotic Vesicle-Associated Membrane Proteins (*Mt*VAMPs) are required (Ivanov et al., 2012). Although the PAM is continuous with the PM it has a distinct protein composition. Blue copper binding protein 1 (*Mt*BCP1) is located at the trunk domain of the PAM and the surrounding PM, whereas Phosphate transporter 4 (*Mt*PT4) is exclusively located at the PAM (Pumplin and Harrison, 2009). The same was found for ammonia transporters

*Mt*AMT2/3 and the sucrose transporter/sensor SUT2 of *Solanum lycopersicum* (*Sl*) (Bitterlich et al., 2014; Breuillin-Sessoms et al., 2015). Recent studies delivered convincing evidence that not only sugars but also 16:0 β-monoacylglycerols (16:0 β-MAGs) are translocated from plant to fungus, presumably via the half-size ATP-binding cassette (ABC) transporters Stunted arbuscule 1 (*Mt*STR1) and *Mt*STR2 (Helber et al., 2011; Bravo et al., 2017; Jiang et al., 2017; Keymer et al., 2017; Luginbuehl et al., 2017). On the fungal site, it was proposed that the arbuscule- and hyphae-localized Monosaccharide transporter 2 (MST2) is involved in sugar transport, as it is important for proper arbuscule development (Helber et al., 2011). Apart from being the matrix for nutrients exchange, the PAS contains β-1,4-glucans, non-esterified homogalacturonans, xyloglucans, hydroxyproline-rich proteins, arabinogalactan proteins, subtilases (*Lj*SbtM1 and *Lj*SbtM3), as well as the protease-inhibitor/peptidase pair *Mt*KPI106/*Mt*SCP1 (Takeda et al., 2009; Rech et al., 2013). Based on several lines of evidence including the analysis of plant phosphate transporter mutants and knockdowns of fungal hexose transporters, there is indication that the arbuscule lifetime is defined by nutrient delivery performance (Javot et al., 2007; Guether et al., 2009; Baier et al., 2010; Helber et al., 2011; Kiers et al., 2011; Yang et al., 2012; Paszkowski and Gutjahr, 2013; Kobae et al., 2014). Insufficiently performing arbuscules are separated from the fungal mycelium via septae formation and completely degraded, after 2 to 10 days (Bonfante-Fasolo, 1984; Toth and Miller, 1984; Floss et al., 2017; Gutjahr and Parniske, 2017).

1.3 Root nodule symbiosis

The major evolutionary invention of RNS is the development of a new symbiont-containing lateral root organ, called the root nodule. RNS is exclusively formed by species that belong to a single phylogenetic clade, comprising four orders: the Fabales, Fagales, Cucurbitales and Rosales (FaFaCuRo) (Soltis et al., 1995). Whereas members of the Fabales are nodulated by gram-negative α- and β-protobacteria collectively referred to as rhizobia, species in the orders of Fagales, Cucurbitales and Rosales form actinorhizal RNS with gram-positive *Frankia* bacteria (Geurts et al., 2012). The only exception is *Parasponia* species (Rosales), which engage in RNS with rhizobia (van Velzen et al., 2019).

The oldest fossil records of a putative nodule are estimated to be 84 million years old (Herendeen et al., 1999), whereas the last common ancestor (LCA) of FaFaCuRo species presumably existed 92-110 million-years-ago (MYA) (Wang et

al., 2009; Bell et al., 2010). To bridge the conceptional gap between the appearance of nodulation and the LCA, the acquisition of an evolutionary advantageous genetic predisposition by the LCA was suggested (Soltis et al., 1995), and a recent opinion argues that this genetic predisposition may have enabled the intracellular accommodation of bacteria in living plant cells (Parniske, 2018). Within the FaFaCuRo clade, only ten out of twenty-eight families contain nodulating plants and in nine out of these ten families, nodulating genera represent the minority (Soltis et al., 1995; Doyle, 2011). To explain this scattered distribution of RNS from an evolutionary perspective, multiple independent gains and subsequent losses of nodulation were proposed (Swensen, 1996; Doyle, 2011). However, a recent genome-wide phylogenomic analysis with members of the FaFaCuRo clade suggests a more parsimonious evolutionary trajectory, in which RNS was gained once and lost multiple times independently (Griesmann et al., 2018). Although RNS evolution is subject to on-going discussion, symbiotic mutant analysis established the widely accepted dogma that RNS evolved on the back of AM, by co-opting existing genetic components to function in a new context (Kistner and Parniske, 2002).

In the best studied RNS between legumes and rhizobia, bacterial attachment to root hairs (RH) depends on plant as well as bacterial surface molecules like lectins and glucomannans (Diaz et al., 1989; Kijne et al., 1997; Hirsch, 1999). Bacterial contact elicits root hair curling (RHC), enclosing individual bacteria within a so-called infection chamber (Geurts et al., 2005; Fournier et al., 2008). Entrapped bacteria continue to divide, resulting in the formation of a microcolony (Oldroyd et al., 2011). From the infection chamber, a tubular invagination of the PM initiates the development of an infection thread (IT), in which rhizobia are guided towards the base of the epidermal cell and further towards the cortex (Fournier et al., 2008; Oldroyd, 2013). Analogous to PPA formation in AM, IT progression is preceded by the formation of a pre-infection thread (PIT), which consists of longitudinally arranged components of the cytoskeleton and ER (Timmers et al., 1999; Fournier et al., 2008). Concomitantly to IT formation, periclinal cell divisions in cortical and pericycle cells are initiated to form a nodule primordium (Roy et al., 2019). Although they are happening in parallel in a precisely coordinated manner, rhizobia infection and nodule organogenesis are genetically distinct processes that can be uncoupled from each other (Tirichine et al., 2006; Murray et al., 2007). Once ITs have reached the developing nodule primordium they ramify and subsequently release rhizobia into nodule primordia cells (Popp and Ott, 2011). In this exocytosis-like process, rhizobia are surrounded by a plant-derived

peribacterial membrane, thereby preventing direct contact of the bacteria with the plant's cytoplasm (Limpens et al., 2009; Ivanov et al., 2012; Gavrin et al., 2016). Membrane surrounded rhizobia then differentiate into N-fixing bacteroids and constitute the organelle-like structure of the symbiosome (Brewin, 2010; Coba de la Peña et al., 2018).

During PIT formation, the longitudinal rearrangements of the cytoskeleton and the ER depend on the actin polymerization driving SCAR/WAVE complex proteins NAP1 and PIR1, as respective *L. japonicus* mutants are impaired in rhizobial infection (Yokota et al., 2009; Miyahara et al., 2010). A prerequisite for IT initiation from the infection chamber and cell-to-cell transition through the cell layers of the root is local weakening of the cell wall. The identification of a mutant in which infection is blocked at the microcolony state revealed that this process might be dependent on *Nodule Pectate Lyase* (*LjNPL*) (Xie et al., 2012). The extension of ITs requires the continuous delivery of membrane vesicles to the tip of the developing IT (Gage, 2004). Only recently, a trimeric protein complex consisting of *Mt*VPY, the putative E3 ligase Lumpy infections (*Mt*LIN) and the cytoplasmic exocyst subunit *Mt*Exo70H4 has been implicated to play a role in the polar growth of ITs (Liu et al., 2019a). Furthermore, IT formation depends on the coiled-coil domain containing protein Rhizobium-directed Polar Growth (RPG), as *rpg* mutants in *M. truncatula* rarely form infected nodules due to abnormally thick and slowly progressing ITs (Arrighi et al., 2006).

Once rhizobia have reached the central nodule tissue, bacteroid differentiation is triggered by low oxygen conditions (Mergaert, 2018). In some but not all RNS forming plant species nodule-specific cysteine-rich (NCR) peptides trigger terminal differentiation of bacteroids, which is characterized by an arrest of bacterial cell division and multiple genome replications, resulting in large bacterial cells with highly permeable membranes (Mergaert et al., 2006; Van de Velde et al., 2010). The oxygen-reduced environment within the root nodule, allows fixation of atmospheric nitrogen (N_2) via the oxygen-sensitive bacterial nitrogenase enzyme complex (Tjepkema and Winship, 1980; Hoffman et al., 2014). In return for nitrogenase-produced ammonia, the plant delivers photosynthetically fixed carbon mainly in the form of malate and amino acids, as well as a multitude of ions to the symbiont (Udvardi and Day, 1997; Colebatch et al., 2004; Downie, 2014; Roy et al., 2019; Mergaert et al., 2020). Nutrient exchange between bacteroids and the plant is mediated by multiple transport systems at the bacterial and the peribacteroid membrane. Those include an aquaporin and transporters for citrate, sulphate, copper, zinc, molybdate, as well as a putative iron transporter (Krusell

et al., 2005; Hakoyama et al., 2012; Tejada-Jiménez et al., 2015; Abreu et al., 2017; Kryvoruchko et al., 2018; Senovilla et al., 2018; Gil-Díez et al., 2019). Due to developmental and environmental cues like nodule age, nutrient re-allocation, altered nutrient availability or reduced photosynthesis, nodules can be terminated and undergo senescence (Seabra et al., 2012; Cabeza et al., 2014a; Cabeza et al., 2014b; Liese et al., 2017; Deng et al., 2019). They are broken down in a controlled manner and their macromolecular components are remobilized to other plant organs (Van de Velde et al., 2006).

2 Signalling in root endosymbioses

2.1 Symbiotic partner perception at the plasma membrane

Prior to symbiotic contact, a reciprocal communication between the host plant and its symbiont takes place. Under P-limiting conditions, plants exude the carotenoid compounds strigolactones (SL) into the rhizosphere (Yoneyama et al., 2007; Yoneyama et al., 2008; Kretzschmar et al., 2012). Experiments with the synthetic strigolactone GR24 indicated that concentrations as low as 10 nM are sufficient to induce fungal responses, including spore germination, hyphal growth and hyphal branching (Besserer et al., 2006; Besserer et al., 2008). Hyphal branching and fungal transcriptional changes also depend on the N-acetylglucosamine (GlcNAc) transporter No Perception 1 (*Oryza sativa* (*Os*)/*Zea mays* (*Zm*)NOPE1), which indicates that GlcNAc is involved in priming the fungus for symbiosis (Nadal et al., 2017). In response to SL perception AMF exude a mixture of signalling molecules that are collectively referred to as mycorrhization factors (MFs). MFs include lipochitooligosaccharides (Myc-LCOs), which are made up of β-1,4-linked N-acetyl-D-glucosamine monomers that are substituted with a N-acyl group at the C2 position of the terminal non-reducing sugar, and short-chained chitooligosaccharides (COs) (reviewed in Oldroyd et al., 2013). The exogenous application of MFs promotes AM formation and induces transcriptional reprogramming, symbiotic Ca^{2+} responses, lateral root formation and starch accumulation in host plants (Kosuta et al., 2003; Oláh et al., 2005; Gutjahr et al., 2009; Kuhn et al., 2010; Maillet et al., 2011; Genre et al., 2013; Sun et al., 2015).

For both RNS and AM, Lysine Motif (LysM) receptor-like kinases (Lyk) are involved in symbiotic signal perception. Although direct binding to Lyks was demonstrated for rhizobial LCOs, the hunt for MF receptors has proven substantially more difficult. A recent study demonstrated direct binding of Myc-LCOs to *Sl*Lyk10, which is an orthologue of *M. truncatula* Nod Factor Perception

(NFP) and *L. japonicus* Nod Factor Receptor 5 (NFR5) (Girardin et al., 2019). Together with a reduction in colonisation by the AM-forming fungus *Rhizophagus irregularis* (*R. irregularis*) upon mutation (*Sllyk10-1*) or downregulation of *SlLYK10* transcripts, this is strong indication that *Sl*Lyk10 is directly involved in the perception of Myc-LCOs (Buendia et al., 2016; Girardin et al., 2019). Interestingly, *SlLyk10* and its orthologue from petunia (*PhLyk10*) complement RNS in *nfp* and *nfr5* mutants, suggesting that *Lyk10* could have been recruited from AM- to RNS-signalling (Girardin et al., 2019). Although *NFR5* is required for LCO perception, its corresponding mutant is not impaired in AM formation (Rasmussen et al., 2016).

In *Oryza sativa*, the LysM domain containing Chitin Elicitor Receptor Kinase 1 (CERK1) mediates plant immunity in response to COs (Ao et al., 2014). Interestingly, mutation of *CERK1* not only impairs immune responses but also AM formation, suggesting an additional role of COs in AM signalling (Zhang et al., 2015; Carotenuto et al., 2017). Although CERK1 was shown to interact with the high affinity chitin receptor Chitin Elicitor Binding Protein (CEBiP) in *O. sativa* (Shimizu et al., 2010)), *cebip* mutant plants establish AM normally, therefore suggesting that differential protein-protein interaction at the PM mediate a bifurcation between immunity and symbiotic signalling (Miyata et al., 2014).

Besides AM, nutrient limitation also promotes the formation of RNS. Under nitrogen-limiting conditions, legumes increase their secretion of (iso)flavonoid to the rhizosphere (Coronado et al., 1995). (Iso)flavonoids are recognized by the bacterial transcriptional activator *nodD*, which induces the expression of Nod Factor (NF) biosynthesis genes (Peters et al., 1986; Lerouge et al., 1990). NFs are LCOs that are structurally similar to Myc-LCOs and can be decorated with methyl, fucosyl, acetyl and sulphate groups (Oldroyd, 2013). NF decoration together with the cocktail of (iso)flavonoids produced by the plant are thought to be two but not all factors that contribute to host-symbiont specificity (Radutoiu et al., 2007; Poole et al., 2018).

NF recognition is mediated by two LysM receptors, namely NFR1 and NFR5 (Lyk3 and NFP in *M. truncatula*), which form heterodimers at the PM (Madsen et al., 2003; Broghammer et al., 2012). In *L. japonicus*, NF receptor (NFR) complexes interact with additional PM-spanning signalling components, including the Leucine Rich Repeat Receptor Like Kinase (LRR-RLK) Symbiosis Receptor-like Kinase SymRK (Does Not Make Infection 2 (DMI2) in *M. truncatula*), an epidermal LysM receptor

(NFRe) (Antolin-Llovera et al., 2014; Murakami et al., 2018) and a recently identified LRR-RLK called Rhizobial Infection Receptor-like Kinase 1 (RINKRK1) (Li et al., 2019). To prevent endocytosis and to stabilize symbiotic signalling, NFR complexes are recruited into nanodomains in a remorin- and flotillin-dependent process (Liang et al., 2018). Cytosolic regulatory factors and signalling components associated with NF perception include NFR5-interacting Cytoplasmic Kinase 4 (NiCK4), NFP-interacting Rho-like small GTPase 6 (ROP6) (Ke et al., 2012; Wong et al., 2019), NFR1-interacting Regulator of G-Signalling (RGS), as well as multiple SymRK-interacting proteins described in 2.2. Apart from NFs, legumes also recognize bacterial exopolysaccharides (EPS), which bind to the LysM domain containing Exopolysaccharide Receptor 3 (EPR3) in *L. japonicus* (Kawaharada et al., 2015). The identification and analysis of *EPR3* revealed a system for the determination of host-symbiont compatibility that is acting downstream of NF signalling (Kawaharada et al., 2015; Kawaharada et al., 2017).

2.2 Common symbiotic signal transduction

The perception of symbiotic signals elicits characteristic calcium responses on the plant side, including cytosolic calcium influxes and periodic calcium oscillations in and around the nucleus, called calcium spiking (Kosuta et al., 2003; Sieberer et al., 2009; Chabaud et al., 2011). The earliest calcium spiking responses can be observed six minutes post NF application and it has been estimated that approximately 36 consecutive spikes are required for symbiotic gene expression (Miwa et al., 2006). Interestingly, there are no significant differences in the calcium response upon perception of rhizobia, AMF, MFs or NFs (Sieberer et al., 2012; Sun et al., 2015). Both the generation of and the transcriptional response to calcium spiking depends on a set of genes, called common symbiosis genes, that are required for both AM and RNS (Stracke et al., 2002; Levy et al., 2004; Mitra et al., 2004; Imaizumi-Anraku et al., 2005; Kistner et al., 2005; Kanamori et al., 2006; Saito et al., 2007; Yano et al., 2008; Groth et al., 2010; Murray et al., 2011; Roberts et al., 2013). Due to their function at the PM, the nuclear envelope and the nucleoplasm a subset of the common symbiosis gene products have been arranged into a conceptual signalling cascade, which transmits information from the PM to the nucleus and initiates symbioses specific transcriptional responses (Figure 1) (Parniske, 2008; Singh and Parniske, 2012; Oldroyd, 2013).

The PM localized Lectin Nucleotide Phosphohydrolase (LNP) binds NFs directly and its RNAi-mediated downregulation in *L. japonicus* results in loss of calcium

spiking, reduced arbuscule and nodule formation as well as a reduction in the expression of the RNS maker gene *Nodule Inception* (*NIN*) (Etzler et al., 1999; Roberts et al., 2013). SymRK/DMI2 is localized at the PM as well and is required for both AM and RNS (Endre et al., 2002; Stracke et al., 2002). Although *symrk/dmi2* mutants retain root hair swelling, they are defective in rhizobial infection and nodule formation, as well as in fungal penetration of the epidermis. Interestingly, *symrk/dmi2* mutants retain cytosolic calcium influxes in root hairs upon symbiont perception, but do not display calcium spiking (Miwa et al., 2006). Based on these experiments and epistatic analysis with *NFR1*, *NFR5* and *SymRK*, it is currently assumed that SymRK/DMI2 acts downstream of LCO perception but upstream of calcium spiking (Madsen et al., 2010; Ried et al., 2014). SymRK/DMI2 interacts with additional cytosolic proteins, including the ARID domain containing SymRK interacting protein 1 (SIP1) (Zhu et al., 2008), the mitogen activated protein kinase kinase (MAPKK) SymRK interacting protein 2 (SIP2) (Chen et al., 2012), the plant U-box E3 ubiquitin ligase PUB1 (Vernié et al., 2016), the E3 ubiquitin ligase Seven In Absentia 4 (SINA4) (Den Herder et al., 2012), the SymRK-interacting E3 ubiquitin ligase (SIE3) (Yuan et al., 2012), and the 3-hydroxy-3-methylglutaryl CoA reductase 1 (HMGR1) (Kevei et al., 2007). The latter is involved in the production of mevalonate (MVA) (Venkateshwaran et al., 2015). As RNAi-mediated downregulation of *HMGR1* transcripts in *M. truncatula* results in reduced calcium spiking in response to rhizobial and fungal signals as well as a decrease in nodule formation (Kevei et al., 2007), it has been proposed that MVA could link microbial perception at the PM to the generation of calcium spiking in the nucleus, via a yet to be identified secondary messenger.

Within the nucleus, multiple components are thought to be involved in the generation of calcium spiking. In *L. japonicus*, those include the cation channels Castor and Pollux/*Mt*DMI1, as *castor* and *pollux*/*Mtdmi1* mutants do not display calcium spiking and are impaired in fungal and rhizobial infection, as well as in nodule organogenesis (Ané et al., 2004; Imaizumi-Anraku et al., 2005). Both proteins form homodimers at the nuclear envelope and until recently they were implicated in the release of potassium from the nucleoplasm, to counteract the positive charge that is generated by the increase in nuclear calcium concentration during calcium spiking (Charpentier et al., 2008). However, recent studies delivered compelling evidence that at least Castor acts as a calcium-regulated calcium channel, supposedly releasing calcium from the nucleoplasm (Kim et al., 2019). In *M. truncatula*, the function of DMI1 could be supported by the sarco/endoplasmic reticulum calcium ATPase (SERCA) MCA8, which is assumed

to decrease the nuclear calcium concentration by pumping it back into the ER lumen (Capoen et al., 2011). Based on their calcium permeability and a reduction in AM-, IT- and nodule-formation in *M. truncatula* mutant plants, it was proposed that three Cyclic Nucleotide-Gated Channels (CNGC15a, CNGC15b, CNGC15c) release calcium into the nucleoplasm upon symbiont perception (Charpentier et al., 2016). Additional components involved in the generation of calcium spiking are the nuclear porins (NUP) 85 and 133, as well as the WD40 repeat protein Nena (Kanamori et al., 2006; Saito et al., 2007; Groth et al., 2010). All three proteins have been identified in *L. japonicus,* are part of the nuclear pore complex (NPC) and were suggested to be involved in the transport of a yet to be identified common symbiotic signalling component (Genre and Russo, 2016), and/or proper subcellular targeting of proteins required for symbiotic signalling (Binder and Parniske, 2018).

Within the nucleus, the Calcium- and Calmodulin-dependent Kinase CCaMK (Does not Make Infections 3 (DMI3) in *M. truncatula*) and the coiled-coil containing transcription factor Cyclops (Interacting Protein of DMI3 (IPD3) in *M. truncatula*) function downstream of calcium spiking (Miwa et al., 2006). As CCaMK and DNA-binding Cyclops form a complex in which Cyclops serves as a phosphorylation substrate, CCaMK is assumed to translate common symbiotic signalling information into a transcriptional readout, in a Cyclops dependent manner (Yano et al., 2008; Singh et al., 2014; Genre and Russo, 2016).

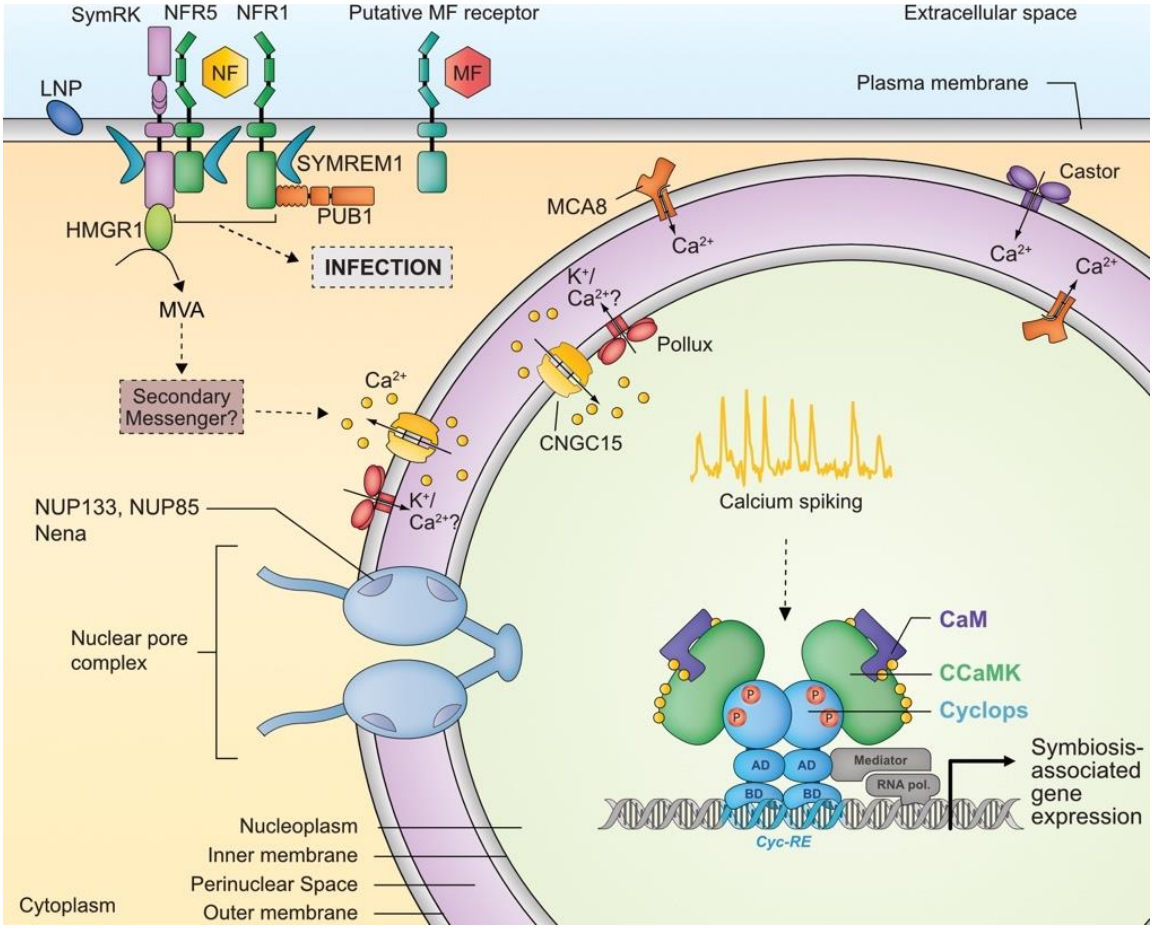

Figure 1: Symbiotic partner perception at the plasma membrane and common symbiotic signal transduction.
At the PM, Nod Factors (NFs) are bound by *Lj*LNP and LysM-receptor-like kinases (LYK), including Nod factor receptor (NFR) 1 and NFR5 in *Lotus japonicus* and LYK3 and NFP in *Medicago truncatula* (Roberts et al., 2013, Amor et al., 2003, Arrighi et al., 2006, Smit et al., 2007, Radutoiu et al., 2003, Madsen et al., 2003). A yet to be identified LYK is proposed to be involved in the perception of AMF derived Mycorrhization factors (MF). NFR-interacting leucine rich repeat receptor-like kinase (LRR-RLK) SymRK is required for both fungal and rhizobial infection, as well as nodule organogenesis (Stracke et al., 2002, Demchenko et al., 2014). Recruitment of NFRs into microdomains, additional regulatory NFR- and SymRK-interacting proteins and putative secondary messengers related to calcium responses are described in 2.1 and 2.2. The nuclear core complex components NUP85, NUP133 and Nena (Kanamori et al., 2006, Saito et al., 2007, Groth et al., 2010), calcium channels Castor, Pollux/DMI1 (Ané et al., 2004, Imaizumi-Anraku et al., Charpentier et al., 2008, Kim et al., 2019) and CNGC15 proteins (Charpentier et al., 2015), as well as calcium pump MCA8 (Capoen et al., 2011) are all required to generate calcium oscillations (calcium spiking) in and around the nucleus, which can be observed minutes after LCO (NF or MF) perception (Ehrhardt et al., 1996, Kistner and Parniske, 2012). Calcium spiking is supposedly decoded by CCaMK/DMI3, which interacts with and phosphorylates the transcriptional activator Cyclops/IPD3 (Levy et al., 2004, Tirichine et al., 2006, Messinese et al., 2007, Yano et al., 2008, Singh et al., 2014). Cyclops binds to palindrome-containing *Cyclops-esponse elements* (*Cyc-Re*) in the promoters of symbiosis related genes, in a DNA-binding domain (BD) dependent manner (Pimprikar et al., 2016, Singh et al., 2014, Cerri et al., 2017). Phosphorylation of dimeric Cyclops is indicated by two key sites (P), which are necessary for DNA-binding and its transcription factor activity (Singh et al., 2014). Cyclops is proposed to interact with mediator proteins, via an activation domain (AD) (Singh et al., 2014). Figure was modified based on Singh and Parniske, 2012 and Singh et al., 2014.

3 Transcriptional regulators and networks in root endosymbioses

To accommodate AMF and enable rhizobial infection as well as nodule organogenesis, extensive transcriptional responses are initiated. Although multiple common symbiosis genes have been identified, the gene regulatory networks governing the development of AM and RNS are different (Pimprikar and Gutjahr, 2018; Roy et al., 2019). Due to its transcriptional regulation of key transcription factors that are involved in both symbioses, Cyclops has been positioned on top of the gene regulatory networks for both AM and RNS (Huisman and Geurts, 2020). Interestingly, many of the gene products that are regulated in a Cyclops-dependent manner were identified to either directly or indirectly interact with the CCaMK/Cyclops complex (summarized in Figure 2). Apart from regulation via the common symbiosis genes, transcriptional networks in root endosymbioses are also subject to regulation via hormonal and nutritional cues. The integration of information from all signalling pathways is crucial for the establishment of both symbioses (Maekawa et al., 2009; Gutjahr et al., 2015; Gamas et al., 2017; Nishida and Suzaki, 2018).

3.1 Arbuscular mycorrhiza

On the plant side, AM formation is initiated by the secretion of strigolactones (SL) into the rhizosphere. Although they were initially identified as factors involved in RNS signalling, it was demonstrated that the GRAS proteins Nodulation Signalling Pathway (NSP) 1 and NSP2 are involved in regulating the expression of SL biosynthesis gene *DWARF27* (*D27*) as well (Liu et al., 2011; Alder et al., 2012). The accumulation orobanchol in mutant plants suggests an additional role for NSP2 in later steps of the SL biosynthesis pathway (Liu et al., 2011). Consistent with a role during this early communication between plant host and AMF, *nsp1* mutants display a reduced colonization level but the number of arbuscules in colonized root patches is not reduced (Liu et al., 2011; Delaux et al., 2013).

Once fungal signals have been perceived, they are translated into a transcriptional response. Due to reduced hyphopodium formation, a reduced number of internal fungal hyphae and the formation of malformed and stunted arbuscules in mutant plants, *Required for Mycorrhization 1* (*RAM1*) was suggested to play a key role during fungal infection and arbuscule development (Gobbato et al., 2012; Rich et al., 2015). *RAM1* encodes for a GRAS domain transcriptional regulator that is required for the induction of a multitude of genes involved in AM development (Park et al., 2015). Among those, the glycerol-3 phosphate-O-acyltransferase

(GPAT) *Required for Arbuscular Mycorrhiza 2* (*RAM2*) is involved in fatty acid biosynthesis and its promoters was shown to be directly bound by *RAM1, in vitro* (Gobbato et al., 2012).

The expression of *RAM1* itself is regulated by the CCaMK/Cyclops complex and Cyclops was demonstrated to directly bind to a palindrome-containing *Cyclops-response Element* (*Cyc-RE*$_{RAM1}$) in the *RAM1* promoter (Pimprikar et al., 2016). Transactivation experiments in tobacco leaves demonstrated that the CCaMK/Cyclops dependent expression of *RAM1* is significantly increased in presence of DELLA proteins and interaction experiments revealed that DELLA1 directly interacts with Cyclops (Pimprikar et al., 2016). Due to a reduction in arbuscule numbers and *NSP1* and *NSP2* transcripts in *della1 della2* double mutant plants, DELLA proteins had been implicated in AM before (Floss et al., 2013) and the direct interaction with Cyclops suggested they participate in MF-dependent signaling. However, a Cyclops-independent function of DELLA cannot be excluded, since overexpression of gibberellic acid (GA) insensitive DELLA1 (della1$^{\Delta 18}$) partially rescues the AM phenotype of an *ipd3* mutant in *M. truncatula* (Floss et al., 2013; Lindsay et al., 2019). Due to their GA-dependent degradation (Davière and Achard, 2016), DELLA proteins are considered as integrators of symbiotic and phytohormone signaling during AM.

To understand the role of DELLA proteins in AM in more detail, the DELLA orthologue from *O. sativa* (SLR1) was used in a yeast two-hybrid (Y2H) approach to screen for interaction partners (Yu et al., 2014). From this analysis, DELLA Interacting Protein 1 (DIP1) was identified. *DIP1* encodes a GRAS protein that is induced upon mycorrhizal infection and RNAi-mediated downregulation of *DIP1* transcripts results in a reduced root colonization. In addition to DELLA, interaction between DIP1 and RAM1 was demonstrated (Yu et al., 2014).

Besides DIP1, the GRAS protein Required for Arbuscule Development 1 (RAD1) was identified as an additional interactor of RAM1 (Xue et al., 2015). During early stages of AM development, ranging from 2-6 days post inoculation (dpi), *rad1* mutants do not display a significant AM-defective phenotype (Park et al., 2015). However, at later stages, ranging from 3-7 weeks post inoculation (wpi), *rad1* mutants display an overall decreased colonization rate compared to wildtype (WT) plants (Park et al., 2015). The increase in small and stunted arbuscules, septae formation and premature arbuscule degradation in the *rad1* mutant suggests that this gene is involved in arbuscule morphogenesis and maintenance (Xue et al., 2015).

Accommodation of fungal structures in cortical cells requires morphological adaptions of the plant root. To identify players in this process, Heck and colleagues (2016) performed a Protein-BLAST (pBLAST) analysis with RAM1, NSP1 and NSP2. This approach led to the identification of Mycorrhiza-Induced GRAS (MIG) proteins. Members of the *MIG* family, are strongly induced 25 dpi with AMF and a transcriptional fusion of the *MIG1* promoter to the *uidA* gene, encoding *β-glucuronidase* (*GUS*), demonstrated that it is specifically expressed in arbuscule containing cells (Heck et al., 2016). Overexpression of *MIG1* resulted in an increased width of cortical cells and an increased number of cortical cell layers (Heck et al., 2016). This effect was phenocopied by the application of the GA synthesis inhibitor paclobutrazol (PAC) or by expression of della1$^{\Delta 18}$, and it was fully reverted by the application of GA. Downregulation of *MIG1* resulted in the formation of malformed arbuscules, which could be rescued by the expression of della1$^{\Delta 18}$. Furthermore, Bimolecular fluorescence complementation (BiFC) studies in tobacco leaves revealed a direct interaction between MIG1 and DELLA1 (Heck et al., 2016). Collectively, these results suggest that MIG1 and DELLA are involved in arbuscule branching and the remodeling of arbuscule containing cortex cells.

Due to insufficient nutrient delivery, arbuscules can be isolated from the fungal mycelium via septae formation and be terminated (Gutjahr and Parniske, 2013). Transcriptional profiling of *pt4* mutants, revealed that the MYB-like transcription factor MYB1 is associated with a transcriptional program for arbuscule degeneration (Floss et al., 2017). Mutation of *MYB1* reduces the expression of arbuscule degeneration associated genes and *MYB1* overexpression resulted in induction of those respective genes in absence of fungus (Floss et al., 2017). In inoculated plants, the overexpression of *MYB1* results in reduced colonization levels, a reduced length of infected root patches, an overall reduction in arbuscule formation and an increase in the numbers of degenerated arbuscules (Floss et al., 2017). Expression analysis of degeneration-associated genes in the *della1 della2* double mutant and in *nsp1* and *nsp2* single mutants revealed that *DELLAs* and *NSP1*, but not *NSP2*, are required for *MYB1*-dependent transcriptional responses. Subsequently, Y2H analysis demonstrated direct interaction between MYB1 and DELLA1/2, as well as NSP1 (Floss et al., 2017).

3.2 Root nodule symbiosis

The earliest morphological responses to NF perception can be observed in root hairs preparing for rhizobial infection and over the course of recent years, the two transcriptional regulators *ERF Required for Nodulation 1* (*ERN1*) and *NIN* have emerged as key players for this process in legumes (Schauser et al., 1999; Middleton et al., 2007; Liu et al., 2019b). Upon mutation of *ern1* in *L. japonicus*, IT formation is blocked very early, and rhizobia remain outside of the root and are occasionally trapped within infection chambers (Cerri et al., 2017). *ERN1* appears to be specific for the infection process, as nodule primordia are still formed in *ern1* mutant plants (Middleton et al., 2007). In *M. truncatula, ERN1* function is supported by *ERN2,* a gene which is absent in *L. japonicus* (Cerri et al., 2016; Cerri et al., 2017). In line with their role in early symbiotic processes, *ERNs* are upregulated as early as 1 h after NF perception (Cerri et al., 2016; Cerri et al., 2017). Translational fusion with Yellow Fluorescent Protein (YFP) demonstrated that ERN1 specifically accumulates in the nuclei of IT-containing and IT-anticipating cells (Cerri et al., 2012). ERN1 regulates the expression of *Early Nodulin 11* (*ENOD11*), via direct binding to a NF-responsive element (NF-box) in its promoter (Andriankaja et al., 2007; Cerri et al., 2012). However, root hair transcriptomic experiments demonstrated that ERN1 is involved in regulating a plethora of additional genes during infection (Liu et al., 2019b). Transactivation assays with the *ERN1* promoter in transiently transformed tobacco leave cells demonstrated that the expression of *ERN1* is synergistically activated by NSP1 and NSP2 (Cerri et al., 2012). *nsp1* and *nsp2* mutants retain the ability to initiate calcium spiking upon rhizobia perception, but they fail to initiate IT and nodule formation (Oldroyd and Long, 2003; Heckmann et al., 2006). Y2H and BiFC experiments revealed that NSP1 and NSP2 form homo- and hetero-dimers, which have been positioned to act downstream of CCaMK (Kaló et al., 2005; Smit et al., 2005; Hirsch et al., 2009). Electrophoretic mobility shift assays (EMSA) suggest that NSP1, but not NSP2, can bind DNA via an AATTT-motif in the promoter of *ENOD11* (Hirsch et al., 2009). In addition to NSP1 and NSP2, *ERN1* expression is regulated by the CCaMK/Cyclops complex. Cyclops in the presence of the autoactive ($CCaMK^{1-314}$ activates the expression of *ERN1* promoter driven *GUS* in *N. benthamiana* leaves and promoter deletion analyses identified a palindrome containing 30 bp motif (*Cyc-RE*$_{ERN1}$), which is directly bound by Cyclops (Cerri et a., 2017). Congruently, the expression of *ERN1* in the *cyclops-3* mutant (G_{2241} to A, W_{371} to stop) (Yano et al., 2008) is severely reduced at 7 days post inoculation (dpi) with rhizobia (Cerri et al., 2017). Interestingly, *GUS* expression analyses with a 2.2kb fragment of the

ERN1 promoter in the *cyclops-3* mutant revealed the expression of *GUS* in nodule primordia, 14 dpi (Cerri et al., 2017). These results suggest that *ERN1* expression is regulated by Cyclops in the epidermis, but not the cortex.

Multiple recent studies demonstrated that the function of NSPs is tightly connected to DELLA proteins. In RNS, exogenous application of GA or *della* mutation results in a reduction in IT formation and nodule numbers, and *DELLA* transcripts are increased in response to inoculation with rhizobia (Fonouni-Farde et al., 2016; Jin et al., 2016). Chromatin Immuno-Precipitation (ChIP) experiments from inoculated *M. truncatula* roots revealed that DELLA1 associates with the *ERN1* promoter *in planta*, and transactivation assays in *A. thaliana* protoplasts with the *ERN1* promoter demonstrated that the NSP1/NSP2 mediated expression of *ERN1* is significantly increased in presence of DELLA1 (Fonouni-Farde et al., 2016; Jin et al., 2016). Due to its direct interaction with Cyclops and NSP2, it was therefore hypothesised that DELLAs serve as bridging factors between the CCaMK/Cyclops complex and the NSP1/NSP2 complex during the regulation of symbiotic gene expression (Jin et al., 2016). In addition to Cyclops and NSP2, DELLA proteins interact with Nuclear Factor-YA 1 (NF-YA1) and transactivation assays demonstrated that DELLA1 and NF-YA1 together promote the expression of *ERN1*, compared to DELLA1 and NF-YA1 alone (Fonouni-Farde et al., 2016).

The second key player during rhizobial infection is the transcription factor *NIN*, which is upregulated as early as two hours after NF perception (Schauser et al., 1999). *nin* mutants display extensive root hair curling and swelling upon perception of NFs, but infection chamber and IT formation, as well as nodule organogenesis are completely blocked (Schauser et al., 1999; Fournier et al., 2015). EMSA experiments demonstrated that Cyclops directly binds to a palindrome-containing sequence within the *NIN* promoter (*Cyc-RE*$_{NIN}$) (Singh et al., 2014), and the abundance of *NIN* transcripts is strongly reduced in rhizobia-inoculated *cyclops-3* mutant plants (Yano et al., 2008). As *NIN*, *ERN1* and *Cyclops* all function during the rhizobial infection process, a recent study aimed to characterize their interplay in more detail. Collectively, this study revealed that ERN1 contributes to the expression of *NIN* during rhizobial infection, in addition to Cyclops (Liu et al., 2019d). However, the additive defects in IT development of the *ern1 cyclops* double mutant compared to the respective single mutants, the lack of IT complementation upon ectopic expression of *NIN* in the *ern1* mutant and transcriptomics data from root hairs suggest that there is an additional *NIN*-independent role for *ERN1* during the infection process (Liu et al., 2019b; Liu et al., 2019d).

An additional factor involved in the expression of *NIN* was identified in a Y2H screen for NSP2 interacting proteins. Interacting Protein of NSP2 (IPN2) directly binds the promoters of *NIN, NPL* and *ERN1* in EMSA experiments and transactivation assays demonstrated that IPN2 promotes the expression of all three genes (Kang et al., 2014; Xiao et al., 2020). Promoter deletion experiments revealed that IPN2-binding to the *NIN* promoter is mediated via a 31 bp fragment, which is also bound by NSP1 (Xiao et al., 2020). Interestingly, co-transformation of *IPN2*, *NSP1* and *NSP2* into *N. benthamiana* leaves results in strong reporter expression via the *NIN* promoter, indicating that a trimeric complex of these proteins is involved in the transcriptional regulation of *NIN* (Xiao et al., 2020). Knock-down experiments of *IPN2* results in reduced IT and nodule numbers and the subsequent isolation and characterization of an *ipn2* mutant revealed an additional role for *IPN2* in regulating vasculature identity, a function which correlates with the role of its close homologue *Altered Phloem Development* (*APL*) in *A. thaliana* (Kang et al., 2014; Xiao et al., 2020).

A recent transcriptomics analysis of *M. truncatula* root hairs revealed *NIN* as the key hub for the transcriptional networks involved in the rhizobial infection process. Gene network analysis and the overlap with ChIP-seq data obtained in an earlier study (Soyano et al., 2014), suggest that approximately 100 genes could be directly targeted by NIN for transcriptional regulation during the infection process ((Liu et al., 2019b). This includes the previously discussed *RPG* and *NPL*, as well as members of the *NF-Y* family.

Members of the NF-Y family form trimeric complexes which are conserved in all eukaryotes and exert transcriptional regulation via direct DNA-binding of a conserved CCAAT-box (NF-YA) and chromatin remodelling (NF-YB and NF-YC) (Calvenzani et al., 2012; Hackenberg et al., 2012). Although EMSA experiments demonstrated that the promoters of *NF-YA1* and *NF-YB1* are both directly bound by NIN, there is a significantly stronger induction in *NF-YA1* expression in response to NF treatment or rhizobial inoculation, compared to *NF-YB1* (Soyano et al., 2013; Laloum et al., 2014; Laporte et al., 2014). Detailed analysis of *nf-ya* mutants demonstrated a requirement for IT progression (Laloum et al., 2014), which is in line with the finding that NF-YA1 interacts with DELLA proteins and associates with the promoter of *ERN1, in planta* (Fonouni-Farde et al., 2016). However, a reduction in nodule development upon *NF-YA1* transcript knock-down, abnormal cell division in the cortex as well as the formation of malformed lateral roots upon overexpression of *NF-Y* subunits suggests that there is an

additional role for NF-Ys in the control of cortical cell divisions (Soyano et al., 2013).

Due to their identity as lateral root organs, lateral roots and nodules display some level of developmental overlap (Bensmihen, 2015), and recent studies argue that *NIN* may have recruited genetic components of lateral root development to evolve nodule organogenesis. ChIP-seq analysis in *L. japonicus* and EMSA experiments demonstrated that NIN associates with introns of *Asymmetric Leaves 2-like 18/Lateral organ Boundaries Domain 16a* (*ASL18/LBD16a*) (Soyano et al., 2019). Interestingly, in non-legume plants orthologues of *ASL18/LBD16a* are required for lateral root development (Goh et al., 2012; Goh et al., 2019). A reduction of nodule number and size in *asl18/lbd16*a mutants under high nitrate conditions suggests that this gene is involved in nodule growth in *L. japonicus* (Soyano et al., 2019). Interestingly, ASL18/LB16a directly interacts with both NF-YA1 and NF-YB1 and their simultaneous overexpression results in the induction cortical cell divisions in roots (Soyano et al., 2019). Transcriptional analysis of the *lbd16* mutants in *M. truncatula* and the finding that NF-YA1 directly binds the promoters of *Stylish* (*STY*) genes suggest that NF-Y subunits and ASL18/LBD16a work together to regulate nodule development in legumes, via the regulation of local auxin concentrations (Hossain et al., 2016; Schiessl et al., 2019).

Besides auxin, cytokinin was shown to be a key plant hormone involved in RNS. This is exemplified by spontaneous nodule development due to constitute activation of the cytokinin receptor Lotus Histidine Kinase 1 (LHK1) in the *L. japonicus spontaneous nodule formation 2* (*snf2*) (Tirichine et al., 2007). Recently, a *cytokinin response-element* (*CE*) was identified in the *NIN* promoter of legumes and it was suggested that *NIN* expression in the cortex is regulated in a cytokinin dependent manner, whereas epidermal *NIN* expression is regulated by the CCaMK/Cyclops complex (Liu et al., 2019c). Overall, a precisely regulated spatio-temporal expression of *NIN* was found to be crucial for RNS development and is therefore subject to extensive research (Soyano et al., 2014; Yoro et al., 2014; Yoro et al., 2019).

As RNS is an energetically costly process, plants keep a tight control of nodule numbers via a negative systemic pathway, called Autoregulation of Nodulation (AON) (Magori and Kawaguchi, 2009). In the root, NIN regulates the expression of *Clavata3/embryo surrounding region-related* (*CLE*) peptides by direct binding to their promoters (Soyano et al., 2014). CLE peptides translocate to the shoot where they are bound by the LRR containing receptor kinase Hypernodulation Aberrant Root Formation 1 (HAR1) (Okamoto et al., 2013). Via additional signalling

components, HAR1 relays an inhibitory signal back to the root (Suzaki et al., 2015; Tsikou et al., 2018). Accordingly, overexpression of *CLE* peptides reduces and knockout of *HAR1* increases nodule numbers, respectively (Nishimura et al., 2002; Mortier et al., 2012; Okamoto et al., 2013). Interestingly, *NIN* also controls a positive systemic pathway, which depends on shoot-located LRR-RLK Compact Root Architecture 2 (CRA2), by directly regulating the expression of C-terminally encoded peptides (CEPs) (Huault et al., 2014; Mohd-Radzman et al., 2016; Imin et al., 2018). CEPs function antagonistically to CLE peptides in the root and downregulation of CEPs results in reduced nodule numbers (Laffont et al., 2020). The regulatory influence of NIN is further expanded by its involvement in the integration of nutritional cues into RNS development. Under high nitrate concentrations nodulation is inhibited (Streeter and Wong, 1988). A recent study in *M. truncatula* demonstrated that the NIN-like Protein 1 (NLP1) translocates into the nucleus under high nitrate conditions, interacts with NIN and directly binds to the promoters of NIN target genes (Lin et al., 2018). The observed suppression of NIN-dependent gene induction by NLP1 therefore suggests transcriptional regulation of NIN target genes by competition for DNA binding sites.

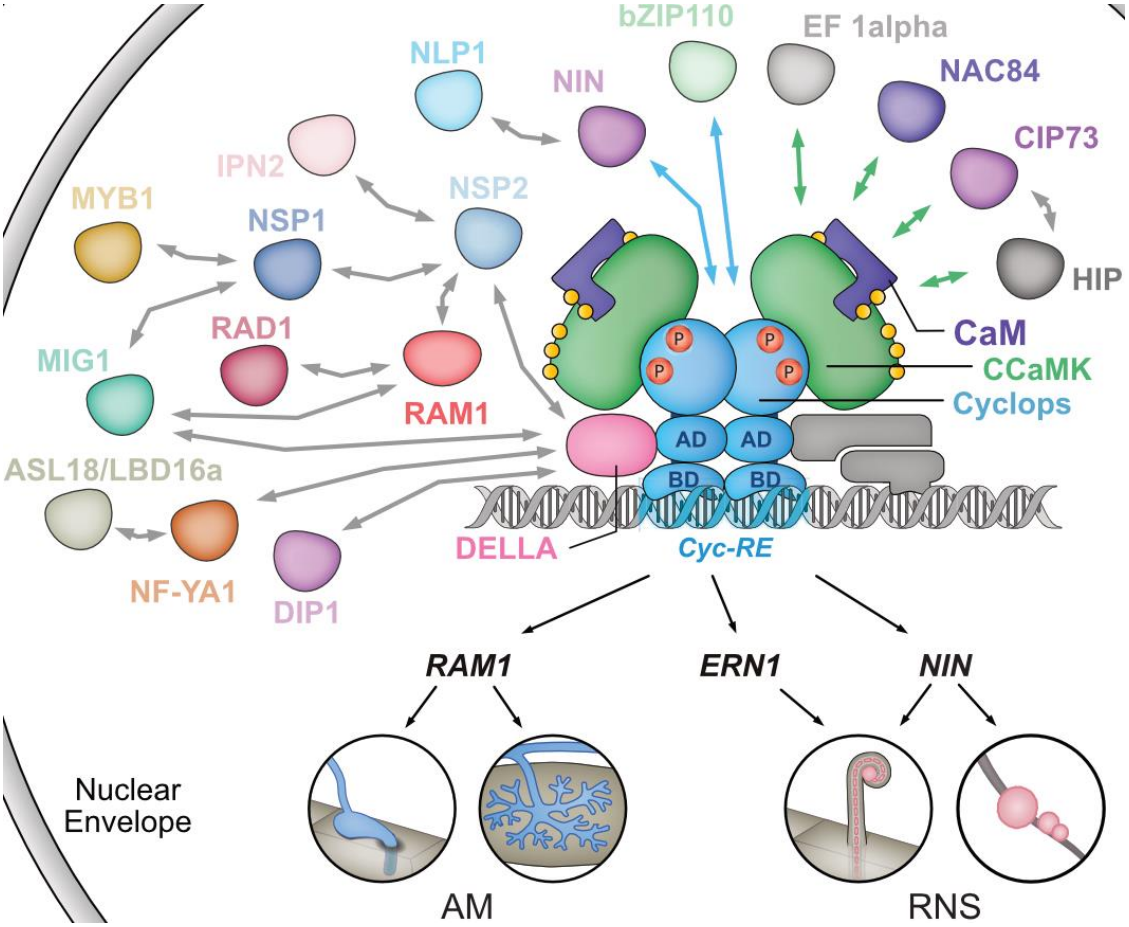

Figure 2: Proteins that are directly or indirectly interacting with the CCaMK/Cyclops complex and are involved in the transcriptional regulation of AM and RNS.
In the nucleus, the CCaMK/Cyclops complex interacts with multiple proteins (colored arrows), which connects it to a large protein-protein-interaction network (grey arrows). CCaMK interacts with CCaMK interacting Protein of approximately 73 kD (CIP73) and specifically phosphorylate its N-terminus (Kang et al., 2011). CIP73 contains a Scythe_N Ubiquitin-like domain and RNAi knockdown reduces nodules numbers and results premature arrest of IT progression (Kang et al., 2011). CIP73 and CCaMK simultaneously interact with cochaperone protein HSC/HSP70 interacting protein (HIP), which is proposed to play a negative role in nodulation (Kang et al., 2015). Elongation factor 1 α (EF1α) and the NAC84 transcription factor were identified as interaction partners and phosphorylation substrates of CCaMK in *L. longiflorum* and *Z. mays*, respectively (Zhu et al., 2016, Wang et al., 1999). Whereas no distinct biological function was assigned to EF1α yet, NAC84 is involved in ABA induced antioxidant defence. In addition to bZIP110 (Katzer, 2017) Cyclops interacts with NIN (Andrade Aguirre., 2021), which itself interacts with NLP1 to regulate RNS in a nitrate concentration dependent manner (Lin et al., 2018). Cyclops is connected to a complex network of interacting GRAS, NF-Y and MYB coiled-coil transcription factors via DELLA proteins, which were shown to interact with NSP2, NF-YA1 and DIP1 (Fonouni-Farde et al., 2016, Yu et al., 2014). Recently the interaction of ASL18/LBD16a with NF-YA1 was reported, with an implicated role in the nodulation process (Schiessl et al., 2019, Soyano et al., 2019). Besides its interaction with NSP1, NSP2 interacts with RAM1 and IPN2, with proposed roles in *RAM2* and *NIN* expression, respectively (Hirsch et al., 2009, Kang et al., 2014, Gobbato et al., 2012, Xiao et al., 2020). Additionally, interactions between RAM1 and RAD1, as well as RAM1 and DIP1 were found (Xue et al., 2015, Yu et al., 2014). Besides its interaction with DELLA, MIG1 interaction with NSP1 was also demonstrated (Heck et al., 2016). Furthermore, NSP1 was found to interact with the GRAS protein MYB1 (Floss et al., 2017). The bi-lipid layer of the nuclear envolope is depicted schematically.

4 CCaMK and Cyclops

4.1 CCaMK

Due to its nuclear localization and its ability to bind calcium in a free and in a calmodulin- (CaM-) bound manner, CCaMK is currently proposed as the decoder of symbiotic calcium spiking (Miller et al., 2013). CCaMK is a plant specific protein kinase that consists of a N-terminal serine/threonine kinase domain, a centrally located CaM binding domain (CBD) and a C-terminal visinin-like domain, which contains three EF hands (Sathyanarayanan et al., 2000; Takeda et al., 2012; Poovaiah et al., 2013). The biochemical characterization of CCaMK function furthermore revealed the presence of an inhibitory domain, which overlaps with the CBD (Ramachandiran et al., 1997).

CCaMK most likely evolved from a calcium-dependent protein kinase (CDPK) in the LCA of charophytes and land plants (Delaux et al., 2015). As *CCaMK* is conserved in AM- and RNS-forming plants but lost in non-symbiotic plants like *A. thaliana*, its main function appears to be in symbiotic signalling (Hrabak et al., 2003). However, an additional role for CCaMK in brassinosteroid (BR) and abscisic acid (ABA) induced antioxidant defence responses in *O. sativa* and *Z. mays* was reported. The latter is mediated by the NAC transcription factor NAC84, which interacts with and is phosphorylated by CCaMK (Zhu et al., 2016). Furthermore, the expression and activity of CCaMK was found to be directly influenced by nitric oxide (NO) and H_2O_2 (Ma et al., 2012; Shi et al., 2012; Yan et al., 2015; Ni et al., 2019). Although *CCaMK* was cloned from anthers of *Lilium longiflorum* (*Ll*), in legumes it is mainly expressed in uninoculated roots, inoculated roots and nodules. (Patil et al., 1995; Tirichine et al., 2006). CCaMK is essential for both AM and RNS, since *ccamk* loss-of-function (LOF) mutants retain LCO-elicited root hair swelling and calcium spiking in response to both microbial signals, but are completely deficient in rhizobial and fungal infections, as well as nodule organogenesis (Ane et al., 2002; Levy et al., 2004; Mitra et al., 2004).

The characterization of CCaMK gain-of-function (GOF) versions led to a more detailed picture about the biological role of this kinase during the establishment of root endosymbioses. Expression of $CCaMK^{T265I}$ by the *L. japonicus spontaneous nodule formation 1* (*snf1*) mutant results in nodule formation in absence of rhizobia (Tirichine et al., 2006). Interestingly, $CCaMK^{T265I}$ renders calcium spiking during early symbiotic signalling dispensable, as evidenced by a low frequency of both AM and RNS formation in the *symrk snf1* double mutant (Madsen et al., 2010). However, the absence of epidermal ITs in *nfr1-1 snf1*, *nfr5-2 snf1*, *nfr1-1 nfr5-2 snf1*

and *nfr1-1 nfr5-2 symrk3 snf1* mutants indicates that both NFRs are indispensable for IT formation in the epidermis (Madsen et al., 2010). Together with the observation that *symrk* mutants retain cytosolic calcium influxes in response to NF perception but *nfr* mutants do not (Miwa et al., 2006), these results raised the hypothesis that there is an alternative epidermal infection signalling pathway, which branches at the NF receptors and may act in parallel to CCaMK.

To further decipher its biological function, AM and RNS complementation assays with truncated or mutated CCaMK versions were conducted. These analyses suggest that its EF-hands and its CBD domain regulate CCaMK activity in a negative manner (Miller et al., 2013). Despite the negative regulatory role of the CBD for CCaMK function, CaM binding seems to be specifically required for IT, but not for arbuscule or nodule formation (Shimoda et al., 2012). In additional CCaMK mutant versions like CCaMK^{T265I}, CCaMK^{T265D} and CCaMK^{T265A}, the isolated kinase domain of CCaMK (CCaMK$^{1-314}$/DMI3$^{1-311}$) mediates symbiosis related responses as well (Gleason et al., 2006; Banba et al., 2008; Hayashi et al., 2014). Interestingly, the symbiosis specific responses upon expression *CCaMK^{T265D}* or *CCaMK$^{1-314}$* in the *ccamk-3* mutant (encoding the kinase-dead CCaMK^{G30E}) are not identical. Complementation with *CCaMK$^{1-314}$* results in a generally higher expression of genes required for both RNS (*NIN, SbtM4, SbtS*) and AM (*SbtM1, PT4*), compared to *CCaMK^{T265D}* (Takeda et al., 2012). In particular, the expression of the AM specific gene *SbtM1* is induced in *ccamk-3* plants expressing *CCaMK$^{1-314}$*, but not in plants expressing *CCaMK^{T265D}*. Interestingly, *CCaMK$^{1-314}$* complements for fungal, but not rhizobial infection in the *ccamk-3* mutant (Takeda et al., 2012). Furthermore, the visualisation of the *StbM1* promoter activity by a transcriptional fusion with a YFP variant (*SbtM1$_{pro}$:Venus*) revealed the formation of PPA-like structures in plants expressing *CCaMK$^{1-314\ T265D}$*, in absence of AM fungus (Takeda et al., 2012).

In order to delimit the cell-type specific requirements of individual CCaMK domains during the establishment of RNS, Hayashi and colleagues (2014) expressed truncated versions of CCaMK ubiquitously under the *Cauliflower Mosaic Virus 35S* promoter, or specifically in the epidermis using a promoter region from the *A. thaliana ExpansinA7* gene. These results revealed that both CCaMK$^{1-314}$ and CCaMK$^{1-340}$ are sufficient for nodule organogenesis and rhizobia infection in the cortex, whereas full-length CCaMK is required for the infection process in the epidermis (Hayashi et al., 2014).

4.2 Cyclops

The dimeric transcriptional regulator Cyclops/IPD3 interacts with and is phosphorylated by CCaMK/DMI3 (Messinese et al., 2007; Yano et al., 2008; Singh et al., 2014; Jin et al., 2018). The promoters of multiple key transcriptional regulators in root endosymbioses were found to be directly targeted by Cyclops, suggesting that Cyclops participates in the translation of CCaMK activity into a transcriptional readout (Yano et al., 2008; Singh et al., 2014; Pimprikar et al., 2016; Cerri et al., 2017). Cyclops contains a regulatory N-terminal domain, an activation domain (AD) and a coiled-coil containing DNA binding domain (BD) (Singh et al., 2014). In *L. japonicus*, *cyclops* mutants are impaired in AMF hyphal penetration of the epidermis and IT formation is arrested at the infection chamber stage, but they retain the ability to develop empty nodule primordia upon rhizobia inoculation (Yano et al., 2008). Expression of *Cyclops* under an epidermis-specific promoter results in the complementation of epidermal but not cortical IT development in *cyclops-3* mutants, demonstrating that Cyclops function is required in both cell types (Hayashi et al., 2014). A recent study revealed that *Cyclops* is conserved in all species engaging in intracellular symbiotic associations, which supports its important role for the intracellular infection process (Radhakrishnan et al., 2020). In addition, there is indication that the biochemical function of Cyclops is conserved amongst endosymbiotic land-plant species, as *Cyclops* from the AM-forming liverwort *Marchantia palaceae* or from the AM-forming monocot *O. sativa* supports the formation of rhizobia-containing nodules in *ipd3-2* or *cyclops-3* mutants, respectively (Yano et al., 2008; Radhakrishnan et al., 2020).

Despite their close functional connection, there are phenotypical discrepancies between *ccamk/dmi3* and *cyclops/ipd3* mutants. In the fast-neutron bombardment mutant *ipd3-1* (*M. truncatula* subspecies *truncatula* Jemalong), IT formation is delayed but abnormally thick and crooked ITs with enlarged, blister-like structures can form (Horvath et al., 2011). Moreover, fully elongated nodules with uninfected cells are observed with low frequency. Interestingly, in the *Tnt1*-insertion mutant *ipd3-2* (*M. truncatula* subspecies *trycala* R108) IT formation is blocked at the infection chamber stage (Horvath et al., 2011). Both *ipd3-1* and *ipd3-2* only display a quantitative reduction in AM formation and fully developed arbuscules can form (Horvath et al., 2011; Floss et al., 2013). Together with the spontaneous formation of full-sized nodules upon overexpression of $CCaMK^{T265D}$ in the bump-forming *cyclops-4* mutant (C_{996} to T, Q_{107} to stop) (Yano et al., 2008), these observations suggest genetic redundancy at the level of *Cyclops/IPD3*. The recent identification of *IPD3-like* (*IPD3L*) in *M. truncatula* partially confirmed this

assumption (Jin et al., 2018). IPD3L appears to have a supporting role in nodule formation, as evidenced by the complete absence of nodule organogenesis in the *ipd3-2 ipd3l* double mutant compared to the *ipd3-2* mutant (Jin et al., 2018). Interestingly, *ipd3 ipd3l* double mutants retain a reduced level of arbuscule formation and induction of AM-related gene expression, indicating that additional genetic components might be involved in arbuscule formation, at least in *M. truncatula*.

A recent study uncovered that *IPD3*/*IPD3L* participate in the regulation of AM in a phosphate concentration dependent manner. In the *idp3-2 ipd3l-2* double mutant, arbuscule formation is reduced by 8-fold under high phosphate conditions compared to low phosphate conditions, whereas a 2-fold reduction was reported for wild-type plants (Lindsay et al., 2019). Interestingly, although a block in epidermal penetration and the complete lack of arbuscule formation was reported for the *cyclops-3* mutant (Yano et al., 2008), a re-evaluation of this mutant revealed a low frequency in arbuscule formation, which was reduced under increasing phosphate concentrations (Lindsay et al., 2019). It was therefore proposed that *IPD3*/*Cyclops* and *IPD3L* are involved in maintaining symbiotic signalling under high phosphate conditions.

4.3 Regulation of the CCaMK/Cyclops complex

CCaMK can bind free or CaM-bound calcium and its phosphorylation activity is differentially regulated by binding of both species (Patil et al., 1995). The current model of CCaMK function proposes that calcium is directly bound in an EF-hand dependent manner, at basal concentrations (Miller et al., 2013). Direct binding of calcium promotes CCaMK autophosphorylation activity of T265 (T267 in *Ll*CaMK, T271 in DMI3) and Transmission Electron Microscopy (TEM) revealed that calcium dependent autophosphorylation at this residue promotes the formation of complex network-like protein structures (Sathyanarayanan and Poovaiah, 2002). An exponential increase in autophosphorylation upon increasing CCaMK concentrations in *in vitro* studies furthermore suggests an intermolecular mechanism for CCaMK autophosphorylation (Tirichine et al., 2006).

Due to the introduction of a negative charge, the replacement of phospho-residues by aspartic acid (D) is considered to mimic the function of phosphorylation (Sweeney et al., 1994; Gilbert et al., 2012). Conversely, substitution with non-modifiable alanine (A), renders the according amino acid phosphoablative. Based on the autoactive nature of CCaMK^{T265D} (Banba et al., 2008), it was therefore

proposed that phosphorylation of this residue activates CCaMK (Shimoda et al., 2012; Singh and Parniske, 2012). However, this was in sharp contrast with the observation that CCaMK^{T271I}, CCaMK^{T271A} and EF-hand mutants led to the formation of spontaneous nodules (Gleason et al., 2006; Tirichine et al., 2006; Miller et al., 2013), and that substrate phosphorylation activity of CCaMK is decreased upon autophosphorylation (Sathyanarayanan and Poovaiah, 2002). Based on extensive structural modelling, which revealed that phosphorylation of T265 promotes the formation of a hydrogen bond network with residues located in the CCaMK CBD, a revised model for CCaMK function was suggested: under basal Ca^{2+} concentrations, phosphorylation at T265 inactivates CCaMK. An increase in nuclear calcium concentrations during symbiotic calcium spiking promotes the binding of calcium saturated CaM to the CBD of CCaMK, releasing its autoinhibition and promoting substrate phosphorylation (Miller et al., 2013). In this scenario, mutation of T265 releases autoinhibition and results in a low but constant substrate phosphorylation by CCaMK.

Besides T265, additional CCaMK phosphorylation sites were determined. Amongst those, S337 is located within the CBD and *ccamk-14* mutant analysis (encoding CCaMK^{S337N}) indicated a regulatory role for this residue in cortical IT development and fungal penetration of the epidermis (Liao et al., 2012). Phosphomimetic CCaMK^{S337D} revealed that phosphorylation of this residues decreases binding of CaM to CCaMK and substrate phosphorylation (Liao et al., 2012). In *M. truncatula*, DMI3^{S344} was identified as the analogous autophophorlyation site of CCaMK^{S337} (Routray et al., 2013). Accordingly, the phosphomimetic replacement DMI3^{S334D} reduces CaM binding, substrate phosphorylation activity and impairs nodulation, AM formation as well as the interaction with IPD3 (Routray et al., 2013). Interestingly, there is no significant alteration of CCaMK^{S337} mutants in the interaction with Cyclops (Liao et al., 2012). Overall, binding of CaM to CCaMK correlates with a switch for its kinase activity, from autophosphorylation to substrate phosphorylation. Interestingly, autophosphorylation of CCaMK is increased in the presence of non-interacting substrates like Myelin Basic Protein (MBP), in comparison to interacting substrates like Cyclops (Liao et al., 2012).

Amongst the multiple described GOF versions of CCaMK, substrate phosphorylation activity of CCaMK^{T265} mutants is still regulated by calcium and CaM. Incorporation of radiolabelled ATP in *in vitro* kinase assays revealed that substrate phosphorylation by CCaMK^{T265I} is increased in upon addition of calcium and CaM (Tirichine et al., 2006). In contrast, a comparison of DMI3 mutant versions

demonstrated that DMI3$^{1-311}$ is not regulated by calcium and CaM anymore and that it reaches substrate phosphorylation levels of approximately 40% compared to calcium/CaM activated wildtype DMI3 (Gleason et al., 2006).

The interaction with and phosphorylation of the CCaMK Interacting Protein of approximately 73 kD (CIP73), which belongs to the large ubiquitin superfamily, indicates that ubiquitination might be involved in CCaMK regulation (Kang et al., 2011). Although RNAi-mediated knockdown of *CIP73* transcripts in *L. japonicus* resulted in a reduction of nodules numbers, a functional connection between ubiquitination and CCaMK function remains to be demonstrated. Both CIP73 and CCaMK interact with cochaperone protein HSC/HSP70 interacting protein (HIP), and an increase in nodule numbers upon knockdown of *HIP* suggests a negative role in nodulation (Kang et al., 2015)

Although CCaMK-dependent phosphorylation of Elongation Factor 1α (EF-1α) was reported in *L. longiflorum*, a symbiosis-related function remains to be demonstrated (Wang and Poovaiah, 1999). Therefore, the main symbiosis-relevant phosphorylation substrate of CCaMK/DMI3 known to date is Cyclops/IPD3. Y2H analyses with truncated Cyclops versions revealed that its interaction domain with CCaMK, overlaps with its transcriptional activation domain (AD) (Yano et al., 2008; Singh et al., 2014). Interestingly, CCaMK-dependent *in vitro* phosphorylation is increased upon truncation of Cyclops, indicating that the sterical conformation of native Cyclops could influence its phosphorylation degree (Yano et al., 2008). Mass spectrometry analysis in *M. truncatula* demonstrated the phosphorylation of IPD3, *in planta*. Whereas S50 and S154 are phosphorylated under sterile conditions, inoculation with *Sinorhizobium meliloti* yielded 9 additional *in vivo* phosphorylation sites (Grimsrud et al., 2010; Marx et al., 2016). Kinase assays with DMI3 (Jin et al., 2018) and unpublished results from *in vitro* phosphorylation of Cyclops by CCaMK or CCaMK^{T265D} (Diploma Katja Katzer, 2011) revealed a total number of 27 additional *in vitro* phosphorylation. Due to a certain degree of overlap amongst all identified sites, this results in a total number of 32 Cyclops phosphorylation sites known to date.

So far, only a small subset of those sites was functionally characterized. Phosphoablative replacement of S50 and S154 with alanine (A) (Cyclops^{AA}) revealed that phosphorylation at these positions is necessary for fungal and rhizobia infection and for binding to the *Cyc-RE$_{NIN}$* (Singh et al., 2014). Interestingly, the phosphomimetic replacement of S50 and S154 by D (Cyclops^{DD})

is sufficient for *NIN* expression via an 870 bp *NIN* promoter fragment and via the *2xCyc-RE$_{NIN}$*, *NIN* expression in the *ccamk-13* mutant (7 bp insertion after G$_{462}$, frame shift) (Perry et al., 2009), and nodule formation in non-inoculated *cyclops-3*, or rhizobia-inoculated *ccamk-13* plants (Singh et al., 2014).

Like Cyclops^{DD}, the removal of an N-terminal fragment of Cyclops (resulting in Cyclops^{min}, aa 255-518) results in spontaneous *GUS* expression via the *2xCyc-RE$_{NIN}$* in *N. benthamiana* (Singh et al., 2014). In *cyclops-3* mutants plants, the transformation with *Cyclops^{min}* results in *GUS* expression via the *2xCyc-RE$_{NIN}$* in 33% of all transformed root systems (Singh et al., 2014). In addition to the *2xCyc-RE$_{NIN}$*, Cyclops^{min} is sufficient to bind the *Cyc-REs* from the promoters of *ERN1* (*2xCyc-RE$_{ERN1}$*) and *RAM1* (*2xCyc-RE$_{RAM1}$*) (Pimprikar et al., 2016; Cerri et al., 2017). In contrast to Cyclops^{DD}, Cyclops^{min} is neither sufficient for *GUS* expression via an 870 bp long fragment of the *NIN* promoter, nor for the complementation of RNS in the *cyclops-3* mutant background (Singh et al., 2014).

Even though Cyclops^{DD} induces nodule development in the *ccamk-13* mutant, it is not sufficient for the complementation of the fungal or the rhizobial infection process (Singh et al., 2014). Therefore, it was proposed that alternative phosphorylation targets of CCaMK exist, or that additional phosphorylation sites of Cyclops might be involved in its regulation (Singh et al., 2014). In *M. truncatula*, the biological role of phosphorylation sites other than S50 and S154 was investigated. Based on the combination of 3 newly and 5 previously characterized phosphorylation sites, an IPD3^{8D} version was generated (Jin et al., 2018). Compared to *IPD3^{WT}* and *IPD3^{2D}* (corresponding version of Cyclops^{DD}), the expression of *IPD3^{8D}* in rhizobia-inoculated *ipd3-2 ipd3l* root systems resulted in a reduced formation of infected nodules (Jin et al., 2018). Interestingly, this correlated with a reduced expression of the RNS-related genes *NIN, ENOD11* and *FLOT4* in those root systems, compared to both *IPD3^{WT}* and *IPD3^{2D}*. In uninoculated *ipd3-2 ipd3l* and *dmi3-1* root systems, expression of *IDP3^{8D}* resulted in a reduced formation of spontaneous nodules compared to *IPD3^{2D}* (Jin et al., 2018). These results demonstrated that IPD3^{8D} is a less active phosphomimetic versions of IPD3, compared to IPD3^{2D}.

Apart from regulating the binding to DNA, phosphorylation is known to modulate protein-protein interactions as well (Holmberg et al., 2002). In the case of IPD3, quantitative Y2H experiments suggest, that phosphorylation or the phosphomimetic replacement of S50 and S154 increase its interaction with DELLA2 (Jin et al., 2016). Furthermore, there is indication that the presence of DELLA2 increases the DMI3-mediated phosphorylation status of IPD3 (Jin et al.,

2016). To investigate the effect of Cyclops phosphorylation on complex formation with CCaMK, Singh and colleagues (2014) employed Fluorescence Lifetime Imaging (FLIM) of GFP- and mOrange-tagged Cyclops and CCaMK, respectively. Interestingly, the phosphomimetic or phosphoablative replacement of S50 and S154 had no effect on the composition of the CCaMK/Cyclops complex (Singh et al., 2014). In addition to CCaMK and DELLA2, NIN was recently identified as Cyclops interaction partner (Andrade Aguirre, 2021). NIN inhibits the activity of Cyclops in *N. benthamiana* and interacts with Cyclops via an N-terminal fragment (NIN^{N}, aa 1-296) (Andrade Aguirre, 2021). FLIM analysis of GFP-Cyclops and mCherry-NIN revealed that the presence of $CCaMK^{T265D}$ or $CCaMK^{1-314}$ increases the Fluorescence Lifetime (FLT) of GFP, suggesting that Cyclops phosphorylation affects the interaction between Cyclops and NIN (Andrade Aguirre, 2021).

The cumulative data obtained on Cyclops suggest that its transcription factor activity and its interaction with additional proteins can be modulated by its phosphorylation status.

VI Aim of this thesis

To establish root endosymbioses with rhizobia or AMF, legumes engage in extensive signalling processes. A central mechanism of these signalling processes is the generation of calcium oscillations in an around the nucleus in response to the perception of signalling molecules exuded by the symbionts (Sieberer et al., 2009; Sieberer et al., 2012; Charpentier, 2018). Due to its molecular make up, CCaMK has been suggested to be the main decoder of symbiotic calcium spiking (Miller et al., 2013) and to date, Cyclops is the only reported symbiosis relevant phosphorylation substrate of CCaMK. Cyclops is a dimeric transcriptional regulator, which binds palindrome containing sequences in the promoters of *NIN*, *RAM1* and *ERN1* (Singh et al., 2014; Pimprikar et al., 2016; Cerri et al., 2017). Phenotypical analysis revealed that *cyclops* mutants are severely impaired in the symbiotic infection processes, as rhizobial IT formation is arrested at the infection chamber stage and fungal hyphae fail to penetrate epidermal cell layers (Yano et al., 2008; Horvath et al., 2011; Ovchinnikova et al., 2011). The importance of *Cyclops* function for root endosymbioses is demonstrated by phylogenetic analyses, which revealed that *Cyclops* is conserved in plants that house their symbionts intracellularly but is lost in plants that engage in extracellular symbiosis and in non-symbiotic plants (Radhakrishnan et al., 2020). Multiple *in vitro* and *in vivo* studies demonstrated the phosphorylation of Cyclops by CCaMK, resulting in a total number of 32 phosphorylation sites known to date (Grimsrud et al., 2010; Singh et al., 2014; Marx et al., 2016; Jin et al., 2018; Diploma Katja Katzer, 2011). Using phosphoablative and phosphomimetic amino acid replacements, the detailed characterization of S50 and S154 ($Cyclops^{AA}$ and $Cyclops^{DD}$, respectively) indicated that phosphorylation of those two residues is necessary and sufficient for the nodule organogenesis process and binding of Cyclops to DNA (Singh et al., 2014). However, the observation that $Cyclops^{DD}$ is not sufficient to complement *ccamk* mutant plants for the rhizobial and the fungal infection raised the hypothesis that additional phosphorylation sites contribute to the regulation Cyclops function. To test this hypothesis, the work of this doctoral thesis aimed to investigate the influence of 26 *in vitro* phosphorylation sites on the transcription factor activity of Cyclops and its protein-protein interactions. Therefore, transactivation assays in *N. benthamiana* and *Saccharomyces cerevisiae*, complementation assays of *L. japonicus* mutants as well as interaction studies in *S. cerevisiae* in *N. benthamiana* were conducted.

VII Results

1 Cyclops activity is modulated by autoactive versions of CCaMK

To test if the transcription factor activity of Cyclops is modulated by different autoactive versions of CCaMK, we performed transactivation assays with Cyclops target promoters. Therefore, we fused the promoters of *NIN* (*NIN*$_{pro}$) and *RAM1* (*RAM1*$_{pro}$) to the *GUS* reporter gene and monitored its expression in transiently transformed *N. benthamiana* leaves, co-expressing Cyclops^{WT} with CCaMK^{T265D} or CCaMK$^{1-314}$. As Cyclops^{DD} does not complement AM formation in the *ccamk-13* mutant background, we furthermore tested whether Cyclops^{DD} can activate the expression of the *GUS* reporter gene when driven by the *RAM1*$_{pro}$.

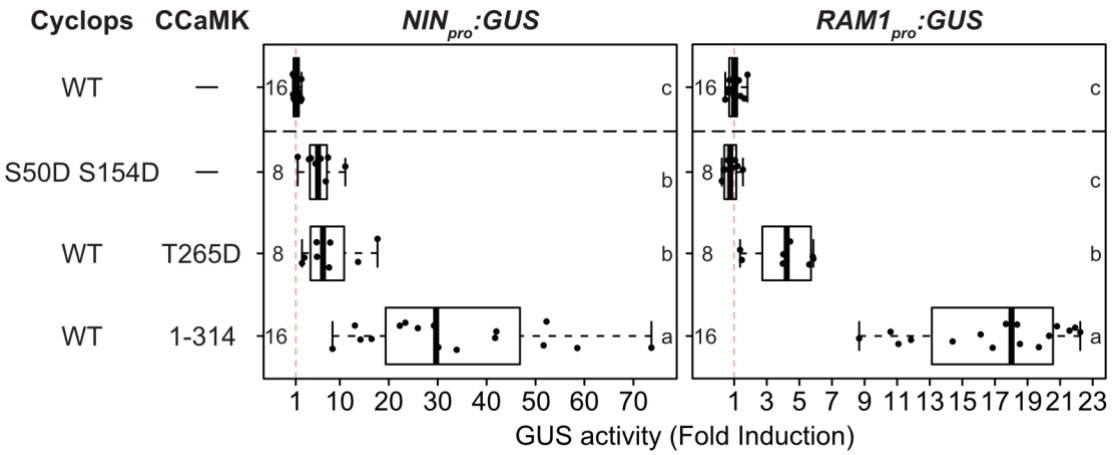

Figure 3: The Cyclops-dependent expression of *GUS* driven by the *NIN* and *RAM1* promoters is modulated by two auto-active versions of CCaMK.
Transactivation assays in *N. benthamiana* leaves, as explained in material and methods. Versions of Cyclops and presence or absence (-) of CCaMK^{T265D} or CCaMK$^{1-314}$ are indicated on the left, Promoter:GUS (*uidA*) reporter fusions are indicated above boxes. Boxplots represent GUS activity as fold induction compared to the median of the negative control (Cyclops^{WT} in absence of CCaMK, red dotted line). Black dots: individual leaf discs measured from two independent infiltrations, black line: median, box: interquartile range, whiskers: lowest and highest data point within 1.5 interquartile range. Empty circles: data points outside of 1.5 interquartile range. Small numbers left of boxplots: number of leaf discs used to measure GUS activity. Data were subjected to Kruskal-Wallis and post-hoc Fishers least significant difference analysis, using Bonferroni correction (p-value ≤ 0.05). Letters right of boxplots indicate statistically different groups.

As previously reported (Singh et al., 2014), Cyclops^{DD} activated *GUS* expression driven by the *NIN*$_{pro}$ to the same level as Cyclops^{WT} in presence of CCaMK^{T265D} (Figure 3, left panel). Although Cyclops^{WT} together with CCaMK^{T265D} led to *RAM1*$_{pro}$ dependent *GUS* expression, Cyclops^{DD} alone did not (Figure 3, right panel). Compared to CCaMK^{T265D}, the presence of CCaMK$^{1-314}$ increased the Cyclops^{WT} mediated *GUS* expression by 4.3- to 4.4-fold for the *NIN*$_{pro}$ and the

RAM1$_{pro}$, respectively. These results demonstrate that Cyclops activity is differentially modulated in presence of CCaMK^{T265D} and CCaMK$^{1-314}$ and that Cyclops^{DD} is not sufficient for the activation of *RAM1* expression.

2 Multiple Cyclops phosphorylation sites are phylogenetically conserved

As the activity of Cyclops was modulated in presence of CCaMK^{T265D} or CCaMK$^{1-314}$, we hypothesized that is due to different Cyclops phosphorylation levels. Interestingly, S50 and S154 are not the only phosphorylation sites of Cyclops. To date, there is a total number of 32 phosphorylation sites that were identified from *in vitro* and *in vivo* studies, of which 8 of have been functionally characterized using phosphoablative and phosphomimetic substitutions (Table 1) (Singh et al., 2014; Jin et al., 2018). To investigate the conservation level of all Cyclops phosphorylation sites, we generated a multiple sequence alignment using the Cyclops amino acids sequences from members of the Fabales, Fagales, Cucurbitales and Rosales, as well as from the AM-forming species *S. lycopersicum* and *O. sativa* (Figure 4). This alignment revealed that S50, S154 and 7 additional sites (S14, S152, S155, S221, S236, S412, S415) were conserved to 100% (Table 1). Interestingly, 6 phosphorylation sites (S33, T81, S134, S145, S220, T414) were not completely conserved, but the respective residues were substituted with phosphorylatable aa like S or tyrosine (T) (Table 1). Overall, these observations suggest that there are phosphorylation sites other than S50 and S154 that could play an important role for the function of Cyclops.

Besides their conservation level, we also investigated the distribution of Cyclops phosphorylation sites within its amino acids sequence. Based on a functional characterisation by Singh and colleagues (2014), Cyclops can be separated into two fragments, encompassing the first 255 aa (Cyclops$^{1-255}$) and aa 255 – 518 (Cyclops^{min}). Cyclops^{min} contains two predicted nuclear localization signals (NLS), and the empirically determined activation and DNA-binding domains (AD and BD, respectively) (Figure 4). Amongst the 32 known Cyclops phosphorylation sites, 27 map to Cyclops$^{1-255}$ and only 5 phosphorylation sites map between the two predicted NLS within Cyclops^{min} (Figure 4). Amongst the 27 phosphorylation sites of Cyclops$^{1-255}$, 13 locate to a previously mapped CCaMK interaction domain and 4 of those 13 sites map to predicted coiled-coil (CC) domains (Yano et al., 2008, Singh et al., 2014). Fourteen additional sites map to Cyclops$^{1-255}$ but are not located within any predicted domain.

Table 1: All known Cyclops phosphorylation sites identified *in vitro* and *in vivo*.
All known phosphorylation sites of Cyclops ordered according to experimental design and author, using the *L. japonicus* sequence as coordinate. List is based on alignment in Figure 4 [a] Sites identified in *M. truncatula*. [b] Site was functionally characterized in Singh et al., 2014 and Jin et al., 2018. [c] Site was functionally characterized in Jin et al., 2018.. * Substituted with phosphorylatable T or S in all species analysed in Figure 4.

Identified *in vitro*			**Identified *in vivo***		**Conservation level in %, according to Figure 4**
Diploma Katja Katzer, 2011	**Singh et al., 2014**	**Jin et al., 2018[a]**	**Grimsrud et al., 2010[a]**	**Marx et al., 2016[a]**	
S7				S7	85.71
				Y10	71.43
S14	S14[b]	S14[b]		S14[b]	100
S33					57.14*
S43				S43	85.71
				T48	57.14
S50	S50[b]		S50[b]	S50[b]	100
		T59[c]			85.71
S66					57.14
S67					57.14
S68					85.71
S72					57.14
S73					42.58
S80[c]		S80[c]			71.43
T81					71.43*
S87[c]		S87[c]			71.43
S116					71.43
S134					85.71*
S145					85.71*
				S152	100
	S154[b]		S154[b]	S154[b]	100
				S155	100
Y197					28.57
S220					85.71*
S221					100
S236					100
S251[b]	S251[b]				57.14
				S406	57.14
S412[b]	S412[b]			S412[b]	100
T414					85.71*
S415					100
S418				S418	85.71

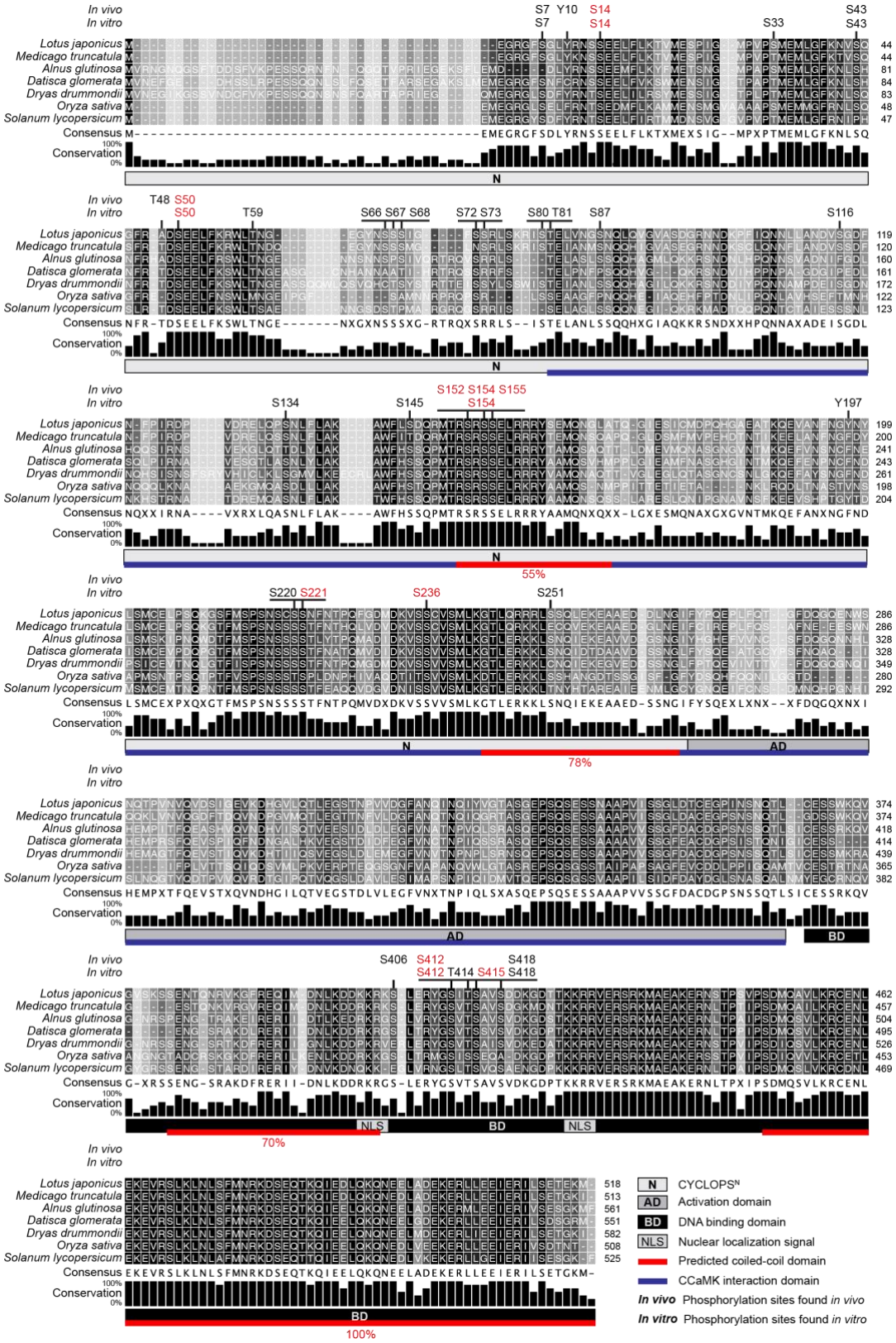

Figure 4: Phylogenetic analysis reveals conservation level of *in vivo* and *in vitro* phosphorylation sites
Amino-acid sequence alignment of Cyclops orthologues from members of the Fabales, Fagales, Cucurbitales, Rosales, Poales and Solanales. Sites phosphorylated i*n vivo* or *in vitro* are indicated on top of the alignment, numbered according to the *Lotus japonicus* sequence. Red letters indicate 100% conservation. Consensus sequence is shown below the alignment. Ambiguous residues are indicated as X. Conservation level is shown in greyscaled boxes per amino acid and as black bar from 0% to 100%. Missing residues are shown as dash. Legend describes Cyclops domains.

3 Phosphoablative mapping reveals *in vitro* phosphorylation sites that are required for symbiosis promoter activation

To identify functionally relevant sites this study focused on *in vitro* phosphorylation sites that were identified in our laboratory und not published so far (Diploma Katja Katzer, 2011) (Table 1, Figure 5A). We therefore employed a successive mapping approach using Cyclops versions that harboured phosphoablative or phosphomimetic substitutions of its *in vitro* phosphorylation sites. Initially, we grouped adjacent phosphorylation sites into 7 cohorts ($Cyclops^{m1, m3, m4, m6, m1346, m4a, m4b}$) (Figure 5B) and tested the corresponding multi-site ablative versions for reporter expression in the presence of $CCaMK^{1-314}$. Compared to the positive control ($Cyclops^{WT}$ in the presence of $CCaMK^{1-314}$), phosphoablation of the sites comprising $Cyclops^{m4b}$ led to a 5-fold and 3.75-fold reduction in *GUS* expression driven by the *RAM1* and the *NIN* promoters, respectively (Figure 5C). For $Cyclops^{m1}$, we observed a small but not significant reduction in *GUS* expression for both promoters. In contrast, the phosphoablative replacements comprising $Cyclops^{m3}$ and $Cyclops^{m6}$ did not affect *GUS* expression strength. Hence, we concluded that phosphorylation sites necessary for Cyclops activity are most likely amongst those mutated in $Cyclops^{m4b}$. To identify individual phosphorylation sites that are necessary for Cyclops activity, we generated single phosphoablative Cyclops versions, based on $Cyclops^{m4b}$ (Figure 6A). Replacements S236A and S251A significantly reduced *GUS* expression driven by the $RAM1_{pro}$ and S251A slightly reduced NIN_{pro}-driven *GUS* expression (Figure 6B). We could not evaluate $Cyclops^{S220}$, as Western Blot analysis failed to detect its presence (Figure 6C). Overall, these data indicate that the phosphorylation of S236 and S251 possibly contributes to the activity of Cyclops on its target promoters *NIN* and *RAM1*.

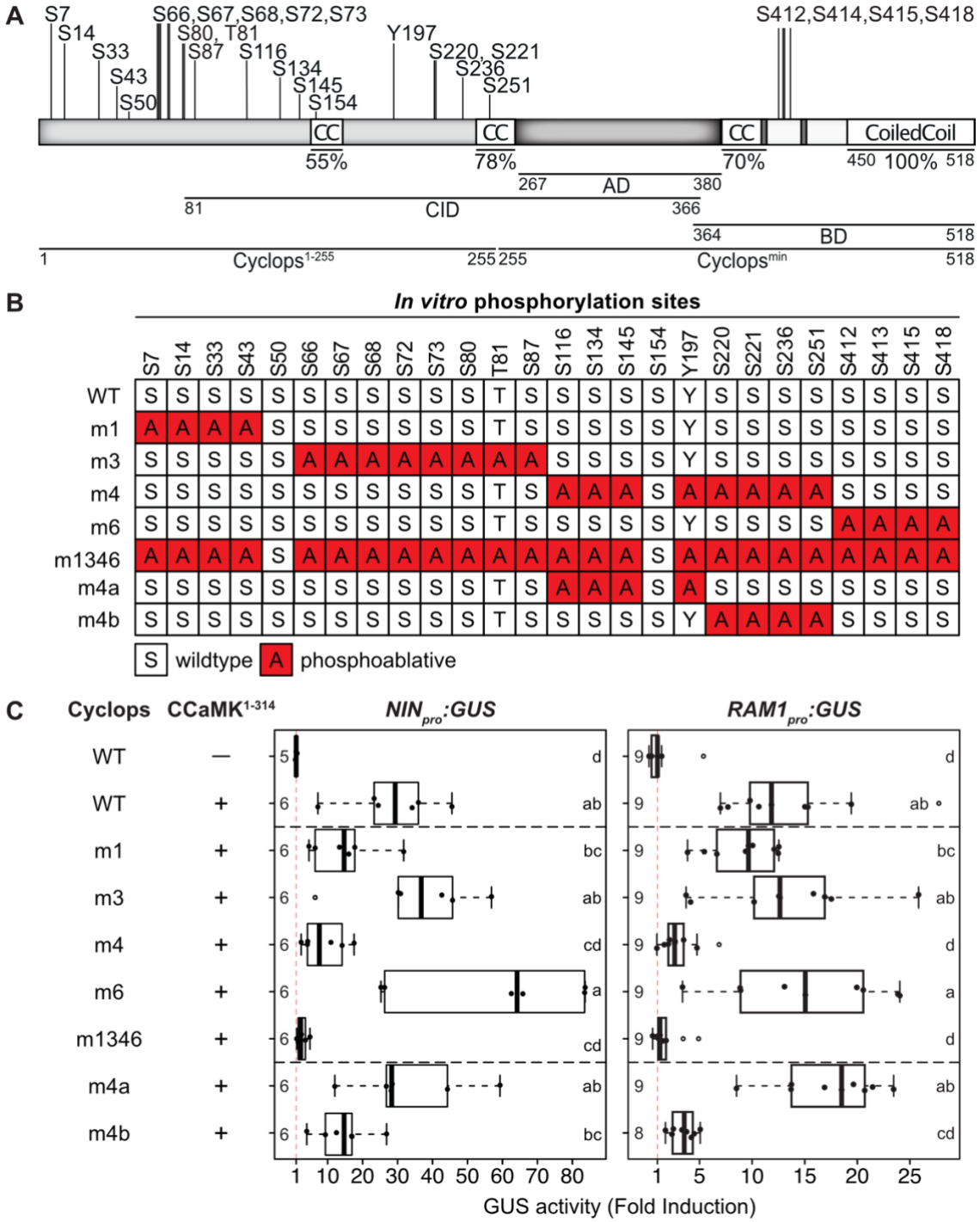

Figure 5: Phosphoablative replacements of Cyclops reveal phosphorylation sites that are required for the CCaMK$^{1-314}$ dependent expression of the *GUS* reporter gene under the control of the *NIN* and *RAM1* promotors, in *N. benthamiana*.

(A) Distribution of characterized Cyclops phosphorylation sites along the *Lotus japonicus* Cyclops protein sequence. Serines (S), threonines (T) and tyrosines (Y) are indicated with their according amino acid numbers. The locations of phosphorylation site S154, the coiled-coil domains (coiled-coil, CC), the activation domain (AD, black), the DNA-binding domain (BD, light grey) and the nuclear localization signals (NLS, black lines) are indicated as predicted or determined by Singh et al. (2014) and the location of the CCaMK interaction domain (CID) is indicated as determined by Yano et al. (2008). Based on the characterisation of Cyclops in Singh et al., 2014, the N-terminal and C-terminal fragments of Cyclops are indicated as Cyclops$^{1-255}$ and Cyclops^{min}, respectively. **(B)** Matrix representation of Cyclops *in vitro* phosphorylation sites substituted with alanine (A). Numbers on top indicate amino acid positions within Cyclops from *L. japonicus* Gifu (B-129). Names of the phosphoversions are indicated on the left. **(continuation of figure legend on page 52)**

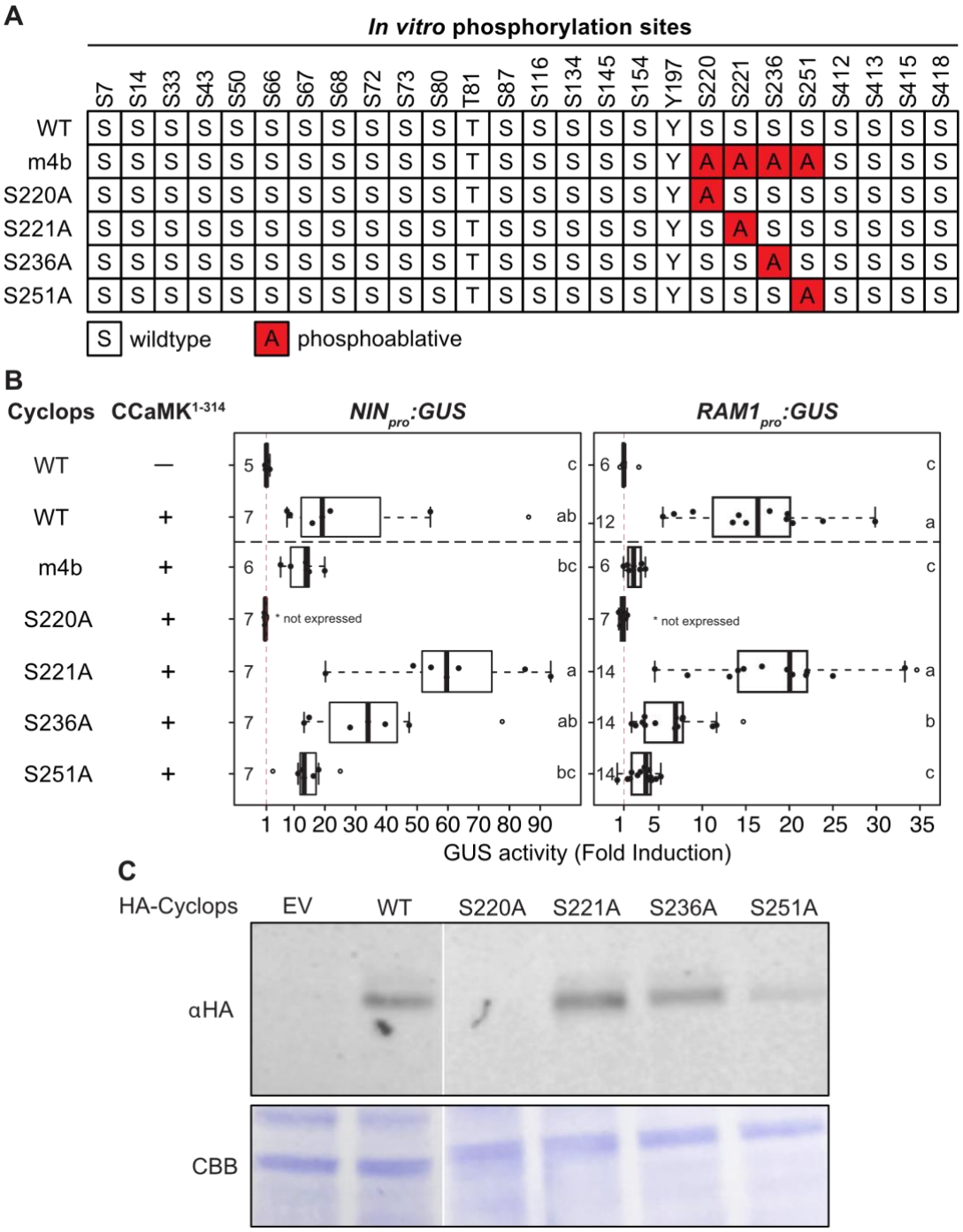

Figure 6: Replacement of either Cyclops S236 or S251 to A reduces the *NIN*$_{pro}$ - and *RAM1*$_{pro}$ -dependent expression of *GUS*, in *N. benthamiana*.

(A) Matrix of Cyclops *in vitro* phosphorylation sites. For description see Figure 5. **(B)** Transactivation assays in *N. benthamiana* leaves, as described in materials and methods. Boxplots represent GUS activity as fold induction compared to the median of the negative control (Cyclops^{WT} in absence of CCaMK$^{1-314}$, red dotted line). Black dots: individual leaf discs measured from one infiltration, black line: median, box: interquartile range, whiskers: lowest and highest data point within 1.5 interquartile range. Empty circles: data points outside of the 1.5 interquartile range. Small numbers left of boxplots indicate the numbers of leaf discs used to measure GUS activity. Data were subjected to Kruskal-Wallis and *post-hoc* Fishers least significant difference analysis, using Bonferroni correction (p-value ≤ 0.05). Letters left of boxplots indicate statistically different groups. **(C)** Western blot analysis of Cyclops versions with phosphoablative replacements. 48 hpi, leaf discs were harvested to perform crude protein extraction from infiltrated leaves used in (B). An antibody against hemagglutinin (αHA) was used to detect the presence of Cyclops (upper panel). The blotting membrane was stained with Coomassie Brilliant Blue (CBB) to visualise relative protein loading (lower panel).

4 Phosphomimetic mapping reveals hyperactive versions of Cyclops and potential consecutive phosphorylation events

To confirm that the phosphorylation of the sites in Cyclops^{m4b} increases the activity of Cyclops, we replaced S220, S221, S236 and S251 with phosphomimetic aspartic acid residues (Figure 7A). As the dual replacement of S50D and S154D was previously published as being supportive for Cyclops function (Singh et al., 2014), we included them in the newly generated Cyclops version (Cyclops^{6D}). To identify the contribution of individual sites to Cyclops activity, we also generated Cyclops versions which contained aspartic acid replacements of only S220, S236 or S251 in addition to D50 and D154 (Cyclops^{3D-1}, Cyclops^{3D-2} and Cyclops^{3D-3}). Because Cyclops^{S221A} did not reduce *GUS* expression for both promoters in the presence of CCaMK$^{1-314}$ (Figure 6B), the phosphomimetic replacement of S221 was not included in this analysis. In the case of the *NIN$_{pro}$*, we observed that Cyclops^{6D} in absence of CCaMK$^{1-314}$ was sufficient to activate *GUS* expression to a similar level as the positive control (Cyclops^{WT} in the presence of CCaMK$^{1-314}$) (Figure 7B, left panel). Cyclops^{3D-1}, Cyclops^{3D-2} and Cyclops^{3D-3} activated *GUS* expression to the same levels as Cyclops^{DD} (Figure 7B, left panel). Interestingly, the presence of CCaMK$^{1-314}$ inhibited *GUS* expression mediated by Cyclops^{6D} but did not significantly change *GUS* expression mediated by Cyclops^{DD}, Cyclops^{3D-1} and Cyclops^{3D-3}. In contrast, Cyclops^{3D-2} in the presence of CCaMK$^{1-314}$ activated *GUS* expression to the same levels as the positive control. When *GUS* was under the control of the *RAM1$_{pro}$* and CCaMK$^{1-314}$ was not present, Cyclops^{DD} did not activate the expression of the reporter gene, there was a slight but not significant expression mediated by Cyclops^{6D} and there was no expression mediated by Cyclops^{3D-1}, Cyclops^{3D-2} and Cyclops^{3D-3} (Figure 7B, right panel). In the presence of CCaMK$^{1-314}$, Cyclops^{DD} activated *GUS* expression to approximately 30% compared to the positive control (Figure 7B, right panel). We observed the same pattern for Cyclops^{6D} and Cyclops^{3D-1} but not for Cyclops^{3D-3}. Similar to the observation made with the *NIN$_{pro}$*, Cyclops^{3D-2} in the presence of CCaMK$^{1-314}$ activated *GUS* expression to the same levels as the positive control.

Legend Figure 5: continued

(C) Transactivation assays in *N. benthamiana* leaves, as explained in material and methods. Versions of Cyclops and presence (+) or absence (-) of CCaMK$^{1-314}$ are indicated on the left, *GUS* (*uidA*) reporter constructs are indicated above boxes. Boxplots represent GUS activity as fold induction compared to the median of the negative control (Cyclops^{WT} in absence of CCaMK$^{1-314,}$ red dotted line). Black dots: individual leave discs measured from two to three independent infiltrations, black line: median, box: interquartile range, whiskers: lowest and highest data point within 1.5 interquartile range. Empty circles: data points outside of 1.5 interquartile range. Small numbers left of boxplots: number of leaf discs used to measure GUS activity. Data were subjected to Kruskal-Wallis and post-hoc Fishers least significant difference analysis, using Bonferroni correction (p-value ≤ 0.05). Letters right of boxplots indicate statistically different groups.

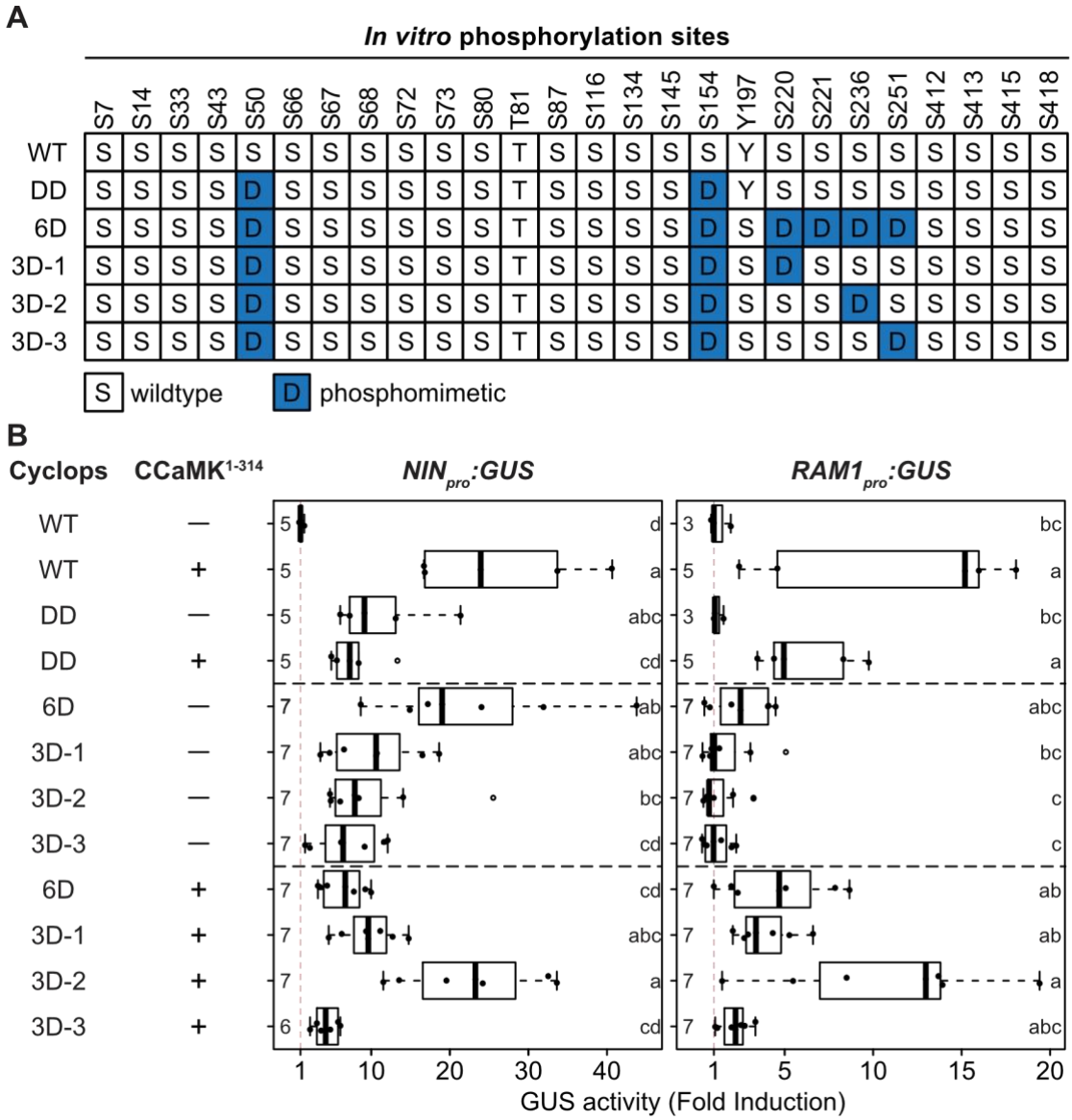

Figure 7: Three triple phosphomimetic replacements of Cyclops are not sufficient for strong *GUS* via the *NIN* and *RAM1* promoters in absence of CCaMK$^{1-314}$, and two block *GUS* expression in presence of CCaMK$^{1-314}$, in *N. benthamiana*.

(A) Matrix representation of Cyclops *in vitro* phosphorylation sites substituted with aspartic acid (D). Numbers on top indicate amino acid positions within Cyclops from *L. japonicus* Gifu (B-129). Names of the phosphoversions are indicated on the left **(B)** Transactivation assays in *N. benthamiana* leaves, as described in material and methods. Boxplots represent GUS activity as fold induction compared to the median of the negative control (Cyclops^{WT} in absence of CCaMK$^{1-314}$, red dotted line). Black dots: individual leaf discs measured from one infiltration, black line: median, box: interquartile range, whiskers: lowest and highest data point within 1.5 interquartile range. Empty circles: data points outside of the 1.5 interquartile range. Small numbers left of boxplots indicate the numbers of leaf discs used to measure GUS activity. Data were subjected to Kruskal-Wallis and *post-hoc* Fishers least significant difference analysis, using Bonferroni correction (p-value ≤ 0.05). Letters right of boxplots indicate statistically different groups.

Overall, these data demonstrate that potentially a higher number of phosphomimetic replacements are required for significant expression of *GUS* via the *RAM1*$_{pro}$ compared to the *NIN*$_{pro}$ and that the phosphomimetic replacements S220D and S251D can inhibit the CCaMK$^{1-314}$ mediated activity of Cyclops.

To identify additional sites that are required for *RAM1*$_{pro}$ dependent expression of *GUS*, we investigated additional phosphorylation sites by phosphomimetic replacement. A slightly reduced *GUS* expression mediated by Cyclops^{m1} and a significant reduction in *GUS* expression mediated by Cyclops^{m4} (Figure 5C) suggested that these additional sites are amongst the ones mutated in the respective Cyclops versions. Therefore, we performed a phosphomimetic mapping approach in absence of CCaMK$^{1-314}$, focusing on the sites in Cyclops^{m1} and Cyclops^{m4} (Figure 8A).

A version of Cyclops in which all phosphorylation sites comprising Cyclops^{m4} were mutated to aspartic acid (called Cyclops^{10D}) activated *GUS* expression to approximately 50% - 75% compared to the positive control (Figure 8B; Figure 9B, right panel). Based on the observation that they inhibited the transcription factor activity of Cyclops in presence of CCaMK$^{1-314}$ (Figure 7B), we removed the phosphomimetic replacements of S220, S221 and S251 from Cyclops^{10D}. The resulting Cyclops^{7D} version displayed the same activity as Cyclops^{10D} (Figure 8B). We tested the contribution of D116, D134, D145 and D197 by generating the Cyclops versions Cyclops$^{4D\ 1-4}$ (Figure 8A). Cyclops^{4D-2} and Cyclops^{4D-3} displayed approximately 30% *GUS* expression compared to the positive control (Cyclops^{WT} in presence of CCaMK$^{1-314}$) (Figure 8B, left panel). Cyclops^{4D-1} and Cyclops^{4D-4} mediated negligible *GUS* expression and were therefore not considered anymore. The combination of Cyclops^{4D-2} and Cyclops^{4D-3} into Cyclops^{5D} (Figure 9A) did not increase the activity of Cyclops and resulted in approximately 30% *GUS* expression (Figure 9B). For the *in vitro* phosphorylation sites S7 – S50, only the combination of all phosphomimetic replacements into Cyclops^{Nphos} activated *GUS* expression to approximately 30% - 50% compared to the positive control (Figure 8C; Figure 9B, right panel). To further increase *GUS* expression, we combined Cyclops^{Nphos} and Cyclops^{5D} into Cyclops^{9D} (Figure 9A). We observed that Cyclops^{9D} mediated approximately 50% expression of *GUS* (Figure 9B, right panel).

After the identification and characterization of Cyclops versions with phosphomimetic replacements that activate the *RAM1*$_{pro}$ in absence of CCaMK$^{1-314}$, we tested their effect on the expression of the *GUS* reporter, when driven by the *NIN*$_{pro}$. All versions displayed a higher expression of *GUS* compared to Cyclops^{DD} (Figure 9B, left panel).

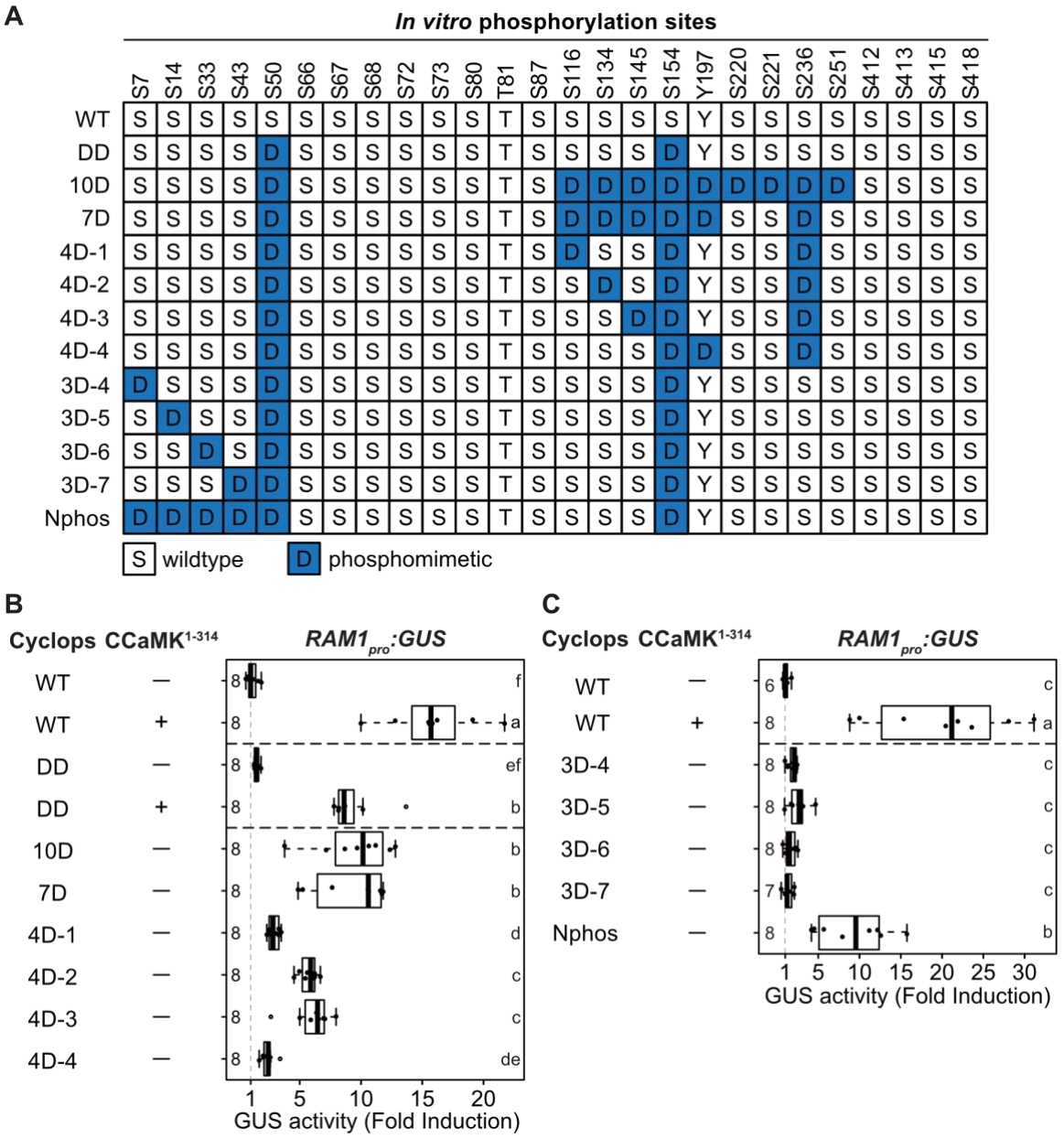

Figure 8: A mapping approach with phosphomimetic replacements identifies Cyclops versions that promote *GUS* expression driven by the *RAM1* promoter in absence of CCaMK$^{1-314}$, in *N. benthamiana*
(A) Matrix representation of Cyclops *in vitro* phosphorylation sites as explained in Figure 7 **(B)- (C)** Transactivation assays in *N. benthamiana* leaves, as described in material and methods. Boxplots represent GUS activity as fold induction compared to the median of the negative control (Cyclops^{WT} in absence of CCaMK$^{1-314}$, red dotted line). Black dots: individual leaf discs measured, black line: median, box: interquartile range, whiskers: lowest and highest data point within 1.5 interquartile range. Empty circles: data points outside of the 1.5 interquartile range. Small numbers left of boxplots indicate the numbers of leaf discs used to measure GUS activity. Data were subjected to Kruskal-Wallis and *post-hoc* Fishers least significant difference analysis, using Bonferroni correction (p-value ≤ 0.05) (B), or to ANOVA and *post-hoc* Tukey HSD analysis (*RAM1$_{pro}$:GUS* $F_{7,53} = 31.13$, p-value ≤ 0.001) (C). Letters right of boxplots indicate statistically different groups.

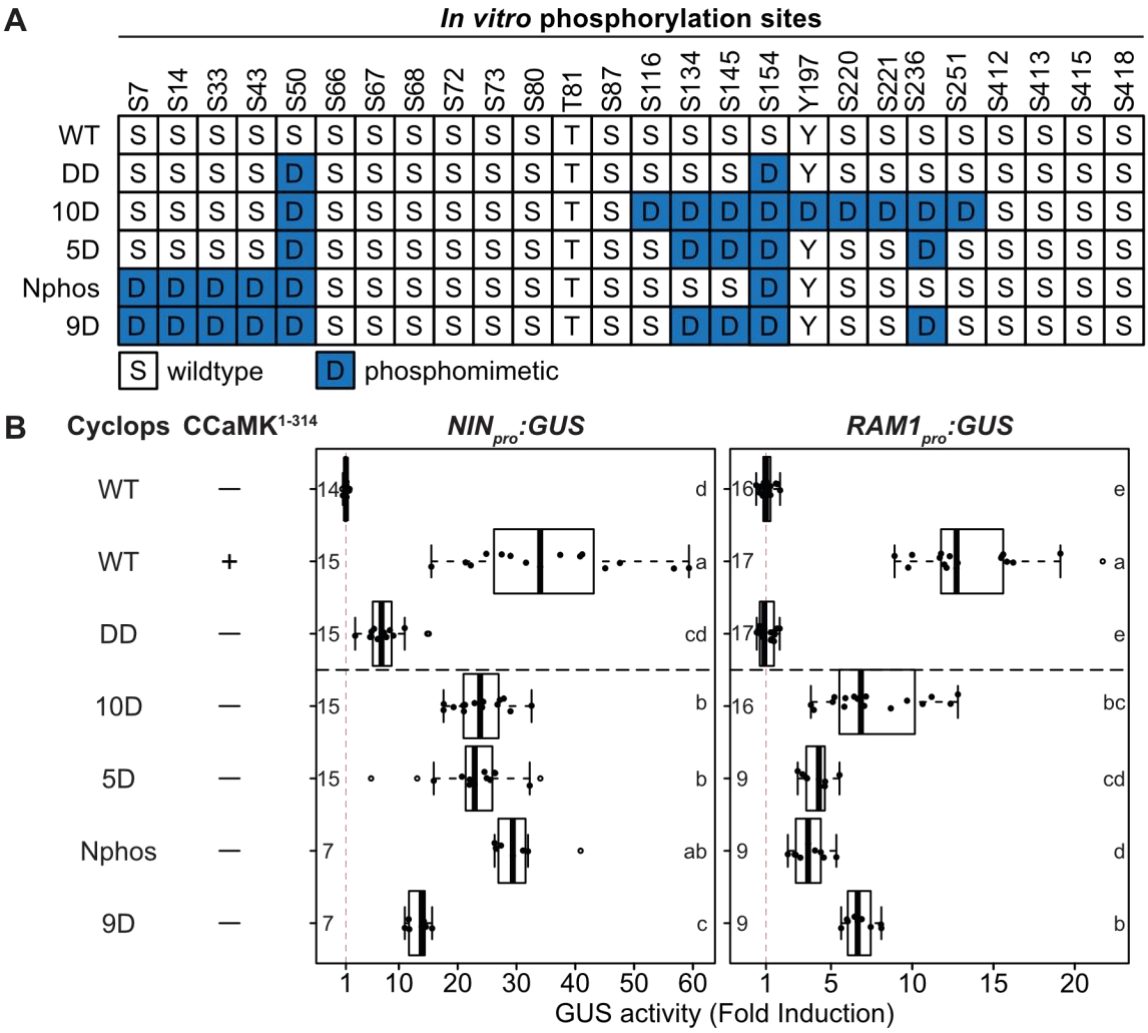

Figure 9: Four new Cyclops versions with phosphomimetic replacements display an increased activity in transactivation assays in *N. benthamiana*, compared to Cyclops^{DD}.

(A) Matrix representation of Cyclops *in vitro* phosphorylation as explained in Figure 7 **(B)** Transactivation assays in *N. benthamiana* leaves, as explained in material and methods. Boxplots represent GUS activity as fold induction compared to the median of the negative control (Cyclops^{WT} in absence of CCaMK$^{1-314}$, red dotted line). Black dots: individual leaf discs measured, from two independent infiltrations, black line: median, box: interquartile range, whiskers: lowest and highest data point within 1.5 interquartile range. Data were subjected to Kruskal-Wallis and post-hoc Fishers least significant difference analysis, using Bonferroni correction (p-value ≤ 0.05). Letters on top of boxplots indicate statistically different groups

5 Phosphomimetic versions of Cyclops increase spontaneous nodule formation

To investigate the effect of an increased number of phosphomimetic replacements in the Cyclops protein *in planta*, we transformed *Cyclops^{DD}*, *Cyclops^{10D}*, *Cyclops^{5D}*, *Cyclops^{Nphos}* and *Cyclops^{9D}* into the *ccamk-13* mutant background. We expressed *CCaMK* as positive control and the human influenza hemagglutinin (HA)- tag as a negative (EV) control. All transgenes were expressed under their endogenous promoters (*Cyc$_{pro}$:2.4kb* and *CCaMK$_{pro}$1.9kb*, respectively). We observed that the transformation of Cyclops versions containing phosphomimetic replacements resulted in the formation of nodules on *ccamk-13* root systems (Figure 10A). We did not observe nodule formation on *ccamk-13* root systems transformed with *CCaMK* and therefore conclude that those nodules formed spontaneously. Compared to *Cyclops^{DD}*, which was demonstrated to induce spontaneous nodule (SN) formation before (Singh et al., 2014), *ccamk-13* roots transformed with *Cyclops^{10D}*, *Cyclops^{5D}*, *Cyclops^{Nphos}* and *Cyclops^{9D}* resulted in an increased frequency of SN formation (plants with SN/all plants analysed) and in the number of SN formed per root system (Figure 10A). These results demonstrate that an increased number of phosphomimetic replacements within Cyclops correlates with an increase in nodule formation.

As Cyclops^{10D}, Cyclops^{5D}, Cyclops^{Nphos} and Cyclops^{9D} mediate spontaneous expression of *GUS* when driven by the *RAM1$_{pro}$* (Figure 9B, right panel) we tested if these Cyclops versions are sufficient to complement the *ccamk-13* mutant for AM formation. After two weeks of co-cultivation with the AMF *R. irregularis* all transformed root systems had extracellular hyphae on their surface (Figure 10B). We observed that 80% (12/15) of the *ccamk-13* root systems transformed with *CCaMK* contained arbuscules, whereas roots transformed with the EV control or with versions of *Cyclops* that contained phosphomimetic replacements did not display any arbuscule formation (Figure 10B). These data demonstrate that the phosphomimetic replacements of the *in vitro* phosphorylation sites we investigated in this study are not sufficient to complement the AM phenotype of the *ccamk-13* mutant.

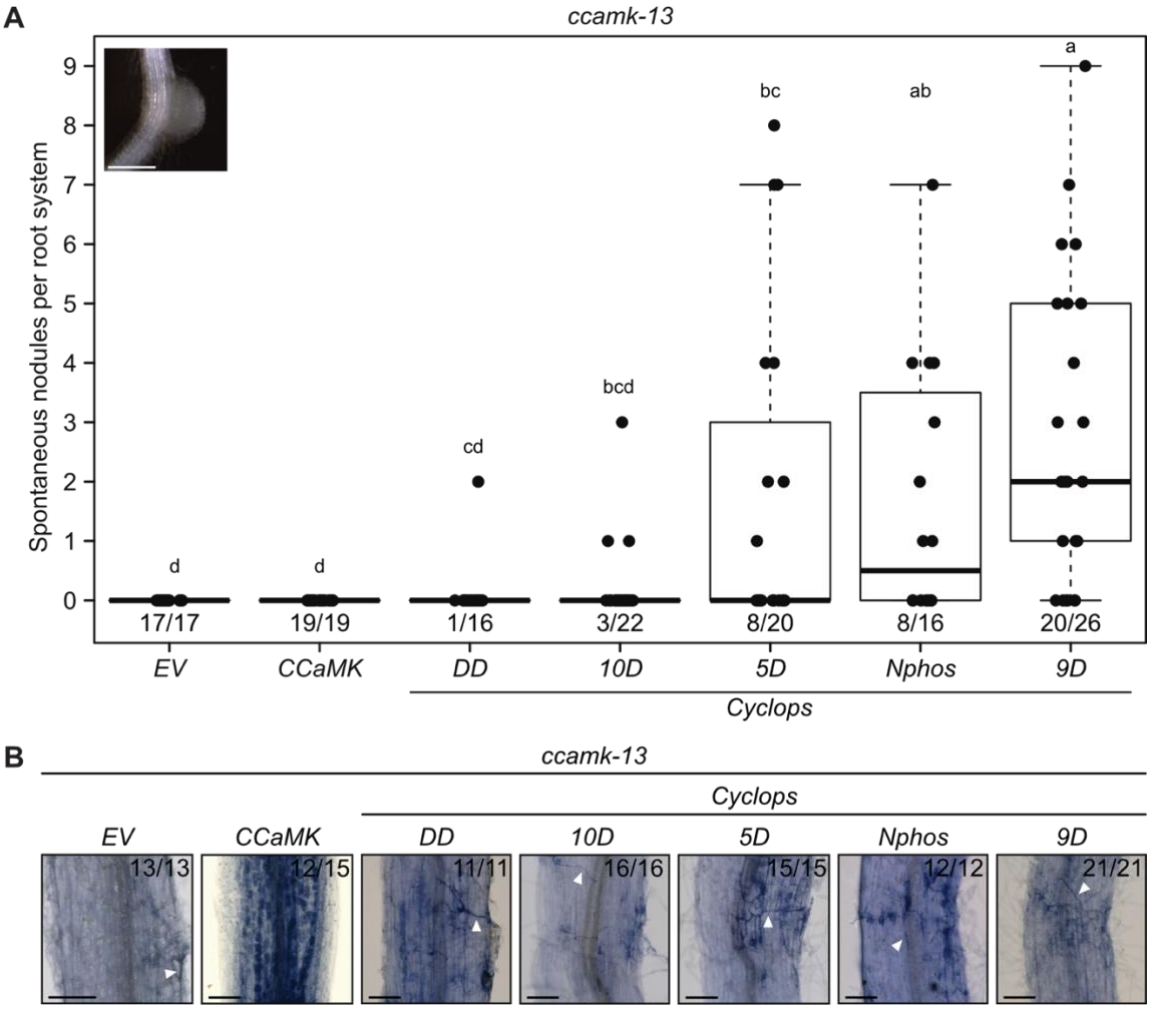

Figure 10: An increased number of serine or threonine to aspartic acid replacements in Cyclops lead to nodule organogenesis on *ccamk-13* root systems in the presence of AMF.
(A) Phenotypic analysis of *ccamk-13* mutant root systems, transformed with *Cyc*$_{pro}$*2.4kb:HA-gCyclops* versions, *CCaMK*$_{pro}$*1.9kb:Myc-gCCaMK* or *EV* (*Cyc*$_{pro}$*2.4kb:HA*). Nodule-shaped structures were scored 7 weeks post *A. rhizogenes* mediated hairy root transformation, including 2 weeks of co-cultivation with *Rhizophagus irregularis* in open pots. Boxplots display the number of spontaneous nodules formed on transgenic *ccamk-13* root systems. Black dots: nodule number on individual root systems, black line: median, box: interquartile range, whiskers: lowest and highest data point within 1.5 interquartile range. Data were subjected to Kruskal-Wallis and post-hoc Fishers least significant difference analysis, using Bonferroni correction (p-value ≤ 0.05). Letters on top of boxplots indicate statistically different groups. Numbers below boxplots indicates the number of root systems with the respective phenotype per all root systems analysed. Representative microscopic brightfield image of a spontaneous nodule is depicted as inlet. Scale bar = 500 µm. **(B)** Representative images of c*camk-13* root systems transformed with *CYC*$_{pro}$*2.4kb:HA-gCyclops* phosphomimetic versions, *CCaMK*$_{pro}$*1.9kb:Myc-gCCaMK* or *EV* (*CYCpro2.4kb:HA*). Plants were analysed 7 weeks post *A. rhizogenes* mediated hairy root transformation, including 2 weeks of co-cultivation with *Rhizophagus irregularis.* Numbers in images indicate how many root systems with the depicted phenotype have been observed, per all root systems analysed. Small white arrows indicate fungal hyphae on the root surface. Scale bars: 500 µm.

6 Phosphomimetic replacements of Cyclops phosphorylation sites enable bacterial presence in nodules

To test if Cyclops^{DD}, Cyclops^{10D}, Cyclops^{5D}, Cyclops^{Nphos} and Cyclops^{9D} are sufficient to complement the rhizobial infection process, we transformed them into *ccamk-13* root systems and inoculated them with *Mesorhizobium loti* MAFF 303099 expressing *Ds*Red (*M. loti Ds*Red). *CCaMK* was used as a positive control. After two weeks of co-cultivation with *M. loti Ds*Red, all Cyclops versions containing phosphomimetic replacements induced nodule organogenesis on *ccamk-13* mutant roots (Figure 11). For *Cyclops^{DD}*, 17.4% (5/23) of all analysed plants formed uninfected nodules (Figure 11, right panel). Except for *Cyclops^{10D}* (10.7%, 3/28), this number was increased in plants transformed with *Cyclops^{5D}* (25.9%, 5/27), *Cyclops^{Nphos}* (53.3%, 16/30) and *Cyclops^{9D}* (35.3%, 6/17). The total number of uninfected nodules per root system varied between the constructs and we observed the highest number of uninfected nodules on *ccamk-13* root systems transformed with *Cyclops^{Nphos}* (Figure 11, right panel). There were no uninfected nodules on *ccamk-13* root systems transformed with *Cyclops^{WT}*. On *ccamk-13* root systems transformed with *Cyclops^{10D}*, *Cyclops^{5D}*, *Cyclops^{Nphos}* and *Cyclops^{9D}* we observed nodules that displayed a *Ds*Red signal and therefore seemed to be infected by rhizobia (Figure 11, left panel). These events were only observed at very low frequency (1 – 2 nodules) on very few (1 – 2) *ccamk-13* root systems. We did not observe nodules that appeared to be infected on *ccamk-13* roots transformed with *Cyclops^{DD}*.

To confirm the presence of rhizobia within nodules that displayed a *Ds*Red signal, we sectioned the nodules using a vibratome. In nodules formed on *ccamk-13* roots transformed with *CCaMK,* rhizobia localized within nodule cells (Figure 12, lower panel) and we observed epidermal infection threads (eIT) (Figure 12, upper panel). We did not observe any *Ds*Red signal in nodules formed on *ccamk-13* roots transformed with *Cyclops^{DD}*, and there were no eITs. In contrast to *Cyclops^{DD}*, there was a *Ds*Red signal in nodules formed on *ccamk-13* roots transformed with *Cyclops^{10D}*, *Cyclops^{Nphos}*, *Cyclops^{9D}* and *Cyclops^{5D}* (Figure 12, lower panels). Interestingly, the *Ds*Red signal in those nodules localized to the apoplast and not to the inside of nodule cells. Additionally, we did not observe eITs on *ccamk-13* roots systems transformed with *Cyclops^{10D}*, *Cyclops^{Nphos}*, *Cyclops^{9D}* and *Cyclops^{5D}* (Figure 12, upper panel). Collectively, these observations indicate that an increase in the number of phosphomimetic replacements in Cyclops increases nodule organogenesis in *ccamk-13* roots and enables the presence of rhizobia in nodules formed on respective root systems.

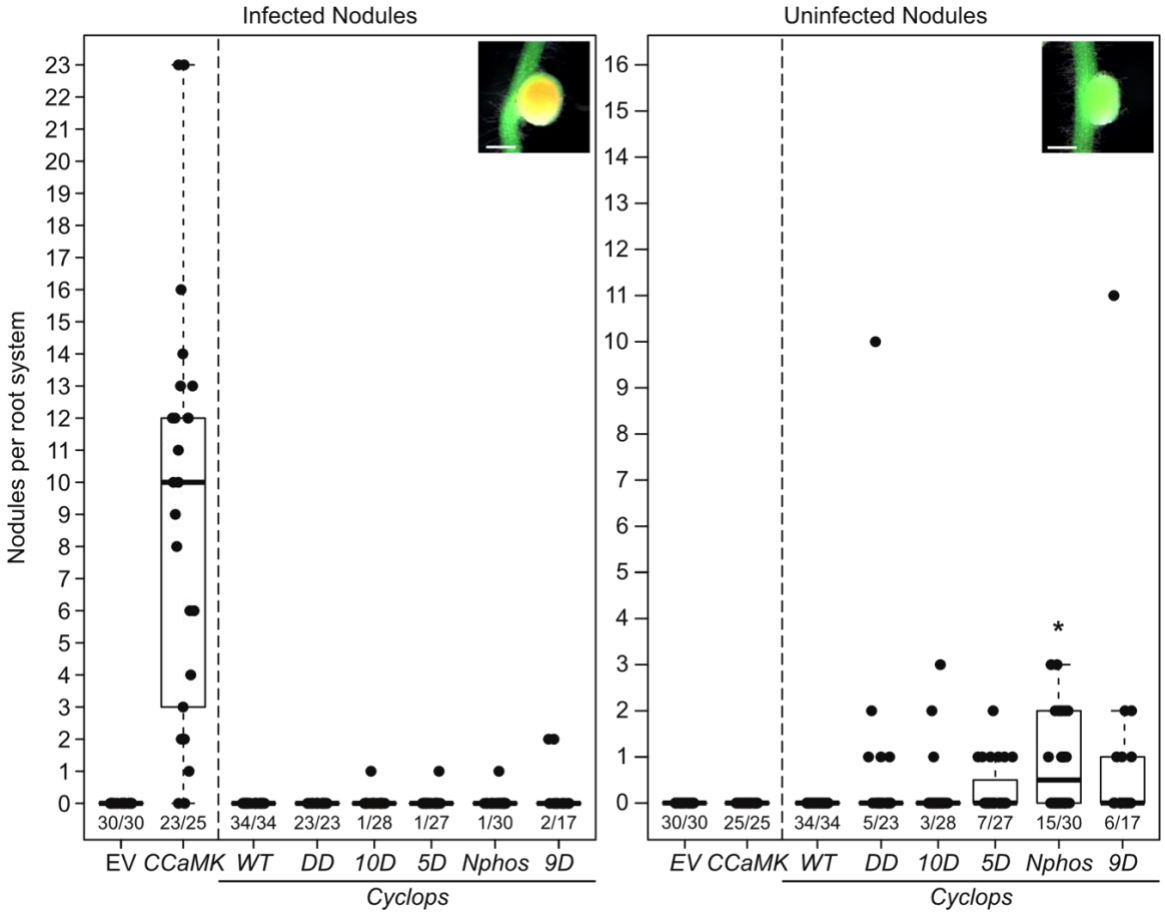

Figure 11: Multiple Cyclops versions with phosphomimetic replacements mediate the formation of infected and uninfected nodules on *ccamk-13* root systems.

Phenotypic analysis of c*camk-13* root systems, transformed with *CYC$_{pro}$2.4kb:HA-gCyclops* phosphomimetic versions, *CCaMK$_{pro}$1.9kb:Myc-gCCaMK* or *EV* (*CYC$_{pro}$2.4kb:HA*). Nodule formation was scored 7 weeks post *A. rhizogenes* mediated hairy root transformation, including 2 weeks of co-cultivation with *M.loti* MAFF 303099, expressing *Ds*Red. Boxplots show respective quantitative analysis of nodule formation on transgenic root systems. Black dots: nodule number on individual root systems, black line: median, box: interquartile range, whiskers: lowest and highest data point within 1.5 interquartile range. Data were subsected to statistical analysis using a Wilcoxon test. Asteriks indicate statistical differences between *Cylops^{10D}*, *Cyclops^{5D}*, *Cyclops^{Nphos}* or *Cyclops^{9D}* and *Cyclops^{DD}* (*$p \leq 0.05$). Numbers below boxplots indicates the number of root systems with the respective phenotype, per all root systems analysed. Representative microscopic images of infected and uninfected nodules are depicted as inlets. Green: *LjUbi$_{pro}$:2xNLS-GFP* transformation marker. Red: *M. loti*. Scale bars = 500 µm.

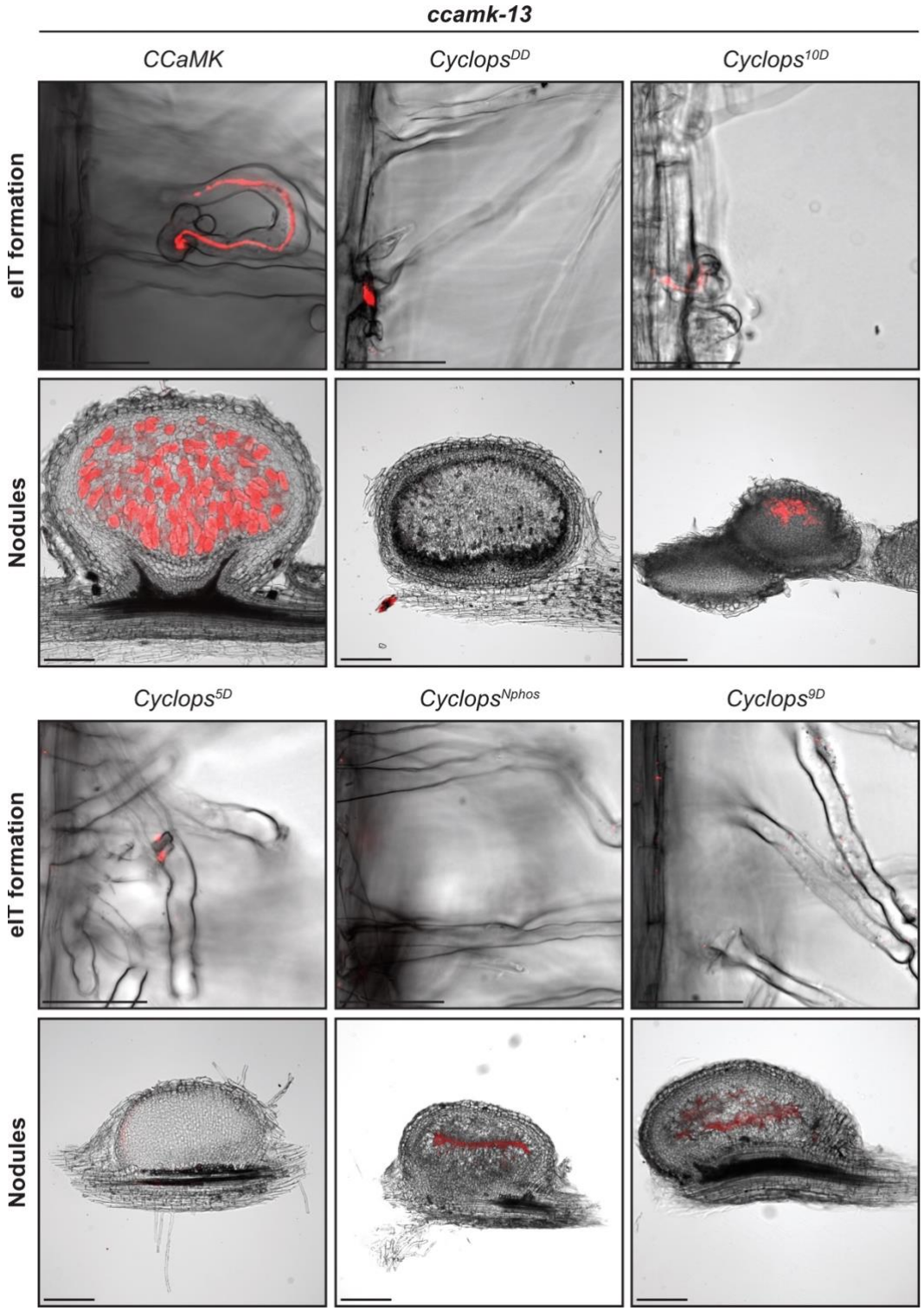

Figure 12: An increased number of phosphomimetic replacements in Cyclops enables bacterial presence in nodules formed on *ccamk-13* root systems.
Phenotypic analysis of c*camk-13* root systems, transformed with *HA-gCyclops* versions containing phosphomimetic replacements, or with *Myc-gCCaMK*. All transgenes were expressed under their endogenous promoters ($CYC_{pro}2.4kb$ or $CCaMK_{pro}1.9kb$). Images in upper panel display representative images of epidermal infection threads (eIT) formation. Images in lower panels display vibratome sections of nodules that appeared to be infected in Supplemental Figure 8. Red fluorescence indicates the presence of *M. loti* MAFF 303099 expressing *Ds*Red. Nodules were analyzed 7 weeks post *A. rhizogenes* mediated hairy root transformation, including 2 weeks of co-cultivation with *M. loti* MAFF 303099. Scale bars: upper panels = 50 µm, lower panels = 200 µm.

7 Phosphomimetic versions of Cyclops fail to complement the rhizobial infection process in the *cyclops-3* mutant

In the *cyclops-3* mutant, the expression of *Cyclops^{DD}* leads to the formation of infected (30-40%) and uninfected nodules (60-70%) (Singh et al., 2014). To investigate if the new phosphomimetic versions we generated in this study increase the proportion of infected nodules, we transformed them into the *cyclops-3* mutant background, using *A. rhizogenes* mediated hairy root transformation. We scored nodule formation after two weeks of co-cultivation with *M. loti Ds*Red. Upon transformation with *Cyclops^{DD}*, 9/11 *cyclops-3* root systems formed uninfected nodules and 4/11 root systems formed infected nodules (Figure 13). Infected and uninfected nodules occurred on the same root systems. For root systems transformed with *Cyclops^{10D}*, *Cyclops^{Nphos}* and *Cyclops^{9D}* there was a reduction of infected nodules per root systems and a reduced number of nodule-forming root systems, compared to *Cyclops^{DD}*. *For Cyclops^{5D}*, we observed an increase in the formation of infected nodules per root system compared to *Cyclops^{DD}*, as well as an increase in nodule-forming root systems. For the formation of uninfected nodules, there was a reduction for all phosphomimetic *Cyclops* constructs compared to *Cyclops^{DD}*.

Regarding the ratio between infected and uninfected nodules on transformed root systems, we observed a shift towards the formation of infected nodules for all Cyclops versions, except for Cyclops^{5D}. Overall, the transformation of Cyclops^{DD} resulted in the highest total number of nodules formed amongst all Cyclops versions with phosphomimetic replacements.

These results indicate that the phosphomimetic status of Cyclops influences its function during the infection process *in planta*, and that a higher activity of Cyclops in *N. benthamiana* does not necessarily correlate with an improved biological function of Cyclops, at least in the *cyclops-3* mutant.

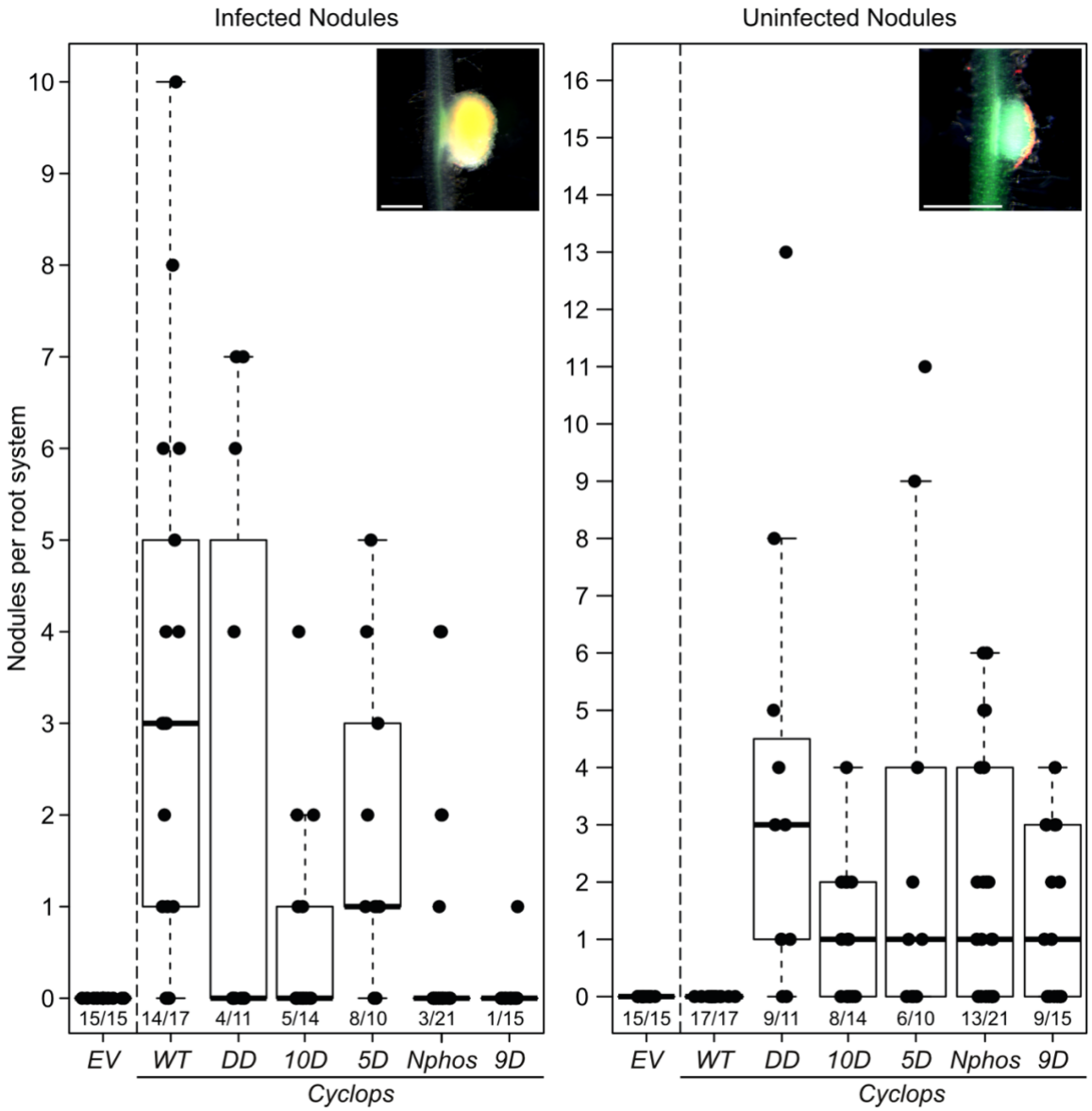

Figure 13: Cyclops versions with phosphomimetic replacements mediate the formation of infected and uninfected nodules on *cyclops-3* root systems.
Phenotypic analysis of *cyclops-3* root systems transformed with *CYC$_{pro}$2.4kb:HA-gCyclops* phosphomimetic versions or *EV* (*CYC$_{pro}$2.4kb:HA*). Nodule formation was scored 7 weeks post *Agrobacterium rhizogenes* mediated hairy root transformation, including 2 weeks of co-cultivation with *M.loti* MAFF 303099, expressing *Ds*Red. Boxplots show quantitative analysis of nodule formation on transgenic root systems. Black dots: nodule number on individual root systems, black line: median, box: interquartile range, whiskers: lowest and highest data point within 1.5 interquartile range. Data were subsected to statistical analysis using a Wilcoxon test. No statistical differences in nodules numbers between root systems transformed with *Cyclops^{DD}* and *Cyclops^{10D}*, *Cyclops^{5D}*, *Cyclops^{Nphos}* and *Cyclops^{9D}* were determined. Numbers below boxplots indicate the number of root systems with the respective phenotype per all root systems analysed. Representative microscopic images of infected and uninfected nodules are depicted as inlets. Green: *LjUbi$_{pro}$:2xNLS-GFP* transformation marker. Red: *M.loti*. Scale bars = 500 μm.

8 Phosphomimetic replacements in Cyclops$^{1-255}$ are sufficient to mediate Cyclops activity

Singh and colleagues (2014) demonstrated that Cyclops^{min} mediates the expression of the *GUS* reporter when fused to the *2xCyc-RE$_{NIN}$*, but fails to express *GUS* when fused to an 870 bp fragment of the *NIN* promoter (*NIN$_{pro870}$*) and is not sufficient to complement the RNS phenotype of the *cyclops-3* mutant. As all the phosphorylation sites we investigated with phosphomimetic replacements in this study map to amino acids 1-255 of Cyclops (Cyclops$^{1-255}$) (Figure 5A), we hypothesized that this N-terminal part of Cyclops positively contributes to its function as a transcription factor, in a phosphorylation-status dependent manner.

To test this, the full-length version of Cyclops (Cyclops^{FL}, aa 1-518) or versions of Cyclops$^{1-255}$ were fused to the DNA binding domain (BD) of the yeast transcription factor Gal4 (Gal4^{BD}-Cyclops$^{FL/N}$) and tested for *Gal4 upstream activating sequence* (*UAS*) responsive reporter expression (Figure 14B). As a negative control, we fused CCaMK to the Gal4^{BD} (Gal4^{BD}-CCaMK). In *N. benthamiana*, neither Gal4^{BD}-Cyclops^{FL}, nor Gal4^{BD}-Cyclops$^{1-255\ WT}$ and Gal4^{BD}-Cyclops$^{1-255\ DD}$ activated the expression of a *5xUAS:eGFP-GUS* reporter compared to the negative control (Figure 14C, right panel). In contrast, Gal4^{BD}-Cyclops$^{1-255\ 10D}$, Gal4^{BD}-Cyclops$^{1-255\ 5D}$, Gal4^{BD}-Cyclops$^{1-255\ Nphos}$ and Gal4^{BD}-Cyclops$^{1-255\ 9D}$ resulted in a significant reporter expression compared to the negative control (Figure 14C, right panel).

It has been proposed that Cyclops mediates target gene expression via interaction with components of the basal transcriptional machinery (Singh et al., 2014). As yeast (*S. cerevisiae*) does not contain any plant-related transcriptional regulators, we used this organism to test whether Cyclops$^{1-255}$ regulates gene expression via this mechanism. Compared to the negative control, Gal4^{BD}-Cyclops^{FL} mediated a small but significant expression of a *5xUAS:Luciferase* reporter (Figure 14C, left panel). We did not observe this for Gal4^{BD}-Cyclops$^{1-255\ WT}$. This observation is in line with the previous identification of a transcriptional activation domain (AD) in Cyclops^{min} (Singh et al., 2014). Interestingly, Gal4^{BD}-Cyclops$^{1-255\ DD}$ mediated the same level of reporter expression as Gal4^{BD}-Cyclops^{FL} (Figure 14C, left panel). Similar to the strong reporter expression we observed in *N. benthamiana*, Gal4^{BD}-Cyclops$^{1-255\ 10D}$, Gal4^{BD}-Cyclops$^{1-255\ 5D}$, Gal4^{BD}-Cyclops$^{1-255\ Nphos}$ and Gal4^{BD}-Cyclops$^{1-255\ 9D}$ mediated a significantly increased reporter expression compared to the negative control and compared to Gal4^{BD}-Cyclops^{FL}, Gal4^{BD}-Cyclops$^{1-255\ DD}$ and Gal4^{BD}-Cyclops$^{1-255\ WT}$ (Figure 14C, left panel). These results indicate that the N-terminus of Cyclops contributes to its transcriptional regulation, in a manner that depends on the number of its phosphomimetic amino acids.

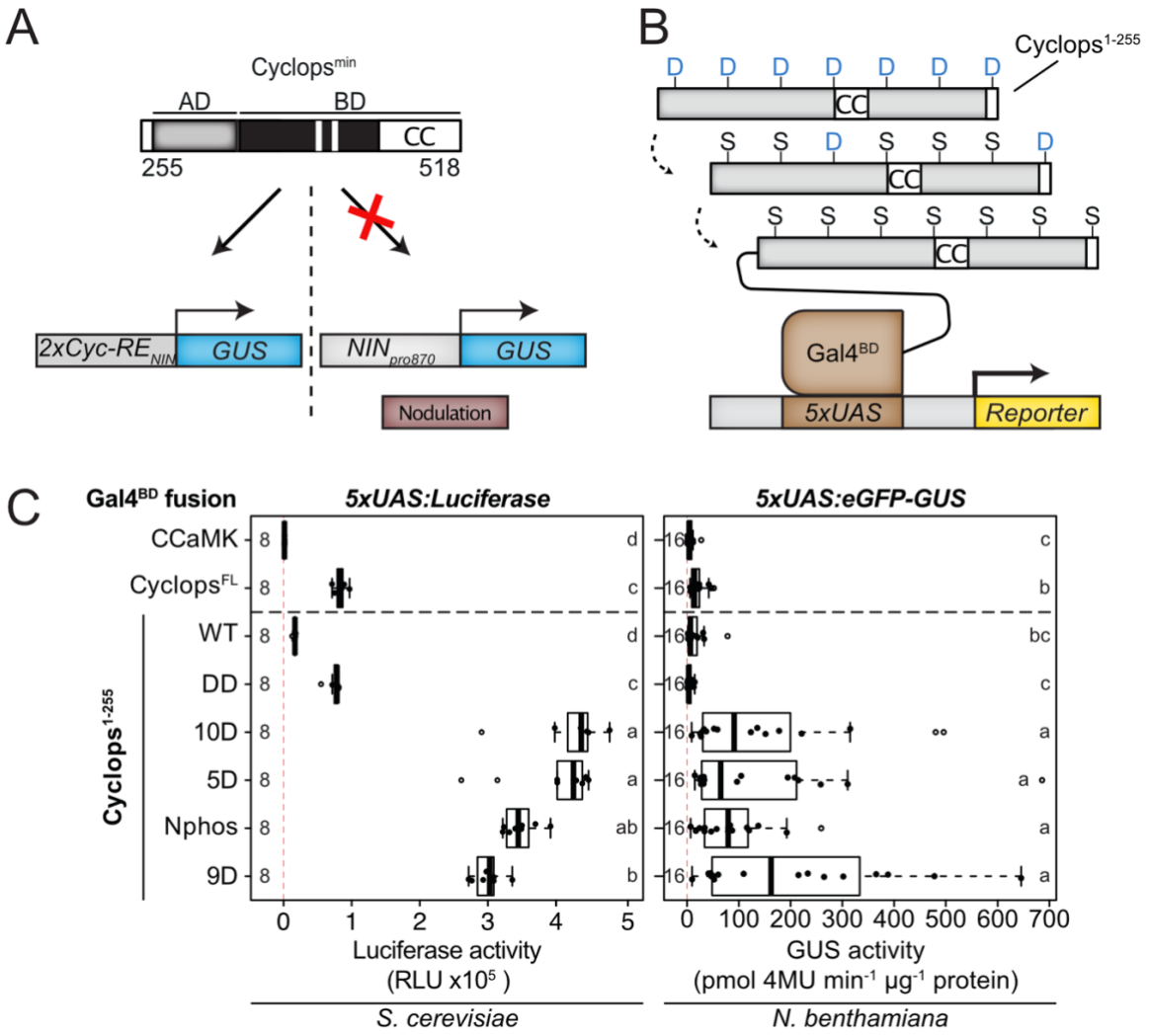

Figure 14: Cyclops$^{1\text{-}255}$-mediated reporter expression depends on its phosphomimetic status in *S. cerevisiae* and *N. benthamiana*.

A) Cyclops^{min} (amino acids 255-518) is sufficient for *GUS* expression via the *2xCyc-RE$_{NIN}$* but not sufficient for *GUS* expression via an 870 bp fragment of the *NIN$_{pro}$* (*NIN$_{pro870}$*) and nodule formation, in the *cyclops-3* mutant (Singh et al., 2014). AD: activation domain, BD: DNA binding domain, CC: coiled-coil, two white bars indicate location of NLS sequences **(B)** Experimental setup: Cyclops$^{1\text{-}255}$ (amino acids 1-255) with phosphomimetic replacements was fused to the Gal4 DNA binding domain (Gal4^{BD}) and tested for *Gal4 upstream activating sequence* (*UAS*)-responsive reporter expression in *N. benthamiana* leaf tissue (*5xUAS:eGFP-GUS*) and *S. cerevisiae* cells (*5xUAS:Luciferase*) **(C)** Boxplots represent reporter activity from 8 technical replicates of one overnight colony (*S. cerevisiae*) or 16 individual leave discs (*N. benthamiana*), 48 hpi. Black dots: individual measurements of colonies or individual measurements of leave discs, black line: median, box: interquartile range, whiskers: lowest and highest data point within 1.5 interquartile range. Empty circles: data points outside of the 1.5 interquartile range. Luciferase activity is depicted as relative light units (RLU). Full length Cyclops (Gal4^{BD}-Cyclops^{FL}, amino acids 1-518) and GAL4^{BD}-CCaMK were included as positive and negative control, respectively. Red dotted line presents the activation values of the negative control. Data were subjected to Kruskal-Wallis and *post-hoc* Fishers least significant difference analysis, using Bonferroni correction (p-value ≤ 0.05). Letters right of boxplots indicate statistically different groups.

9 The phosphomimetic status of Cyclops^{S236} and the mutation of CCaMK^{T265} modulate the interaction between those proteins

Previous studies delivered indications that the phosphorylation of Cyclops can influence its interaction with additional proteins (Jin et al., 2016; Andrade Aguirre, 2021). To test if the phosphomimetic amino acids replacements we investigated in this study influence the interaction of Cyclops and CCaMK, we performed a Y2H analysis. CCaMK was used as a Gal4^{BD} fusion (Bait) and full-length Cyclops was used as a Gal4^{AD} fusion (Prey) (Figure 15). We confirmed the presence of Prey and Bait constructs by growth on SD medium lacking leucine (-L) and tryptophane (-W), respectively. To test the interaction between Bait and Prey we monitored the growth of transformed yeast cells on SD medium lacking adenine (-A) and histidine (-H), and measured the expression of a *UAS*-driven Luciferase reporter (Figure 15). Presence of the *Luciferase* reporter gene was confirmed by growth on synthetic dropout (SD) medium lacking uracil (-U). The well-established interaction between Cyclops and CCaMK (Singh et al., 2014; Pimprikar et al., 2016; Andrade Aguirre, 2021) was used as a positive control. Gal4^{BD}-CCaMK in combination with a Gal4^{AD}-fusion of the large T antigen of Simian Vacuolating Virus 40 (SV40) was used as negative control.

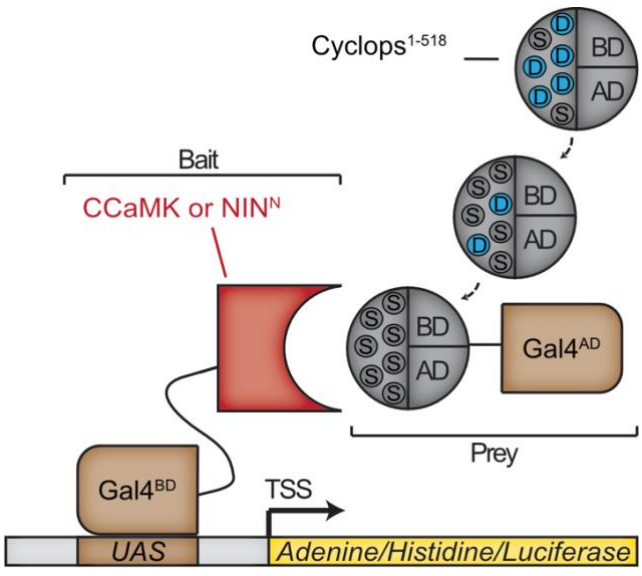

Figure 15: Establishment of a quantitative, Luciferase reporter system.
CCaMK or NIN^{N} (aa 1-296) were used as Gal4^{BD} fusions (Bait) and full-length Cyclops phosphomimetic versions were used as Gal4^{AD} fusions (Prey). The interaction status of Bait and Prey combinationss was assessed using I) growth complementation of the strain *S. cerevisiae* Y8800 on synthetic dropout medium (SD) lacking adenine (A) or histidine (H), and II) quantitatively using the stably integrated Firefly *Luciferase* gene. To drive the expression of adenine and histidine, the promoters endogenous to *S. cerevisiae* strain Y8800 were used (James et al., 1996). To drive the expression of *Luciferase*, the *Gal2*$_{pro}$ from *S. cerevisiae* strain AH109 was used. TSS: transcriptional start site.

As reported in previous studies (Yano et al., 2008; Singh et al., 2014) both Cyclops^{WT} and Cyclops^{DD} interacted with CCaMK (Figure 16B). We also observed interaction between Cyclops^{Nphos} and CCaMK. In contrast, Cyclops^{10D}, Cyclops^{9D} and Cyclops^{5D} did not interact with CCaMK. Since Cyclops^{5D} represented the non-interacting Cyclops version with the lowest number of phosphomimetic replacements, we hypothesized that S134D, S145D or S236D caused the loss of interaction with CCaMK. To test this hypothesis, we reverted the phosphomimetic replacements of those sites individually, yielding Cyclops^{QP1}, Cyclops^{QP2} and Cyclops^{QP3} (Figure 16A). Amongst those versions, only Cyclops^{QP3} interacted with CCaMK (Figure 16C). This indicated that the phosphomimetic replacement S236D was sufficient for the loss of interaction. We confirmed this assumption by generating Cyclops^{S236D}, which did not interact with CCaMK (Figure 16C).

To further characterize the role of S236 phosphorylation in regulating the interaction of Cyclops and CCaMK, we generated a phosphoablative version of S236 (Cyclops^{S236A}) (Figure 17A). If phosphorylation of S236 is sufficient to block the interaction between Cyclops and CCaMK, we expected a constitutive interaction between Cyclops^{S236A} and CCaMK. To test if phosphorylation of S236 is required to block the interaction with CCaMK, we also tested the interaction between Cyclops^{S236A} and autoactive CCaMK^{T265D}. For CCaMK and Cyclops^{S236A}, we observed an increased expression of the *Luciferase* reporter gene compared to CCaMK and Cyclops^{WT}, indicating an increased interaction strength of CCaMK and Cyclops^{S236A} (Figure 17B). We furthermore observed that the interaction strength between CCaMK^{T265D} and Cyclops^{WT} was significantly higher compared to CCaMK and Cyclops^{WT} (Figure 17B). In addition, the interaction strength between CCaMK^{T265D} and Cyclops^{S236A} was increased by 5-fold, compared to CCaMK^{T265D} and Cyclops^{WT}. From these observations we conclude that the phosphomimetic replacement CCaMK^{T265D} and the phosphorylation status of S236 jointly influence the interaction between CCaMK and Cyclops.

To confirm the results obtained in these Y2H experiments, we used a fluorophore-based method to monitor protein-protein interactions in nuclei of *N. benthamiana* leaves. Upon close proximity (< 10 nm), Förster Resonance Energy Transfer (FRET) from a donor to an acceptor fluorophore leads to a reduction of the fluorescence lifetime (FLT) of the donor fluorophore (Lampugnani et al., 2018). Fluorescence Lifetime Imaging (FLIM) can serve as a readout for FRET efficiency (FLIM-FRET) between the FRET pair GFP (FRET donor) and mCherry (FRET acceptor). In fluorophore-fusion proteins like GFP-Cyclops and mCherry-CCaMK, changes in the FLT of GFP in presence of mCherry can therefore be used as indication for

altered protein-protein interaction between Cyclops and CCaMK. To prevent CCaMK-dependent phosphorylation of Cyclops in *N. benthamiana* leaves, we used kinase-dead version of CCaMK, which harbours a D186N amino acid substitution in the activation loop of its kinase domain (CCaMK^{NFG}) (Chloé Cathebras, unpublished).

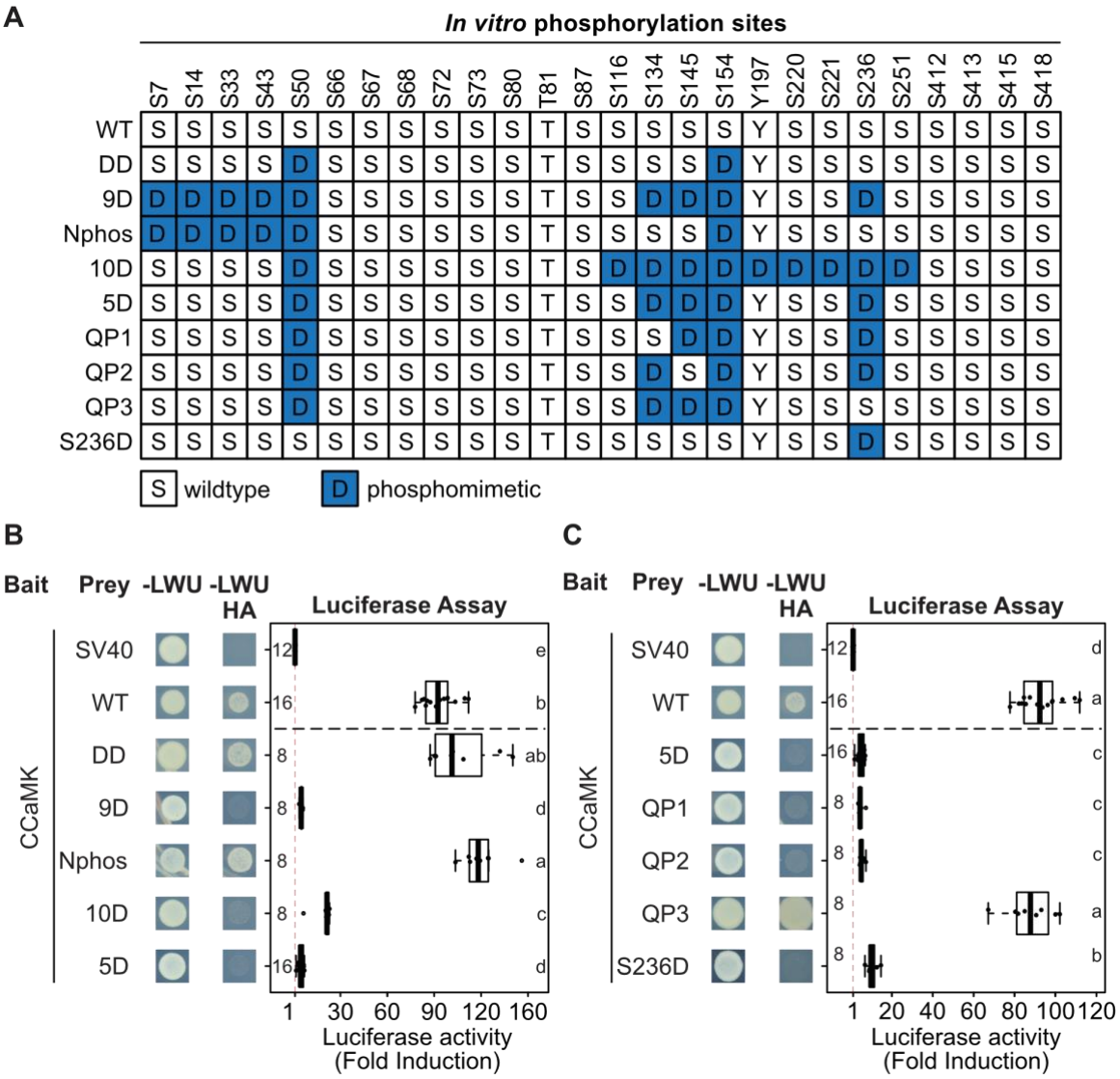

Figure 16: The phosphomimetic replacement of S236 is sufficient to block the interaction between Cyclops and CCaMK, in Y2H experiments.

(A) Matrix representation of Cyclops *in vitro* phosphorylation sites substituted with aspartic acid (D). Numbers on top indicate amino acid positions within Cyclops from *L. japonicus* Gifu (B-129). Names of the phosphoversions are indicated on the left. **(B) – (C)** Y2H experiments with CCaMK as bait and Cyclops versions or SV40 as prey. Assays were performed as described in material and methods. Boxplots represent Luciferase activity of individual overnight colonies (small numbers left of boxplots). Black dots: measurements from individual colonies, black line: median, box: interquartile range, whiskers: lowest and highest data point within 1.5 interquartile range. Empty circles: data points outside of the 1.5 interquartile range. Luciferase activity is displayed as fold induction compared to the negative control (CCaMK + SV40, red dotted line). Data were subjected to Kruskal-Wallis and *post-hoc* Fishers least significant difference analysis, using Bonferroni correction (p-value ≤ 0.05). Letters on the right of boxplots indicate statistically different groups.

A translational fusion between mCherry and GFP was used as a positive control (NLS-mCherry-GFP) and free NLS-mCherry in the presence of GFP-Cyclops^{WT} was used as a negative control. The average FLT of GFP was 2.4 ns for GFP-Cyclops^{WT} in presence of free NLS-mCherry (Figure 17C). For GFP-Cyclops^{WT} or GFP-Cyclops^{S236D} the presence of mCherry-CCaMK^{NFG} reduced the average FLT of GFP to 2.3 ns. This indicated that both GFP-Cyclops^{WT} and GFP-Cyclops^{S236D} interacted with mCherry-CCaMK^{NFG}.

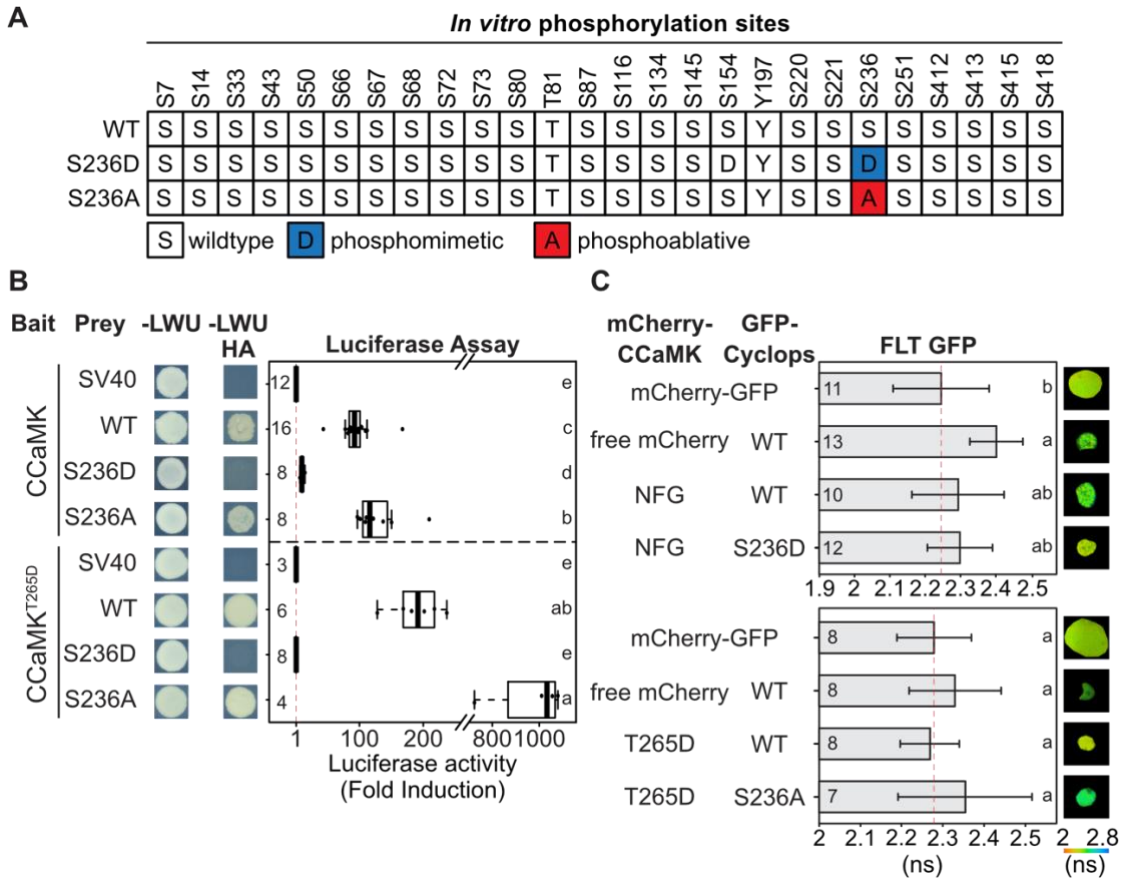

Figure 17: Phosphomimetic and phosphoablative replacements of Cyclops^{S236} as well as the mutation of CCaMK^{T265} modulate the interaction between Cyclops and CCaMK, in Y2H experiments
(A) Matrix representation of Cyclops *in vitro* phosphorylation sites substituted with alanine (A) or aspartic acid (D). Numbers on top indicate amino acid positions within Cyclops from *L. japonicus* Gifu (B-129). Names of the phosphoversions are indicated on the left. **(B)** Y2H experiments with CCaMK as bait and Cyclops versions or SV40 as prey, as described in materials and methods. Data were subjected to Kruskal-Wallis and *post-hoc* Fishers least significant difference analysis, using Bonferroni correction (p-value ≤ 0.05). Letters left of boxplots indicate statistically different groups. **(C)** *In vivo* FLIM-FRET analysis of the CCaMK/Cyclops interaction, using GFP as FRET donor and mCherry as FRET acceptor, in nuclei of *N. benthamiana* leaf cells 48 hours post infiltration. A translational fusion of NLS-mCherry-GFP was used as positive control, free NLS-mCherry in presence of GFP-Cyclops^{WT} was used as negative control. Bar charts represent the average fluorescence lifetime (FLT) of GFP in nano seconds (ns), from individual nuclei (small numbers). Error bars represent standard deviation. Red dotted line indicates the FLT measured for GFP-Cyclops^{WT} in presence of mCherry-CCaMK$^{NFG/T265D}$. Data were subjected to Kruskal-Wallis and *post-hoc* Fishers least significant difference analysis, using Bonferroni correction (p-value ≤ 0.05). Letters on the right of boxplots indicate statistically different groups. Images on the far right depict FLT of GFP as representative colour coded images of measured nuclei. Scale is shown below.

VIII Discussion

Cyclops is an essential regulator of the rhizobial and the fungal infection process during the establishment of RNS and AM, respectively (Yano et al., 2008). Its interaction with and phosphorylation by CCaMK suggests that Cyclops participates in the translation of common symbiotic signalling into a symbiont specific transcriptional response. As phosphomimetic replacements of the Cyclops phosphorylation sites S50 and S154 (Cyclops^{DD}) complement the *ccamk-13* mutant for nodulation but not for the rhizobial or fungal infection process, it was suggested that additional phosphorylation sites are involved in the regulation of Cyclops activity (Singh et al., 2014). To test this hypothesis, we functionally characterized 26 *in vitro* phosphorylation sites, using a combination of transactivation assays in *N. benthamiana*, complementation assays of symbiotic mutants as well as protein-protein interaction studies.

1 The biological role of Cyclops phosphorylation

1.1 Modulation of Cyclops activity *in planta*

The characterization of S50 and S154 revealed that phosphorylation at those two positions is necessary, but not sufficient to mediate all biological functions of Cyclops (Singh et al., 2014). In this study, we have demonstrated that the activity of Cyclops increases, as its phosphomimetic status increases (Figure 9, Figure 10, Figure 14). Hence, the question arises: what is the functional role of modulating the activity of Cyclops via its phosphorylation status? Phosphoproteomic analysis of rhizobium (*Sinorhizobium meliloti*) inoculated *M. truncatula* plants revealed that Cyclops/IPD3 is phosphorylated at 12 residues *in vivo* (Marx et al., 2016). In contrast, a previous *in vivo* study of the same legume grown under non-inoculated conditions only found two phosphorylated residues, namely S50 and S154 (Grimsrud et al., 2010). Collectively, these results suggest that the phosphorylation status of Cyclops is increased in response to a symbiont and that phosphorylation of S50 and S154 has a function under non-symbiotic conditions. The finding that phosphorylation at S50 and S154 is necessary for binding to a palindrome containing *Cyc-RE* from the NIN_{pro} *in vitro* suggests that this function is DNA binding (Singh et al., 2014). This is supported by ChIP-seq experiments performed in non-inoculated *cyclops-3* plants, in which ectopically expressed Cyclops^{DD} associated with the promoter of not only *NIN*, but also with the promoter of *RAM1* (Emmanoulis Bastakis, unpublished).

The analyses of Cyclops^{DD} demonstrated that phosphorylation of S50 and S154 is not only required for DNA-binding, but also resulted in transcription factor activity of Cyclops (Singh et al., 2014). This implies an expression of Cyclops target genes even under non-symbiotic conditions. Interestingly, RNAse protection assays and the analysis of the transposon footprint mutant *nin-2* demonstrated that this is the case, at least for *NIN* (Schauser et al., 1999; Andrade Aguirre, 2021). A potential non-symbiotic biological role for *NIN* arises from the recent identification of *ASL18*/*LBD16a* as transcriptional target of NIN, which is proposed to have a dual function in lateral root formation via auxin signalling and in nodule formation via physical interaction with NF-YA1 and NF-YB1 (Soyano et al., 2019). Therefore, it could be that plants forming endosymbiotic associations Cyclops participates in the homeostasis of the root system architecture, via the transcriptional regulation of *NIN*. However, a direct connection of Cyclops to the formation of lateral roots remains to be demonstrated.

1.2 How is a dynamic phosphorylation status of Cyclops mediated?

Since it has been identified as the only kinase to phosphorylate Cyclops to date, modulation of the Cyclops phosphorylation status most likely depends on CCaMK. Although it was proposed that CCaMK is inactive under basal nuclear calcium levels (Miller et al., 2013), multiple *in vitro* studies demonstrated substrate phosphorylation activity in absence of calcium and CaM, or presence of only calcium (Tirichine et al., 2006; Liao et al., 2012; Diploma Katja Katzer, 2011). These findings could explain the identification of phosphorylated S50 and S154 under non-symbiotic conditions *in vivo*, as observed by Grimsrud and colleagues (2010). Extensive biochemical experimentation and mathematical modelling resulted in a model of CCaMK function, in which CCaMK-dependent substrate phosphorylation increases in a logarithmic manner over the course of approximately 30 min of calcium spiking, accounting for 20 calcium spikes (Miller et al., 2013). Interestingly, it was previously determined that approximately 36 spikes are necessary for the expression of *ENOD11*, a gene which is under the control of common symbiotic signalling (Miwa et al., 2006). Overall, these data suggest that certain level of Cyclops phosphorylation must be achieved to induce the expression of its targets in response to symbiont perception. An increased transcriptional function of Cyclops by multiple phosphomimetic versions that we tested in this study supports this idea (Figure 9, Figure 10, Figure 14).

Increasing phosphorylation levels can in principle lead to two kinds of responses. In a switch-like response the function of the phosphorylation substrate is only elicited upon reaching a certain phosphorylation level threshold (Nash et al., 2001; Kõivomägi et al., 2011). In a graded response the increase in its phosphorylation level correlates with an increased function of the substrate (Pufall et al., 2005; Strickfaden et al., 2007). For Cyclops, the type of response is unclear at this stage. On the one hand, transcriptional activation experiments with the N-terminal fragment of Cyclops in yeast indicate a switch-like behaviour, with Cyclops^{5D} being the minimal phosphorylation level required to induce a strong transcriptional response compared to Cyclops^{DD} (Figure 14). We observed a similar tendency in transactivation assays with the *NIN$_{pro}$* and the *RAM1$_{pro}$* (Figure 9). On the other hand, nodulation frequencies in complemented *ccamk-13* plants indicate a gradual increase of the Cyclops activity, which correlates with an increased number of phosphomimetic replacements (Figure 10). An exception to this pattern is Cyclops^{10D}, indicating that not only the number of phosphorylated residues could influence Cyclops function, but also their distribution within the Cyclops protein. Overall, a more detailed investigation of individual phosphorylation sites is necessary, to exactly determine their functional influence on Cyclops activity.

1.3 Cyclops phosphorylation as a specificity factor for RNS or AM

The biochemical properties of Cyclops appear to be highly conserved in root endosymbioses forming species. *Cyclops* from *O. sativa*, which forms AM but not RNS, complements both AM and RNS in the *cyclops-3* mutant (Yano et al., 2008). This was further confirmed by Radhakrishnan and colleagues (2020), who demonstrated that ectopic expression of *Cyclops* from the AM-forming liverwort *M. paleacea* complements the rhizobial infection process of the *ipd3-2* mutant. As Cyclops is both required for AM and RNS, these observations point to a long-standing conundrum in symbioses research: how can a single transcriptional regulator be responsible for symbioses-specific transcriptional responses? As Cyclops is phosphorylated by CCaMK, it is tempting to speculate that differential phosphorylation of Cyclops could be the specificity-mediating agent during the transcriptional responses to bacterial or fungal perception. In principle, multisite phosphorylation of transcription factors by a single kinase can mediate differential transcriptional responses. In the case of the yeast transcription factor Pho4, one amongst six phosphorylation sites mediates the expression of a specific subset of target genes, which are required in intermediate phosphate conditions (Springer

et al., 2003). This specific transcriptional response correlates with specific binding of partially phosphorylated Pho4 to its target promoters.

In the case of Cyclops, there are indications speaking in favour and against this hypothesis. A direct comparison of symbiotic gene expression in *ccamk-3* plants expressing CCaMK^{T265D} or CCaMK$^{1-314}$ revealed that AM-specific *SbtM1* is only expressed upon transformation of *CCaMK$^{1-314}$* (Takeda et al., 2012). Interestingly, fungal infection of *ccamk-3* mutant plants is supported both by CCaMK^{T265D} and CCaMK$^{1-314}$, whereas rhizobial infection is only supported by CCaMK^{T265D} (Takeda et al., 2012). Lastly, Takeda and colleagues (2012) observed cytological changes in *ccamk-3* mutants transformed with *CCaMK$^{1-314}$* harbouring a T265D mutation (*CCaMK$^{1-314\ TD}$*), which resembled the PPA. Collectively, these results demonstrate that CCaMK$^{1-314}$ and its variants have functions that are more specifically required for AM rather than RNS and it is likely that those functions are mediated via Cyclops phosphorylation.

However, these results are deduced from studies with the truncated CCaMK, which is not regulated by calcium and CaM anymore (Singh, 2014). Based on our current knowledge, differential phosphorylation of Cyclops would require symbiosis specific activity of native CCaMK. Due to the activation of CCaMK by perinuclear calcium spiking, it is likely that differential CCaMK activity is encoded in distinct calcium spiking profiles in response to bacterial or fungal perception. However, this has not been observed yet (Miwa et al., 2006). In contrast, the spiking profiles of epidermal root hair cells in *M. truncatula* are similar in response to bacterial and fungal perception (Sieberer et al., 2012). Furthermore, the observations made in this study rather indicate that the phosphorylation level of Cyclops modulates the expression of its target genes in general, opposed to mediating transcriptional specificity (Figure 9). The only exception to this observation is Cyclops^{DD}, which mediates weak expression of *NIN* but no expression of *RAM1* at all (Figure 7, Figure 8, Figure 9). As Cyclops^{DD} associates with both the promoters of *NIN* and *RAM1 in vivo* (Emmanoulis Bastakis, unpublished), it is likely that the physical structure of promoter regions can influence the activity of Cyclops as well.

Overall, the results obtained in this study indicate that not the phosphorylation pattern of Cyclops, but rather alternative genetic factors could mediate specific transcriptional responses during symbiotic associations. At least in the case of RNS, a pathway acting in parallel to common symbiotic signalling has been suggested. Whereas *symrk* mutants retain cytosolic calcium influxes and root hair deformation, *nfr1* and *nfr5* mutants do not (Radutoiu et al., 2003). These non-

congruent phenotypes are indicative for a parallel pathway that diverges at the level of *NFR1* and *NFR5*, and it has been suggested that *Cyclops* partakes in cross-signalling between common symbiotic signalling and this hypothetical pathway (Madsen et al., 2010). Although the clear identification of a MF receptor has not been achieved yet, these observations exemplify that additional symbiosis related signalling pathways could be involved in the (transcriptional) activation of genetic factors that could mediate Cyclops specificity.

To unravel the mechanistic functions of Cyclops in RNS- and AM-related gene expression, immunoprecipitation from nodulated and mycorrhized roots followed by the determination of interacting proteins and/or the Cyclops phosphorylation pattern via mass spectrometry analysis could represent a strategy which could be employed by future studies.

1.4 The role of the Cyclops N-terminus

It has been proposed that the main function of the Cyclops N-terminus ($Cyclops^{1-255}$) is the inhibition of Cyclops function, which is released upon phosphorylation of S50 and S154 (Singh et al., 2014). However, in this study we have demonstrated that an increased number of phosphomimetic replacements in $Cyclops^{1-255}$ correlates with an increased activity of this Cyclops fragment in both yeast and *N. benthamiana* (Figure 14). Our data therefore indicate the phosphorylation level of $Cyclops^{1-255}$ positively contributes to Cyclops activity in a phosphorylation status dependent manner, suggesting that the N-terminus of Cyclops can function as an additional and inducible AD. ADs can in principle bear four characteristics: they can be glutamine (Q) rich (containing repeats like QQQXXXQQQ) (Courey et al., 1989), they can be proline (P) rich (containing repeats like PPPXXXPPP) (Mermod et al., 1989), they can be isoleucine (I) rich (containing repeats like IIXXII) (Attardi and Tjian, 1993), or they can contain acidic domains (rich in aspartic acid or glutamic acid) (Sadowski et al., 1988). Acidic ADs are often found to harbour amphipathic α-helices, in which negatively charged residues are exposed to the outside surface of the protein and hydrophobic residues are buried towards the inside of the protein (Hunter and Karin, 1992). It was previously proposed that transcription factor phosphorylation can potentiate the activation capacity of α-helices containing ADs, due to an increase in the net negative charge (Ptashne, 1988). Interestingly, in $Cyclops^{1-255}$ there are two coiled-coil forming α-helices predicted (Figure 5A) (Singh et al., 2014), making this mechanism a possible scenario for the transactivation function of the Cyclops N-terminus.

In both yeast and *N. benthamiana*, Cyclops$^{1\text{-}255\ 5D}$ and Cyclops$^{1\text{-}255\ Nphos}$ mediated *UAS*-responsive reporter expression to similar levels as Cyclops$^{1\text{-}255\ 9D}$ and Cyclops$^{1\text{-}255\ 10D}$, in both yeast and *N. benthamiana* (Figure 14). This indicates that phosphorylation of the N-terminus promotes a switch-like behaviour for its transactivation function as discussed earlier. However, this is not clearly reflected in nodule numbers in complemented *ccamk-13* plants (Figure 10). Interestingly, there was a small discrepancy in *UAS*-responsive reporter expression mediated by the N-terminal fragment of Cyclops^{DD} between yeast and *N. benthamiana*. Whereas Cyclops^{DD} activated reporter expression in yeast to levels comparable to Gal4^{BD}-Cyclops^{FL}, it did not in *N. benthamiana* (Figure 14). This could indicate that the transactivation function of Cyclops$^{1\text{-}255}$ is regulated by additional factors, *in planta*.

Acidic ADs of yeast or human transcription factors have been demonstrated to interact with general co-activators of transcription, including TATA-binding protein (TBP)-associated factors (TAFs) (Uesugi et al., 1997), mediator of RNA polymerase II transcription subunit 15 (MED15) (Jedidi et al., 2010) and members of the p300-CREB-binding protein (CBP) coactivator family (Teufel et al., 2007). Although interaction with the basic transcriptional machinery has been suggested for the previously mapped AD of Cyclops (Singh et al., 2014), the transactivation function in yeast suggest that the same could be the case for the N-terminal fragment of Cyclops. Interestingly, recent work reported on the identification of the putative mediator complex protein *Lack of Symbiont Accommodation* (*LAN*), which is involved in the rhizobial infection process (Suzaki et al., 2019). *LAN* is a putative orthologue of *MED2* from *A. thaliana*, which is proposed to be a component of the mediator complex (Suzaki et al., 2019). However, neither LAN nor additional mediator complex proteins interacted with Cyclops^{WT} or Cyclops^{5D} in Y2H experiments (data not shown). At least for LAN the lack of interaction with Cyclops supports the proposition that both proteins act in parallel pathways (Suzaki et al., 2019), and further studies are required to proof that Cyclops is directly interacting with general co-activator components in a phosphorylation dependent manner.

1.5 A comparison to other phosphomimetic Cyclops versions

Previous work has identified and characterized *in vitro* phosphorylation sites of IPD3 (Jin et al., 2018). However, those results contrast with the observations made in this study, since the multi-phosphomimetic versions of IPD3 tested by Jin and colleagues (2018) were less active in RNS marker gene expression and nodule

formation, compared to IPD3^{2D}. Although the sites investigated in both studies located to the N-terminal half of Cyclops/IPD3, there is only a partial overlap. Out of the 14 phosphomimetic sites investigated here and the 8 phosphomimetic sites investigated by Jin and colleagues (2018), only 5 sites are identical (Table 1). S50 and S154 are included in those 5 sites. Amongst the remaining 3 overlapping sites, S80 and S87 located to a region that did not have an effect in the phosphoablative mapping experiments performed here (Cyclops^{m3}, Figure 5B). Hence, the experimental design used here presumably missed the inhibitory function of S80 and S87. Overall, the observations made in these two studies indicate that Cyclops phosphorylation may not only have an activating, but also an inhibitory effect on its activity. Activating and inhibitory phosphorylation sites have been shown in a single transcription factor before. The human Heat Shock Factor 1 (HSF1) is phosphorylated by Ca^{2+} Dependent Protein Kinase II (CDPKII) in response to stress and phosphorylation of S303, S307 and S363 repress its activity, whereas phosphorylation of S230 promotes it (Kline and Morimoto, 1997; Holmberg et al., 2001). Overall, the molar ratio of activating and repressing phosphorylation sites of HSF1 modulates its transcriptional output and the cumulative data on the function of its phosphorylation sites suggests the same for Cyclops.

2 Cyclops phosphorylation could modulate the interaction with CCaMK

We employed our new phosphomimetic versions at hand as a starting point to investigate the influence of Cyclops phosphorylation on the interaction with CCaMK. Based on phosphomimetic and phosphoablative substitutions we gathered indications that the phosphorylation state of Cyclops^{S236} strongly influences the interaction with CCaMK, at least in yeast (Figure 16C, Figure 17B): The lack of interaction between CCaMK and Cyclops^{S236D} in Y2H experiments indicated that phosphorylation at this residue could block the interaction with CCaMK, whereas the interaction between Cyclops^{S236A} with CCaMK or CCaMK^{T265D} indicated that unphosphorylated S236 could promote the interaction with CCaMK (Figure 17B). Alternatively, it cannot be excluded that there is an overaccumulation of Cyclops^{S236A}, leading to an increased reporter gene expression. Although this has not been observed for Cyclops^{S236A} in *N. benthamiana* (Figure 6C), western blot analyses in yeast are required to exclude this possibility. Even though multiple S236D-containing versions of Cyclops were shown to be active in transactivation assays in *N. benthamiana* and it can therefore be assumed

that those protein were present in the leave cells, the same experimental approach should be taken to confirm the presence of Cyclops^{S236D} in yeast cells.

Interestingly, the phosphomimetic mutation CCaMK^{T265D} influenced the interaction strength with Cyclops as well, as observed from an increased reporter expression when Cyclops interacted with CCaMK^{T265D} compared to CCaMK (Figure 17B). The function of CCaMK has been under thorough investigations. Autophosphorylation of CCaMK at S343 and S344 leads to the repulsion of CaM, and could therefore represent the first step of CCaMK deactivation during or after Ca^{2+} spiking (Liao et al., 2012; Miller et al., 2013). Interestingly, it was demonstrated that CCaMK autophosphorylation is increased in the presence of non-interacting substrates like MBP, as compared to an interacting substrate like Cyclops (Liao et al., 2012). The results presented here on non-interacting phosphomimetic verions of Cyclops could indicate that Cyclops is released from CCaMK upon phosphorylation of S236, ultimately leading to increased CCaMK autophosphorylation and subsequent kinase deactivation. Interestingly, an increased interaction between CCaMK^{T265D} and Cyclops (Figure 17B) could indicate that its phosphorylation not only leads to repulsion of Cyclops but could also increase interaction with CCaMK. However, substrate phosphorylation activity of CCaMK^{T265D} in yeast remains to be demonstrated. Alternatively, increased interaction between Cyclops and CCaMK^{T265D} could also be due to conformational changes of CCaMK, which have been proposed upon mutation of T265 (Miller et al., 2013). In FLIM-FRET experiments in *N. benthamiana* nuclei there were no FLT differences of GFP in Cyclops^{WT}/CCaMK^{NFG} complexes compared to Cyclops^{S236D}/CCaMK^{NFG} complexes and there was an increase in the FLT of GFP in Cyclops^{S236A}/CCaMK^{T265D} complexes compared to Cyclops^{WT}/CCaMK^{T265D} complexes (Figure 17C). Hence, these results did not reflect the results obtained in Y2H experiments. Interestingly, the protein accumulation of CCaMK kinase mutants was demonstrated to be decreased compared to wildtype CCaMK in *L. japonicus* hairy root experiments (Shimoda et al., 2019). It is therefore advisable to repeat the interaction studies of Cyclops^{S236D} with wildtype CCaMK, to ensure sufficient abundance of the mCherry FRET acceptor proteins in *N. benthamiana*. The observed discrepancies between Y2H and FLIM-FRET experiments could also be due to additional plant factors that are not present in yeast and thorough investigation of the interaction between Cyclops phosphosite mutants and CCaMK have to be conducted, using additional methods including Co-IP and/or pulldown experiments. Although with limitations, the observations made in this study are first indications that the phosphorylation status of Cyclops could serve

as a "molecular timer" for CCaMK deactivation. Based on the observation that the phosphorylation status modulates its transcriptional activity, this implies the existence of consecutive phosphorylation events. Only upon achievement of a phosphorylation status that is sufficient for appropriate target gene expression, Cyclops is released from CCaMK through phosphorylation of S236. A 100% phylogenetic conservation of S236 amongst the species analysed in this study (Figure 4) indicates that this mechanism may not only function in *L. japonicus*, but in root endosymbiosis forming species in general.

The basis of consecutive phosphorylation events could be different phosphorylation rates of individual amino acids. For the mouse transcription factor Elk-1 this has been demonstrated (Mylona et al., 2016). Elk-1 is phosphorylated by ERK2 and sites that are phosphorylated at fast rates promote the interaction of Elk-1 with components of the mediator complex, whereas sites that are phosphorylated at slower rates block its interaction with mediator components. In contrast to CCaMK, there are no detailed biochemical investigations on the mechanistic events of Cyclops phosphorylation. Similar to Mylona and colleagues (2016), a Nuclear Magnetic Resonance (NMR) spectroscopy approach could be taken, to greatly improve the knowledge on how exactly Cyclops is phosphorylated by CCaMK in order to regulate its functions and interactions with other proteins.

Apart from CCaMK, multiple studies identified proteins that are directly or indirectly interacting with Cyclops (Figure 2). Based on biochemical experiments and interaction studies in yeast, Jin and colleagues (2016) proposed that the phosphorylation of Cyclops increases its interaction with DELLA and the presence of DELLA increases the interaction between CCaMK and Cyclops. Based on the observations that DELLAs interact with additional symbiosis related transcriptional regulators like NSP2, a model was suggested in which DELLA proteins serve as bridging factors between the CCaMK/Cyclops complex and NPS2 (Jin et al., 2016). Due to the interaction between NSP2 and NSP1 and the proposed DNA-binding properties of NSP1 (Hirsch et al., 2009), DELLA proteins could therefore promote cooperative promoter binding to regulate symbiotic gene expression. However, in this study we demonstrated that an increased phosphomimetic status of Cyclops$^{1\text{-}255}$ is sufficient to promote gene expression in yeast on its own. Therefore, the interplay between the influence of phosphorylation on transcriptional factor activity and DELLA interaction remains to be entangled. Currently it cannot be excluded that both mechanisms exist in

parallel, as the Cyclops interaction domains with DELLA and/or components of the basal transcriptional machinery have not been determined yet.

3 Complementation of the *ccamk-13* and *cyclops-3* mutants with phosphomimetic versions of Cyclops

Inoculation of *ccamk-13* plants that were complemented with higher-order phosphomimetic versions of Cyclops resulted in the presence of *Ds*Red-expressing *M. loti* in the apoplast of nodules (Figure 11). However, IT formation and intracellular presence of *M. loti* cells was not observed. Furthermore, complemented *ccamk-13* plants did not form arbuscules upon inoculation with AMF (Figure 10B). In complemented *cyclops-3* plants the transformation of phosphomimetic Cyclops versions resulted in the formation of infected and uninfected nodules (Figure 13). However, except for Cyclops^{5D} the number of infected nodules was reduced compared to Cyclops^{WT} and Cyclops^{DD} transformed plants.

As previously discussed, there are no differences in calcium signatures in epidermal cells during the infection by rhizobia or AMF (Sieberer et al., 2009). However, cell-type specific differences in calcium spiking frequency have been observed. Symbiont containing cells display high frequency calcium spiking, whereas symbiont anticipating cells or cells adjacent to symbiont containing cells display low frequency spiking (Sieberer et al., 2012). These observations suggest that CCaMK and Cyclops are only activated in specific cells and that this activation happens successively in different cell types, following the infection progress of the symbiont.

The importance of a tight spatiotemporal regulation during the expression of symbiotic players is exemplified by the Cyclops target gene *NIN*. In the *L. japonicus daphne* mutant a chromosomal translocation perturbs the *NIN* promoter 7 kb upstream of the transcriptional start site (TSS), resulting in loss of nodulation, a hyperinfection phenotype and an increased epidermal expression area of *NIN* compared to wildtype plants (Yoro et al., 2014). Cortex specific expression and grafting experiments including the *daphne* and the hypernodulating *har1* mutants revealed that the cortical expression of *NIN* acts inhibitory on IT formation, in a local and systemic manner (Yoro et al., 2019). The isolation of a *daphne-like* mutant in *M. truncatula* further suggests that *NIN* expression in the cortex and nodulation may be controlled by a cytokinin responsive element (*CE*) that is located approximately 18 kb upstream of the TSS (Liu et al., 2019c). Interestingly,

simultaneous expression of *NIN* in cortex and epidermis mediated by CCaMK$^{1\text{-}314,\ T265D}$ does not complement the *ccamk-3* mutant for rhizobial infection (Takeda et al., 2012). Taken together, these results suggest that the initiation of *NIN* expression in the epidermis by Cyclops, followed by a cytokinin-dependent cortical expression is crucial for successful RNS establishment. Due to their irreversible nature, it is likely that phosphomimetic versions of Cyclops are constitutively active in all *Cyclops*-expressing cells. Hence, they are not able to mimic the delicate spatiotemporal expression of its target genes, resulting in incomplete complementation of at least the *ccamk* and *cyclops* mutants.

If not via ITs, how could *M.loti* cells enter nodules formed on complemented *ccamk-13 plants*? Alternative to infection via root hair, nodules can be colonized by rhizobia via natural cracks in the root epidermis (Sprent and James, 2007). Those cracks predominantly occur at sites of lateral root organ formation, as epidermal cell layers are "pushed aside" by the newly formed structure which is emerging from the root cortex or pericycle. At this stage, it cannot be excluded that rhizobia entered those nodules via cracks in the root surface and a more detailed microscopic investigation has to be conducted to follow the infection mode of rhizobia into *cyclops-3* plants expressing *Cyclops* versions with phosphomimetic mutations.

4 A potential model for the functions of Cyclops phosphorylation

Although with limitations, the data obtained in this study together with observations from previous reports allow the construction of a working model for the functions of Cyclops phosphorylation (Figure 18). Cyclops phosphorylated at S50 and S154 is present in the nucleus under non-symbiotic conditions and the interaction between CCaMK and Cyclops^{DD} suggests those two proteins form a complex that is assembled prior to the onset of symbiotic signalling (Singh et al., 2014). This is confirmed by FLIM-FRET measurements in *L. japonicus* root hair cells (Chloe Cathebras, unpublished). Biochemical data from EMSA analyses with Cyclops suggest that the complex is bound to DNA at this stage (Singh et al., 2014), potentially mediating a low-level expression of *NIN* (Schauser et al., 1999). This is supported by a slight reduction of *NIN* expression in the *cyclops-3* mutant (Singh et al., 2014). Upon symbiont perception, CCaMK is activated by perinuclear Ca^{2+} spiking, resulting in phosphorylation of Cyclops. The data obtained in this study suggest that an increased phosphorylation status of Cyclops results in an increased expression of its target genes. Transactivation assays in yeast suggest that this increase could be mediated via an increased interaction strength with components of the basal transcriptional machinery. Y2H experiments furthermore indicate that phosphorylation of S236 could subsequently block the interaction between Cyclops and CCaMK, which could lead to the onset of CCaMK deactivation. Although it is likely that phosphorylation of S236 is one of the last phosphorylation events on Cyclops, it is currently not possible to deduce if the release of CCaMK or the potential interaction with basal transcriptional machinery components comes first.

Overall, phosphorylation appears to have complex regulatory effects on Cyclops. Due to the identification of multiple sites *in vivo* and *in vitro*, the exact mechanistic interplay of those sites and the determination of the role of individual sites pose a big challenge. This work has partially decrypted the function of some of those sites. However, stringent evidence on the biological role of those sites *in planta* remains to be accumulated.

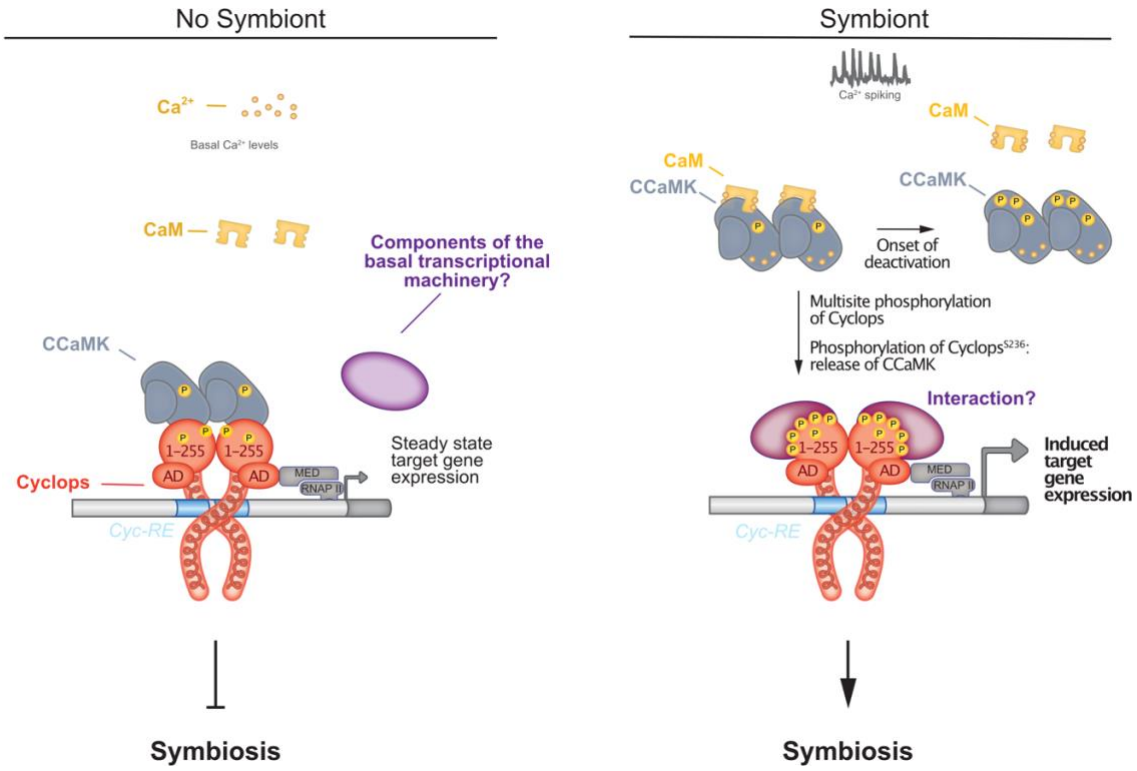

Figure 18: A hypothetical model for the regulation of Cyclops and CCaMK by phosphorylation.
Under non-symbiotic conditions, Cyclops phosphorylated at positions S50 and S154 resides at the DNA of its target promoters (Grimsrud et al., 2010, Singh et al., 2014, Pimprikar et al., 2016, Emmanoulis Bastakis, unpublished), interacting with CCaMK. A low level expression of symbiotic Cyclops target genes (Schauser et al., 1999) is insuficient to establish symbiosis. In presence of symbiont, Ca^{2+}- and CaM-activated CCaMK phosphorylates Cyclops. The highly phosphorlyated N-terminal part of Cyclops (aa 1-255) may interact with components of the basal transcriptional machinery, ultimately inducing full target gene expression leading to symboisis establishment. CCaMK is released from Cyclops upon phosphorylation of S236. Model does not display exact temporal events and simultaneous interaction of Cyclops with CCaMK and components of the basal transcriptional machinery cannot be excluded. MED: previously proposed mediator complex components that interact with a mapped Cyclops AD and the RNA polymerase II (RNAP II) (Singh et al., 2014). Not depicted: interaction between Cyclops and DELLA.

IX Materials and Methods

1 Plant media and solutions

1.1 Nodulation FAB

Component	Concentration [µM]
$MgSO_4$ *$7H_2O$	500
KH_2PO_4	250
KCl	250
$CaCl_2$ *H_2O	250
KNO_3	100
FE-EDDHA	25
H_3BO_3	50
$MnSO_4$ *H_2O	25
$ZnSO_4$*$7H_2O$	10
Na_2MoO_4 *$2H_2O$	0.50
$CuSO_4$ *$5H_2O$	0.20
$CoCl_2$ *$6H_20$	0.20
MES-KOH buffer pH 5.7	2

1.2 ¼ strength Hoagland medium

Component	Concentration [mM]
KH_2PO_4	1
KNO_3	5
$Ca(NO_3)_2$ x $4H_2O$	5
$MgSO_4$ x $7H_2O$	2
Microelement stock (1000x)	1x
Chelated iron stock solution (200x)	0.2
pH	Adjust to 5.8 with KOH

1.3 1000x microelement stock for Hoagland medium

Component	Amount
H_3BO_3	2.86 g
$MnCl_2$ x $4H_2O$	1.81 g
$ZnSO_4$ x $7H_2O$	0.22 g
$CuSO_4$ x $5H_2O$	0.08 g
Na_2MoO_4 x $2H_2O$	0.025 g
$CoCl_2$ x $6H_2O$	0.025 g
ddH_2O	To 1 l

1.4 200x chelated iron stock solution for Hoagland medium

Component	Amount
$FeSO_4$ x $7H_2O$	5.56
Na_2-EDTA	7.45
ddH_2O	To 1 l

1.5 1x B5 medium

Component	Amount
m-inositol	100 mg
Pyridoxine HCl	1 g
Nicotinic acid	1 g
Thiamine	10 g
ddH_2O	To 1 l
Sterile filtrate	0.45 μm filter

1.6 Infiltration mix *N. benthamiana* transformation

Component	Concentration [mM]
MES-KOH pH 5.6	10
$MgCl_2$	10
Acetosyringon	0.15

2 Bacterial media and solutions

2.1 LB medium

Component	Amount
Bacto Tryptone	10 g
Bacto Yeast Extract	5 g
NaCl	10 g
Bacto agar (only for plates)	15 g
ddH_2O	To 1 l

2.2 TY medium

Component	Amount
Bacto Tryptone	5 g
Bacto Yeast Extract	3 g
Bacto agar (only for plates)	15 g
ddH_2O	To 1 l

2.3 SOC medium

Component	Amount
Bacto Tryptone	20 g
Bacto Yeast Extract	5 g
NaCl	0.5
KCl	0.186 g
$MgCl_2$	0.952 g
$MgSO_4$	1.204 g
Glucose	3.603 g
ddH_2O	To 1 l

3 Yeast media and solutions

3.1 YPAD medium

Component	Amount
Yeast Extract	10 g
Peptone	10 g
Adenine	80 mg
Bacto agar (only for plates)	20 g
20% autoclaved Glucose	100 ml
ddH_2O	To 1 l

3.2 SD medium

Component	Amount
Yeast nitrogen base	6.7 g
Dropout powder (-LWAHU)	1.6 g
Leu (0.5 g/50 ml ddH_2O)	10 ml
Try (0.5 g/50 ml ddH_2O)	2 ml
Ala	80 mg
His (0.5 g/50 ml ddH_2O)	2 ml
Bacto agar	20 g
20% autoclaved glucose	100 ml
ddH_2O	To 1 l
pH	Adjust to 5.8 - 6 with KOH

3.3 Yeast transformation mix

Component	Amount for 1 transformation
Filtrated PEG 3350 (50% w/v)	240 µl
Filtrated LiAc (1M)	36 µl
Boiled salmon sperm DNA (2mg/ml)	50 µl

3.4 Yeast dropout powder mix –LWAHU

Component	MW [g/mol]	Amount in mix [g]	Final µM in solution
Arginine	174.2	1	0.50350
Asparagine	132.1	1	0.66403
Aspartic Acid	133.1	1	0.65904
Cysteine	121.2	1	0.7237
Glutamine	147.1	1	0.59632
Glutamic Acid	146.2	1	0.59999
Glycine	75.1	1	1.16803
myo-Inositole	180.16	1	0.48689
Isoleucine	131.16	1	0.66859
Lysine	146.2	1	0.59999
Methionine	149.2	1	0.58793
para-Amaminobenzoic acid	137.14	0.1	0.06396
Phenylalanine	164.2	1	0.53098
Proline	115.1	1	0.76211
Serine	105.1	1	0.83462
Threonine	119.1	1	0.73651
Tyrosine	181.2	1	0.48410
Valine	117.1	1	0.74909

4 Plant lines used

Line	Ecotype	Genotype	Progenitor	Seedbag Number	Reference
Wild type	Gifu B-129	wildtype		111212, 111204, 111217, 111219	
ccamk-13	Gifu	homozygous	cac57.9	111570, 91262,	Perry et al., 2009
cyclops-3	Gifu	homozygous	EMS126 line	111560	Perry et al., 2009

5 Bacterial strains used

Strain	Reference
Agrobacterium tumefaciens GV3101	(Holsters et al., 1980)
Agrobacterium tumefaciens AGL1	(Lazo et al., 1991)
Agrobacterium rhizogenes AR1193	(Stougaard et al., 1987)
Mesorhizobium loti MAFF303099 *Ds*RED	(Maekawa et al., 2009)
Escherichia coli TOP10	Invitrogen

6 Yeast strains used

Strain	Genotype	Auxotrophies	Reference
Y8800-*GAL2*$_{pro}^{AH109}$*:Luciferase*	*MATa* leu2-3,112 trp1-901 his3-200 Gal2^{AH109}-LUC gal4Δ gal80Δ GAL2-ADE2 LYS2::GAL1-HIS3 MET2::GAL7-lacZ cyh2^{R}	Leu, Trp, His, Ade	Gift by Dr. David Chiasson

7 Transformation protocols

7.1 *E. coli*

Chemically competent *E. coli* TOP10 cells were stored at -80°C, in 15% glycerol. For transformation cells were thawed on ice, for 5 min. 50 µl of cells were transferred into a 1.5 ml reaction tube. 1 µl of plasmid or 5 µl of cut-ligation reaction was added and mixed by gentle flicking. Cells were incubated on ice for 2-5 minutes, prior to a heat shock at 42°C for 40-60 s. Cells were transferred to ice and incubated for 5 min. 600 µl of LB medium was added and cells were incubated at 37°C for 45-60 min, under continuous shaking at 180 rpm. 10 µl to all cells were plated onto LB plates containing the required antibiotic as selection marker and incubated at 37°C, overnight. Integrity of the transformed plasmid was tested by colony PCR or plasmid isolation followed by restriction digest.

7.2 *Agrobacterium*

Electrocompetent *A. rhizogenes* AR1193 or *A. tumefaciens* AGL1/GV3101 cells were stored at -80°C, in 10% glycerol. Cells were thawed on ice for 10 min. 20 µl of cells were transferred into 1.5 ml reaction tubes and kept on ice. 1 µl of plasmid DNA was added and mixed by gentle pipetting. Cells were transferred into an electroporation cuvette. Cuvette was gently tapped onto the work bench, prior to electroporation. Cells were transformed with the BIORAD MicroPulser™, using the program EC1. After the electro pulse, cells were immediately retrieved from the cuvette, by adding 200 µl SOC medium into the cuvette and pipetting up and down. Cells were transferred into a 2 ml reaction tube, containing 1 ml SOC medium. After an incubation of 2 h at 28°C and continuous shaking at 180 rpm, 10 µl of cells were plated onto LB plates containing the required antibiotics combination as selection marker for successful transformation. Plates were closed with parafilm and incubated at 28°C, for 2-3 days.

7.3 Yeast

Yeast strains were stored in 25% glycerol at -80°C. For usage, strains were streaked onto YPAD plates and grown at 28°C, for 2-3 days. For transformation, strains on plate were inoculated into 3 ml liquid YPAD medium using an inoculation needle and grown over night at 28°C, under continuous shaking at 180 rpm. In the morning OD_{600} was determined using a photo spectrometer. For 10 transformations a total volume of 50 ml YPAD was inoculated at an OD_{600} of 0.15. Yeast cells were grown in a 200 ml Erlenmeyer flask at 28°C for 4 h, under continuous shaking at 180 rpm. Cells were pelleted at 4000 g, for 7 min. YPAD was decanted and the pellet was washed with sterile ddH_2O, by vigorous vortexing. This was repeated two times. Pellet was resuspended in 1 ml ddH_2O and transferred to a 1.5 ml reaction tube. Cells were pelleted at 13000 g, for 30 s. Supernatant was removed using a pipet and pellet was resuspended in 0.5 ml ddH_2O. For each transformation, 50 µl of cells were aliquoted into 1.5 ml reaction tubes, containing 200 ng per plasmid (400 ng total amount for double transformation). 310 µl of cold transformation mix was added followed by immediate vortexing. Cells were incubated at RT for 15 min, followed by an incubation of 30 min at 42°C. Cells were pelleted at 13000 g for 30 s. Supernatant was removed with a pipet and cells were resuspended in 1 ml of sterile ddH_2O. 200 µl were plated onto synthetic dropout (SD) medium lacking Leu, Try, or both. Cells were grown at 28°C for 2-3 days. Individual colonies were re-streaked onto a fresh SD plate and grown at 28°C for 2-3 days again and kept at 4°C for long term storage.

7.4 *L. japonicus* hairy root transformation

L. japonicus seeds were scratched in a mortar using sandpaper. Seeds were transferred into 2 ml reaction tubes, submerged in 1 ml sterilisation solution (1.2 % NaOCl, 0.1% SDS) and incubated for 6 min on a rotation wheel. Seeds were washed with a minimum volume of 100 ml sterile ddH_2O and incubated on a rotation wheel at RT, for at least 2 h. Alternatively, incubation of seeds was performed on a rotation wheel overnight, at 4°C. Swollen seeds were plated onto 0.8% water-agar and incubated in dark for 2 days. Seeds were transferred to light and incubated for another 4 days. In parallel, *A. rhizogenes* strains AR1193 harbouring the required LIII expression plasmids were streaked from glycerol stocks (25 % glycerol, stored at -80°C) onto LB plates supplemented with respective antibiotics. After incubation at 28°C for 3 days, a small amount of bacterial culture was resuspended in 200 µl liquid LB medium. Bacterial suspension was plated uniformly onto fresh LB plates and incubated at 28°C for 1 day. For hairy root transformation, bacteria were scraped from LB plates using a bent Pasteur glass pipet and resuspended in 5-7 ml sterile ddH_2O. Bacterial suspension was transferred to a sterile square petri dish. *L. japonicus* seedling were cut at the hypocotyl region using a sterile scalpel. After cutting, seedlings were dipped into bacterial suspension and transferred to 1x B5 plates lacking sucrose. Plates were closed with Parafilm. At the top facing side of the plates, Parafilm was cut open with a scalpel and closed again with Micropore tape (3M). Plates were incubated in the dark for 3 days, at approximately 20°C. Plates were transferred to light and incubated for 4 days. 7 days post transformation, seedlings were transferred to B5 plates containing 2% sucrose and 300 µg/ml cefotaxime. Plants were grown on B5 plates with sucrose and cefotaxime for 4 additional weeks. During this time plants were shifted onto fresh B5 plates 1-2 times per week. Before transfer to Weck jars, plants were screened for nuclear GFP signal indicating successful transformation, using a stereo microscope. Non-transformed plants were discarded. Light refers to long day light conditions with cycles of 16 h light and 8 h dark, at 24°C.

7.5 Transient transformation of *N. benthamiana* leaf tissue

A. tumefaciens strains AGL1 or GV3101 containing binary vectors required for individual experiments were streaked from glycerol stocks (25% glycerol, -80°C) onto LB plates, containing the required antibiotic combination. For vectors used see experiments. For detailed description of vectors see 19.2 and 19.3. Bacteria were grown at 28°C, for 3 days. 24 h before infiltration, bacteria were inoculated in liquid LB medium and incubated at 28°C, 180 rpm. Bacterial cultures were transferred to

50 ml Falcon tubes and pelleted at 4347 g, 15 min. LB medium was decanted thoroughly. Pellet was resuspended in 1 ml infiltration mix by tapping on the bench and vigorous vortexing. OD_{600} was determined using a photospectrometer. Bacterial suspensions were diluted to an OD of 1 in infiltration mix. Based on a pre-defined infiltration scheme, bacterial suspensions were mixed yielding a total OD of 1, with individual ODs of 0.25. Mixture was incubated in the dark for 1.5 h, prior to infiltration. Counting from the youngest emerging leaf, leaves 5 and 6 of 14 days old *N. benthamiana* plants were infiltrated with approximately 1 ml bacterial mixture per leaf, using a 1 ml syringe. Per condition, two plants were used. Plants were grown for 48 h in cycles of 16h light and 8 h dark, at 24°C and were used for transactivation assays, Western Blot, FLIM-FRET imaging or RNA extraction.

8 Root Nodule Symbiosis assay

For nodulation assays, *M. loti* MAFF 303099 expressing *Ds*Red were streaked from glycerol stock (25% glycerol at -80°C) onto TY agar plates, supplemented with gentamycin (12.5 µg/ml) and $CaCl_2$ (6 mM). Bacteria were grown at 28°C, for 3 days. 50 ml of liquid TY medium was inoculated with bacteria and grown at 28°C, for 2-3 days. Bacterial culture was transferred to a 50 ml Falcon tube and pelleted at 4347 g, for 10 min. Supernatant was decanted and pellet was resuspended in 10 ml Nodulation FAB. Centrifugation and resuspension were repeated 2 times. Pellet was resuspended in 1 ml Nodulation FAB and OD600 was determined. Bacteria were diluted to an OD of 0.05 in Nodulation FAB. 40 ml of this dilution were pipetted into Weck jars, pre-filled with 300 g of sterile sand-vermiculite mixture (1:2). Bacteria were evenly distributed by thorough stirring with a large forceps. 10-12 plants with transformed root systems were transplanted from B5 plates into the prepared Weck jars (5 weeks post hairy root transformation). Jars were closed with 1 layer of micropore tape. Plants were grown in long day conditions (16 h light, 8 h dark), at 24°C, for 2 weeks. Infection thread as well as nodule formation was scored using a stereo microscope.

9 Arbuscular Mycorrhiza Symbiosis assay

Arbuscular Mycorrhiza development was tested with the fungus *Rhizophagus irregularis*. For fungal infection of *L. japonicus* plants the chive (*Allium schoenoprasum*) nursing pot system was used (Demchenko et al., 2004). Prior to *L. japonicus* transfer chive nursing plants were cut below the stem using a scissor or

scalpel. A sterile sand-vermiculite mixture (1:2) was used as substrate. Plants were watered with twelfth strength Hoagland medium, 2 times per week. 2 weeks post co-cultivation, root systems were subjected to Black Ink staining to visualize arbuscular mycorrhiza development. Black Ink stained root systems were mounted on a glass slide and visually inspected for presence or absence of arbuscules.

10 Transactivation assays in *N. benthamiana*

Tobacco plants were infiltrated and harvested according to 7.5. To test *GUS* expression the binary vectors *pBI101-pNIN870:GUS* (Singh et al., 2014), *LIIβF A-B pRAM1:GUS* (Pimprikar et al., 2016) *5xUAS$_{Gal4}$:eGFP-GUS* (Weijers et al., 2003) were co-infiltrated with phosphosite mutants of *HA-Cyclops*, *Myc-CCaMK^{T265D}*, *Myc-CCaMK$^{1-314}$*, an EV (HA-tag) control, Gal4^{BD}-Cyclops^{FL}, phosphomimetic versions of Gal4^{BD}-Cyclops^{N}, Gal4^{BD}-CCaMK. For combinations used and detailed description of constructs used see experiments and 19.3 and 0. Leaf discs were harvested using a tissue puncher (7 mm diameter). Leaf discs were placed into deepwell plates floating on liquid nitrogen, containing 6-8 glass beads (2.6 mm diameter) per well. Deepwell plates were closed thoroughly with rubber lids. Leaf discs were pulverised using a Retsch mill (30 Hz, 45 s, 2 repetitions). Leaf powder was spun down (3220 g, 1 min) and 350 µl extraction buffer (50 mM NaPi buffer pH 7, 10 mM ß-mercaptoethanol, 10 mM Na_2-EDTA pH 8, 0.1 % Triton-X100, 0.1 % N-laurylsarcosine, 1x PPIC) was added per well. Plates were closed again with a rubber lid, kept on ice and occasionally inverted until extraction buffer turned liquid. Plates were centrifuged at 3220 g, 30 min, 4°C. A 96 well PCR plate was filled with 100 µl of GUS buffer (50 mM NaPi buffer pH 7, 10 mM β-mercaptoethanol, 10 mM Na_2-EDTA pH 8, 0.1 % Triton-X100, 0.1 % N-laurylsarcosine, 1 mM 4-methylumbelliferyl glucuronide) per well and pre-heated at 37°C. From the supernatant of the protein extracts, 10 µl of per well was transferred into 100 µl GUS buffer. Reaction was incubated for 20 min, at 37°C, in a 96 well heat block. Reaction was stopped by transferring 10 µl per well to a black 96 well plate, pre-filled with 100 µl of 0.2 M Na_2CO_3 per well. Plates were covered with aluminium foil until measurement. For quantification of protein content, 1 µl of the supernatant from the protein extract was transferred into transparent 96 well plates, pre-filled with 100 µl of Bradford solution (dilution of 1:5 in ddH_2O). 4-methylumbelliferone (4-MU) production was determined in a TECAN plate reader (shaking: 3 s with a linear amplitude of 3 mm, excitation wavelength: 360 nm, emission wavelength: 450 nm, gain: 50, integration time: 40 µs, 25 flashes). Protein

amount was determined in a TECAN plate reader (shaking: 3 s with a linear amplitude of 3 mm, absorbance: 595 nm, 25 flashes). For quantification a 4-MU standard curve with following µM concentrations was used: 0.5, 1. 10, 25, 50, 100, 500, 1000. 4-MU standard curve was prepared in extraction buffer. A 4-MU stock of 10 mM in ddH_2O was kept at -20°C for long time storage. For protein quantification a BSA standard curve with following µg/µl concentrations was used: 0, 0.125, 0.25, 0.5, 0.75, 1.0, 1.5, 2. BSA standard curve was prepared in extraction buffer. A working stock solution of 2 mg/ml in extraction buffer was stored at -20°C. Data evaluation was done with Microsoft Excel.

11 SDS-PAGE and Western Blot

Protein extracts were mixed with 4x SDS loading dye (0.125 mM TRIS-HCl pH 6.8, 7 % SDS, 40 % glycerol, 0.3 g DTT, dash of bromphenol blue) and boiled 95°C, for 5 min. 12-15 µl of samples was loaded onto a polyacrylamide gel. Polyacrylamide gel consisted of a 5 % stacking gel and a 12 % separation gel. Gel was prepared according to the guideline of the Cold Spring Harbour Laboratory Press protocol. PAGE was performed in 1x SDS running buffer (3 g/l TRIS, 14.4 g/l glycine, 1 g/l SDS) using a Hoefer Mighty Small II Vertical Protein Electrophoresis unit. Samples were separated at 50 V for 15 min followed by 150 V for 90 min, or until the front marker lane had exited the gel. Protein transfer to a PVDF (GE Healthcare) membrane was performed in 1x transfer buffer (3 g/l TRIS, 14.4 g/l glycine, pH 8.3 with HCl) at 30 V, 4°C, overnight using a BIORAD wet blotting system. After transfer membranes were transferred to 50 ml amber Falcon tubes. Membranes transferred to a rolling shaker and blocked with 5 % skim milk powder in 1x PBS (pH 7.4) at 4°C, for 8 h. Blocking solution was removed and membranes were washed with PBS, 4x. Membranes were incubated with primary antibodies on a rolling shaker at 4°C, overnight. α-HA (Roche 3F10, rat) was used at a concentration of 1:1000 and α-Myc (Santa-Cruz 9E10, mouse) was used at a concentration of 1:3000. Both primary antibodies were diluted in PBS-T 0.1 % (PBS + 0.1 % Tween 20). Membranes were washed with 10 ml PBS-T 0.2%, for 4x 5 min. Incubation with secondary antibodies was performed on a rolling shaker at RT. Secondary antibodies were diluted to 1:15000 in PBS-T 0.1%, supplemented with 1% skim milk powder and 0.02 % SDS. IRDye680 (α-rat, LICOR) and IRDye800 (α-mouse, LICOR) were used. Image acquisition was performed with an Odyssey scanner (LICOR).

12 Black Ink staining

Plants were harvested and cut at the hypocotyl region. Root systems were transferred to 2 ml or 5 ml reaction tubes, dependent on root system size. Roots were submerged in 10 % KOH. Tubes were transferred to 95°C and incubated for 15 min, or to 60°C for overnight incubation. In case of strong coloration of the KOH solution it was removed and replaced by fresh KOH. Second incubation was performed at 60°C, for 3-4 h. Root systems were washed three times with tap water. Root systems were washed once with 10 % acetic acid. After removal of acetic acid root systems were submerged in Black Ink staining solution (5 % Black Ink in 5 % acetic acid) and incubated at 95°C, for 5 min. Staining solution was removed and root systems were washed three times with tap water. Root systems were destained with 5 % acetic acid at RT, for a minimum of 20 min. Material was kept in 5 % acetic acid, at 4°C for long term storage.

13 Formaldehyde fixation

Formaldehyde solution (4 % formaldehyde in 50 Mm PIPES buffer, pH 7) was used for fixation of entire transgenic root systems or individual nodules. Plant material was harvested into 50 ml Falcon tubes or 2 ml reaction tubes. Plant material was covered with fixation solution and vacuum infiltrated for 5-7 min, using a desiccator connected to an air pump. Infiltration was repeated 3-4 times. In between infiltrations vacuum was released slowly. Samples were stored in fixation solution at 4°C, overnight. Fixation solution was discarded and samples were washed for 3 times with 50 mM PIPES buffer. Samples were kept at 4°C for long term storage.

14 Nodule sections

Nodules were removed from formaldehyde fixed root systems, using a scalpel. Nodules were embedded in 7% low-melt agarose (Roth). Sectioning was performed with a Leica VT100S vibratome, equipped with a razor blade. Nodules were cut into 55 µm thin sections, at a speed and frequency of 5. Sections were mounted onto glass slides and inspected with a Leica upright microscope.

15 Luciferase assay for Y2H

Individual colonies were inoculated in single wells of a sterile 96 deepwell plate, containing 250 µl sterile SD medium per well. For inoculation a yellow pipet tip

was used. Colonies were suspended by pipetting up and down, using a multi-channel pipet. Plate was closed with a rubber lid. Plate was placed in an empty blue pipet tip box, tilted to the front and fixed with sticky tape. Colonies were grown overnight (28°C, 350 rpm). Colonies were quickly spun down (3220 g, 30 s). 100 µl were transferred to a transparent 96 well Sarstedt plate and OD_{600} was determined using a TECAN plate reader (Absorbance at 600 nm, 25 flashes, shake for 3s at 4 mm linear amplitude). Measured values were multiplied by a scaling factor of 12.1. Scaling factor was determined empirically by comparing OD_{600} of an overnight culture measured with a 1 ml cuvette in a photospectrometer, with the OD_{600} of 100 µl of the same culture measured in a TECAN plate reader.

$$Scaling\ Factor = \frac{OD_{600}\ (1\ ml\ photospectrometer\ cuvette)}{OD_{600}\ (100\ \mu l\ TECAN\ plate)}$$

Based on the obtained OD_{600} values, cultures were inoculated in a fresh 96 deepwell plate at an OD of 0.5 and grown at 28°C, 350 rpm. After 4 h, 100 µl were transferred to a transparent 96 well Sarstedt plate and OD_{600} was determined (Absorbance at 600 nm, 25 flashes, shake for 3 s at 4 mm linear amplitude). From the same cultures, 100 µl were transferred to a white 96 well COSTAR plate and used for luminescence measurement. 100 µl luciferin substrate (1 mM D-luciferin in 0.1 M sodium citrate) was injected at following parameters: 3 s shaking at 3 mm linear amplitude, injection speed 200 µl/s, refill speed 200 µl/s. All parameters were applied in a well-wise manner. Luminescence values were normalised to OD_{600} values. Evaluation was done in Microsoft Excel. During the experiment, luciferin substrate was kept in dark at all times. A luciferin stock (100 mM D-luciferin in ddH_2O) was kept at -80°C for long term storage.

16 Spotting assay for Y2H

For spotting assays overnight cultures were grown in the same way like for luciferase assays. OD_{600} was determined and individual cultures were diluted to an OD of 0.5 in ddH_2O. From this, 3 consecutive 10-fold dilutions were generated resulting in ODs 0.5, 0.05, 0.005, 0.0005. 5 µl per dilution were dropped onto SD –LWU as well as SD –LWAHU plates. Yeast growth was evaluated after 48-72 h at 28°C.

17 Plasmid isolation from *E. coli* cells

For plasmid isolation from *E. coli* cells, individual colonies were inoculated in LB medium supplemented with the according antibiotic selection marker, using a

sterile toothpick. Liquid cultures were incubated at 37°C for 5 h or overnight, at continuous shaking at 180 rpm. 2 ml of liquid cultures were transferred to 2 ml reaction tubes and pelleted at 20238 g for 1 min. Supernatant was decanted and pellets were resuspended in 200 µl of cold buffer P1 (50 mM TRIS base, 10 mM $Na_2EDTA * 2H_2O$, 5mg/ml RNase A, pH 8). 200 µl of sterile filtrated buffer P2 (0.2 M NaOH, 1% SDS) was added and tubes were inverted 8-15 times. 350 µl of cold buffer P3 (3M potassium acetate, pH 5.5) was added and tubes were inverted 8-15 times. Tubes were centrifuged at 15871 g for 3 min. 600 µl of supernatant was transferred to 1.5 ml reaction tubes, containing 600 µl isopropanol. Tubes were inverted and plasmid DNA (pDNA) was pelleted by centrifugation at 20238 g for 3 min. Supernatants were decanted and tubes were tapped on paper tissue, to remove remaining supernatant. 600 µl of ethanol (70%) was added. Tubes were centrifuged at 20238 g for 3 min. Ethanol was carefully removed using a pipet equipped with a yellow tip on top of a blue tip. Pellets were dried at RT for 30 min or at 60°C for 10 min. pDNA was resuspended in 50 µl ddH_2O.

18 Cut-ligations

All cut-ligations were performed in a reaction volume of 15 µl. All plasmids were used at a concentration of 100 ng/µl. PCR fragments were used at the concentration yielded from PCR product clean up (ThermoFisher GeneJet PCR Purification kit, according to manufacturer's guidelines). 1 µl of plasmid or PCR fragment was used in cut-ligations, together with 1.5 µl of reaction buffer, 1.5 µl of 10 mM ATP, 0.75 µl of BsaI-HF or BpiI and 0.75 µl of T4 DNA ligase. Remaining volume was filled up with ddH_2O. For BsaI-HF, NEB Cutsmart buffer was used. For BpiI, ThermoFisher Buffer G buffer was used. All BsaI-HF cut-ligations were performed using the following program: [37°C for 10 min, 16°C for 10 min] x 6; 37°C for 10min; 65°C for 20 min. For BpiI cut-ligations the following program was used: [37°C for 2 min, 16°C for 5 min] x 50; 37°C for 10min; 65°C for 20 min.

19 Plasmid list and construction

In this study, Golden Gate and Gateway plasmids were used. All plasmids generated in this study were constructed using the Golden Gate cloning system (Binder et al., 2014). The following tables contain a detailed description of the plasmid identity and their construction or reference. TA = transcriptional activation assay in *N. benthamiana* or *S. cerevisiae*, Y2H = Y2H assay, FLIM-FRET = FLIM-FRET analysis in *N. benthamiana*, HR = hairy root transformation in *Lotus*

japonicus, pPB = plasmid Philipp Bellon, gPB = glycerol stock Philipp Bellon, pGG = plasmid Giulia Gobatto, pKK = plasmid Katja Katzer, pMC = plasmid Marion Cerri, SDM = Site directed mutagenesis, M = designates WT cloning module of gCyclops, m = designates phosphoablative cloning module of gCyclops.

19.1 L0 plasmids

Table 2: L0 plasmids used in this study

Purpose	Plasmid name and description	Construction/Reference	Plasmid ID
Cloning	gCYC-M1-S50D	SDM on pKK24 with PB003 and PB004, to remove internal BpiI site, PCR with PB019 and PB007 on pKK24, SmaI or StuI CL into BB1	pPB001
Cloning	gCYC-M1-S50	SDM on pPB001 with PB026 and PB027	pPB038
Cloning	gCYC-m1-S50D	SDM on pKK14 with PB003 and PB004, to remove internal BpiI site, PCR with PB019 and PB007 on pKK14, SmaI or StuI CL into BB1	pPB002
Cloning	gCYC-m1-S50	SDM on pPB002 with KK21D and KK22D, D50S	pPB036
Cloning	gCYC-M1_Nphos	Eurofins fragment, SmaI or StuI CL into BB2	pPB112
Cloning	gCYC-M2-WT	PCR with PB008 and PB009 on pKK25, A-tailing into pSEVA191-XcmI	pPB003
Cloning	gCYC-M3_WT	PCR with PB010 and PB011 on pMC9, A-tailing into pSEVA191-XcmI	pPB005
Cloning	gCYC-m3	PCR with PB010 and PB011 on pKK26, SmaI or BpiI CL into BB2	pPB006

Cloning	gCYC-M4_S154D	PCR with PB012 and PB025 on pMC9, A-tailing into pSEVA191-XcmI	pPB007
Cloning	gCYC-M4_WT	SDM on pPB007 with KK23C and KK24C	pPB037
Cloning	gCYC-m4-S154D	PCR with PB012 and PB025 on pKK20, SmaI or StuI CL into BB2	pPB008
Cloning	gCYC-M4_9*D	Eurofins Fragment, SmaI or StuI CL into BB1	pPB010
Cloning	gCYC-m4-b	Eurofins Fragment, SmaI or StuI CL into BB1	pPB012
Cloning	gCYC-m4-a	Eurofins Fragment, SmaI or StuI CL into BB1	pPB013
Cloning	gCYC-m4_S220A	SDM on pPB037 with PB028 and PB029	pPB058
Cloning	gCYC-m4_S221A	SDM on pPB037 with PB036 and PB037	pPB059
Cloning	gCYC-m4_S226A	SDM on pPB037 with PB 038 and PB039	pPB060
Cloning	gCYC-m4_S251A	SDM on pPB037 with PB040 and PB041	pPB061
Cloning	gCYC-M5_WT	PCR with PB023 and PB015 on pKK30, SmaI or BpiI CL into BB1	pPB014
Cloning	gCYC-M6_WT	PCR with PB016 and PB017 on pKK31, SmaI or BpiI CL into	pPB016
Cloning	gCYC-m6	PCR with PB016 and PB017 on pKK22, A-tailing into pSEVA191-XcmI	pPB017

Cloning	gCYC-M7	SDM on pKK32 with PB026 and PB027 to remove internal BpiI site, PCR with PB018 and PB020 on pKK32 A-tailing into pSEVA191-XcmI	pPB018
Cloning	gCYC-F1-S50 (M1-M3)	PCR on pPB042 with PB019 and PB011, SmaI or StuI CL into BB1	pPB080
Cloning	gCYC-F2-S50D (M1-M3)	PCR on pPB089 with PB019 and PB011, SmaI or StuI CL into BB1	pPB094
Cloning	gCYC-F3 (M5-M7)	PCR on pPB042 with PB023 and PB020, SmaI or StuI CL in BB1	pPB082
Cloning	gCYC-F6_S154D (M2-4)	PCR on pPB089 with PB008 and PB025, BpiI CL into BB1	pPB180
Cloning	gCYC-F7_S154 (M2-4)	PCR on pPB042 with PB008 and PB025, BpiI CL into BB1	pPB181

19.2 LI plasmids

Table 3: LI plasmids used in this study

Purpose	Plasmid name and description	Construction/Reference	Plasmid ID
Cloning	gCyclops^{WT}	Assembled via BpiI CL with pPB038, pPB003, pPB005, pPB037, pPB014, pPB016, pPB018 into pENTR-BpiI	pPB042
Cloning	cCyclops^{WT}	RT-PCR on *N. benthamiana* expressed	pGG015

		pPB050, with PB019 and GG016	
Cloning	gCyclops^{m1}	Assembled via BpiI CL with pPB036, pPB003, pPB005, pPB037, pPB014, pPB016, pPB018, into pENTR-BpiI	pPB043
Cloning	gCyclops^{m3}	Assembled via BpiI CL with pPB038, pPB003, pPB006, pPB037, pPB014, pPB016. pPB018, into pENTR-BpiI	pPB044
Cloning	gCyclops^{m4}	Assembled via BpiI CL with pPB038, pPB003, pPB005, pB035, pPB014, pPB016, pPB018 into pENTR-BpiI	pPB045
Cloning	gCyclops^{m6}	BpiI CL with pPB038, pPB003, pPB005, pPB037, pPB014, pPB017, pPB018 into pENTR-BpiI	pPB046
Cloning	gCyclops^{m1346}	Assembled via BpiI CL with pPB036, pPB003, pPB006, pB035, pPB014, pPB017, pPB018 into pENTR-BpiI	pPB047
Cloning	gCyclops^{m4a}	Assembled via BpiI CL with pPB038, pPB003, pPB012, pPB014, pPB016, pPB018, into pENTR-BpiI	pPB048
Cloning	gCyclops^{m4b}	Assembled via BpiI CL with pPB038, pPB003,	pPB049

		pPB013, pPB014, pPB016, pPB018, into pENTR-BpiI	
Cloning	gCyclops^{S220A}	Assembled via BpiI CL with pPB038, pPB003, pPB005, pPB058, pPB014, pPB016, pPB018 into BpiI	pPB079
Cloning	gCyclops^{S221A}	Assembled via BpiI CL with pPB038, pPB003, pPB005, pPB059, pPB014, pPB016, pPB018 into Bpi	pPB071
Cloning	gCyclops^{S236A}	Assembled via BpiI CL with pPB038, pPB003, pPB005, pPB060, pPB014, pPB016, pPB018 into Bpi	pPB072
Cloning	cCyclops^{S236A}	PCRs on pGG015 with PB019/PB294 and PB293/PB020, BpiI CL into BB3	pPB493
Cloning	gCyclops^{S251A}	Assembled via BpiI CL with pPB038, pPB003, pPB005, pPB061, pPB014, pPB016, pPB018 into pENTR-Bpi	pPB073
Cloning	gCyclops^{DD}	Assembled via BpiI CL with pPB001, pPB003, pPB005, pPB037, pPB014, pPB016, pPB018, into pENTR-BpiI	pPB089
Cloning	cCyclops^{DD}	RT-PCR on *N. benthamiana* expressed	pGG016

		pPB172, with PB019 and GG016	
Cloning	gCyclops^{6D}	Assembled via BpiI CL with pPB096, pPB062, pPB082	pPB070
Cloning	gCyclops^{3D-1}	PCR on pPB089 with PB019/PB073 and PB072/PB020, BpiI CL into pENTR-BpiI	pPB075
Cloning	gCyclops^{3D-2}	PCR on pPB089 with PB019/PB274 and PB273/PB020, BpiI CL into pENTR-BpiI	pPB077
Cloning	gCyclops^{3D-3}	PCR on pPB089 with PB019/PB079 and PB078/PB020, BpiI CL into pENTR-BpiI	pPB078
Cloning	gCyclops^{10D}	Assembled via BpiI CL with pPB001, pPB003, pPB005, pPB010, pPB014, pPB016, pPB018 into pENTR-BpiI	pPB031
Cloning	cCyclops^{10D}	RT-PCR on *N. benthamiana* expressed pPB031, with PB019 and GG016	pGG021
Cloning	gCyclops^{7D}	Assembled via BpiI CL with pPB094, pPB103 pPB082 into pENTR-BpiI	pPB135
Cloning	gCyclops^{4D-1}	Assembled via BpiI CL with pPB094, pPB104 pPB082 into pENTR-BpiI	pPB136

Cloning	gCyclops^{4D-2}	Assembled via BpiI CL with pPB094, pPB105 pPB082 into pENTR-BpiI	pPB137
Cloning	gCyclops^{4D-3}	Assembled via BpiI CL with pPB094, pPB106 pPB082 into pENTR-BpiI	pPB138
Cloning	gCyclops^{4D-4}	Assembled via BpiI CL with pPB094, pPB107 pPB082 into pENTR-BpiI	pPB139
Cloning	gCyclops^{3D-4}	Assembled via BpiI CL with pPB113, pPB180, pPB082 into pENTR-BpiI	pPB145
Cloning	gCyclops^{3D-5}	Assembled via BpiI CL with pPB114, pPB180, pPB082 into pENTR-BpiI	pPB146
Cloning	gCyclops^{3D-6}	Assembled via BpiI CL with pPB115, pPB180, pPB082 into pENTR-BpiI	pPB147
Cloning	gCyclops^{3D-7}	Assembled via BpiI CL with pPB116, pPB180, pPB082 into pENTR-BpiI	pPB148
Cloning	gCyclops^{Nphos}	Assembled via BpiI CL with pPB112, pPB180, pPB082 into pENTR-BpiI	pPB144
Cloning	cCyclops^{Nphos}	RT-PCR on *N. benthamiana* expressed	pGG020

		pPB245, with PB019 and GG016	
Cloning	gCyclops^{5D}	PCR on pPB137 with PB019/PB276 and PB275/PB020, BpiI CL into pENTR-BpiI	pPB198
Cloning	cCyclops^{5D}	RT-PCR on *N. benthamiana* expressed pPB218, with PB019 and GG016	pGG018
Cloning	gCyclops^{9D}	PCR on pPB144 with PB019 and PB011, PCR on pPB198 with PB012 and PB020, BpiI CL into pENTR-BpiI	pPB293
Cloning	cCyclops^{9D}	RT-PCR on *N. benthamiana* expressed pPB306 with PB019 and GG016	pGG019
Cloning	cCyclops$^{S50D-S154D-S236D}$	PCR on pGG016 with PB019/PB274 and PB273/PB020, BpiI CL into BB3	pPB407
Cloning	cCyclops^{QP1}	PCR of pPB407 with PB019/PB276 and PB275/PB020, BpiI CL into pENTR-BpiI	pPB409
Cloning	cCyclops^{QP2}	PCR of pPB407 with PB019/PB278 and PB277/PB020, BpiI CL into pENTR-BpiI	pPB408
Cloning	cCyclops^{QP3}	PCR of pPB409 with PB019/PB278 and PB277/PB020, BpiI CL into BB3	pPB465

Cloning	cCyclops^{3D-8}	PCR on pGG016 with PB019/PB278 and PB277/PB020, BpiI CL into BB3	pPB463
Cloning	cCyclops^{3D-9}	PCR on pGG016 with PB019/PB276 and PB275/PB020, BpiI CL into BB3	pPB464
Cloning	cCyclops^{S134D}	PCR on pGG015 with PB019/PB278 and PB277/PB020, BpiI CL into BB3	pPB410
Cloning	cCyclops^{S145D}	PCR on pGG015 with PB019/PB276 and PB275/PB020, BpiI CL into BB3	pPB411
Cloning	cCyclops^{S236D}	PCR on pGG015 with PB019/PB274 and PB273/GG016, BpiI Cl into pENTR-BpiI	pPB466
Cloning	cCyclops$^{N, WT}$	PCR with PB019 and GG018 on pGG015, BpiI CL into BB3	pGG023
Cloning	cCyclops$^{N, DD}$	PCR with PB019 and GG018 on pGG016, BpiI CL into BB3	pGG024
Cloning	cCyclops$^{N, 10D}$	PCR with PB019 and GG018 on pGG021, BpiI CL into BB3	pGG029
Cloning	cCyclops$^{N, 5D}$	PCR with PB019 and GG018 on pGG018, BpiI CL into BB3	pGG026
Cloning	cCyclops$^{N, Nphos}$	PCR with PB019 and GG018 on pGG020, BpiI CL into BB3	pGG028

Cloning	cCyclops$^{N, 9D}$	PCR with PB019 and GG018 on pGG019, BpiI CL into BB3	pGG027
Cloning	cCCaMK	Gift by David Chiasson	
Cloning	cCCaMK^{T265D}	Gift by David Chiasson	
Cloning	cNIN^{N}	Gift by David Chiasson	
Cloning	Gal4^{AD}	Gift by David Chiasson	
Cloning	Gal4^{BD}	Gift by David Chiasson	
Cloning	Gal4^{BDplant_codon} (plant codons)	Gift by David Chiasson	
Cloning	SV40	Gift by David Chiasson	
Cloning	*Cyc$_{pro}$2.4kb*	Gift by Chloe Cathebras	
Cloning	*CCaMK$_{pro}$1.9kb*	Gift by Chloe Cathebras	
Cloning	*ScSac6$_{pro}$*	Gift by David Chiasson	
Cloning	*ScADH1$_{pro}$*	Gift by David Chiasson	
Cloning	*ScADH1$_{pro}$ 1-400*	Gift by David Chiasson	
Cloning	*ScTDH1t*	Gift by David Chiasson	
Cloning	*ScADH1t*	Gift by David Chiasson	
Cloning	gCCaMK	Gift by Chloe Cathebras	
Cloning	gCCaMK^{T265D}	Gift by Chloe Cathebras	
Cloning	gCCaMK^{NFG}	Gift by Chloe Cathebras	

19.3 LII plasmids

Table 4: LII plasmids used in this study

Purpose	**Plasmid name and description**	**Construction/Reference**	**Plasmid ID**
TA	LIIβ F 3-4 *LjUbi$_{pro}$:Myc-gCCaMK$^{1-314}$:NOS$_t$*	Gift by Chloe Cathebras	Chloe Cathebras L2 #40
TA	LIIβ F 1-2 *LjUbi$_{pro}$:HA:NOS$_t$*	Assembled via BsaI CL with LI A-B *LjUbi$_{pro}$* (G007), LI B-C HA-tag (G067), LI C-D dy (BB7), LI D-E dy (BB8), LI E-F	pPB027

		NOS_t (G006), LI F-G dy (BB9) into BB20	
TA	LIIβ F 1-2 *$LjUbi_{pro}$:HA-gCyclops^{WT}:NOS_t*	Assembled via BsaI CL with LI A-B *$LjUbi_{pro}$* (G007), LI B-C HA-tag (G067), LI C-D gCyclops (pPB042), LI D-E dy (BB8), LI E-F NOS_t (G006), LI F-G dy (BB9) into BB20	pPB050
TA	LIIβ F 1-2 *$LjUbi_{pro}$:HA-gCyclops^{m1}:NOS_t*	Assembled via BsaI CL with LI A-B *$LjUbi_{pro}$* (G007), LI B-C HA-tag (G067), LI C-D gCyclops (pPB043), LI D-E dy (BB8), LI E-F NOS_t (G006), LI F-G dy (BB9) into BB20	pPB051
TA	LIIβ F 1-2 *$LjUbi_{pro}$:HA-gCyclops^{m3}:NOS_t*	Assembled via BsaI CL with LI A-B *$LjUbi_{pro}$* (G007), LI B-C HA-tag (G067), LI C-D gCyclops (pPB044), LI D-E dy (BB8), LI E-F NOS_t (G006), LI F-G dy (BB9) into BB20	pPB052
TA	LIIβ F 1-2 *$LjUbi_{pro}$:HA-gCyclops^{m4}:NOS_t*	Assembled via BsaI CL with LI A-B *$LjUbi_{pro}$* (G007), LI B-C HA-tag (G067), LI C-D gCyclops (pPB045), LI D-E dy (BB8), LI E-F NOS_t (G006), LI F-G dy (BB9) into BB20	pPB053
TA	LIIβ F 1-2 *$LjUbi_{pro}$:HA-gCyclops^{m6}:NOS_t*	Assembled via BsaI CL with LI A-B *$LjUbi_{pro}$*	pPB054

		(G007), LI B-C HA-tag (G067), LI C-D gCyclops (pPB046), LI D-E dy (BB8), LI E-F NOS_t (G006), LI F-G dy (BB9) into BB20	
TA	LIIβ F 1-2 *LjUbi$_{pro}$:HA-gCyclops^{m1346}:NOS$_t$*	Assembled via BsaI CL with LI A-B *LjUbi$_{pro}$* (G007), LI B-C HA-tag (G067), LI C-D gCyclops (pPB047), LI D-E dy (BB8), LI E-F NOS_t (G006), LI F-G dy (BB9) into BB20	pPB055
TA	LIIβ F 1-2 *LjUbi$_{pro}$:HA-gCyclops^{m4a}:NOS$_t$*	Assembled via BsaI CL with LI A-B *LjUbi$_{pro}$* (G007), LI B-C HA-tag (G067), LI C-D gCyclops (pPB048), LI D-E dy (BB8), LI E-F NOS_t (G006), LI F-G dy (BB9) into BB20	pPB056
TA	LIIβ F 1-2 *LjUbi$_{pro}$:HA-gCyclops^{m4b}:NOS$_t$*	Assembled via BsaI CL with LI A-B *LjUbi$_{pro}$* (G007), LI B-C HA-tag (G067), LI C-D gCyclops (pPB049), LI D-E dy (BB8), LI E-F NOS_t (G006), LI F-G dy (BB9) into BB20	pPB057
TA	LIIβ F 1-2 *LjUbi$_{pro}$:HA-gCyclops^{S220A}:NOS$_t$*	Assembled via BsaI CL with LI A-B *LjUbi$_{pro}$* (G007), LI B-C HA-tag (G067), LI C-D gCyclops (pPB079), LI D-E dy (BB8), LI E-F NOS_t	pPB0086

		(G006), LI F-G dy (BB9) into BB20	
TA	LIIβ F 1-2 *LjUbi$_{pro}$:HA-gCyclops^{S221A}:NOS$_t$*	Assembled via BsaI CL with LI A-B *LjUbi$_{pro}$* (G007), LI B-C HA-tag (G067), LI C-D gCyclops (pPB071), LI D-E dy (BB8), LI E-F NOS$_t$ (G006), LI F-G dy (BB9) into BB20	pPB083
TA	LIIβ F 1-2 *LjUbi$_{pro}$:HA-gCyclops^{S236A}:NOS$_t$*	Assembled via BsaI CL with LI A-B *LjUbi$_{pro}$* (G007), LI B-C HA-tag (G067), LI C-D gCyclops (pPB072), LI D-E dy (BB8), LI E-F NOS$_t$ (G006), LI F-G dy (BB9) into BB20	pPB084
TA	LIIβ F 1-2 *LjUbi$_{pro}$:HA-gCyclops^{S251A}:NOS$_t$*	Assembled via BsaI CL with LI A-B *LjUbi$_{pro}$* (G007), LI B-C HA-tag (G067), LI C-D gCyclops (pPB073), LI D-E dy (BB8), LI E-F NOS$_t$ (G006), LI F-G dy (BB9) into BB20	pPB085
TA	LIIβ F 1-2 *LjUbi$_{pro}$:HA-gCyclops^{DD}:NOS$_t$*	Assembled via BsaI CL with LI A-B *LjUbi$_{pro}$* (G007), LI B-C HA-tag (G067), LI C-D gCyclops (pPB089), LI D-E dy (BB8), LI E-F NOS$_t$ (G006), LI F-G dy (BB9) into BB20	pPB172
TA	LIIβ F 1-2 *LjUbi$_{pro}$:HA-gCyclops^{6D}:NOS$_t$*	Assembled via BsaI CL with LI A-B *LjUbi$_{pro}$*	pPB095

		(G007), LI B-C HA-tag (G067), LI C-D gCyclops (pPB070), LI D-E dy (BB8), LI E-F NOS_t (G006), LI F-G dy (BB9) into BB20	
TA	LIIβ F 1-2 *LjUbi$_{pro}$:HA-gCyclops^{3D-1}:NOS$_t$*	Assembled via BsaI CL with LI A-B *LjUbi$_{pro}$* (G007), LI B-C HA-tag (G067), LI C-D gCyclops (pPB075), LI D-E dy (BB8), LI E-F NOS_t (G006), LI F-G dy (BB9) into BB20	pPB096
TA	LIIβ F 1-2 *LjUbi$_{pro}$:HA-gCyclops^{3D-2}:NOS$_t$*	Assembled via BsaI CL with LI A-B *LjUbi$_{pro}$* (G007), LI B-C HA-tag (G067), LI C-D gCyclops (pPB077), LI D-E dy (BB8), LI E-F NOS_t (G006), LI F-G dy (BB9) into BB20	pPB097
TA	LIIβ F 1-2 *LjUbi$_{pro}$:HA-gCyclops^{3D-3}:NOS$_t$*	Assembled via BsaI CL with LI A-B *LjUbi$_{pro}$* (G007), LI B-C HA-tag (G067), LI C-D gCyclops (pPB078), LI D-E dy (BB8), LI E-F NOS_t (G006), LI F-G dy (BB9) into BB20	pPB098
TA	LIIβ F 1-2 *LjUbi$_{pro}$:HA-gCyclops^{10D}:NOS$_t$*	Assembled via BsaI CL with LI A-B *LjUbi$_{pro}$* (G007), LI B-C HA-tag (G067), LI C-D gCyclops (pPB023), LI D-E dy (BB8), LI E-F NOS_t	pPB031

		(G006), LI F-G dy (BB9) into BB20	
TA	LIIβ F 1-2 *LjUbi$_{pro}$:HA-gCyclops^{7D}:NOS$_t$*	Assembled via BsaI CL with LI A-B *LjUbi$_{pro}$* (G007), LI B-C HA-tag (G067), LI C-D gCyclops (pPB135), LI D-E dy (BB8), LI E-F NOS$_t$ (G006), LI F-G dy (BB9) into BB20	pPB163
TA	LIIβ F 1-2 *LjUbi$_{pro}$:HA-gCyclops^{4D-1}:NOS$_t$*	Assembled via BsaI CL with LI A-B *LjUbi$_{pro}$* (G007), LI B-C HA-tag (G067), LI C-D gCyclops (pPB136), LI D-E dy (BB8), LI E-F NOS$_t$ (G006), LI F-G dy (BB9) into BB20	pPB164
TA	LIIβ F 1-2 *LjUbi$_{pro}$:HA-gCyclops^{4D-2}:NOS$_t$*	Assembled via BsaI CL with LI A-B *LjUbi$_{pro}$* (G007), LI B-C HA-tag (G067), LI C-D gCyclops (pPB137), LI D-E dy (BB8), LI E-F NOS$_t$ (G006), LI F-G dy (BB9) into BB20	pPB165
TA	LIIβ F 1-2 *LjUbi$_{pro}$:HA-gCyclops^{4D-3}:NOS$_t$*	Assembled via BsaI CL with LI A-B *LjUbi$_{pro}$* (G007), LI B-C HA-tag (G067), LI C-D gCyclops (pPB138), LI D-E dy (BB8), LI E-F NOS$_t$ (G006), LI F-G dy (BB9) into BB20	pPB166
TA	LIIβ F 1-2 *LjUbi$_{pro}$:HA-gCyclops^{4D-4}:NOS$_t$*	Assembled via BsaI CL with LI A-B *LjUbi$_{pro}$*	pPB167

		(G007), LI B-C HA-tag (G067), LI C-D gCyclops (pPB139), LI D-E dy (BB8), LI E-F NOS_t (G006), LI F-G dy (BB9) into BB20	
TA	LIIβ F 1-2 *LjUbi$_{pro}$:HA-gCyclops^{3D-4}:NOS$_t$*	Assembled via BsaI CL with LI A-B *LjUbi$_{pro}$* (G007), LI B-C HA-tag (G067), LI C-D gCyclops (pPB145), LI D-E dy (BB8), LI E-F NOS_t (G006), LI F-G dy (BB9) into BB20	pPB184
TA	LIIβ F 1-2 *LjUbi$_{pro}$:HA-gCyclops^{3D-5}:NOS$_t$*	Assembled via BsaI CL with LI A-B *LjUbi$_{pro}$* (G007), LI B-C HA-tag (G067), LI C-D gCyclops (pPB146), LI D-E dy (BB8), LI E-F NOS_t (G006), LI F-G dy (BB9) into BB20	pPB185
TA	LIIβ F 1-2 *LjUbi$_{pro}$:HA-gCyclops^{3D-6}:NOS$_t$*	Assembled via BsaI CL with LI A-B *LjUbi$_{pro}$* (G007), LI B-C HA-tag (G067), LI C-D gCyclops (pPB147), LI D-E dy (BB8), LI E-F NOS_t (G006), LI F-G dy (BB9) into BB20	pPB246
TA	LIIβ F 1-2 *LjUbi$_{pro}$:HA-gCyclops^{3D-7}:NOS$_t$*	Assembled via BsaI CL with LI A-B *LjUbi$_{pro}$* (G007), LI B-C HA-tag (G067), LI C-D gCyclops (pPB148), LI D-E dy (BB8), LI E-F NOS_t	pPB247

		(G006), LI F-G dy (BB9) into BB20	
TA	LIIβ F 1-2 *LjUbi$_{pro}$:HA-gCyclops^{Nphos}:NOS$_t$*	Assembled via BsaI CL with LI A-B *LjUbi$_{pro}$* (G007), LI B-C HA-tag (G067), LI C-D gCyclops (pPB144), LI D-E dy (BB8), LI E-F NOS$_t$ (G006), LI F-G dy (BB9) into BB20	pPB245
TA	LIIβ F 1-2 *LjUbi$_{pro}$:HA-gCyclops^{5D}:NOS$_t$*	Assembled via BsaI CL with LI A-B *LjUbi$_{pro}$* (G007), LI B-C HA-tag (G067), LI C-D gCyclops (pPB198), LI D-E dy (BB8), LI E-F NOS$_t$ (G006), LI F-G dy (BB9) into BB20	pPB218
TA	LIIβ F 1-2 *LjUbi$_{pro}$:HA-gCyclops^{9D}:NOS$_t$*	Assembled via BsaI CL with LI A-B *LjUbi$_{pro}$* (G007), LI B-C HA-tag (G067), LI C-D gCyclops (pPB293), LI D-E dy (BB8), LI E-F NOS$_t$ (G006), LI F-G dy (BB9) into BB20	pPB306
Y2H	LII Trp 3-4 CEN *ScADH1$_{pro}$1-400:Gal4^{BD}-cCCaMK:TDH1$_t$*	Assembled via BsaI CL with LI A-B *ScADH1$_{pro}$1-400,* LI B-C Gal4^{BD}, LI C-D cCCaMK, LI D-E dy (BB8), LI E-F TDH1$_t$, LI F-G dy (BB9) into LII Trp 3-4 CEN	pGG117
Y2H	LII Trp 3-4 CEN *ScADH1$_{pro}$1-400:Gal4^{BD}-cCCaMK^{T265D}:TDH1$_t$*	Assembled via BsaI CL with LI A-B *ScADH1$_{pro}$1-400,* LI B-C Gal4^{BD}, LI C-	pGG115

		D cCCaMK^{T265D}, LI D-E dy (BB8), LI E-F TDH1$_t$, LI F-G dy (BB9) into LII Trp 3-4 CEN	
TA	LII Trp 3-4 CEN *ScSac6$_{pro}$:Gal4^{BD}-cCyclops^{WT}:TDH1$_t$*	Assembled via BsaI CL with LI A-B *ScSac6$_{pro}$*, LI B-C Gal4^{BD}, LI C-D cCyclops (pGG015), LI D-E dy (BB8), LI E-F TDH1$_t$, LI F-G dy (BB9) into LII Trp 3-4 CEN	pGG105
TA	LII Trp 3-4 CEN *ScSac6$_{pro}$:Gal4^{BD}-cCyclops^{N,WT}:TDH1$_t$*	Assembled via BsaI CL with LI A-B *ScSac6$_{pro}$*, LI B-C Gal4^{BD}, LI C-D cCyclops (pGG023), LI D-E dy (BB8), LI E-F TDH1$_t$, LI F-G dy (BB9) into LII Trp 3-4 CEN	pGG067
TA	LII Trp 3-4 CEN *ScSac6$_{pro}$:Gal4^{BD}-cCyclops^{N,DD}:TDH1$_t$*	Assembled via BsaI CL with LI A-B *ScSac6$_{pro}$*, LI B-C Gal4^{BD}, LI C-D cCyclops pGG023), LI D-E dy (BB8), LI E-F TDH1$_t$, LI F-G dy (BB9) into LII Trp 3-4 CEN	pGG068
TA	LII Trp 3-4 CEN *ScSac6$_{pro}$:Gal4^{BD}-cCyclops^{N,10D}:TDH1$_t$*	Assembled via BsaI CL with LI A-B *ScSac6$_{pro}$*, LI B-C Gal4^{BD}, LI C-D cCyclops (pGG029), LI D-E dy (BB8), LI E-F TDH1$_t$, LI F-G dy (BB9) into LII Trp 3-4 CEN	pGG073
TA	LII Trp 3-4 CEN *ScSac6$_{pro}$:Gal4^{BD}-cCyclops^{N,5D}:TDH1$_t$*	Assembled via BsaI CL with LI A-B *ScSac6$_{pro}$*, LI B-C Gal4^{BD}, LI C-D cCyclops (pGG026), LI	pGG070

		D-E dy (BB8), LI E-F $TDH1_t$, LI F-G dy (BB9) into LII Trp 3-4 CEN	
TA	LII Trp 3-4 CEN *$ScSac6_{pro}$:$Gal4^{BD}$-$cCyclops^{N, Nphos}$:$TDH1_t$*	Assembled via BsaI CL with LI A-B *$ScSac6_{pro}$*, LI B-C $Gal4^{BD}$, LI C-D cCyclops (pGG028), LI D-E dy (BB8), LI E-F $TDH1_t$, LI F-G dy (BB9) into LII Trp 3-4 CEN	pGG072
TA	LII Trp 3-4 CEN *$ScSac6_{pro}$:$Gal4^{BD}$-$cCyclops^{N, 9D}$:$TDH1_t$*	Assembled via BsaI CL with LI A-B *$ScSac6_{pro}$*, LI B-C $Gal4^{BD}$, LI C-D cCyclops (pGG027), LI D-E dy (BB8), LI E-F $TDH1_t$, LI F-G dy (BB9) into LII Trp 3-4 CEN	pGG071
TA	LIIβ F 5-6 *$LjUbi_{pro}$:$Gal4^{BDplant_codon_codon}$_cCCaMK:$NOS_t$*	Assembled via BsaI CL with LI A-B *$LjUbi_{pro}$* (G007), LI B-C $Gal4^{BDplant\_codon}$, LI C-D cCCaMK, LI D-E dy (BB8), LI E-F NOS_t (G006), LI F-G dy (BB9) into BB28	pPB388
TA	LIIβ F 5-6 *$LjUbi_{pro}$:$Gal4^{BDplant_codon}$_$cCyclops^{WT}$:NOS_t*	Assembled via BsaI CL with LI A-B *$LjUbi_{pro}$* (G007), LI B-C $Gal4^{BDplant\_codon}$, LI C-D cCyclops (pGG015), LI D-E dy (BB8), LI E-F NOS_t (G006), LI F-G dy (BB9) into BB28	pPB389
TA	LIIβ F 5-6 *$LjUbi_{pro}$:$Gal4^{BDplant_codon}$_$cCyclops^{N, WT}$:NOS_t*	Assembled via BsaI CL with LI A-B *$LjUbi_{pro}$* (G007), LI B-C	pPB375

		$Gal4^{BDplant\_codon}$, LI C-D cCyclops (pGG023), LI D-E dy (BB8), LI E-F NOS_t (G006), LI F-G dy (BB9) into BB28	
TA	LIIβ F 5-6 *$LjUbi_{pro}$:$Gal4^{BDplant_codon}$_ $cCyclops^{N,\ DD}$:NOS_t*	Assembled via BsaI CL with LI A-B *$LjUbi_{pro}$* (G007), LI B-C $Gal4^{BDplant\_codon}$, LI C-D cCyclops (pGG024), LI D-E dy (BB8), LI E-F NOS_t (G006), LI F-G dy (BB9) into BB28	pPB376
TA	LIIβ F 5-6 *$LjUbi_{pro}$:$Gal4^{BDplant_codon}$_ $cCyclops^{N,\ 10D}$:NOS_t*	Assembled via BsaI CL with LI A-B *$LjUbi_{pro}$* (G007), LI B-C $Gal4^{BDplant\_codon}$, LI C-D cCyclops (pGG028), LI D-E dy (BB8), LI E-F NOS_t (G006), LI F-G dy (BB9) into BB28	pPB380
TA	LIIβ F 5-6 *$LjUbi_{pro}$:$Gal4^{BDplant_codon}$_ $cCyclops^{N,\ 5D}$:NOS_t*	Assembled via BsaI CL with LI A-B *$LjUbi_{pro}$* (G007), LI B-C $Gal4^{BDplant\_codon}$, LI C-D cCyclops (pGG026), LI D-E dy (BB8), LI E-F NOS_t (G006), LI F-G dy (BB9) into BB28	pPB378
TA	LIIβ F 5-6 *$LjUbi_{pro}$:$Gal4^{BDplant_codon}$_ $cCyclops^{N,Nphos}$:NOS_t*	Assembled via BsaI CL with LI A-B *$LjUbi_{pro}$* (G007), LI B-C $Gal4^{BDplant\_codon}$, LI C-D $cCyclops^{WT}$ (pGG029), LI D-E dy (BB8), LI E-F	pPB382

		NOS_t (G006), LI F-G dy (BB9) into BB28	
TA	LIIβ F 5-6 *$LjUbi_{pro}$:$Gal4^{BDplant\_codon}$-$cCyclops^{N,\ 9D}$:NOS_t*	Assembled via BsaI CL with LI A-B *$LjUbi_{pro}$* (G007), LI B-C $Gal4^{BDplant\_codon}$, LI C-D cCyclops (pGG027), LI D-E dy (BB8), LI E-F NOS_t (G006), LI F-G dy (BB9) into BB28	pPB379
Y2H	pGADT7 *$ScADH1_{pro}$:HA-cSV40:$T7_t$*	Gift by David Chiasson	pGG076
Y2H	LII Leu 1-2 CEN *$ScSac6_{pro}$:$Gal4^{AD}$-$cCyclops^{WT}$:$ADH1_t$*	Assembled via BsaI CL with LI A-B *$ScSac6_{pro}$*, LI B-C $Gal4^{AD}$, LI C-D cCyclops (pGG015), LI D-E dy (BB8), LI E-F $ADH1_t$, LI F-G dy (BB9) into LII Leu 1-2 CEN	pGG059
Y2H	LII Leu 1-2 CEN *$ScSac6_{pro}$:$Gal4^{AD}$-$cCyclops^{DD}$:$ADH1_t$*	Assembled via BsaI CL with LI A-B *$ScSac6_{pro}$*, LI B-C $Gal4^{AD}$, LI C-D $cCyclops^{DD}$ (pGG016), LI D-E dy (BB8), LI E-F $ADH1_t$, LI F-G dy (BB9) into LII Leu 1-2 CEN	pGG060
Y2H	LII Leu 1-2 CEN *$ScSac6_{pro}$:$Gal4^{AD}$-$cCyclops^{10D}$:$ADH1_t$*	Assembled via BsaI CL with LI A-B *$ScSac6_{pro}$*, LI B-C $Gal4^{AD}$, LI C-D cCyclops (pGG021), LI D-E dy (BB8), LI E-F $ADH1_t$, LI F-G dy (BB9) into LII Leu 1-2 CEN	pGG065
Y2H	LII Leu 1-2 CEN	Assembled via BsaI CL with LI A-B *$ScSac6_{pro}$*, LI B-C $Gal4^{AD}$, LI C-D	pGG062

	ScSac6$_{pro}$:Gal4^{AD}-cCyclops^{5D}:ADH1$_t$	cCyclops (pGG018), LI D-E dy (BB8), LI E-F ADH1$_t$, LI F-G dy (BB9) into LII Leu 1-2 CEN	
Y2H	LII Leu 1-2 CEN *ScSac6$_{pro}$:Gal4^{AD}-cCyclops^{Nphos}:ADH1$_t$*	Assembled via BsaI CL with LI A-B *ScSac6$_{pro}$*, LI B-C Gal4^{AD}, LI C-D cCyclops (pGG020), LI D-E dy (BB8), LI E-F ADH1$_t$, LI F-G dy (BB9) into LII Leu 1-2 CEN	pGG064
Y2H	LII Leu 1-2 CEN *ScSac6$_{pro}$:Gal4^{AD}-cCyclops^{9D}:ADH1$_t$*	Assembled via BsaI CL with LI A-B *ScSac6$_{pro}$*, LI B-C Gal4^{AD}, LI C-D cCyclops (pGG019), LI D-E dy (BB8), LI E-F ADH1$_t$, LI F-G dy (BB9) into LII Leu 1-2 CEN	pGG063
Y2H	LII Leu 1-2 CEN *ScSac6$_{pro}$:Gal4^{AD}-cCyclops^{QP1}:ADH1$_t$*	Assembled via BsaI CL with LI A-B *ScSac6$_{pro}$*, LI B-C Gal4^{AD}, LI C-D cCyclops (pPB409), LI D-E dy (BB8), LI E-F ADH1$_t$, LI F-G dy (BB9) into LII Leu 1-2 CEN	pPB441
Y2H	LII Leu 1-2 CEN *ScSac6$_{pro}$:Gal4^{AD}-cCyclops^{QP2}:ADH1$_t$*	Assembled via BsaI CL with LI A-B *ScSac6$_{pro}$*, LI B-C Gal4^{AD}, LI C-D cCyclops (pPB408), LI D-E dy (BB8), LI E-F ADH1$_t$, LI F-G dy (BB9) into LII Leu 1-2 CEN	pPB440
Y2H	LII Leu 1-2 CEN *ScSac6$_{pro}$:Gal4^{AD}-cCyclops^{QP3}:ADH1$_t$*	Assembled via BsaI CL with LI A-B *ScSac6$_{pro}$*, LI B-C Gal4^{AD}, LI C-D cCyclops (pPB465), LI	pPB469

		D-E dy (BB8), LI E-F ADH1$_t$, LI F-G dy (BB9) into LII Leu 1-2 CEN	
Y2H	LII Leu 1-2 CEN *ScSac6$_{pro}$:Gal4^{AD}-cCyclops^{3D-8}:ADH1$_t$*	Assembled via BsaI CL with LI A-B *ScSac6$_{pro}$*, LI B-C Gal4^{AD}, LI C-D cCyclops (pPB463), LI D-E dy (BB8), LI E-F ADH1$_t$, LI F-G dy (BB9) into LII Leu 1-2 CEN	pPB467
Y2H	LII Leu 1-2 CEN *ScSac6$_{pro}$:Gal4^{AD}-cCyclops^{3D-9}:ADH1$_t$*	Assembled via BsaI CL with LI A-B *ScSac6$_{pro}$*, LI B-C Gal4^{AD}, LI C-D cCyclops (pPB464), LI D-E dy (BB8), LI E-F ADH1$_t$, LI F-G dy (BB9) into LII Leu 1-2 CEN	pPB468
Y2H	LII Leu 1-2 CEN *ScSac6$_{pro}$:Gal4^{AD}-cCyclops^{S134D}:ADH1$_t$*	Assembled via BsaI CL with LI A-B *ScSac6$_{pro}$*, LI B-C Gal4^{AD}, LI C-D cCyclops (pPB410), LI D-E dy (BB8), LI E-F ADH1$_t$, LI F-G dy (BB9) into LII Leu 1-2 CEN	pPB442
Y2H	LII Leu 1-2 CEN *ScSac6$_{pro}$:Gal4^{AD}-cCyclops^{S145D}:ADH1$_t$*	Assembled via BsaI CL with LI A-B *ScSac6$_{pro}$*, LI B-C Gal4^{AD}, LI C-D cCyclops (pPB411), LI D-E dy (BB8), LI E-F ADH1$_t$, LI F-G dy (BB9) into LII Leu 1-2 CEN	pPB443
Y2H	LII Leu 1-2 CEN *ScSac6$_{pro}$:Gal4^{AD}-cCyclops^{S236D}:ADH1$_t$*	Assembled via BsaI CL with LI A-B *ScSac6$_{pro}$*, LI B-C Gal4^{AD}, LI C-D cCyclops (pPB466), LI D-E dy (BB8), LI E-F	pPB470

		ADH1$_t$, LI F-G dy (BB9) into LII Leu 1-2 CEN	
Y2H	LII Leu 1-2 CEN *ScSac6$_{pro}$:Gal4^{AD}-cCyclops^{S236A}:ADH1$_t$*	Assembled via BsaI CL with LI A-B *ScSac6$_{pro}$*, LI B-C Gal4^{AD}, LI C-D cCyclops (pPB493), LI D-E dy (BB8), LI E-F ADH1$_t$, LI F-G dy (BB9) into LII Leu 1-2 CEN	pPB494
Y2H	*LII Trp 3-4 CEN ScADH1$_{pro}$1-400:Gal4^{BD}-NIN^{N}:TDH1$_t$*	Assembled via BsaI CL with LI A-B *ScADH1$_{pro}$1-400*, LI B-C Gal4^{BD}, LI C-D cNIN^{N} , LI D-E dy (BB8), LI E-F TDH1$_t$, LI F-G dy (BB9) into LII Trp 3-4 CEN	pGG125
FLIM-FRET	LIIβ F 1-2 *35S$_{pro}$:NLS-mCherry-linker-GFP:35S$_t$*	Gift by Anna Isabel Seidler	gPB135
FLIM-FRET	LIIβ F 1-2 *LjUbi$_{pro}$:NLS-mCherry:35S$_t$*	Assembled via BsaI CL with LI A-B *LjUbi$_{pro}$* (G007), LI B-C NLS (G60), LI C-D mCherry (G23), LI D-E dy (BB8), LI E-F 35S$_t$ (G059), LI F-G dy (BB9) into BB20	pPB279
FLIM-FRET	LIIβ F 5-6 *LjUbi$_{pro}$:gCCaMK^{T265D}-mCherry:NOS$_t$*	Assembled via BsaI CL with LI A-B *LjUbi$_{pro}$* (G007), LI B-C dy (BB6), LI C-D gCCaMK,, LI D-E mCherry (G025), LI E-F NOS$_t$ (G6), LI F-G dy (BB9) into BB28	pPB527
FLIM-FRET	LIIβ F 5-6	Assembled via BsaI CL with LI A-B *LjUbi$_{pro}$* (G007), LI B-C dy (BB6),	pPB528

	LjUbi$_{pro}$:gCCaMK^{NFG}-mCherry:NOS$_t$	LI C-D gCCaMK^{NFG},, LI D-E mCherry (G025), LI E-F NOS$_t$ (G6), LI F-G dy (BB9) into BB28	
FLIM-FRET	LIIβ F 5-6 *LjUbi$_{pro}$:sGFP-gCyclops^{WT}:NOS$_t$*	Assembled via BsaI CL with LI A-B *LjUbi$_{pro}$* (G007), LI B-C sGFP (G028), LI C-D gCyclops (pPB089) LI D-E dy (BB8), LI E-F NOS$_t$ (G6), LI F-G dy (BB9) into BB28	pPB272
FLIM-FRET	LIIβ F 5-6 *LjUbi$_{pro}$:sGFP-gCyclops^{S236D}:NOS$_t$*	Assembled via BsaI CL with LI A-B *LjUbi$_{pro}$* (G007), LI B-C sGFP (G028), LI C-D gCyclops (pPB151) LI D-E dy (BB8), LI E-F NOS$_t$ (G6), LI F-G dy (BB9) into BB28	pPB523
FLIM-FRET	LIIβ F 5-6 *LjUbi$_{pro}$:sGFP-gCyclops^{S236A}:NOS$_t$*	Assembled via BsaI CL with LI A-B *LjUbi$_{pro}$* (G007), LI B-C sGFP (G028), LI C-D gCyclops (pPB072) LI D-E dy (BB8), LI E-F NOS$_t$ (G6), LI F-G dy (BB9) into BB28	pPB526
HR	LIIβ F 5-6 *LjCyc$_{pro}$2.4kb:HA:NOS$_t$*	Assembled via BsaI CL with LI A-B LjCyc$_{pro}$2.4kb, LI B-C HA-tag (G067), LI C-D dy (BB7) LI D-E dy (BB8), LI E-F NOS$_t$ (G6), LI F-G dy (BB9) into BB28	pPB239

HR	LIIβ F 5-6 *LjCCaMK$_{pro}$1.9kb:Myc-gCCaMK:NOS$_t$*	Assembled via BsaI CL with LI A-B LjCCaMK$_{pro}$1.9kb, LI B-C Myc-tag (G069), LI C-D gCCaMK, LI D-E dy (BB8), LI E-F NOS$_t$ (G6), LI F-G dy (BB9) into BB28	pPB240
HR	LIIβ F 5-6 *LjCyc$_{pro}$2.4kb:HA-gCyclops^{WT}:NOS$_t$*	Assembled via BsaI CL with LI A-B LjCyc$_{pro}$2.4kb, LI B-C HA-tag (G067), LI C-D gCyclops (pPB042) LI D-E dy (BB8), LI E-F NOS$_t$ (G6), LI F-G dy (BB9) into BB28	pPB235
HR	LIIβ F 5-6 *LjCyc$_{pro}$2.4kb:HA-gCyclops^{DD}:NOS$_t$*	Assembled via BsaI CL with LI A-B LjCyc$_{pro}$2.4kb, LI B-C HA-tag (G067), LI C-D gCyclops (pPB089) LI D-E dy (BB8), LI E-F NOS$_t$ (G6), LI F-G dy (BB9) into BB28	pPB236
HR	LIIβ F 5-6 *LjCyc$_{pro}$2.4kb:HA-gCyclops^{10D}:NOS$_t$*	Assembled via BsaI CL with LI A-B LjCyc$_{pro}$2.4kb, LI B-C HA-tag (G067), LI C-D gCyclops (pPB091) LI D-E dy (BB8), LI E-F NOS$_t$ (G6), LI F-G dy (BB9) into BB28	pGG033
HR	LIIβ F 5-6 *LjCyc$_{pro}$2.4kb:HA-gCyclops^{5D}:NOS$_t$*	Assembled via BsaI CL with LI A-B LjCyc$_{pro}$2.4kb, LI B-C HA-tag (G067), LI C-D	pPB238

		gCyclops (pPB198) LI D-E dy (BB8), LI E-F NOS_t (G6), LI F-G dy (BB9) into BB28	
HR	LIIβ F 5-6 *$LjCyc_{pro}$2.4kb:HA-$gCyclops^{Nphos}$:NOS_t*	Assembled via BsaI CL with LI A-B $LjCyc_{pro}$2.4kb, LI B-C HA-tag (G067), LI C-D gCyclops (pPB144) LI D-E dy (BB8), LI E-F NOS_t (G6), LI F-G dy (BB9) into BB28	pGG032
HR	LIIβ F 5-6 *$LjCyc_{pro}$2.4kb:HA-$gCyclops^{9D}$:NOS_t*	Assembled via BsaI CL with LI A-B $LjCyc_{pro}$2.4kb, LI B-C HA-tag (G067), LI C-D gCyclops (pPB293) LI D-E dy (BB8), LI E-F NOS_t (G6), LI F-G dy (BB9) into BB28	pGG031
HR	LIIα F 1-2 *$AtUBI10_{pro}$:2xNLS-GFP:$35S_t$*	Gift by Chloe Cathebras	

19.4 LIII plasmids

Table 5: LIII plasmids used in this study

Purpose	Plasmid name and description	Construction/Reference	Plasmid ID
HR	LIIIβ F A-B *LjCyc$_{pro}$2.4kb:HA:NOS$_t$*	Assembled via BpiI CL with 1-2 *AtUBI10$_{pro}$:2xNLS-GFP:35S$_t$*, 2-3 insulator (BB43), 3-4 dy (BB64), 4-5 insulator (BB44), 5-6 HA-tag (pPB293) into BB53	pGG049
HR	LIIIβ F A-B *LjCCaMK$_{pro}$1.9kb:Myc-gCCaMK:NOS$_t$*	Assembled via BpiI CL with 1-2 *AtUBI10$_{pro}$:2xNLS-GFP:35S$_t$*, 2-3 insulator (BB43), 3-4 dy (BB64), 4-5 insulator (BB44), 5-6 gCCaMK (pPB240) into BB53	pGG050
HR	LIIIβ F A-B *LjCyc$_{pro}$2.4kb:HA-gCyclops^{WT}:NOS$_t$*	Assembled via BpiI CL with 1-2 *AtUBI10$_{pro}$:2xNLS-GFP:35S$_t$*, 2-3 insulator (BB43), 3-4 dy (BB64), 4-5 insulator (BB44), 5-6 gCyclops (pPB235) into BB53	pPB258
HR	LIIIβ F A-B *LjCyc$_{pro}$2.4kb:HA-gCyclops^{DD}:NOS$_t$*	Assembled via BpiI CL with 1-2 *AtUBI10$_{pro}$:2xNLS-GFP:35S$_t$*, 2-3 insulator (BB43), 3-4 dy (BB64), 4-5 insulator (BB44), 5-6 gCyclops (pPB236) into BB53	pPB259

HR	LIIIβ F A-B *LjCyc$_{pro}$2.4kb:HA-gCyclops^{10D}:NOS$_t$*	Assembled via BpiI CL with 1-2 *AtUBI10$_{pro}$:2xNLS-GFP:35S$_t$*, 2-3 insulator (BB43), 3-4 dy (BB64), 4-5 insulator (BB44), 5-6 gCyclops (pGG033) into BB53	pGG036
HR	LIIIβ F A-B *LjCyc$_{pro}$2.4kb:HA-gCyclops^{5D}:NOS$_t$*	Assembled via BpiI CL with 1-2 *AtUBI10$_{pro}$:2xNLS-GFP:35S$_t$*, 2-3 insulator (BB43), 3-4 dy (BB64), 4-5 insulator (BB44), 5-6 gCyclops (pPB238) into BB53	pGG048
HR	LIIIβ F A-B *LjCyc$_{pro}$2.4kb:HA-gCyclops^{Nphos}:NOS$_t$*	Assembled via BpiI CL with 1-2 *AtUBI10$_{pro}$:2xNLS-GFP:35S$_t$*, 2-3 insulator (BB43), 3-4 dy (BB64), 4-5 insulator (BB44), 5-6 gCyclops (pGG032) into BB53	pGG035
HR	LIIIβ F A-B *LjCyc$_{pro}$2.4kb:HA-gCyclops^{9D}:NOS$_t$*	Assembled via BpiI CL with 1-2 *AtUBI10$_{pro}$:2xNLS-GFP:35S$_t$*, 2-3 insulator (BB43), 3-4 dy (BB64), 4-5 insulator (BB44), 5-6 gCyclops (pGG031) into BB53	pGG034

19.5 Gateway plasmids

Table 6: Gateway plasmids used in this study

Purpose	Plasmid name and description	Construction/Reference	Plasmid ID
	pBI101-pNIN870:GUS	Singh et al., 2014	gPB026
	LIIβF A-B pRAM1:GUS	Pimprikar et al., 2016	gPB011
	5xUAS$_{pro}$:eGFP-GUS	Weijers et al., 2003	-

20 Oligo list

Table 7: Oligos used in this study

Primer ID	5′ – 3′ sequence	Purpose	Source
PB003	GTTCCTGAAAACAGTGATGG	Cloning	This study
PB004	CCATCACTGTTTTCAGGAAC	Cloning	This study
PB007	TAGAAGACAAGTAACATGATCTTG CCTCTCCA	Cloning	This study
PB008	TAGAAGACAATTACCTTGTTCTTTG TTGTTGTTTC	Cloning	This study
PB009	TAGAAGACAAATCAATAGAAAGGA ATTGAAAATCAGA	Cloning	This study
PB010	TAGAAGACAATGATGTATCTTTGTT TTCTAAATCAGG	Cloning	This study
PB011	TAGAAGACAAAGGCTACACCAACT TGTAGCTGA	Cloning	This study
PB012	TAGAAGACAAGCCTCAGATGGAAG AAACAA	Cloning	This study
PB015	TAGAAGACAACTGCACAATTTAGC AGAATTAACC	Cloning	This study
PB016	TAGAAGACAAGCAGAGAAAAAGT CTAGAAAGATATGG	Cloning	This study
PB017	TAGAAGACAAAATGCATGTTTTAG AGCACAATG	Cloning	This study
PB018	TAGAAGACAACATTAGAATTTTGAT TCTCTTTATTG	Cloning	This study
PB019	ATGAAGACTTTACGGGTCTCACACC ATGGAAGGGAGGGGG	Cloning	This study
PB020	ATGAAGACTTCAGAGGTCTCTCCTT CATTTTTTCAGTTTCTGATAG	Cloning	This study

PB023	TAGAAGACAAAAGCTGCAGAAGATGACTTAAATG	Cloning	This study
PB025	TAGAAGACAAGCTTCTTTCTCAAGTTG	Cloning	This study
PB026	CAGATAGAAGATCTTCAGAAG	Cloning	This study
PB027	CTTCTGAAGATCTTCTATCTG	Cloning	This study
PB028	CTCATGTGCATCTAACTTCAAC	Cloning	This study
PB029	GTTGAAGTTAGATGCACATGAG	Cloning	This study
PB036	GTCCAACTCATGTTCAGCTAACTTCAACACAC	Cloning	This study
PB037	GTGTGTTGAAGTTAGCTGAACATGAGTTGGAC	Cloning	This study
PB038	GCGACATGGATAAAGTTTCAGCTTGTGTAAGTATGCTGAAAG	Cloning	This study
PB038	CTTTCAGCATACTTACACAAGCTGAAACTTTATCCATGTCGC	Cloning	This study
PB040	CATTACAACGCCGGAGACTCGCCAGTCAACTTGAGAAAGAAG	Cloning	This study
PB041	CTTCTTTCTCAAGTTGACTGGCGAGTCTCCGGCGTTGTAATG	Cloning	This study
PB072	TAGAAGACAAGATTCTAACTTCAACACACCTC	Cloning	This study
PB073	TAGAAGACAAAATCACATGAGTTGGACGGAG	Cloning	This study
PB078	TAGAAGACAAGACAGTCAACTTGAGAAAGAAGCTGCAG	Cloning	This study
PB079	TAGAAGACAATGTCGAGTCTCCGGCGTTGTAATG	Cloning	This study
PB273	TAGAAGACAAGATTGTGTAAGTATGCTGAAAGG	Cloning	This study
PB274	TAGAAGACAAAATCTGAAACTTTATCCATGTCG	Cloning	This study
PB275	TAGAAGACAAGATGATCAACGAATGACAAGAAG	Cloning	This study
PB276	TAGAAGACAACATCGAGAAACCAGGCCTTG	Cloning	This study

PB277	TAGAAGACAAGATAACTTGTTTCTAGCCAAGG	Cloning	This study
PB278	TAGAAGACAATATCAGGTTGCAGTTCTCTATC	Cloning	This study
PB293	TAGAAGACAAGCTTGTGTAAGTATGCTGAAAGG	Cloning	This study
PB294	TAGAAGACAAAAGCTGAAACTTTATCCATGTCG	Cloning	This study
KK21D	CGCGCAGATAGCGAGGAGCTTTTC	Cloning	Katja Katzer
KK22D	GAAAAGCTCCTCGCTATCTGCGCG	Cloning	Katja Katzer
KK23C	GACAAGAAGCCGGTCCTCTGAATTGC	Cloning	Katja Katzer
KK24C	GCAATTCAGAGGACCGGCTTCTTGTC	Cloning	Katja Katzer
GG034	TGCAGATCTTCGTCAAGACC	qPCR*LjUbi*	This study (Giulia Gobbato)
GG035	ACCTCCCCTCAGACGAAG	qPCR*LjUbi*	This study (Giulia Gobbato)
GG036	CATGCATTGAATCATGCTACGT	qPCR*LjRAM1*	This study (Giulia Gobbato)
GG037	CCTTGTGGAGACCATCCATT	qPCR*LjRAM1*	This study (Giulia Gobbato)
GG038	CACGTTGTTAGGACCCCAAT	qPCR*LjSbtM1*	This study (Giulia Gobbato)
GG039	TTGAGCAGCACCCTCTCTAT	qPCR*LjSbtM1*	This study (Giulia Gobbato)

GG040	GCTATCTCACAGAAGAGACC	qPCR*LjVPY*	This study (Giulia Gobbato)
GG041	AACAGAGTCACCAGAACCAG	qPCR*LjVPY*	This study (Giulia Gobbato)
GG042	CTTGTCCACCTCAATCCAAC	qPCR*LjERN1*	This study (Giulia Gobbato)
GG043	CTAGCTGCATCAATCATGCC	qPCR*LjERN1*	This study (Giulia Gobbato)
GG044	GAAGCTGCTTCAACCTTAAAGT	qPCR*LjNF-YA1*	This study (Giulia Gobbato)
GG045	GAGATGTAGAACTGAACTTGTC	qPCR*LjNF-YA1*	This study (Giulia Gobbato)
GG046	TGGATCAGCTAGCATGGAATAT	qPCR*LjNIN*	This study (Giulia Gobbato)
GG047	TCTGCTTCTGCTGTTGTCAC	qPCR*LjNIN*	This study (Giulia Gobbato)

21 Microscopy and image processing

Images of *L. japonicus* RNS complementation experiments were taken with a Leica M165 FC stereo microscope equipped with a Planapo 1x objective, a Leica TL5000 Ergo base, a Leica EL6000 UV lamp and a Leica DFC450 C camera. LAS X software was used for image acquisition. Nuclear GFP signal of the transformation marker was detected with a GFP filter and *M. loti* derived DsRED signal was detected with a DsRED filter. Brightfield was used to image histochemical stainings like GUS. Images of *L. japonicus* AM complementation experiments were taken with a Keyence VHX-6000 digital microscope. Post-acquisition image processing was done with Fiji software. Images were adjusted for contrast and brightness. FLIM-FRET analyses were performed with an upright Leica SP5 confocal laser-scanning microscope that was equipped with a HCX PL APO CS 20x/0.7 IMM CORR CS objective. sGFP was excited at 900 nm using a Ti:Sapphire multiphoton laser, running at 80 mHz with a 1.2 ps pulse length. A PMT detector at a resolution of 256x256 pixels was used for photon detection. Cycle number was based on a minimum photon count of 2000. Signals were recorded with the photon counting software TCSPC 2.8 (Becker & Hickl). Lifetime calculation was performed from a selected region of interest, using the SPCImage software (Becker & Hickl). A binning factor of 2 as well as a double exponential decay model was used for lifetime evaluations. Scatter and shift were fixed to zero.

22 Statistics and data visualization

All statistical analysis and datablots were generated with the R Studio Software (R version 1.3.595) (© 2009-2020 RStudio, PBC). Statistical analysis applied is described in figure legends. Adobe Illustrator or Affinity Designer software was used to generate illustrative figure parts.

X References

Abreu, I., Saéz, Á., Castro-Rodríguez, R., Escudero, V., Rodríguez-Haas, B., Senovilla, M., Larue, C., Grolimund, D., Tejada-Jiménez, M., and Imperial, J. (2017). *Medicago truncatula* Zinc-Iron Permease6 provides zinc to rhizobia-infected nodule cells. Plant, cell & environment **40,** 2706-2719.

Alder, A., Jamil, M., Marzorati, M., Bruno, M., Vermathen, M., Bigler, P., Ghisla, S., Bouwmeester, H., Beyer, P., and Al-Babili, S. (2012). The Path from β-Carotene to Carlactone, a Strigolactone-Like Plant Hormone. Science **335,** 1348-1351.

Andrade Aguirre, R.E. (2021). The transcription factor NIN mediates a dynamic balance between gene activation and repression in *L. japonicus* (lmu).

Andriankaja, A., Boisson-Dernier, A., Frances, L., Sauviac, L., Jauneau, A., Barker, D.G., and de Carvalho-Niebel, F. (2007). AP2-ERF transcription factors mediate Nod factor dependent *MtENOD11* activation in root hairs via a novel *cis*-regulatory motif. Plant Cell **19,** 2866-2885.

Ané, J.-M., Kiss, G.B., Riely, B.K., Penmetsa, R.V., Oldroyd, G.E.D., Ayax, C., Lévy, J., Debellé, F., Baek, J.-M., Kalo, P., Rosenberg, C., Roe, B.A., Long, S.R., Dénarié, J., and Cook, D.R. (2004). *Medicago truncatula DMI1* Required for Bacterial and Fungal Symbioses in Legumes. Science **303,** 1364-1367.

Ane, J.M., Levy, J., Thoquet, P., Kulikova, O., de Billy, F., Penmetsa, V., Kim, D.J., Debelle, F., Rosenberg, C., Cook, D.R., Bisseling, T., Huguet, T., and Denarie, J. (2002). Genetic and cytogenetic mapping of *DMI1*, *DMI2*, and *DMI3* genes of *Medicago truncatula* involved in Nod factor transduction, nodulation, and mycorrhization. Mol Plant Microbe Interact **15,** 1108-1118.

Antolin-Llovera, M., Ried, M.K., and Parniske, M. (2014). Cleavage of the SYMBIOSIS RECEPTOR-LIKE KINASE ectodomain promotes complex formation with nod factor receptor 5. Current Biology **24,** 422-427.

Ao, Y., Li, Z., Feng, D., Xiong, F., Liu, J., Li, J.-F., Wang, M., Wang, J., Liu, B., and Wang, H.-B. (2014). *Os*CERK1 and *Os*RLCK176 play important roles in peptidoglycan and chitin signaling in rice innate immunity. The Plant Journal **80,** 1072-1084.

Arrighi, J.F., Barre, A., Ben Amor, B., Bersoult, A., Soriano, L.C., Mirabella, R., de Carvalho-Niebel, F., Journet, E.P., Gherardi, M., Huguet, T., Geurts, R., Denarie, J., Rouge, P., and Gough, C. (2006). The *Medicago truncatula* lysin

motif-receptor-like kinase gene family includes NFP and new nodule-expressed genes. Plant Physiology **142,** 265-279.

Attardi, L.D., and Tjian, R. (1993). Drosophila tissue-specific transcription factor NTF-1 contains a novel isoleucine-rich activation motif. Genes & development **7,** 1341-1353.

Bago, B., Zipfel, W., Williams, R.M., Jun, J., Arreola, R., Lammers, P.J., Pfeffer, P.E., and Shachar-Hill, Y. (2002). Translocation and utilization of fungal storage lipid in the arbuscular mycorrhizal symbiosis. Plant Physiology **128,** 108-124.

Baier, M.C., Keck, M., Gödde, V., Niehaus, K., Küster, H., and Hohnjec, N. (2010). Knockdown of the symbiotic sucrose synthase *MtSucS1* affects arbuscule maturation and maintenance in mycorrhizal roots of *Medicago truncatula*. Plant physiology **152,** 1000-1014.

Banba, M., Gutjahr, C., Miyao, A., Hirochika, H., Paszkowski, U., Kouchi, H., and Imaizumi-Anraku, H. (2008). Divergence of evolutionary ways among common sym genes: *CASTOR* and *CCaMK* show functional conservation between two symbiosis systems and constitute the root of a common signaling pathway. Plant Cell Physiol **49,** 1659-1671.

Bastmeyer, M., Deising, H.B., and Bechinger, C. (2002). Force exertion in fungal infection. Annual Review of Biophysics and Biomolecular Structure **31,** 321-341.

Bell, C.D., Soltis, D.E., and Soltis, P.S. (2010). The age and diversification of the angiosperms re-revisited. American journal of botany **97,** 1296-1303.

Bensmihen, S. (2015). Hormonal Control of Lateral Root and Nodule Development in Legumes. Plants **4,** 523-547.

Besserer, A., Bécard, G., Jauneau, A., Roux, C., and Séjalon-Delmas, N. (2008). GR24, a Synthetic Analog of Strigolactones, Stimulates the Mitosis and Growth of the Arbuscular Mycorrhizal Fungus *Gigaspora rosea* by Boosting Its Energy Metabolism. Plant Physiology **148,** 402-413.

Besserer, A., Puech-Pagès, V., Kiefer, P., Gomez-Roldan, V., Jauneau, A., Roy, S., Portais, J.-C., Roux, C., Bécard, G., and Séjalon-Delmas, N. (2006). Strigolactones stimulate arbuscular mycorrhizal fungi by activating mitochondria. PLoS biology **4,** e226.

Binder, A., and Parniske, M. (2018). The nuclear pore complex in symbiosis and pathogen defence. Annual Plant Reviews online, 229-254.

Bitterlich, M., Krügel, U., Boldt-Burisch, K., Franken, P., and Kühn, C. (2014). The sucrose transporter *Sl*SUT 2 from tomato interacts with brassinosteroid

functioning and affects arbuscular mycorrhiza formation. The Plant Journal **78,** 877-889.

Bonfante-Fasolo, P. (1984). Anatomy and morphology of VA mycorrhizae. VA mycorrhizae **57,** 5-33.

Bravo, A., Brands, M., Wewer, V., Dörmann, P., and Harrison, M.J. (2017). Arbuscular mycorrhiza-specific enzymes FatM and RAM 2 fine-tune lipid biosynthesis to promote development of arbuscular mycorrhiza. New Phytologist **214,** 1631-1645.

Breuillin-Sessoms, F., Floss, D.S., Gomez, S.K., Pumplin, N., Ding, Y., Levesque-Tremblay, V., Noar, R.D., Daniels, D.A., Bravo, A., Eaglesham, J.B., Benedito, V.A., Udvardi, M.K., and Harrison, M.J. (2015). Suppression of Arbuscule Degeneration in *Medicago truncatula phosphate transporter 4* Mutants Is Dependent on the Ammonium Transporter 2 Family Protein AMT2;3. The Plant Cell **27,** 1352.

Brewin, N.J. (2010). Root nodules (legume–rhizobium symbiosis). eLS.

Broghammer, A., Krusell, L., Blaise, M., Sauer, J., Sullivan, J.T., Maolanon, N., Vinther, M., Lorentzen, A., Madsen, E.B., Jensen, K.J., Roepstorff, P., Thirup, S., Ronson, C.W., Thygesen, M.B., and Stougaard, J. (2012). Legume receptors perceive the rhizobial lipochitin oligosaccharide signal molecules by direct binding. PNAS **109,** 13859-13864.

Buendia, L., Wang, T., Girardin, A., and Lefebvre, B. (2016). The LysM receptor-like kinase *SlLYK10* regulates the arbuscular mycorrhizal symbiosis in tomato. New Phytologist **210,** 184-195.

Cabeza, R., Koester, B., Liese, R., Lingner, A., Baumgarten, V., Dirks, J., Salinas-Riester, G., Pommerenke, C., Dittert, K., and Schulze, J. (2014a). An RNA Sequencing Transcriptome Analysis Reveals Novel Insights into Molecular Aspects of the Nitrate Impact on the Nodule Activity of *Medicago truncatula*. Plant Physiology **164,** 400-411.

Cabeza, R.A., Liese, R., Lingner, A., von Stieglitz, I., Neumann, J., Salinas-Riester, G., Pommerenke, C., Dittert, K., and Schulze, J. (2014b). RNA-seq transcriptome profiling reveals that *Medicago truncatula* nodules acclimate N 2 fixation before emerging P deficiency reaches the nodules. Journal of Experimental Botany **65,** 6035-6048.

Calvenzani, V., Testoni, B., Gusmaroli, G., Lorenzo, M., Gnesutta, N., Petroni, K., Mantovani, R., and Tonelli, C. (2012). Interactions and CCAAT-Binding of *Arabidopsis thaliana* NF-Y Subunits. PloS one **7,** e42902.

Capoen, W., Sun, J., Wysham, D., Otegui, M.S., Venkateshwaran, M., Hirsch, S., Miwa, H., Downie, J.A., Morris, R.J., Ane, J.M., and Oldroyd, G.E. (2011). Nuclear membranes control symbiotic calcium signaling of legumes. Proceedings of the National Academy of Sciences, USA **108,** 14348-14353.

Carotenuto, G., Chabaud, M., Miyata, K., Capozzi, M., Takeda, N., Kaku, H., Shibuya, N., Nakagawa, T., Barker, D.G., and Genre, A. (2017). The rice LysM receptor-like kinase *Os*CERK1 is required for the perception of short-chain chitin oligomers in arbuscular mycorrhizal signaling. New Phytologist **214,** 1440-1446.

Cerri, M.R., Frances, L., Laloum, T., Auriac, M.C., Niebel, A., Oldroyd, G.E., Barker, D.G., Fournier, J., and de Carvalho-Niebel, F. (2012). *Medicago truncatula* ERN transcription factors: regulatory interplay with NSP1/NSP2 GRAS factors and expression dynamics throughout rhizobial infection. Plant Physiology **160,** 2155-2172.

Cerri, M.R., Frances, L., Kelner, A., Fournier, J., Middleton, P.H., Auriac, M.C., Mysore, K.S., Wen, J., Erard, M., Barker, D.G., Oldroyd, G.E., and de Carvalho-Niebel, F. (2016). The symbiosis-related ERN transcription factors act in concert to coordinate rhizobial host root infection. Plant Physiol **171,** 1037-1054.

Cerri, M.R., Wang, Q., Stolz, P., Folgmann, J., Frances, L., Katzer, K., Li, X., Heckmann, A.B., Wang, T.L., Downie, J.A., Klingl, A., de Carvalho-Niebel, F., Xie, F., and Parniske, M. (2017). The *ERN1* transcription factor gene is a target of the CCaMK/CYCLOPS complex and controls rhizobial infection in *Lotus japonicus*. New Phytologist **215,** 323-337.

Chabaud, M., Genre, A., Sieberer, B.J., Faccio, A., Fournier, J., Novero, M., Barker, D.G., and Bonfante, P. (2011). Arbuscular mycorrhizal hyphopodia and germinated spore exudates trigger Ca^{2+} spiking in the legume and nonlegume root epidermis. New Phytologist **189,** 347-355.

Charpentier, M. (2018). Calcium signals in the plant nucleus: origin and function. Journal of Experimental Botany **69,** 4165-4173.

Charpentier, M., and Oldroyd, G. (2010). How close are we to nitrogen-fixing cereals? Current opinion in plant biology **13,** 556-564.

Charpentier, M., Bredemeier, R., Wanner, G., Takeda, N., Schleiff, E., and Parniske, M. (2008). *Lotus japonicus* CASTOR and POLLUX are ion channels essential for perinuclear calcium spiking in legume root endosymbiosis. Plant Cell **20,** 3467-3479.

Charpentier, M., Sun, J., Vaz Martins, T., Radhakrishnan, G.V., Findlay, K., Soumpourou, E., Thouin, J., Very, A.A., Sanders, D., Morris, R.J., and Oldroyd, G.E. (2016). Nuclear-localized cyclic nucleotide-gated channels mediate symbiotic calcium oscillations. Science **352,** 1102-1105.

Chen, T., Zhu, H., Ke, D., Cai, K., Wang, C., Gou, H., Hong, Z., and Zhang, Z. (2012). A MAP Kinase Kinase Interacts with SymRK and Regulates Nodule Organogenesis in *Lotus japonicus*. The Plant Cell **24,** 823-838.

Chen, Y.F., Wang, Y., and Wu, W.H. (2008). Membrane transporters for nitrogen, phosphate and potassium uptake in plants. Journal of Integrative Plant Biology **50,** 835-848.

Coba de la Peña, T., Fedorova, E., Pueyo, J.J., and Lucas, M.M. (2018). The symbiosome: legume and rhizobia co-evolution toward a nitrogen-fixing organelle? Frontiers in plant science **8,** 2229.

Colebatch, G., Desbrosses, G., Ott, T., Krusell, L., Montanari, O., Kloska, S., Kopka, J., and Udvardi, M.K. (2004). Global changes in transcription orchestrate metabolic differentiation during symbiotic nitrogen fixation in *Lotus japonicus*. The Plant Journal **39,** 487-512.

Cordell, D., Rosemarin, A., Schröder, J.J., and Smit, A. (2011). Towards global phosphorus security: A systems framework for phosphorus recovery and reuse options. Chemosphere **84,** 747-758.

Coronado, C., Zuanazzi, J.A.S., Sallaud, C., Quirion, J.C., Esnault, R., Husson, H.P., Kondorosi, A., and Ratet, P. (1995). Alfalfa Root Flavonoid Production Is Nitrogen Regulated. Plant Physiology **108,** 533.

Courey, A.J., Holtzman, D.A., Jackson, S.P., and Tjian, R. (1989). Synergistic activation by the glutamine-rich domains of human transcription factor Sp1. Cell **59,** 827-836.

da Silva, V.P., van der Werf, H.M., Spies, A., and Soares, S.R. (2010). Variability in environmental impacts of Brazilian soybean according to crop production and transport scenarios. Journal of environmental management **91,** 1831-1839.

Dalpé, Y., and Monreal, M. (2004). Arbuscular mycorrhiza inoculum to support sustainable cropping systems. Crop management **3,** 1-11.

Davière, J.-M., and Achard, P. (2016). A Pivotal Role of DELLAs in Regulating Multiple Hormone Signals. Molecular Plant **9,** 10-20.

Delaux, P.M., Becard, G., and Combier, J.P. (2013). *NSP1* is a component of the Myc signaling pathway. New Phytologist **199,** 59-65.

Delaux, P.M., Radhakrishnan, G.V., Jayaraman, D., Cheema, J., Malbreil, M., Volkening, J.D., Sekimoto, H., Nishiyama, T., Melkonian, M., Pokorny, L., Rothfels, C.J., Sederoff, H.W., Stevenson, D.W., Surek, B., Zhang, Y., Sussman, M.R., Dunand, C., Morris, R.J., Roux, C., Wong, G.K., Oldroyd, G.E., and Ane, J.M. (2015). Algal ancestor of land plants was preadapted for symbiosis. Proc Natl Acad Sci U S A **112,** 13390-13395.

Demchenko, K., Winzer, T., Stougaard, J., Parniske, M., and Pawlowski, K. (2004). Distinct roles of *Lotus japonicus SYMRK* and *SYM15* in root colonization and arbuscule formation. New Phytologist **163,** 381-392.

Den Herder, G., Yoshida, S., Antolín-Llovera, M., Ried, M.K., and Parniske, M. (2012). *Lotus japonicus* E3 Ligase SEVEN IN ABSENTIA4 Destabilizes the Symbiosis Receptor-Like Kinase SYMRK and Negatively Regulates Rhizobial Infection. The Plant Cell **24,** 1691-1707.

Deng, J., Zhu, F., Liu, J., Zhao, Y., Wen, J., Wang, T., and Dong, J. (2019). Transcription Factor bHLH2 Represses *CYSTEINE PROTEASE77* to Negatively Regulate Nodule Senescence. Plant Physiology **181,** 1683-1703.

Diaz, C.L., Melchers, L.S., Hooykaas, P.J., Lugtenberg, B.J., and Kijne, J.W. (1989). Root lectin as a determinant of host–plant specificity in the Rhizobium–legume symbiosis. Nature **338,** 579-581.

Diploma Katja Katzer, (2011). CYCLOPS phosphorylation sites involved in root endosymbisis. In Institut für Biochemie und Biotechnologie (Martin-Luther-Universität Halle-Wittenberg), pp. 136.

Douglas, A. (2011). The Symbiotic Habit. BioScience **61,** 326-327.

Downie, J.A. (2014). Legume nodulation. Current Biology **24,** R184-R190.

Doyle, J.J. (2011). Phylogenetic perspectives on the origins of nodulation. Molecular Plant-Microbe Interactions **24,** 1289-1295.

Endre, G., Kereszt, A., Kevei, Z., Mihacea, S., Kalo, P., and Kiss, G.B. (2002). A receptor kinase gene regulating symbiotic nodule development. Nature **417,** 962-966.

Etzler, M.E., Kalsi, G., Ewing, N.N., Roberts, N.J., Day, R.B., and Murphy, J.B. (1999). A nod factor binding lectin with apyrase activity from legume roots. Proceedings of the National Academy of Sciences **96,** 5856-5861.

Fester, T., Strack, D., and Hause, B. (2001). Reorganization of tobacco root plastids during arbuscule development. Planta **213,** 864-868.

Fitter, A. (2006). What is the link between carbon and phosphorus fluxes in arbuscular mycorrhizas? A null hypothesis for symbiotic function. New Phytologist **172,** 3-6.

Fixen, P. (2009). World fertilizer nutrient reserves-a view to the future. Better Crops with Plant Food **93,** 8-11.

Floss, D.S., Levy, J.G., Levesque-Tremblay, V., Pumplin, N., and Harrison, M.J. (2013). DELLA proteins regulate arbuscule formation in arbuscular mycorrhizal symbiosis. PNAS **110,** E5025-5034.

Floss, D.S., Gomez, S.K., Park, H.J., MacLean, A.M., Muller, L.M., Bhattarai, K.K., Levesque-Tremblay, V., Maldonado-Mendoza, I.E., and Harrison, M.J. (2017). A Transcriptional Program for Arbuscule Degeneration during AM Symbiosis Is Regulated by MYB1. Curr Biol **27,** 1206-1212.

Fonouni-Farde, C., Tan, S., Baudin, M., Brault, M., Wen, J., Mysore, K.S., Niebel, A., Frugier, F., and Diet, A. (2016). DELLA-mediated gibberellin signalling regulates Nod factor signalling and rhizobial infection. Nature communications **7,** 12636.

Fournier, J., Timmers, A.C., Sieberer, B.J., Jauneau, A., Chabaud, M., and Barker, D.G. (2008). Mechanism of infection thread elongation in root hairs of *Medicago truncatula* and dynamic interplay with associated rhizobial colonization. Plant Physiology **148,** 1985-1995.

Fournier, J., Teillet, A., Chabaud, M., Ivanov, S., Genre, A., Limpens, E., de Carvalho-Niebel, F., and Barker, D.G. (2015). Remodeling of the Infection Chamber before Infection Thread Formation Reveals a Two-Step Mechanism for Rhizobial Entry into the Host Legume Root Hair. Plant Physiology **167,** 1233.

Gage, D.J. (2004). Infection and invasion of roots by symbiotic, nitrogen-fixing rhizobia during nodulation of temperate legumes. Microbiology and Molecular Biology Reviews **68,** 280-300.

Gamas, P., Brault, M., Jardinaud, M.-F., and Frugier, F. (2017). Cytokinins in Symbiotic Nodulation: When, Where, What For? Trends in Plant Science **22,** 792-802.

Gaude, N., Bortfeld, S., Duensing, N., Lohse, M., and Krajinski, F. (2012). Arbuscule-containing and non-colonized cortical cells of mycorrhizal roots undergo extensive and specific reprogramming during arbuscular mycorrhizal development. Plant J **69,** 510-528.

Gavrin, A., Chiasson, D., Ovchinnikova, E., Kaiser, B.N., Bisseling, T., and Fedorova, E.E. (2016). VAMP 721a and VAMP 721d are important for pectin dynamics and release of bacteria in soybean nodules. New Phytologist **210,** 1011-1021.

Genre, A., and Russo, G. (2016). Does a Common Pathway Transduce Symbiotic Signals in Plant–Microbe Interactions? Frontiers in Plant Science **7,** 96.

Genre, A., Chabaud, M., Timmers, T., Bonfante, P., and Barker, D.G. (2005). Arbuscular mycorrhizal fungi elicit a novel intracellular apparatus in *Medicago truncatula* root epidermal cells before infection. Plant Cell **17,** 3489-3499.

Genre, A., Chabaud, M., Faccio, A., Barker, D.G., and Bonfante, P. (2008). Prepenetration apparatus assembly precedes and predicts the colonization patterns of arbuscular mycorrhizal fungi within the root cortex of both *Medicago truncatula* and *Daucus carota*. Plant Cell **20,** 1407-1420.

Genre, A., Chabaud, M., Balzergue, C., Puech-Pagès, V., Novero, M., Rey, T., Fournier, J., Rochange, S., Bécard, G., and Bonfante, P. (2013). Short-chain chitin oligomers from arbuscular mycorrhizal fungi trigger nuclear Ca^{2+} spiking in *Medicago truncatula* roots and their production is enhanced by strigolactone. New Phytologist **198,** 190-202.

George, E., Marschner, H., and Jakobsen, I. (1995). Role of Arbuscular Mycorrhizal Fungi in Uptake of Phosphorus and Nitrogen From Soil. Critical Reviews in Biotechnology **15,** 257-270.

Geurts, R., Fedorova, E., and Bisseling, T. (2005). Nod factor signaling genes and their function in the early stages of Rhizobium infection. Curr Opin Plant Biol **8,** 346-352.

Geurts, R., Lillo, A., and Bisseling, T. (2012). Exploiting an ancient signalling machinery to enjoy a nitrogen fixing symbiosis. Curr Opin Plant Biol **15,** 438-443.

Gianinazzi, S., Gollotte, A., Binet, M.N., van Tuinen, D., Redecker, D., and Wipf, D. (2010). Agroecology: the key role of arbuscular mycorrhizas in ecosystem services. Mycorrhiza **20,** 519-530.

Gil-Díez, P., Tejada-Jiménez, M., León-Mediavilla, J., Wen, J., Mysore, K.S., Imperial, J., and González-Guerrero, M. (2019). *Mt*MOT1. 2 is responsible for molybdate supply to *Medicago truncatula* nodules. Plant, cell & environment **42,** 310-320.

Gilbert, N.C., Rui, Z., Neau, D.B., Waight, M.T., Bartlett, S.G., Boeglin, W.E., Brash, A.R., and Newcomer, M.E. (2012). Conversion of human 5-lipoxygenase to a 15-lipoxygenase by a point mutation to mimic phosphorylation at Serine-663. FASEB J **26,** 3222-3229.

Girardin, A., Wang, T., Ding, Y., Keller, J., Buendia, L., Gaston, M., Ribeyre, C., Gasciolli, V., Auriac, M.-C., Vernié, T., Bendahmane, A., Ried, M.K.,

Parniske, M., Morel, P., Vandenbussche, M., Schorderet, M., Reinhardt, D., Delaux, P.-M., Bono, J.-J., and Lefebvre, B. (2019). LCO Receptors Involved in Arbuscular Mycorrhiza Are Functional for Rhizobia Perception in Legumes. Current Biology **29,** 4249-4259.e4245.

Gleason, C., Chaudhuri, S., Yang, T., Munoz, A., Poovaiah, B.W., and Oldroyd, G.E. (2006). Nodulation independent of rhizobia induced by a calcium-activated kinase lacking autoinhibition. Nature **441,** 1149-1152.

Gobbato, E., Marsh, J.F., Vernie, T., Wang, E., Maillet, F., Kim, J., Miller, J.B., Sun, J., Bano, S.A., Ratet, P., Mysore, K.S., Denarie, J., Schultze, M., and Oldroyd, G.E. (2012). A GRAS-type transcription factor with a specific function in mycorrhizal signaling. Curr Biol **22,** 2236-2241.

Goh, T., Joi, S., Mimura, T., and Fukaki, H. (2012). The establishment of asymmetry in *Arabidopsis* lateral root founder cells is regulated by LBD16/ASL18 and related LBD/ASL proteins. Development **139,** 883-893.

Goh, T., Toyokura, K., Yamaguchi, N., Okamoto, Y., Uehara, T., Kaneko, S., Takebayashi, Y., Kasahara, H., Ikeyama, Y., Okushima, Y., Nakajima, K., Mimura, T., Tasaka, M., and Fukaki, H. (2019). Lateral root initiation requires the sequential induction of transcription factors LBD16 and PUCHI in *Arabidopsis thaliana*. New Phytologist **224,** 749-760.

Griesmann, M., Chang, Y., Liu, X., Song, Y., Haberer, G., Crook, M.B., Billault-Penneteau, B., Lauressergues, D., Keller, J., Imanishi, L., Roswanjaya, Y.P., Kohlen, W., Pujic, P., Battenberg, K., Alloisio, N., Liang, Y., Hilhorst, H., Salgado, M.G., Hocher, V., Gherbi, H., Svistoonoff, S., Doyle, J.J., He, S., Xu, Y., Xu, S., Qu, J., Gao, Q., Fang, X., Fu, Y., Normand, P., Berry, A.M., Wall, L.G., Ané, J.-M., Pawlowski, K., Xu, X., Yang, H., Spannagl, M., Mayer, K.F.X., Wong, G.K.-S., Parniske, M., Delaux, P.-M., and Cheng, S. (2018). Phylogenomics reveals multiple losses of nitrogen-fixing root nodule symbiosis. Science.

Grimsrud, P.A., den Os, D., Wenger, C.D., Swaney, D.L., Schwartz, D., Sussman, M.R., Ane, J.M., and Coon, J.J. (2010). Large-scale phosphoprotein analysis in *Medicago truncatula* roots provides insight into *in vivo* kinase activity in legumes. Plant Physiol **152,** 19-28.

Groth, M., Takeda, N., Perry, J., Uchida, H., Draxl, S., Brachmann, A., Sato, S., Tabata, S., Kawaguchi, M., Wang, T.L., and Parniske, M. (2010). NENA, a *Lotus japonicus* homolog of Sec13, is required for rhizodermal infection by arbuscular mycorrhiza fungi and rhizobia but dispensable for cortical endosymbiotic development. Plant Cell **22,** 2509-2526.

Guether, M., Balestrini, R., Hannah, M., He, J., Udvardi, M.K., and Bonfante, P. (2009). Genome-wide reprogramming of regulatory networks, transport, cell wall and membrane biogenesis during arbuscular mycorrhizal symbiosis in *Lotus japonicus*. New Phytologist **182,** 200-212.

Gutjahr, C., and Parniske, M. (2013). Cell and developmental biology of arbuscular mycorrhiza symbiosis. Annual review of cell and developmental biology **29,** 593-617.

Gutjahr, C., and Parniske, M. (2017). Cell biology: control of partner lifetime in a plant–fungus relationship. Current Biology **27,** R420-R423.

Gutjahr, C., Novero, M., Guether, M., Montanari, O., Udvardi, M., and Bonfante, P. (2009). Presymbiotic factors released by the arbuscular mycorrhizal fungus *Gigaspora margarita* induce starch accumulation in *Lotus japonicus* roots. New Phytologist **183,** 53-61.

Gutjahr, C., Gobbato, E., Choi, J., Riemann, M., Johnston, M.G., Summers, W., Carbonnel, S., Mansfield, C., Yang, S.Y., Nadal, M., Acosta, I., Takano, M., Jiao, W.B., Schneeberger, K., Kelly, K.A., and Paszkowski, U. (2015). Rice perception of symbiotic arbuscular mycorrhizal fungi requires the karrikin receptor complex. Science **350,** 1521-1524.

Hackenberg, D., Wu, Y., Voigt, A., Adams, R., Schramm, P., and Grimm, B. (2012). Studies on Differential Nuclear Translocation Mechanism and Assembly of the Three Subunits of the *Arabidopsis thaliana* Transcription Factor NF-Y. Molecular Plant **5,** 876-888.

Hakoyama, T., Niimi, K., Yamamoto, T., Isobe, S., Sato, S., Nakamura, Y., Tabata, S., Kumagai, H., Umehara, Y., and Brossuleit, K. (2012). The integral membrane protein SEN1 is required for symbiotic nitrogen fixation in *Lotus japonicus* nodules. Plant and Cell Physiology **53,** 225-236.

Harrison, M.J. (2005). Signaling in the arbuscular mycorrhizal symbiosis. Annu. Rev. Microbiol. **59,** 19-42.

Hayashi, T., Shimoda, Y., Sato, S., Tabata, S., Imaizumi-Anraku, H., and Hayashi, M. (2014). Rhizobial infection does not require cortical expression of upstream common symbiosis genes responsible for the induction of Ca^{2+} spiking Plant J **77,** 146-159.

Heck, C., Kuhn, H., Heidt, S., Walter, S., Rieger, N., and Requena, N. (2016). Symbiotic Fungi Control Plant Root Cortex Development through the Novel GRAS Transcription Factor MIG1. Current Biology **26,** 2770-2778.

Heckmann, A.B., Lombardo, F., Miwa, H., Perry, J.A., Bunnewell, S., Parniske, M., Wang, T.L., and Downie, J.A. (2006). *Lotus japonicus* nodulation

requires two GRAS domain regulators, one of which is functionally conserved in a non-legume. Plant physiology **142,** 1739-1750.

Helber, N., Wippel, K., Sauer, N., Schaarschmidt, S., Hause, B., and Requena, N. (2011). A Versatile Monosaccharide Transporter That Operates in the Arbuscular Mycorrhizal Fungus *Glomus* sp Is Crucial for the Symbiotic Relationship with Plants. The Plant Cell **23,** 3812.

Herendeen, P.S., Magallon-Puebla, S., Lupia, R., Crane, P.R., and Kobylinska, J. (1999). A preliminary conspectus of the Allon flora from the Late Cretaceous (late Santonian) of central Georgia, USA. Annals of the Missouri Botanical Garden**,** 407-471.

Hirsch, A.M. (1999). Role of lectins (and rhizobial exopolysaccharides) in legume nodulation. Current opinion in plant biology **2,** 320-326.

Hirsch, S., Kim, J., Munoz, A., Heckmann, A.B., Downie, J.A., and Oldroyd, G.E. (2009). GRAS proteins form a DNA binding complex to induce gene expression during nodulation signaling in *Medicago truncatula*. Plant Cell **21,** 545-557.

Hoffman, B.M., Lukoyanov, D., Yang, Z.Y., Dean, D.R., and Seefeldt, L.C. (2014). Mechanism of nitrogen fixation by nitrogenase: the next stage. Chem Rev **114,** 4041-4062.

Holmberg, C.I., Tran, S.E., Eriksson, J.E., and Sistonen, L. (2002). Multisite phosphorylation provides sophisticated regulation of transcription factors. Trends Biochem Sci **27,** 619-627.

Holmberg, C.I., Hietakangas, V., Mikhailov, A., Rantanen, J.O., Kallio, M., Meinander, A., Hellman, J., Morrice, N., MacKintosh, C., Morimoto, R.I., Eriksson, J.E., and Sistonen, L. (2001). Phosphorylation of serine 230 promotes inducible transcriptional activity of heat shock factor 1. The EMBO journal **20,** 3800-3810.

Holsters, M., Silva, B., Van Vliet, F., Genetello, C., De Block, M., Dhaese, P., Depicker, A., Inzé, D., Engler, G., and Villarroel, R. (1980). The functional organization of the nopaline A. tumefaciens plasmid pTiC58. Plasmid **3,** 212-230.

Horvath, B., Yeun, L.H., Domonkos, A., Halasz, G., Gobbato, E., Ayaydin, F., Miro, K., Hirsch, S., Sun, J., Tadege, M., Ratet, P., Mysore, K.S., Ane, J.M., Oldroyd, G.E., and Kalo, P. (2011). *Medicago truncatula IPD3* is a member of the common symbiotic signaling pathway required for rhizobial and mycorrhizal symbioses. Molecular Plant-Microbe Interactions **24,** 1345-1358.

Hossain, M.S., Shrestha, A., Zhong, S., Miri, M., Austin, R.S., Sato, S., Ross, L., Huebert, T., Tromas, A., and Torres-Jerez, I. (2016). *Lotus japonicus* NF-YA1 plays an essential role during nodule differentiation and targets members of the *SHI*/*STY* gene family. Molecular Plant-Microbe Interactions **29,** 950-964.

Hrabak, E.M., Chan, C.W., Gribskov, M., Harper, J.F., Choi, J.H., Halford, N., Kudla, J., Luan, S., Nimmo, H.G., Sussman, M.R., Thomas, M., Walker-Simmons, K., Zhu, J.K., and Harmon, A.C. (2003). The *Arabidopsis* CDPK-SnRK superfamily of protein kinases. Plant Physiol **132,** 666-680.

Huault, E., Laffont, C., Wen, J., Mysore, K.S., Ratet, P., Duc, G., and Frugier, F. (2014). Local and Systemic Regulation of Plant Root System Architecture and Symbiotic Nodulation by a Receptor-Like Kinase. PLoS genetics **10,** e1004891.

Huisman, R., and Geurts, R. (2020). A roadmap toward engineered nitrogen-fixing nodule symbiosis. Plant communications **1,** 100019.

Hunter, T., and Karin, M. (1992). The regulation of transcription by phosphorylation. Cell **70,** 375-387.

Imaizumi-Anraku, H., Takeda, N., Charpentier, M., Perry, J., Miwa, H., Umehara, Y., Kouchi, H., Murakami, Y., Mulder, L., Vickers, K., Pike, J., Downie, J.A., Wang, T., Sato, S., Asamizu, E., Tabata, S., Yoshikawa, M., Murooka, Y., Wu, G.J., Kawaguchi, M., Kawasaki, S., Parniske, M., and Hayashi, M. (2005). Plastid proteins crucial for symbiotic fungal and bacterial entry into plant roots. Nature **433,** 527-531.

Imin, N., Patel, N., Corcilius, L., Payne, R.J., and Djordjevic, M.A. (2018). CLE peptide tri-arabinosylation and peptide domain sequence composition are essential for SUNN-dependent autoregulation of nodulation in *Medicago truncatula*. New Phytologist **218,** 73-80.

Ivanov, S., Fedorova, E.E., Limpens, E., De Mita, S., Genre, A., Bonfante, P., and Bisseling, T. (2012). Rhizobium–legume symbiosis shares an exocytotic pathway required for arbuscule formation. Proceedings of the National Academy of Sciences **109,** 8316-8321.

Javot, H., Pumplin, N., and Harrison, M.J. (2007). Phosphate in the arbuscular mycorrhizal symbiosis: transport properties and regulatory roles. Plant, cell & environment **30,** 310-322.

Jedidi, I., Zhang, F., Qiu, H., Stahl, S.J., Palmer, I., Kaufman, J.D., Nadaud, P.S., Mukherjee, S., Wingfield, P.T., and Jaroniec, C.P. (2010). Activator Gcn4 employs multiple segments of Med15/Gal11, including the KIX domain, to

recruit mediator to target genes in vivo. Journal of Biological Chemistry **285,** 2438-2455.

Jiang, Y., Wang, W., Xie, Q., Liu, N., Liu, L., Wang, D., Zhang, X., Yang, C., Chen, X., Tang, D., and Wang, E. (2017). Plants transfer lipids to sustain colonization by mutualistic mycorrhizal and parasitic fungi. Science **356,** 1172-1175.

Jin, Y., Chen, Z., Yang, J., Mysore, K.S., Wen, J., Huang, J., Yu, N., and Wang, E. (2018). IPD3 and IPD3L function redundantly in rhizobial and mycorrhizal symbioses. Front Plant Sci **9,** 267.

Jin, Y., Liu, H., Luo, D., Yu, N., Dong, W., Wang, C., Zhang, X., Dai, H., Yang, J., and Wang, E. (2016). DELLA proteins are common components of symbiotic rhizobial and mycorrhizal signalling pathways. Nature communications **7,** 12433.

Kaló, P., Gleason, C., Edwards, A., Marsh, J., Mitra, R.M., Hirsch, S., Jakab, J., Sims, S., Long, S.R., and Rogers, J. (2005). Nodulation signaling in legumes requires NSP2, a member of the GRAS family of transcriptional regulators. Science **308,** 1786-1789.

Kanamori, N., Madsen, L.H., Radutoiu, S., Frantescu, M., Quistgaard, E.M., Miwa, H., Downie, J.A., James, E.K., Felle, H.H., Haaning, L.L., Jensen, T.H., Sato, S., Nakamura, Y., Tabata, S., Sandal, N., and Stougaard, J. (2006). A nucleoporin is required for induction of Ca^{2+} spiking in legume nodule development and essential for rhizobial and fungal symbiosis. PNAS **103,** 359-364.

Kang, H., Zhu, H., Chu, X., Yang, Z., Yuan, S., Yu, D., Wang, C., Hong, Z., and Zhang, Z. (2011). A novel interaction between CCaMK and a protein containing the Scythe_N ubiquitin-like domain in *Lotus japonicus*. Plant Physiol **155,** 1312-1324.

Kang, H., Xiao, A., Huang, X., Gao, X., Yu, H., He, X., Zhu, H., Hong, Z., and Zhang, Z. (2015). A *Lotus japonicus* cochaperone protein interacts with the ubiquitin-like domain protein CIP73 and plays a negative regulatory role in nodulation. MPMI **28,** 534-545.

Kang, H., Chu, X., Wang, C., Xiao, A., Zhu, H., Yuan, S., Yang, Z., Ke, D., Xiao, S., Hong, Z., and Zhang, Z. (2014). A MYB coiled-coil transcription factor interacts with NSP2 and is involved in nodulation in *Lotus japonicus*. New Phytol **201,** 837-849.

Katzer, K. (2017). Structure, function and regulation of the CCaMK/CYCLOPS complex during root symbioses (lmu).

Kawaharada, Y., Nielsen, M.W., Kelly, S., James, E.K., Andersen, K.R., Rasmussen, S.R., Fuchtbauer, W., Madsen, L.H., Heckmann, A.B., Radutoiu, S., and Stougaard, J. (2017). Differential regulation of the *Epr3* receptor coordinates membrane-restricted rhizobial colonization of root nodule primordia. Nature communications **8,** 14534.

Kawaharada, Y., Kelly, S., Nielsen, M.W., Hjuler, C.T., Gysel, K., Muszynski, A., Carlson, R.W., Thygesen, M.B., Sandal, N., Asmussen, M.H., Vinther, M., Andersen, S.U., Krusell, L., Thirup, S., Jensen, K.J., Ronson, C.W., Blaise, M., Radutoiu, S., and Stougaard, J. (2015). Receptor-mediated exopolysaccharide perception controls bacterial infection. Nature **523,** 308-312.

Ke, D., Fang, Q., Chen, C., Zhu, H., Chen, T., Chang, X., Yuan, S., Kang, H., Ma, L., Hong, Z., and Zhang, Z. (2012). The Small GTPase ROP6 Interacts with NFR5 and Is Involved in Nodule Formation in *Lotus japonicus*. Plant Physiology **159,** 131.

Kevei, Z., Lougnon, G., Mergaert, P., Horvath, G.V., Kereszt, A., Jayaraman, D., Zaman, N., Marcel, F., Regulski, K., Kiss, G.B., Kondorosi, A., Endre, G., Kondorosi, E., and Ane, J.M. (2007). 3-hydroxy-3-methylglutaryl coenzyme a reductase 1 interacts with NORK and is crucial for nodulation in *Medicago truncatula*. Plant Cell **19,** 3974-3989.

Keymer, A., Pimprikar, P., Wewer, V., Huber, C., Brands, M., Bucerius, S., Delaux, P.-M., Klingl, V., von Roepenack-Lahaye, E., Wang, T.L., Eisenreich, W., Doermann, P., Parniske, M., and Gutjahr, C. (2017). Lipid transfer from plants to arbuscular mycorrhiza fungi. bioRxiv.

Kiers, E.T., Duhamel, M., Beesetty, Y., Mensah, J.A., Franken, O., Verbruggen, E., Fellbaum, C.R., Kowalchuk, G.A., Hart, M.M., and Bago, A. (2011). Reciprocal rewards stabilize cooperation in the mycorrhizal symbiosis. Science **333,** 880-882.

Kijne, J.W., Bauchrowitz, M.A., and Diaz, C.L. (1997). Root lectins and rhizobia. Plant physiology **115,** 869.

Kim, S., Zeng, W., Bernard, S., Liao, J., Venkateshwaran, M., Ane, J.M., and Jiang, Y. (2019). Ca^{2+}-regulated Ca^{2+} channels with an RCK gating ring control plant symbiotic associations. Nat Commun **10,** 3703.

Kistner, C., and Parniske, M. (2002). Evolution of signal transduction in intracellular symbiosis. Trends Plant Sci **7,** 511-518.

Kistner, C., Winzer, T., Pitzschke, A., Mulder, L., Sato, S., Kaneko, T., Tabata, S., Sandal, N., Stougaard, J., and Webb, K.J. (2005). Seven *Lotus japonicus*

genes required for transcriptional reprogramming of the root during fungal and bacterial symbiosis. Plant Cell **17,** 2217-2229.

Kline, M.P., and Morimoto, R.I. (1997). Repression of the heat shock factor 1 transcriptional activation domain is modulated by constitutive phosphorylation. Mol Cell Biol **17,** 2107-2115.

Kobae, Y., Gutjahr, C., Paszkowski, U., Kojima, T., Fujiwara, T., and Hata, S. (2014). Lipid droplets of arbuscular mycorrhizal fungi emerge in concert with arbuscule collapse. Plant and Cell Physiology **55,** 1945-1953.

Kõivomägi, M., Valk, E., Venta, R., Iofik, A., Lepiku, M., Balog, E.R.M., Rubin, S.M., Morgan, D.O., and Loog, M. (2011). Cascades of multisite phosphorylation control Sic1 destruction at the onset of S phase. Nature **480,** 128-131.

Kosuta, S., Chabaud, M., Lougnon, G., Gough, C., Dénarié, J., Barker, D.G., and Bécard, G. (2003). A diffusible factor from arbuscular mycorrhizal fungi induces symbiosis-specific *MtENOD11* expression in roots of *Medicago truncatula*. Plant physiology **131,** 952-962.

Kretzschmar, T., Kohlen, W., Sasse, J., Borghi, L., Schlegel, M., Bachelier, J.B., Reinhardt, D., Bours, R., Bouwmeester, H.J., and Martinoia, E. (2012). A petunia ABC protein controls strigolactone-dependent symbiotic signalling and branching. Nature **483,** 341-344.

Krusell, L., Krause, K., Ott, T., Desbrosses, G., Krämer, U., Sato, S., Nakamura, Y., Tabata, S., James, E.K., and Sandal, N. (2005). The sulfate transporter SST1 is crucial for symbiotic nitrogen fixation in *Lotus japonicus* root nodules. The Plant Cell **17,** 1625-1636.

Kryvoruchko, I.S., Routray, P., Sinharoy, S., Torres-Jerez, I., Tejada-Jiménez, M., Finney, L.A., Nakashima, J., Pislariu, C.I., Benedito, V.A., and Gonzalez-Guerrero, M. (2018). An iron-activated citrate transporter, *Mt*MATE67, is required for symbiotic nitrogen fixation. Plant Physiology **176,** 2315-2329.

Kuhn, H., Küster, H., and Requena, N. (2010). Membrane steroid-binding protein 1 induced by a diffusible fungal signal is critical for mycorrhization in *Medicago truncatula*. New Phytologist **185,** 716-733.

Laffont, C., Ivanovici, A., Gautrat, P., Brault, M., Djordjevic, M.A., and Frugier, F. (2020). The NIN transcription factor coordinates CEP and CLE signaling peptides that regulate nodulation antagonistically. Nat Commun **11,** 3167.

Laloum, T., Baudin, M., Frances, L., Lepage, A., Billault-Penneteau, B., Cerri, M.R., Ariel, F., Jardinaud, M.F., Gamas, P., de Carvalho-Niebel, F., and Niebel, A. (2014). Two CCAAT-box-binding transcription factors

redundantly regulate early steps of the legume-rhizobia endosymbiosis. Plant J **79,** 757-768.

Lampugnani, E.R., Wink, R.H., Persson, S., and Somssich, M. (2018). The Toolbox to Study Protein–Protein Interactions in Plants. Critical Reviews in Plant Sciences **37,** 308-334.

Lanfranco, L., Fiorilli, V., and Gutjahr, C. (2018). Partner communication and role of nutrients in the arbuscular mycorrhizal symbiosis. New Phytol **220,** 1031-1046.

Laporte, P., Lepage, A., Fournier, J., Catrice, O., Moreau, S., Jardinaud, M.F., Mun, J.H., Larrainzar, E., Cook, D.R., Gamas, P., and Niebel, A. (2014). The CCAAT box-binding transcription factor NF-YA1 controls rhizobial infection. J Exp Bot **65,** 481-494.

Lazo, G.R., Stein, P.A., and Ludwig, R.A. (1991). A DNA transformation-competent Arabidopsis genomic library in *Agrobacterium*. Biotechnology (N Y) **9,** 963-967.

Lerouge, P., Roche, P., Faucher, C., Maillet, F., Truchet, G., Promé, J.C., and Dénarié, J. (1990). Symbiotic host-specificity of *Rhizobium meliloti* is determined by a sulphated and acylated glucosamine oligosaccharide signal. Nature **344,** 781-784.

Levy, J., Bres, C., Geurts, R., Chalhoub, B., Kulikova, O., Duc, G., Journet, E.P., Ane, J.M., Lauber, E., Bisseling, T., Denarie, J., Rosenberg, C., and Debelle, F. (2004). A putative Ca^{2+} and calmodulin-dependent protein kinase required for bacterial and fungal symbioses. Science **303,** 1361-1364.

Li, X., Zheng, Z., Kong, X., Xu, J., Qiu, L., Sun, J., Reid, D., Jin, H., Andersen, S.U., Oldroyd, G.E.D., Stougaard, J., Downie, J.A., and Xie, F. (2019). Atypical Receptor Kinase RINRK1 Required for Rhizobial Infection But Not Nodule Development in *Lotus japonicus*. Plant Physiol **181,** 804-816.

Liang, P., Stratil, T.F., Popp, C., Marín, M., Folgmann, J., Mysore, K.S., Wen, J., and Ott, T. (2018). Symbiotic root infections in *Medicago truncatula* require remorin-mediated receptor stabilization in membrane nanodomains. Proceedings of the National Academy of Sciences **115,** 5289.

Liao, J., Singh, S., Hossain, M.S., Andersen, S.U., Ross, L., Bonetta, D., Zhou, Y., Sato, S., Tabata, S., Stougaard, J., Szczyglowski, K., and Parniske, M. (2012). Negative regulation of CCaMK is essential for symbiotic infection. Plant J **72,** 572-584.

Liese, R., Schulze, J., and Cabeza, R.A. (2017). Nitrate application or P deficiency induce a decline in *Medicago truncatula* N2-fixation by similar changes in the nodule transcriptome. Scientific reports **7,** 46264.

Limpens, E., Ivanov, S., van Esse, W., Voets, G., Fedorova, E., and Bisseling, T. (2009). *Medicago* N2-fixing symbiosomes acquire the endocytic identity marker Rab7 but delay the acquisition of vacuolar identity. The Plant Cell **21,** 2811-2828.

Lin, J.S., Li, X., Luo, Z.L., Mysore, K.S., Wen, J., and Xie, F. (2018). NIN interacts with NLPs to mediate nitrate inhibition of nodulation in *Medicago truncatula*. Nature Plants.

Lindsay, P.L., Williams, B.N., MacLean, A., and Harrison, M.J. (2019). A Phosphate-Dependent Requirement for Transcription Factors IPD3 and IPD3L During Arbuscular Mycorrhizal Symbiosis in *Medicago truncatula*. Molecular Plant-Microbe Interactions® **32,** 1277-1290.

Liu, C.-W., Breakspear, A., Stacey, N., Findlay, K., Nakashima, J., Ramakrishnan, K., Liu, M., Xie, F., Endre, G., and de Carvalho-Niebel, F. (2019a). A protein complex required for polar growth of rhizobial infection threads. Nature communications **10,** 1-17.

Liu, C.W., Breakspear, A., Guan, D., Cerri, M.R., Abbs, K., Jiang, S., Robson, F.C., Radhakrishnan, G., Roy, S., Bone, C., Stacey, N., Rogers, C., Trick, M., Niebel, A., Oldroyd, G.E., de Carvalho-Niebel, F., and Murray, J.D. (2019b). NIN acts as a network hub controlling a growth module required for rhizobial infection. Plant Physiol.

Liu, J., Rutten, L., Limpens, E., van der Molen, T., van Velzen, R., Chen, R., Chen, Y., Geurts, R., Kohlen, W., Kulikova, O., and Bisseling, T. (2019c). A remote *cis*-regulatory region is required for *NIN* expression in the pericycle to initiate nodule primordium formation in *Medicago truncatula*. Plant Cell **31,** 68-83.

Liu, M., Soyano, T., Yano, K., Hayashi, M., and Kawaguchi, M. (2019d). ERN1 and CYCLOPS coordinately activate *NIN* signaling to promote infection thread formation in *Lotus japonicus*. J Plant Res.

Liu, W., Kohlen, W., Lillo, A., Op den Camp, R., Ivanov, S., Hartog, M., Limpens, E., Jamil, M., Smaczniak, C., Kaufmann, K., Yang, W.C., Hooiveld, G.J., Charnikhova, T., Bouwmeester, H.J., Bisseling, T., and Geurts, R. (2011). Strigolactone biosynthesis in *Medicago truncatula* and rice requires the symbiotic GRAS-type transcription factors NSP1 and NSP2. Plant Cell **23,** 3853-3865.

Lohse, S., Schliemann, W., Ammer, C., Kopka, J., Strack, D., and Fester, T. (2005). Organization and metabolism of plastids and mitochondria in arbuscular mycorrhizal roots of *Medicago truncatula*. Plant Physiology **139,** 329-340.

Luginbuehl, L.H., Menard, G.N., Kurup, S., Van Erp, H., Radhakrishnan, G.V., Breakspear, A., Oldroyd, G.E., and Eastmond, P.J. (2017). Fatty acids in arbuscular mycorrhizal fungi are synthesized by the host plant. Science **356,** 1175-1178.

Ma, F., Lu, R., Liu, H., Shi, B., Zhang, J., Tan, M., Zhang, A., and Jiang, M. (2012). Nitric oxide-activated calcium/calmodulin-dependent protein kinase regulates the abscisic acid-induced antioxidant defence in maize. Journal of Experimental Botany **63,** 4835-4847.

Maathuis, F.J.M. (2009). Physiological functions of mineral macronutrients. Current Opinion in Plant Biology **12,** 250-258.

MacLean, A.M., Bravo, A., and Harrison, M.J. (2017). Plant Signaling and Metabolic Pathways Enabling Arbuscular Mycorrhizal Symbiosis. The Plant Cell **29,** 2319.

Madsen, E.B., Madsen, L.H., Radutoiu, S., Olbryt, M., Rakwalska, M., Szczyglowski, K., Sato, S., Kaneko, T., Tabata, S., Sandal, N., and Stougaard, J. (2003). A receptor kinase gene of the LysM type is involved in legume perception of rhizobial signals. Nature **425,** 637-640.

Madsen, L.H., Tirichine, L., Jurkiewicz, A., Sullivan, J.T., Heckmann, A.B., Bek, A.S., Ronson, C.W., James, E.K., and Stougaard, J. (2010). The molecular network governing nodule organogenesis and infection in the model legume *Lotus japonicus*. Nature communications **1,** 10.

Maekawa, T., Maekawa-Yoshikawa, M., Takeda, N., Imaizumi-Anraku, H., Murooka, Y., and Hayashi, M. (2009). Gibberellin controls the nodulation signaling pathway in *Lotus japonicus*. Plant J **58,** 183-194.

Magori, S., and Kawaguchi, M. (2009). Long-distance control of nodulation: molecules and models. Molecules and cells **27,** 129-134.

Maillet, F., Poinsot, V., André, O., Puech-Pagès, V., Haouy, A., Gueunier, M., Cromer, L., Giraudet, D., Formey, D., and Niebel, A. (2011). Fungal lipochitooligosaccharide symbiotic signals in arbuscular mycorrhiza. Nature **469,** 58-63.

Marx, H., Minogue, C.E., Jayaraman, D., Richards, A.L., Kwiecien, N.W., Siahpirani, A.F., Rajasekar, S., Maeda, J., Garcia, K., Del Valle-Echevarria, A.R., Volkening, J.D., Westphall, M.S., Roy, S., Sussman, M.R., Ane, J.M., and Coon, J.J. (2016). A proteomic atlas of the legume *Medicago truncatula*

and its nitrogen-fixing endosymbiont *Sinorhizobium meliloti*. Nature Biotechnology **34,** 1198-1205.

Menge, D.N.L., Hedin, L.O., and Pacala, S.W. (2012). Nitrogen and phosphorus limitation over long-term ecosystem development in terrestrial ecosystems. PloS one **7,** e42045-e42045.

Mergaert, P. (2018). Role of antimicrobial peptides in controlling symbiotic bacterial populations. Natural Product Reports **35,** 336-356.

Mergaert, P., Kereszt, A., and Kondorosi, E. (2020). Gene expression in nitrogen-fixing symbiotic nodule cells in *Medicago truncatula* and other nodulating plants. Plant Cell **32,** 42-68.

Mergaert, P., Uchiumi, T., Alunni, B., Evanno, G., Cheron, A., Catrice, O., Mausset, A.-E., Barloy-Hubler, F., Galibert, F., and Kondorosi, A. (2006). Eukaryotic control on bacterial cell cycle and differentiation in the Rhizobium–legume symbiosis. Proceedings of the National Academy of Sciences **103,** 5230-5235.

Mermod, N., O'Neill, E.A., Kelly, T.J., and Tjian, R. (1989). The proline-rich transcriptional activator of CTF/NF-I is distinct from the replication and DNA binding domain. Cell **58,** 741-753.

Messinese, E., Mun, J.H., Yeun, L.H., Jayaraman, D., Rouge, P., Barre, A., Lougnon, G., Schornack, S., Bono, J.J., Cook, D.R., and Ane, J.M. (2007). A novel nuclear protein interacts with the symbiotic DMI3 calcium- and calmodulin-dependent protein kinase of *Medicago truncatula*. Molecular Plant-Microbe Interactions **20,** 912-921.

Middleton, P.H., Jakab, J., Penmetsa, R.V., Starker, C.G., Doll, J., Kaló, P., Prabhu, R., Marsh, J.F., Mitra, R.M., and Kereszt, A. (2007). An ERF transcription factor in *Medicago truncatula* that is essential for Nod factor signal transduction. The Plant Cell Online **19,** 1221-1234.

Miller, A., and Cramer, M. (2005). Root nitrogen acquisition and assimilation. Plant and soil **274,** 1-36.

Miller, J.B., Pratap, A., Miyahara, A., Zhou, L., Bornemann, S., Morris, R.J., and Oldroyd, G.E. (2013). Calcium/Calmodulin-dependent protein kinase is negatively and positively regulated by calcium, providing a mechanism for decoding calcium responses during symbiosis signaling. Plant Cell **25,** 5053-5066.

Mitra, R.M., Gleason, C.A., Edwards, A., Hadfield, J., Downie, J.A., Oldroyd, G.E., and Long, S.R. (2004). A Ca^{2+}/calmodulin-dependent protein kinase

required for symbiotic nodule development: Gene identification by transcript-based cloning. Proc Natl Acad Sci U S A **101,** 4701-4705.

Mitsuhashi, N., Ohnishi, M., Sekiguchi, Y., Kwon, Y.-U., Chang, Y.-T., Chung, S.-K., Inoue, Y., Reid, R.J., Yagisawa, H., and Mimura, T. (2005). Phytic acid synthesis and vacuolar accumulation in suspension-cultured cells of *Catharanthus roseus* induced by high concentration of inorganic phosphate and cations. Plant physiology **138,** 1607-1614.

Miwa, H., Sun, J., Oldroyd, G.E., and Downie, J.A. (2006). Analysis of calcium spiking using a cameleon calcium sensor reveals that nodulation gene expression is regulated by calcium spike number and the developmental status of the cell. Plant J **48,** 883-894.

Miyahara, A., Richens, J., Starker, C., Morieri, G., Smith, L., Long, S., Downie, J.A., and Oldroyd, G.E. (2010). Conservation in function of a SCAR/WAVE component during infection thread and root hair growth in *Medicago truncatula*. Molecular plant-microbe interactions **23,** 1553-1562.

Miyata, K., Kozaki, T., Kouzai, Y., Ozawa, K., Ishii, K., Asamizu, E., Okabe, Y., Umehara, Y., Miyamoto, A., Kobae, Y., Akiyama, K., Kaku, H., Nishizawa, Y., Shibuya, N., and Nakagawa, T. (2014). The Bifunctional Plant Receptor, *Os*CERK1, Regulates Both Chitin-Triggered Immunity and Arbuscular Mycorrhizal Symbiosis in Rice. Plant and Cell Physiology **55,** 1864-1872.

Mohd-Radzman, N.A., Laffont, C., Ivanovici, A., Patel, N., Reid, D., Stougaard, J., Frugier, F., Imin, N., and Djordjevic, M.A. (2016). Different Pathways Act Downstream of the CEP Peptide Receptor CRA2 to Regulate Lateral Root and Nodule Development. Plant Physiology **171,** 2536-2548.

Mohr, S., and Evans, G. (2013). Projections of future phosphorus production. Philica **380**.

Mortier, V., De Wever, E., Vuylsteke, M., Holsters, M., and Goormachtig, S. (2012). Nodule numbers are governed by interaction between CLE peptides and cytokinin signaling. Plant J **70,** 367-376.

Murakami, E., Cheng, J., Gysel, K., Bozsoki, Z., Kawaharada, Y., Hjuler, C.T., Sorensen, K.K., Tao, K., Kelly, S., Venice, F., Genre, A., Thygesen, M.B., Jong, N., Vinther, M., Jensen, D.B., Jensen, K.J., Blaise, M., Madsen, L.H., Andersen, K.R., Stougaard, J., and Radutoiu, S. (2018). Epidermal LysM receptor ensures robust symbiotic signalling in *Lotus japonicus*. eLife **7**.

Murray, J.D., Karas, B.J., Sato, S., Tabata, S., Amyot, L., and Szczyglowski, K. (2007). A cytokinin perception mutant colonized by *Rhizobium* in the absence of nodule organogenesis. Science **315,** 101-104.

Murray, J.D., Muni, R.R., Torres-Jerez, I., Tang, Y., Allen, S., Andriankaja, M., Li, G., Laxmi, A., Cheng, X., Wen, J., Vaughan, D., Schultze, M., Sun, J., Charpentier, M., Oldroyd, G., Tadege, M., Ratet, P., Mysore, K.S., Chen, R., and Udvardi, M.K. (2011). *Vapyrin,* a gene essential for intracellular progression of arbuscular mycorrhizal symbiosis, is also essential for infection by rhizobia in the nodule symbiosis of *Medicago truncatula*. Plant J **65,** 244-252.

Mylona, A., Theillet, F.X., Foster, C., Cheng, T.M., Miralles, F., Bates, P.A., Selenko, P., and Treisman, R. (2016). Opposing effects of Elk-1 multisite phosphorylation shape its response to ERK activation. Science **354,** 233-237.

Nadal, M., Sawers, R., Naseem, S., Bassin, B., Kulicke, C., Sharman, A., An, G., An, K., Ahern, K.R., Romag, A., Brutnell, T.P., Gutjahr, C., Geldner, N., Roux, C., Martinoia, E., Konopka, J.B., and Paszkowski, U. (2017). An N-acetylglucosamine transporter required for arbuscular mycorrhizal symbioses in rice and maize. Nature Plants **3,** 17073.

Nash, P., Tang, X., Orlicky, S., Chen, Q., Gertler, F.B., Mendenhall, M.D., Sicheri, F., Pawson, T., and Tyers, M. (2001). Multisite phosphorylation of a CDK inhibitor sets a threshold for the onset of DNA replication. Nature **414,** 514-521.

Ni, L., Fu, X., Zhang, H., Li, X., Cai, X., Zhang, P., Liu, L., Wang, Q., Sun, M., Wang, Q.W., Zhang, A., Zhang, Z., and Jiang, M. (2019). Abscisic Acid Inhibits Rice Protein Phosphatase PP45 via H2O2 and Relieves Repression of the Ca(2+)/CaM-Dependent Protein Kinase DMI3. Plant Cell **31,** 128-152.

Nishida, H., and Suzaki, T. (2018). Nitrate-mediated control of root nodule symbiosis. Curr Opin Plant Biol **44,** 129-136.

Nishimura, R., Hayashi, M., Wu, G.J., Kouchi, H., Imaizumi-Anraku, H., Murakami, Y., Kawasaki, S., Akao, S., Ohmori, M., Nagasawa, M., Harada, K., and Kawaguchi, M. (2002). HAR1 mediates systemic regulation of symbiotic organ development. Nature **420,** 426-429.

Nussaume, L., Kanno, S., Javot, H., Marin, E., Pochon, N., Ayadi, A., Nakanishi, T.M., and Thibaud, M.C. (2011). Phosphate Import in Plants: Focus on the PHT1 Transporters. Front Plant Sci **2,** 83.

Okamoto, S., Shinohara, H., Mori, T., Matsubayashi, Y., and Kawaguchi, M. (2013). Root-derived CLE glycopeptides control nodulation by direct binding to HAR1 receptor kinase. Nat Commun **4,** 2191.

Oláh, B., Brière, C., Bécard, G., Dénarié, J., and Gough, C. (2005). Nod factors and a diffusible factor from arbuscular mycorrhizal fungi stimulate lateral root

formation in *Medicago truncatula* via the DMI1/DMI2 signalling pathway. The Plant Journal **44,** 195-207.

Oldroyd, G.E. (2013). Speak, friend, and enter: signalling systems that promote beneficial symbiotic associations in plants. Nature Reviews: Microbiology **11,** 252-263.

Oldroyd, G.E., and Long, S.R. (2003). Identification and characterization of *nodulation-signaling pathway 2,* a gene of *Medicago truncatula* involved in Nod actor signaling. Plant Physiol **131,** 1027-1032.

Oldroyd, G.E., Murray, J.D., Poole, P.S., and Downie, J.A. (2011). The rules of engagement in the legume-rhizobial symbiosis. Annual review of genetics **45,** 119-144.

Orsel, M., Filleur, S., Fraisier, V., and Daniel-Vedele, F. (2002). Nitrate transport in plants: which gene and which control? Journal of Experimental Botany **53,** 825-833.

Ovchinnikova, E., Journet, E.P., Chabaud, M., Cosson, V., Ratet, P., Duc, G., Fedorova, E., Liu, W., den Camp, R.O., Zhukov, V., Tikhonovich, I., Borisov, A., Bisseling, T., and Limpens, E. (2011). IPD3 controls the formation of nitrogen-fixing symbiosomes in pea and *Medicago* spp. MPMI **24,** 1333-1344.

Park, H.J., Floss, D.S., Levesque-Tremblay, V., Bravo, A., and Harrison, M.J. (2015). Hyphal branching during arbuscule development requires *Reduced Arbuscular Mycorrhiza1*. Plant Physiology **169,** 2774-2788.

Parniske, M. (2008). Arbuscular mycorrhiza: the mother of plant root endosymbioses. Nat Rev Microbiol **6,** 763-775.

Parniske, M. (2018). Uptake of bacteria into living plant cells, the unifying and distinct feature of the nitrogen-fixing root nodule symbiosis. Curr Opin Plant Biol **44,** 164-174.

Paszkowski, U., and Gutjahr, C. (2013). Multiple control levels of root system remodeling in arbuscular mycorrhizal symbiosis. Frontiers in plant science **4,** 204.

Patil, S., Takezawa, D., and Poovaiah, B.W. (1995). Chimeric plant calcium/calmodulin-dependent protein kinase gene with a neural visinin-like calcium-binding domain. Proc Natl Acad Sci U S A **92,** 4897-4901.

Perry, J., Brachmann, A., Welham, T., Binder, A., Charpentier, M., Groth, M., Haage, K., Markmann, K., Wang, T.L., and Parniske, M. (2009). TILLING in *Lotus japonicus* identified large allelic series for symbiosis genes and

revealed a bias in functionally defective ethyl methanesulfonate alleles toward glycine replacements. Plant Physiol **151,** 1281-1291.

Peters, N.K., Frost, J.W., and Long, S.R. (1986). A plant flavone, luteolin, induces expression of Rhizobium meliloti nodulation genes. Science **233,** 977-980.

Pfeffer, P.E., Douds, D.D., Bécard, G., and Shachar-Hill, Y. (1999). Carbon uptake and the metabolism and transport of lipids in an arbuscular mycorrhiza. Plant Physiology **120,** 587-598.

Pimprikar, P., and Gutjahr, C. (2018). Transcriptional Regulation of Arbuscular Mycorrhiza Development. Plant and Cell Physiology **59,** 678-695.

Pimprikar, P., Carbonnel, S., Paries, M., Katzer, K., Klingl, V., Bohmer, M.J., Karl, L., Floss, D.S., Harrison, M.J., Parniske, M., and Gutjahr, C. (2016). A CCaMK-CYCLOPS-DELLA complex activates transcription of *RAM1* to regulate arbuscule branching. Current Biology **26,** 1126.

Poole, P., Ramachandran, V., and Terpolilli, J. (2018). Rhizobia: from saprophytes to endosymbionts. Nat Rev Microbiol **16,** 291-303.

Poovaiah, B.W., Du, L., Wang, H., and Yang, T. (2013). Recent advances in calcium/calmodulin-mediated signaling with an emphasis on plant-microbe interactions. Plant Physiol **163,** 531-542.

Popp, C., and Ott, T. (2011). Regulation of signal transduction and bacterial infection during root nodule symbiosis. Curr Opin Plant Biol **14,** 458-467.

Ptashne, M. (1988). How eukaryotic transcriptional activators work. Nature **335,** 683-689.

Pufall, M.A., Lee, G.M., Nelson, M.L., Kang, H.-S., Velyvis, A., Kay, L.E., McIntosh, L.P., and Graves, B.J. (2005). Variable control of Ets-1 DNA binding by multiple phosphates in an unstructured region. Science **309,** 142-145.

Pumplin, N., and Harrison, M.J. (2009). Live-cell imaging reveals periarbuscular membrane domains and organelle location in *Medicago truncatula* roots during arbuscular mycorrhizal symbiosis. Plant physiology **151,** 809-819.

Pumplin, N., Mondo, S.J., Topp, S., Starker, C.G., Gantt, J.S., and Harrison, M.J. (2010). *Medicago truncatula* Vapyrin is a novel protein required for arbuscular mycorrhizal symbiosis. Plant J **61,** 482-494.

Radhakrishnan, G.V., Keller, J., Rich, M.K., Vernié, T., Mbadinga Mbadinga, D.L., Vigneron, N., Cottret, L., Clemente, H.S., Libourel, C., Cheema, J., Linde, A.-M., Eklund, D.M., Cheng, S., Wong, G.K.S., Lagercrantz, U., Li, F.-W., Oldroyd, G.E.D., and Delaux, P.-M. (2020). An ancestral signalling

pathway is conserved in intracellular symbioses-forming plant lineages. Nature Plants **6,** 280-289.

Radutoiu, S., Madsen, L.H., Madsen, E.B., Felle, H.H., Umehara, Y., Grønlund, M., Sato, S., Nakamura, Y., Tabata, S., and Sandal, N. (2003). Plant recognition of symbiotic bacteria requires two LysM receptor-like kinases. Nature **425,** 585-592.

Radutoiu, S., Madsen, L.H., Madsen, E.B., Jurkiewicz, A., Fukai, E., Quistgaard, E.M.H., Albrektsen, A.S., James, E.K., Thirup, S., and Stougaard, J. (2007). LysM domains mediate lipochitin–oligosaccharide recognition and Nfr genes extend the symbiotic host range. The EMBO Journal **26,** 3923-3935.

Ramachandiran, S., Takezawa, D., Wang, W., and Poovaiah, B.W. (1997). Functional Domains of Plant Chimeric Calcium/Calmodulin-Dependent Protein Kinase: Regulation by Autoinhibitory and Visinin-Like Domains1. The Journal of Biochemistry **121,** 984-990.

Rech, S.S., Heidt, S., and Requena, N. (2013). A tandem Kunitz protease inhibitor (KPI106)–serine carboxypeptidase (SCP1) controls mycorrhiza establishment and arbuscule development in *Medicago truncatula*. The Plant Journal **75,** 711-725.

Remy, W., Taylor, T.N., Hass, H., and Kerp, H. (1994). Four hundred-million-year-old vesicular arbuscular mycorrhizae. Proceedings of the National Academy of Sciences **91,** 11841-11843.

Rich, M.K., Schorderet, M., Bapaume, L., Falquet, L., Morel, P., Vandenbussche, M., and Reinhardt, D. (2015). The Petunia GRAS Transcription Factor ATA/RAM1 Regulates Symbiotic Gene Expression and Fungal Morphogenesis in Arbuscular Mycorrhiza. Plant Physiology **168,** 788-797.

Ried, M.K., Antolin-Llovera, M., and Parniske, M. (2014). Spontaneous symbiotic reprogramming of plant roots triggered by receptor-like kinases. eLife **3**.

Roberts, N.J., Morieri, G., Kalsi, G., Rose, A., Stiller, J., Edwards, A., Xie, F., Gresshoff, P.M., Oldroyd, G.E.D., Downie, J.A., and Etzler, M.E. (2013). Rhizobial and Mycorrhizal Symbioses in *Lotus japonicus* Require Lectin Nucleotide Phosphohydrolase, Which Acts Upstream of Calcium Signaling. Plant Physiology **161,** 556-567.

Routray, P., Miller, J.B., Du, L., Oldroyd, G., and Poovaiah, B.W. (2013). Phosphorylation of S344 in the calmodulin-binding domain negatively affects CCaMK function during bacterial and fungal symbioses. Plant J **76,** 287-296.

Roy, S., Liu, W., Nandety, R.S., Crook, A.D., Mysore, K.S., Pislariu, C.I., Frugoli, J.A., Dickstein, R., and Udvardi, M.K. (2019). Celebrating 20 years of genetic discoveries in legume nodulation and symbiotic nitrogen fixation. The Plant Cell**,** tpc.00279.02019.

Sadowski, I., Ma, J., Triezenberg, S., and Ptashne, M. (1988). GAL4-VP16 is an unusually potent transcriptional activator. Nature **335,** 563-564.

Saito, K., Yoshikawa, M., Yano, K., Miwa, H., Uchida, H., Asamizu, E., Sato, S., Tabata, S., Imaizumi-Anraku, H., Umehara, Y., Kouchi, H., Murooka, Y., Szczyglowski, K., Downie, J.A., Parniske, M., Hayashi, M., and Kawaguchi, M. (2007). NUCLEOPORIN85 is required for calcium spiking, fungal and bacterial symbioses, and seed production in *Lotus japonicus*. Plant Cell **19,** 610-624.

Sathyanarayanan, P.V., and Poovaiah, B.W. (2002). Autophosphorylation-dependent inactivation of plant chimeric calcium/calmodulin-dependent protein kinase. Eur J Biochem **269,** 2457-2463.

Sathyanarayanan, P.V., Cremo, C.R., and Poovaiah, B.W. (2000). Plant Chimeric Ca^{2+}/Calmodulin-dependent Protein Kinase: ROLE OF THE NEURAL VISININ-LIKE DOMAIN IN REGULATING AUTOPHOSPHORYLATION AND CALMODULIN AFFINITY. Journal of Biological Chemistry **275,** 30417-30422.

Schauser, L., Roussis, A., Stiller, J., and Stougaard, J. (1999). A plant regulator controlling development of symbiotic root nodules. Nature **402,** 191-195.

Schiessl, K., Lilley, J.L.S., Lee, T., Tamvakis, I., Kohlen, W., Bailey, P.C., Thomas, A., Luptak, J., Ramakrishnan, K., Carpenter, M.D., Mysore, K.S., Wen, J., Ahnert, S., Grieneisen, V.A., and Oldroyd, G.E.D. (2019). *NODULE INCEPTION* recruits the lateral root developmental program for symbiotic nodule organogenesis in *Medicago truncatula*. Curr Biol **29,** 3657-3668 e3655.

Seabra, A.R., Pereira, P.A., Becker, J.D., and Carvalho, H.G. (2012). Inhibition of Glutamine Synthetase by Phosphinothricin Leads to Transcriptome Reprograming in Root Nodules of *Medicago truncatula*. Molecular Plant-Microbe Interactions® **25,** 976-992.

Senovilla, M., Castro-Rodríguez, R., Abreu, I., Escudero, V., Kryvoruchko, I., Udvardi, M.K., Imperial, J., and González-Guerrero, M. (2018). *Medicago truncatula* copper transporter 1 (*Mt*COPT 1) delivers copper for symbiotic nitrogen fixation. New Phytologist **218,** 696-709.

Shachar-Hill, Y., Pfeffer, P.E., Douds, D., Osman, S.F., Doner, L.W., and Ratcliffe, R.G. (1995). Partitioning of intermediary carbon metabolism in vesicular-arbuscular mycorrhizal leek. Plant Physiology **108,** 7-15.

Shen, J., Yuan, L., Zhang, J., Li, H., Bai, Z., Chen, X., Zhang, W., and Zhang, F. (2011). Phosphorus dynamics: from soil to plant. Plant physiology **156,** 997-1005.

Shi, B., Ni, L., Zhang, A., Cao, J., Zhang, H., Qin, T., Tan, M., Zhang, J., and Jiang, M. (2012). OsDMI3 Is a Novel Component of Abscisic Acid Signaling in the Induction of Antioxidant Defense in Leaves of Rice. Molecular Plant **5,** 1359-1374.

Shimizu, T., Nakano, T., Takamizawa, D., Desaki, Y., Ishii-Minami, N., Nishizawa, Y., Minami, E., Okada, K., Yamane, H., Kaku, H., and Shibuya, N. (2010). Two LysM receptor molecules, CEBiP and *Os*CERK1, cooperatively regulate chitin elicitor signaling in rice. The Plant Journal **64,** 204-214.

Shimoda, Y., Imaizumi-Anraku, H., and Hayashi, M. (2019). Kinase activity-dependent stability of calcium/calmodulin-dependent protein kinase of *Lotus japonicus*. Planta **250,** 1773-1779.

Shimoda, Y., Han, L., Yamazaki, T., Suzuki, R., Hayashi, M., and Imaizumi-Anraku, H. (2012). Rhizobial and fungal symbioses show different requirements for calmodulin binding to calcium calmodulin-dependent protein kinase in *Lotus japonicus*. Plant Cell **24,** 304-321.

Siciliano, V., Genre, A., Balestrini, R., Cappellazzo, G., Pierre, J., and Bonfante, P. (2007). Transcriptome analysis of arbuscular mycorrhizal roots during development of the prepenetration apparatus. Plant Physiology **144,** 1455-1466.

Sieberer, B.J., Chabaud, M., Fournier, J., Timmers, A.C., and Barker, D.G. (2012). A switch in Ca^{2+} spiking signature is concomitant with endosymbiotic microbe entry into cortical root cells of *Medicago truncatula*. Plant Journal **69,** 822-830.

Sieberer, B.J., Chabaud, M., Timmers, A.C., Monin, A., Fournier, J., and Barker, D.G. (2009). A nuclear-targeted cameleon demonstrates intranuclear Ca^{2+} spiking in *Medicago truncatula* root hairs in response to rhizobial nodulation factors. Plant Physiol **151,** 1197-1206.

Singh, S. (2014). The calcium signature decoding CCaMK/CYCLOPS complex activates the transcription of symbiosis associated genes (lmu).

Singh, S., and Parniske, M. (2012). Activation of calcium- and calmodulin-dependent protein kinase (CCaMK), the central regulator of plant root endosymbiosis. Current Opinion in Plant Biology **15,** 444-453.

Singh, S., Katzer, K., Lambert, J., Cerri, M., and Parniske, M. (2014). CYCLOPS, a DNA-binding transcriptional activator, orchestrates symbiotic root nodule development. Cell host & microbe **15,** 139-152.

Smil, V. (2004). The roots of nitrogen fixation. Nature **431,** 909-911.

Smit, P., Raedts, J., Portyanko, V., Debelle, F., Gough, C., Bisseling, T., and Geurts, R. (2005). NSP1 of the GRAS protein family is essential for rhizobial Nod factor-induced transcription. Science **308,** 1789-1791.

Smith, D., Owens, P., Leytem, A., and Warnemuende, E. (2007). Nutrient losses from manure and fertilizer applications as impacted by time to first runoff event. Environmental Pollution **147,** 131-137.

Soltis, D.E., Soltis, P.S., Morgan, D.R., Swensen, S.M., Mullin, B.C., Dowd, J.M., and Martin, P.G. (1995). Chloroplast gene sequence data suggest a single origin of the predisposition for symbiotic nitrogen fixation in angiosperms. Proc Natl Acad Sci U S A **92,** 2647-2651.

Soyano, T., Kouchi, H., Hirota, A., and Hayashi, M. (2013). Nodule inception directly targets *NF-Y* subunit genes to regulate essential processes of root nodule development in *Lotus japonicus*. PLoS genetics **9,** e1003352.

Soyano, T., Shimoda, Y., Kawaguchi, M., and Hayashi, M. (2019). A shared gene drives lateral root development and root nodule symbiosis pathways in *Lotus*. Science **366,** 1021-1023.

Soyano, T., Hirakawa, H., Sato, S., Hayashi, M., and Kawaguchi, M. (2014). NODULE INCEPTION creates a long-distance negative feedback loop involved in homeostatic regulation of nodule organ production. PNAS **111,** 14607-14612.

Sprent, J.I., and James, E.K. (2007). Legume evolution: where do nodules and mycorrhizas fit in? Plant physiology **144,** 575-581.

Springer, M., Wykoff, D.D., Miller, N., and O'Shea, E.K. (2003). Partially phosphorylated Pho4 activates transcription of a subset of phosphate-responsive genes. PLoS Biol **1,** e28.

Stougaard, J., Petersen, T.E., and Marcker, K.A. (1987). Expression of a complete soybean leghemoglobin gene in root nodules of transgenic *Lotus corniculatus*. Proc Natl Acad Sci U S A **84,** 5754-5757.

Stracke, S., Kistner, C., Yoshida, S., Mulder, L., Sato, S., Kaneko, T., Tabata, S., Sandal, N., Stougaard, J., Szczyglowski, K., and Parniske, M. (2002). A

plant receptor-like kinase required for both bacterial and fungal symbiosis. Nature **417,** 959-962.

Streeter, J., and Wong, P.P. (1988). Inhibition of legume nodule formation and N2 fixation by nitrate. Critical Reviews in Plant Sciences **7,** 1-23.

Strickfaden, S.C., Winters, M.J., Ben-Ari, G., Lamson, R.E., Tyers, M., and Pryciak, P.M. (2007). A mechanism for cell-cycle regulation of MAP kinase signaling in a yeast differentiation pathway. Cell **128,** 519-531.

Sun, J., Miller, J.B., Granqvist, E., Wiley-Kalil, A., Gobbato, E., Maillet, F., Cottaz, S., Samain, E., Venkateshwaran, M., Fort, S., Morris, R.J., Ane, J.M., Denarie, J., and Oldroyd, G.E. (2015). Activation of symbiosis signaling by arbuscular mycorrhizal fungi in legumes and rice. Plant Cell **27,** 823-838.

Sutton, M.A., Oenema, O., Erisman, J.W., Leip, A., van Grinsven, H., and Winiwarter, W. (2011). Too much of a good thing. Nature **472,** 159-161.

Suzaki, T., Yoro, E., and Kawaguchi, M. (2015). Leguminous plants: inventors of root nodules to accommodate symbiotic bacteria. Int Rev Cell Mol Biol **316,** 111-158.

Suzaki, T., Takeda, N., Nishida, H., Hoshino, M., Ito, M., Misawa, F., Handa, Y., Miura, K., and Kawaguchi, M. (2019). *LACK OF SYMBIONT ACCOMMODATION* controls intracellular symbiont accommodation in root nodule and arbuscular mycorrhizal symbiosis in *Lotus japonicus*. PLoS Genet **15,** e1007865.

Sverdrup, H.U., and Ragnarsdottir, K.V. (2011). Challenging the planetary boundaries II: Assessing the sustainable global population and phosphate supply, using a systems dynamics assessment model. Applied Geochemistry **26,** S307-S310.

Sweeney, H.L., Yang, Z., Zhi, G., Stull, J.T., and Trybus, K.M. (1994). Charge replacement near the phosphorylatable serine of the myosin regulatory light chain mimics aspects of phosphorylation. Proc Natl Acad Sci U S A **91,** 1490-1494.

Swensen, S.M. (1996). The evolution of actinorhizal symbioses: evidence for multiple origins of the symbiotic association. American Journal of Botany **83,** 1503-1512.

Takeda, N., Maekawa, T., and Hayashi, M. (2012). Nuclear-localized and deregulated calcium- and calmodulin-dependent protein kinase activates rhizobial and mycorrhizal responses in *Lotus japonicus*. Plant Cell **24,** 810-822.

Takeda, N., Sato, S., Asamizu, E., Tabata, S., and Parniske, M. (2009). Apoplastic plant subtilases support arbuscular mycorrhiza development in *Lotus japonicus*. Plant J **58,** 766-777.

Taylor, T.N., Remy, W., Hass, H., and Kerp, H. (1995). Fossil arbuscular mycorrhizae from the Early Devonian. Mycologia **87,** 560-573.

Tejada-Jiménez, M., Castro-Rodríguez, R., Kryvoruchko, I., Lucas, M.M., Udvardi, M., Imperial, J., and González-Guerrero, M. (2015). *Medicago truncatula* natural resistance-associated macrophage Protein1 is required for iron uptake by rhizobia-infected nodule cells. Plant Physiology **168,** 258-272.

Teufel, D.P., Freund, S.M., Bycroft, M., and Fersht, A.R. (2007). Four domains of p300 each bind tightly to a sequence spanning both transactivation subdomains of p53. Proceedings of the National Academy of Sciences **104,** 7009-7014.

Timmers, A., Auriac, M.-C., and Truchet, G. (1999). Refined analysis of early symbiotic steps of the *Rhizobium-Medicago* interaction in relationship with microtubular cytoskeleton rearrangements. Development **126,** 3617-3628.

Tirichine, L., Sandal, N., Madsen, L.H., Radutoiu, S., Albrektsen, A.S., Sato, S., Asamizu, E., Tabata, S., and Stougaard, J. (2007). A gain-of-function mutation in a cytokinin receptor triggers spontaneous root nodule organogenesis. Science **315,** 104-107.

Tirichine, L., Imaizumi-Anraku, H., Yoshida, S., Murakami, Y., Madsen, L.H., Miwa, H., Nakagawa, T., Sandal, N., Albrektsen, A.S., Kawaguchi, M., Downie, A., Sato, S., Tabata, S., Kouchi, H., Parniske, M., Kawasaki, S., and Stougaard, J. (2006). Deregulation of a Ca^{2+}/calmodulin-dependent kinase leads to spontaneous nodule development. Nature **441,** 1153-1156.

Tischner, R. (2000). Nitrate uptake and reduction in higher and lower plants. Plant, cell & environment **23,** 1005-1024.

Tjepkema, J.D., and Winship, L.J. (1980). Energy requirement for nitrogen fixation in actinorhizal and legume root nodules. Science **209,** 279-281.

Toth, R., and Miller, R.M. (1984). Dynamics of arbuscule development and degeneration in a *Zea mays* mycorrhiza. American journal of botany **71,** 449-460.

Tsikou, D., Yan, Z., Holt, D.B., Abel, N.B., Reid, D.E., Madsen, L.H., Bhasin, H., Sexauer, M., Stougaard, J., and Markmann, K. (2018). Systemic control of legume susceptibility to rhizobial infection by a mobile microRNA. Science **362,** 233-236.

Udvardi, M.K., and Day, D.A. (1997). Metabolite Transport across Symbiotic Membranes of Legume Nodules. Annu Rev Plant Physiol Plant Mol Biol **48,** 493-523.

Uesugi, M., Nyanguile, O., Lu, H., Levine, A.J., and Verdine, G.L. (1997). Induced α helix in the VP16 activation domain upon binding to a human TAF. Science **277,** 1310-1313.

Vaccari, D.A. (2009). Phosphorus: a looming crisis. Scientific American **300,** 54-59.

Van de Velde, W., Guerra, J.C.P., De Keyser, A., De Rycke, R., Rombauts, S., Maunoury, N., Mergaert, P., Kondorosi, E., Holsters, M., and Goormachtig, S. (2006). Aging in legume symbiosis. A molecular view on nodule senescence in *Medicago truncatula*. Plant physiology **141,** 711-720.

Van de Velde, W., Zehirov, G., Szatmari, A., Debreczeny, M., Ishihara, H., Kevei, Z., Farkas, A., Mikulass, K., Nagy, A., and Tiricz, H. (2010). Plant peptides govern terminal differentiation of bacteria in symbiosis. Science **327,** 1122-1126.

van Velzen, R., Doyle, J.J., and Geurts, R. (2019). A Resurrected Scenario: Single Gain and Massive Loss of Nitrogen-Fixing Nodulation. Trends in Plant Science **24,** 49-57.

Venkateshwaran, M., Jayaraman, D., Chabaud, M., Genre, A., Balloon, A.J., Maeda, J., Forshey, K., den Os, D., Kwiecien, N.W., Coon, J.J., Barker, D.G., and Ane, J.M. (2015). A role for the mevalonate pathway in early plant symbiotic signaling. Proc Natl Acad Sci U S A **112,** 9781-9786.

Vernié, T., Camut, S., Camps, C., Rembliere, C., de Carvalho-Niebel, F., Mbengue, M., Timmers, T., Gasciolli, V., Thompson, R., and Le Signor, C. (2016). PUB1 interacts with the receptor kinase DMI2 and negatively regulates rhizobial and arbuscular mycorrhizal symbioses through its ubiquitination activity in *Medicago truncatula*. Plant Physiology **170,** 2312-2324.

Walan, P., Davidsson, S., Johansson, S., and Höök, M. (2014). Phosphate rock production and depletion: Regional disaggregated modeling and global implications. Resources, Conservation and Recycling **93,** 178-187.

Walder, F., Niemann, H., Natarajan, M., Lehmann, M.F., Boller, T., and Wiemken, A. (2012). Mycorrhizal networks: common goods of plants shared under unequal terms of trade. Plant physiology **159,** 789-797.

Wang, E., Schornack, S., Marsh, J.F., Gobbato, E., Schwessinger, B., Eastmond, P., Schultze, M., Kamoun, S., and Oldroyd, G.E. (2012). A common

signaling process that promotes mycorrhizal and oomycete colonization of plants. Curr Biol **22,** 2242-2246.

Wang, H., Moore, M.J., Soltis, P.S., Bell, C.D., Brockington, S.F., Alexandre, R., Davis, C.C., Latvis, M., Manchester, S.R., and Soltis, D.E. (2009). Rosid radiation and the rapid rise of angiosperm-dominated forests. Proceedings of the National Academy of Sciences **106,** 3853.

Wang, W., and Poovaiah, B.W. (1999). Interaction of Plant Chimeric Calcium/Calmodulin-dependent Protein Kinase with a Homolog of Eukaryotic Elongation Factor-1α. Journal of Biological Chemistry **274,** 12001-12008.

Weijers, D., Van Hamburg, J.-P., Van Rijn, E., Hooykaas, P.J., and Offringa, R. (2003). Diphtheria toxin-mediated cell ablation reveals interregional communication during *Arabidopsis* seed development. Plant Physiology **133,** 1882-1892.

Westhoek, H., Lesschen, J.P., Rood, T., Wagner, S., De Marco, A., Murphy-Bokern, D., Leip, A., van Grinsven, H., Sutton, M.A., and Oenema, O. (2014). Food choices, health and environment: Effects of cutting Europe's meat and dairy intake. Global Environmental Change **26,** 196-205.

Wong, J.E.M.M., Nadzieja, M., Madsen, L.H., Bücherl, C.A., Dam, S., Sandal, N.N., Couto, D., Derbyshire, P., Uldum-Berentsen, M., Schroeder, S., Schwämmle, V., Nogueira, F.C.S., Asmussen, M.H., Thirup, S., Radutoiu, S., Blaise, M., Andersen, K.R., Menke, F.L.H., Zipfel, C., and Stougaard, J. (2019). A *Lotus japonicus* cytoplasmic kinase connects Nod factor perception by the NFR5 LysM receptor to nodulation. Proceedings of the National Academy of Sciences **116,** 14339-14348.

Xiao, A., Yu, H., Fan, Y., Kang, H., Ren, Y., Huang, X., Gao, X., Wang, C., Zhang, Z., Zhu, H., and Cao, Y. (2020). Transcriptional regulation of *NIN* expression by IPN2 is required for root nodule symbiosis in *Lotus japonicus*. New Phytologist **227,** 513-528.

Xie, F., Murray, J.D., Kim, J., Heckmann, A.B., Edwards, A., Oldroyd, G.E.D., and Downie, J.A. (2012). Legume pectate lyase required for root infection by rhizobia. Proceedings of the National Academy of Sciences **109,** 633.

Xue, L., Cui, H., Buer, B., Vijayakumar, V., Delaux, P.M., Junkermann, S., and Bucher, M. (2015). Network of GRAS transcription factors involved in the control of arbuscule development in *Lotus japonicus*. Plant Physiology **167,** 854-871.

Yan, J., Guan, L., Sun, Y., Zhu, Y., Liu, L., Lu, R., Jiang, M., Tan, M., and Zhang, A. (2015). Calcium and ZmCCaMK are involved in brassinosteroid-induced antioxidant defense in maize leaves. Plant and Cell Physiology **56,** 883-896.

Yang, S.-Y., Grønlund, M., Jakobsen, I., Grotemeyer, M.S., Rentsch, D., Miyao, A., Hirochika, H., Kumar, C.S., Sundaresan, V., and Salamin, N. (2012). Nonredundant regulation of rice arbuscular mycorrhizal symbiosis by two members of the *PHOSPHATE TRANSPORTER1* gene family. The Plant Cell **24,** 4236-4251.

Yano, K., Yoshida, S., Müller, J., Singh, S., Banba, M., Vickers, K., Markmann, K., White, C., Schuller, B., and Sato, S. (2008). CYCLOPS, a mediator of symbiotic intracellular accommodation. PNAS **105,** 20540-20545.

Yokota, K., Fukai, E., Madsen, L.H., Jurkiewicz, A., Rueda, P., Radutoiu, S., Held, M., Hossain, M.S., Szczyglowski, K., and Morieri, G. (2009). Rearrangement of actin cytoskeleton mediates invasion of *Lotus japonicus* roots by *Mesorhizobium loti*. The Plant Cell **21,** 267-284.

Yoneyama, K., Xie, X., Kusumoto, D., Sekimoto, H., Sugimoto, Y., Takeuchi, Y., and Yoneyama, K. (2007). Nitrogen deficiency as well as phosphorus deficiency in sorghum promotes the production and exudation of 5-deoxystrigol, the host recognition signal for arbuscular mycorrhizal fungi and root parasites. Planta **227,** 125-132.

Yoneyama, K., Xie, X., Sekimoto, H., Takeuchi, Y., Ogasawara, S., Akiyama, K., Hayashi, H., and Yoneyama, K. (2008). Strigolactones, host recognition signals for root parasitic plants and arbuscular mycorrhizal fungi, from Fabaceae plants. New Phytologist **179,** 484-494.

Yoro, E., Suzaki, T., and Kawaguchi, M. (2019). CLE-HAR1 Systemic Signaling and NIN-Mediated Local Signaling Suppress the Increased Rhizobial Infection in the *daphne* Mutant of *Lotus japonicus*. Mol Plant Microbe Interact, MPMI08190223R.

Yoro, E., Suzaki, T., Toyokura, K., Miyazawa, H., Fukaki, H., and Kawaguchi, M. (2014). A positive regulator of nodule organogenesis, NODULE INCEPTION, acts as a negative regulator of rhizobial infection in *Lotus japonicus*. Plant Physiology **165,** 747-758.

Yu, N., Luo, D., Zhang, X., Liu, J., Wang, W., Jin, Y., Dong, W., Liu, J., Liu, H., Yang, W., Zeng, L., Li, Q., He, Z., Oldroyd, G.E., and Wang, E. (2014). A DELLA protein complex controls the arbuscular mycorrhizal symbiosis in plants. Cell Res **24,** 130-133.

Yuan, S., Zhu, H., Gou, H., Fu, W., Liu, L., Chen, T., Ke, D., Kang, H., Xie, Q., Hong, Z., and Zhang, Z. (2012). A Ubiquitin Ligase of Symbiosis Receptor Kinase Involved in Nodule Organogenesis. Plant Physiology **160,** 106-117.

Zhang, X., Dong, W., Sun, J., Feng, F., Deng, Y., He, Z., Oldroyd, G.E.D., and Wang, E. (2015). The receptor kinase CERK1 has dual functions in symbiosis and immunity signalling. The Plant Journal **81,** 258-267.

Zhu, H., Chen, T., Zhu, M., Fang, Q., Kang, H., Hong, Z., and Zhang, Z. (2008). A novel ARID DNA-binding protein interacts with SymRK and is expressed during early nodule development in *Lotus japonicus*. Plant Physiol **148,** 337-347.

Zhu, Y., Yan, J., Liu, W., Liu, L., Sheng, Y., Sun, Y., Li, Y., Scheller, H.V., Jiang, M., Hou, X., Ni, L., and Zhang, A. (2016). Phosphorylation of a NAC Transcription Factor by a Calcium/Calmodulin-Dependent Protein Kinase Regulates Abscisic Acid-Induced Antioxidant Defense in Maize. Plant Physiology **171,** 1651-1664.

XI List of Figures

XII List of Tables

XIII Declaration of contribution of other researchers

Figure 1: Initially created by Dr. Andreas Binder. Modified by Philipp Bellon.

Figure 2: CCaMK/Cyclops complex and AM and RNS icons were created by Dr. Andreas Binder. Modified by Philipp Bellon.

Figure 5: Experiment was designed by Philipp Bellon and performed by Clara Pappenberger, Data evaluation and figure preparation was done by Philipp Bellon.

Figure 6: Experiment was designed by Philipp Bellon and performed by Clara Pappenberger. Data evaluation and figure preparation was done by Philipp Bellon.

Figure 10: Experiment was designed by Philipp Bellon and performed by Giulia Gobatto. Data evaluation and figure preparation was done by Philipp Bellon.

Figure 14: Experiments were designed by Philipp Bellon and performed by Giulia Gobatto, Lena Weidert and Zoé Möller-Ramon. Data evaluation and figure preparation was done by Philipp Bellon.

XIV Acknowledgements

I would like to express my gratitude to all the people that were on my side during the period of this doctoral thesis

Firstly, I would like to thank my supervisor Prof. Martin Parniske for taking me on as a doctoral student in his lab. I would like to thank him for his support, feedback, the discussions we had and the valuable ideas he brought to the table. I am especially grateful that I could enjoy the freedom to follow my own scientific ideas and for giving me the opportunity to attend scientific conferences and several training courses. Lastly, I would like to thank him for the time he spent on correcting and evaluating proposals, manuscripts, and this thesis.

I would also like to thank the Collaborative Research Centre (SFB924) "Molecular mechanisms regulating yield and yield stability in plants" for funding me as part of the subproject "Spatio-temporal dynamics in the composition and function of the CCaMK/Cyclops complex". Furthermore, I would like to thank SFB924 for traveling grants and the possibility to participate in and organize several scientific and softskill courses. Importantly, a big thanks to the SFB924 Young Investigator Initiative for fun conferences, retreats, evenings, and trainings. I got to know some great people there and I really enjoyed being part of the YII.

To the Genetics members and to my colleagues, I want to express my highest gratitude. Firstly, I would like to thank Dr. Marion Cherri for taking the time to onboard me onto the Genetics ship and introducing me to not only the lab, but also to the research topic. Furthermore, I would like to thank Dr. Katja Katzer and Dr. Victor Gimenez-Oya for continuous discussions, brainstorming at any time, ideas and feedback on the Cyclops phospho-project. I also would like to thank Victor for his cooperation and teamwork in the lab, which I always enjoyed. Many thanks to Prof. David Chiasson for continuous help with cloning and yeast work, and his support during the Bachelor Project. For the Bachelor Project I would also like to thank Dr. Dagmar Hann und Dr. Andreas Brachmann for their cooperation and support. Dr. Andreas Brachmann I would like to additionally thank for helping me with IT problems in the frame of my microscopy responsibility. Andreas´ team-members Ute and Gisela I would like to thank for their sequencing service and taking on samples, even though I was too late quite often.

Throughout the years I had the possibility to supervise and teach Giulia, Clara, Leon, Chiara and the Bachelor Project team Zoé, Alice and Lena, which I always

enjoyed a lot. I would like to thank them for their dedication and the good work they did in the lab. I wish you all the best.

Special thanks go to Dr. Rosa Elena Andrade, Xiaoyun Gong, Chloé Cathebras and Jessica Folgmann. I really enjoyed having you as my colleagues. I not only want to thank you for your scientific input and discussions, but also for the fun times we had and your personal support. I also want to thank current and previous doctoral students for being great colleagues and office mates and making the time in the institute a nice experience: Martin B, Katy Sollweck, Nimisha Panchakshari, Isabell Seidler, Juan Liang, Benjamin Billault-Penneteau, Aline Sandré, Max Griesmann, Constance Tisserant, Fang-Yu and Flo Dunker.

I would also like to thank my parents who always support, believe and never give up on me.

Lastly, I would like to thank Anni. Without your guidance, support and patience I would have not been able to do this. Especially at the end. Thank you for being on my side, always.

XV Curriculum vitae

Philipp Robert Bellon

Work experience

02/2016 – present	**Doctoral Thesis**: Ludwig-Maximilians-Universität München, Faculty of Biology - Genetics, Functional characterization of the transcription factor Cyclops, Prof. Parniske
03/2015 – 12/2015	**Technical Assistant:** Ruprecht-Karls-Universität Heidelberg, Centre for Organismal Studies, Prof. Schumacher
05/2014 – 12/2014	**Master Thesis**: Ruprecht-Karls-Universität Heidelberg, Centre for Organismal Studies, Design of a fluorescent cytosolic nitrate sensor based on *A. thaliana* Nitrate Reductase 1, Prof. Schumacher
07/2012 – 09/2012	**DAAD RISE research internship in Australia**: University of Newcastle, The Tom Farrell Institute for the Environment, Plant Science Group
04/2012 – 06/2012	**Bachelor Thesis**: Ruprecht-Karls-Universität Heidelberg, Institute for Physiology and Pathophysiology, Effects of Nitric Oxide (NO) on biophysical parameter of temporal properties of Ca^{2+} regulation in isolated murine cardiomyocytes, Prof. Fink

Education

09/2012 – 12/2014	**Master of Science**: Ruprecht-Karls-Universität Heidelberg, Molecular Biology of Plants (Grade: 1.2)
10/2009 – 06/2012	**Bachelor of Science**: Ruprecht-Karls-Universität Heidelberg, (Grade:1.8)
09/1999 – 06/2008	**High School**: Graf-Eberhard-Gymnasium Bad Urach (Grade: 1.9)

Additional qualifications, skills, engagements

Courses and Seminars	12/2020: People Management Seminar (initiation, organization, participation) 09/2019: Certified Good Manufacturing Practice course (participation, Grade: 88/100) 04/2019: Project Management Seminar (participation)
IT	Microsoft-Office Package (very good skills) CLC Main Workbench (very good skills) Adobe Illustrator (good skills) Affinity Designer (good skills) R (basic skills)
Languages	German (native), English (excellent), French (basic)
Social	Student representative of the SFB924 Young Investigator Initiative

Publications

09/2018	Poster Presentation: Transcriptional regulation of Cyclops is dependent on its phosphorylation status.", European Nitrogen Fixation Conference (ENFC) 2018, Stockholm, Sweden
10/2017	Poster Presentation: "Multiple phosphorylation sites of Cyclops influence the transcriptional regulation of the *NIN* promoter.", SFB924 Conference, Freising, Germany
08/2016	Poster Presentation: "Do you want to join the complex? Towards the identification of new CCaMK/Cyclops components.", European Nitrogen Fixation Conference (ENFC) 2016, Budapest, Hungary

Private engagements and hobbies

Social	Community Service at DZKJR, Garmisch-Partenkirchen Organizing Member of the annual church summer camp
Sports	Head of Tennis Team Teaching kids and teenagers as certified Tennis Mentor